Conception, Preparation & Characterization of nanoparticles of complex shapes : Study of their in vivo fate

Olivier Cauchois

UNIVERSITÉ PARIS-SUD 11
FACULTÉ DE PHARMACIE DE CHÂTENAY-MALABRY

ÉCOLE DOCTORALE :
INNOVATION THÉRAPEUTIQUE : DU FONDAMENTAL A L'APPLIQUÉ
PÔLE : PHARMACOTECHNIE ET PHYSICO-CHIMIE

ANNÉE 2011 - 2012 SÉRIE DOCTORAT N° 1137

THÈSE DE DOCTORAT
Présentée
À L'UNITÉ DE FORMATION ET DE RECHERCHE
FACULTE DE PHARMACIE DE CHATENAY-MALABRY
UNIVERSITÉ PARIS-SUD 11

pour l'obtention du grade de
DOCTEUR DE L'UNIVERSITÉ PARIS-SUD 11
par

M Olivier CAUCHOIS

Titre de la thèse :

Conception, Préparation & Caractérisation de Nanoparticules de Formes Complexes. Etude de leur Devenir *In Vivo*.

Date de Soutenance : 15 Décembre 2011

JURY :	Mme le Professeur Ijeoma UCHEGBU	Rapporteur
	M le Docteur Christophe TRIBET	Rapporteur
	M le Professeur Elias FATTAL	Examinateur
	Mme le Docteur Nathalie MIGNET	Examinateur
	M le Docteur Nicolas TSAPIS	Examinateur
	M le Professeur Gilles PONCHEL	Directeur de Thèse

À mon grand-père Henri-Jean Martin, homme et chercheur extraordinaire,
source d'inspiration dans ma vie personnelle et professionnelle

À mon fils Eric et à ses futurs frères et sœurs
pour qui j'espère devenir à mon tour une source d'inspiration.

Remerciements

Cette thèse a été réalisée à la faculté de pharmacie de l'Université Paris Sud 11 à Châtenay-Malabry, France, au sein de l'UMR CNRS 8612 Physico-Chimie – Pharmacotechnie – Biopharmacie (dirigée par le Professeur Patrick COUVREUR puis Professeur Elias FATTAL) sous la direction scientifique du Professeur Gilles PONCHEL.

Je tiens à adresser mes plus sincères remerciements

Au Professeur Patrick COUVREUR et au professeur Elias FATTAL pour m'avoir permis de travailler au sein de l'UMR 8612.

Au Professeur Gilles PONCHEL pour m'avoir encadré durant ces trois années, pour sa grande confiance et sa compréhension, pour sa disponibilité, pour toutes nos discussions scientifiques. Merci beaucoup Gilles pour ta patience, je sais que parfois j'ai beaucoup, beaucoup poussé pour faire certaines manips ou publier parce que ce sujet m'a passionné et m'a tenu à cœur, merci de ton soutien. Nos échanges scientifiques ou autres m'ont beaucoup appris.

Au Professeur Ijeoma UCHEGBU, à Christophe TRIBET pour avoir été les rapporteurs de ma thèse, ainsi qu'à Elias FATTAL, à Nathalie MIGNET et à Elias FATTAL pour avoir participé à mon jury de thèse. Merci pour votre discussion et vos conseils !

A Magali NOIRAY pour sa gentillesse et son aide avec l'ITC et la SPR et aussi pour toutes nos discussions sur Eric et Pacôme !

A Christine VAUTHIER pour son aide avec les mesures d'activation du complément et ses conseils sur l'analyse statistique des photos de microscopie électronique à transmission.

A Kawthar BOUCHEMAL pour ses conseils précieux sur l'ITC, pour nos discussions scientifiques et personnelles.

A Danielle JAILLARD pour sa gentillesse et sa disponibilité et qui m'ont permis de me familiariser et de maîtriser la microscopie électronique à transmission.

Au Pr Elias FATTAL pour son soutien amical et sympathique.

A Nicolas TSAPIS, Valérie NICOLAS, Valérie DOMERGUE, et à tous les autres statutaires de l'Unité (ou d'ailleurs) qui m'on donné de leur temps, des conseils, qui m'on prêté du matériel ou des réactifs…

A Freimar SEGURA SANCHEZ qui a été « mon héritage scientifique », pour toute son aide lors de mon arrivée et mais surtout pour tous ses conseils expérimentaux, sa bonne humeur constante et son éternel optimisme.

A Rym SKANJI qui m'a accompagné du jour où je suis arrivé jusqu'à ma soutenance de thèse, qui m'a aidé à évoluer scientifiquement et personnellement.

Un très grand merci aussi aux membres de l'équipe VI, et en particulier mes stagiaires Marion, Myriam, Cindy, Naïla et Abdel, avec qui j'ai eu le plaisir de partager ces trois années. Tous nos échanges me manqueront !

Je voudrais aussi remercier mes collègues et maintenant amis Freimar, Silvia, Giada, Henri, Nadia, Rym, Khairallah, les différentes Bénédictes, Ipek, Laura, Sandrine, Amélie, Nathalie, Nadège, Odile, Samia et tous ceux que j'oublie de citer ici. Vous allez me manquer !

Également un très grand merci à toute l'UMR CNRS 8612, avec qui j'ai eu le plaisir de travailler et de qui j'ai beaucoup appris, qu'ils soient thésards, post-doctorants, stagiaires, Erasmus... qui ont, directement ou indirectement, favorisé l'avancement de cette thèse.

Aux mamans et aux papas de l'unité, qui m'ont bien soutenu lors de l'arrivé d'Eric.

Enfin je dois remercier ma famille. Ils ont toujours su me soutenir même s'ils ne comprenaient pas toujours mes choix.

Merci infiniment à ma chère épouse, Gaëlle, de m'avoir tant aidé pendant toute cette thèse. J'avais grâce à toi à la maison une oreille attentive à toutes mes élucubrations de chercheur fou, peu importait l'heure du jour ou de la nuit tu as toujours été là pour moi. Cette thèse restera toujours une des meilleures périodes de ma vie car nous nous sommes mariés et tu m'as offert un magnifique cadeau : Eric. Sans toi je n'aurai jamais réussi à faire un travail de cette qualité.

Table of content

List of abbreviations

AFM	Atomic force microscopy
BLG-NCA	benzyl-L-glutamate N-carboxy anhydride
CNT	Carbone Nanotube
CVD	Chemical vapor deposition
DCTB	2-[(2E)-3-(4-tert-Butylphenyl)-2-methylprop-2-enylidene]malononitrile
DMF	Dimethylformamide
DMSO	Dimethylsulfoxide
e.g.	Exempli gratia
EDL	Electrostatic double layer interaction
EDTA	Ethylene diamine tetra acetic acid
EPR effect	Enhanced permeability and retention effect
FTIR	Fourier transform infrared spectroscopy
Γ	Aspect ratio (length over width)
His-Tag	Histidine tag, a chain of six Histidine residues
ITC	Isothermal titration calorimetry
IV	Intravenous
MALDI TOF	Matrix-assisted laser desorption/ionisation time of flight
MPS	Macrophage-phagocyte system

MS	Mass spectroscopy
MW	Molecular weight
MWNT	Multi wall nanotube
NCA	N-carboxy anhydride
NMR	Nuclear magnetic resonance
NTA	Nitriloacetic acid
ODE	1-octadecene
PBLG	Poly(gamma-benzyl-L-glutamate)
PECL	Poly(epsilon caprolactone)
PEG	Poly(ethylene glycol)
PFPE	Perfluoropolyether
PLA	Poly(lactic acid)
PRINT	Particle replication in non wetting templates
PVA	Poly(vinyl alcohol)
PS	Polystyrene
QD	Quantum Dot
RGD sequence	Arginine - Glycine - Aspartic acid
SPR	Surface plasmon resonance
SEM	Scanning electron microscopy
SWNT	Single wall nanotube
TEC	Triethylcitrate

TEM	Transmission electron microscopy
THF	Tetrahydrofuran
USPIO	Ultra small particles of iron oxide

General Introduction

General introduction

Whatever the route of delivery in the body, an active pharmaceutical ingredient undergoes a number of phenomena from its absorption to its elimination. At a given dosage, the therapeutic efficacy of these molecules, their eventual side effects and toxicity all depend on their distribution in the organism, organs, cells and even sub-cellular compartments. This distribution depends only on the physico-chemical properties of these molecules, combined with the physiological and biological properties of the subject. Therefore and not surprisingly drug efficiency depends on the amount of drug reaching effectively the target cells, which results mainly from the capacity of the drug to pass through many physico-chemical and biochemical barriers raised between the administration site and the therapeutic target of the active ingredient. In order to better control this distribution, one of the current strategies is to associate the active ingredient to a carrier that will impose its own biodistribution properties until reaching the target, while masking temporarily the active molecule. Ideal carriers should possess a series of attributes required to cross each of these barriers efficiently. Furthermore, once the target is reached, these carriers must be able to release the active ingredient in the targeted organ or tissue. Ideally the carrier should then be easy to eliminate. As a result the drug targeting strategy should allow the increase of the local concentration of active ingredient at the target site and/or to decrease the drug toxicity and/or the secondary effects in other territories.

If this strategy holds high promises for therapeutic developments, for example in cancer treatments and in many other pathologies, it requires to be able to engineer vectors possessing simultaneously very different functionalities. Still this strategy is giving high hopes for the improvement of active ingredient efficiency by increasing their therapeutic index and is currently at the center of a significant research effort both at academic and industrial levels.

These research efforts are currently focused on creating efficient carriers, which can have various structures, ranging from macromolecules to particulate carriers. In the case of particulate carriers, some parameters are classically finely tuned including: (i) the size of the carrier, (ii) the surface charge of the carrier, (iii) the chemical groups or more complex molecules presented on the surface of the carrier. If the impact of each of these parameters is now better understood, one can wonder how to further increase the efficiency of these vectors.

Obviously a better control of their surface characteristics has to be achieved for gaining in selectivity during distribution. Indeed, following their delivery, the carriers have simultaneously to not develop interactions with biological molecules and cells, for escaping premature capture, but also to recognize specifically their target site. This is expected to depend on how certain molecules, including recognition ligands, are presented at the surface of the carrier. This is a key functionality for maximizing the desired recognition properties and for which many carriers deserve to be optimized.

However the distribution in the organs of particulate carriers and their interactions with biological fluids and cells should also depend on their morphology. Indeed there are many examples in the living world, ranging from biological macromolecules, to their supramolecular organization, from cells organites to micro-organisms which show that the geometry and the shape play a major role in life. Thus, we believe that understanding the influence of shape over the micro or nanoparticles traffic in the body would help achieve significant progress in the field of drug targeting.

A review of particulate carriers intended for drug targeting applications shows that the shape parameter has been really neglected so far. Indeed many carriers with varying internal structures have been imagined and fabricated, but most of them are spheres, including micro and nanoparticles. This is probably due to the fact that most preparation methods lead quite easily to spherical geometry, while preparing in a reproducible way non spherical carriers, with desired pharmaceutical characteristics, is much more difficult. Whatever the reasons for it, when looking at the different phenomena involved during the distribution of a targeted delivery system in the body, one can wonder if the sphere is the most efficient shape and what could be the influence of shape on these phenomena. For example after intravenous injection of a nanoparticles suspension, the particles will be rapidly diluted in the blood and distributed in the whole body via the vasculature. However what will be the influence of the shape on the ability of the particles to move in biological fluids (blood, interstitial liquids, cytosol…)? Afterwards the particles have to extravasate through the endothelium lining the veins and capillaries to get out of the blood flow, then to diffuse through the interstitial liquids to attain the desired cells. What will be the influence of the shape on the ability of the particles to be sieved through the endothelium or on the contrary will they be prone to adhere to endothelial surfaces? Finally the carrier must either release the drug in the vicinity of these cells (or

organ) or enter the cells and undergo intracellular traffic before delivering its drug cargo. What will be the influence of the shape on their biodistribution in organs and cells?

Intuitively the answer to these questions is that indeed shape should influence the fate of these carriers along their path from the blood to their target.

In this context, the aim of the thesis was to investigate the influence of the shape of non spherical polymeric nanoparticles on their interactions with cells and their overall distribution after intravenous (IV) delivery. For this purpose, different strategies were investigated for producing sufficiently large amounts of particles with non spherical geometries. These particles were characterized and finally the effect of shape has been studied *ex*- and *in vivo*.

This dissertation falls into seven chapters. The first chapter reviews many studies that have been published so far about the effect of the shape of particles on different biological and physical phenomena involved in their biodistribution; it comprises also an overview of the available fabrication techniques, while keeping in mind that these particles have to be used for pharmaceutical applications. The second chapter is dedicated to the experimental preparation of non spherical nano and microparticles through the film stretching technique, a method in which spherical particles are encased in a polymer film, liquefied, and finally deformed by stretching of the film. The third chapter describes how the auto-assembly of polymers can lead to the creation of non-spherical particles. In this case, poly(γ-benzyl-L-glutamate), a polypeptide forming α-helices, has been used for preventing the nanoparticles from being spherical, thus leading to the fabrication of ellipsoids. The aspect ratio of the particles (length over width) was related to the molecular weight of the polymer they are composed of. The fourth chapter aims to investigate the effect of morphology on the capacity of elongated particles to interact when they bear recognition ligands on their surface. For this purpose an experimental model of elongated nanoparticles, able to be easily functionalized after their production, an original strategy, is proposed and consists in making profit of the possibility to attach His-tagged proteins to nitriloacetic residues in the presence of Ni^{2+}. Indeed many potential ligands are commercially available with an His-tag. Using these tools chapter 5 reports an *in vitro* study describing the impact of shape on nanoparticles-cell interaction. The sixth chapter presents an *in vivo* study of the effect of nanoparticles shape on their biodistribution in rats demonstrating the impact of morphology on the fate of particles in the body. Finally the dissertation ends by a general discussion of the experimental results in

order to replace them in the pharmaceutical context and to put them in perspective for future investigations.

Chapter I

Shape and Drug Targeting

Chapter 1. Shape and drug targeting

Introduction:

Drug targeting is a strategy that consists in modifying the biodistribution properties of a drug by those of a carrier in which it is transported. Consequently, understanding the *in vivo* fate of the carriers is a critical step in their development. This strategy aims not only to reduce the amount of administered drugs, but also to improve the benefit/risk ratio for the patient by enhancing the delivery of the carrier in a specific organ, dedicated cells or subcellular compartments. Ideal carriers should increase specificity while toxic effects caused by non specific delivery should be weakened.

Various carriers have been proposed, which are not only able to encapsulate the therapeutic molecules, but are also meant to vehiculate the drug in the body from the site of delivery to the target organ, and finally to interact efficiently with the targeted cells. From this point of view, polymer nanoparticles are interesting objects because they present a unique combination of a nanometric size and the possibility to considerably modulate their physico-chemical properties. A survey of the literature shows that these carriers are mostly spherical particles and that until now only their sizes, surfaces charge and composition were studied[1], the effect of the particles morphology on their behavior in the body has been almost ignored. The reasons for it probably stems from the difficulty to prepare and to obtain micro and nano objects with non spherical shapes, prepared from materials of pharmaceutical interest; also from the lack of basic data on the role of morphology on the behavior of these objects in the body, when in contact with biological fluids and faced to various cellular environments, for example when particles-cells interactions occur.

This situation is quite surprising as, when looking at living bodies, the notion of shape appears so ubiquitous and having so much implications in the machinery of life. For example, at the micron range, it is well known that the morphology of microorganisms has a great influence over their life[2-4]: Many studies describe to which extent morphology dictates not only their motion but also their capacity to be phagocytosed by macrophages.

This review aims to present the available knowledge concerning the shape and the morphology of carriers of pharmaceutical interest and envision the incidence of this parameter in drug delivery, more specifically in drug targeting applications. A first section will comprise a discussion of the different phenomena occurring after carriers administration in the body on which shape can have an influence. The second section presents the different methods available to obtain non spherical particles and discuss their interest for producing carriers of pharmaceutical interest.

1.1. Shape vs. biological phenomena implicated in drug delivery

When a carrier is administered to a patient, whatever the pathway, it is subjected to many biological phenomena. Depending on the administration routes, various barriers should be crossed before reaching the target. These barriers can be tissular barriers, epithelia (e.g. the intestinal epithelium in the case of the oral route), endothelia in the case of IV delivery, biological barriers, e.g. the premature capture of carriers by the immune system, and many others. Efficient drug targeting is under the precise control of these factors. The knowledge of these phenomena is critical in many situations. The targeting of tumors gives an emblematic example of this problematic. Indeed, it is well known that in growing tumors, new blood vessels are created rapidly and present gaps through which only sufficiently small particles can permeate and reach cancerous cells. This occurrence is better known as the Enhance Permeability and Retention (EPR) effect[5]. We can only wonder how the effect of shape and the EPR effect will mesh.

In this context the first part of this review focuses on describing the phenomena that will rule the *in vivo* fate of non spherical micro and nanoparticles by envisioning some situations these carriers face following their delivery in the body and discusses the possible influence of their geometry. Several questions of importance can be raised: (i) What is the influence of the shape on the ability of a particle to move inside biological fluids (blood, interstitial liquids, cytosol…)? (ii) What is the influence of the shape on the ability to interact and to adhere to biological objects (vessels endothelia, cells…)? (iii) What is the influence of the shape on biodistribution? …

These phenomena are caused by surface or volume forces. It is noteworthy to mention some general considerations on the volume and on the specific surface of spherical micro- and nanoparticles to see how size will impact the forces applied on particles. Microparticles have a typical size comprised between 1 and 100µm, whereas nanoparticles of pharmaceutical interest have typical sizes between 5 and 500nm. The size factor is around 200. This variation has dramatic effects on volume forces (e.g. gravity), which will be $200^3=8*10^6$ times stronger on a microparticle than on a nanoparticle, whereas surface forces (e.g. electric repulsion) will be $200^2 = 4*10^4$ times stronger for microparticles compared to nanoparticles. Furthermore the

specific surface is three orders of magnitude higher for nanoparticles considering the same volume of nanoparticles as microparticles (Figure 1.1).

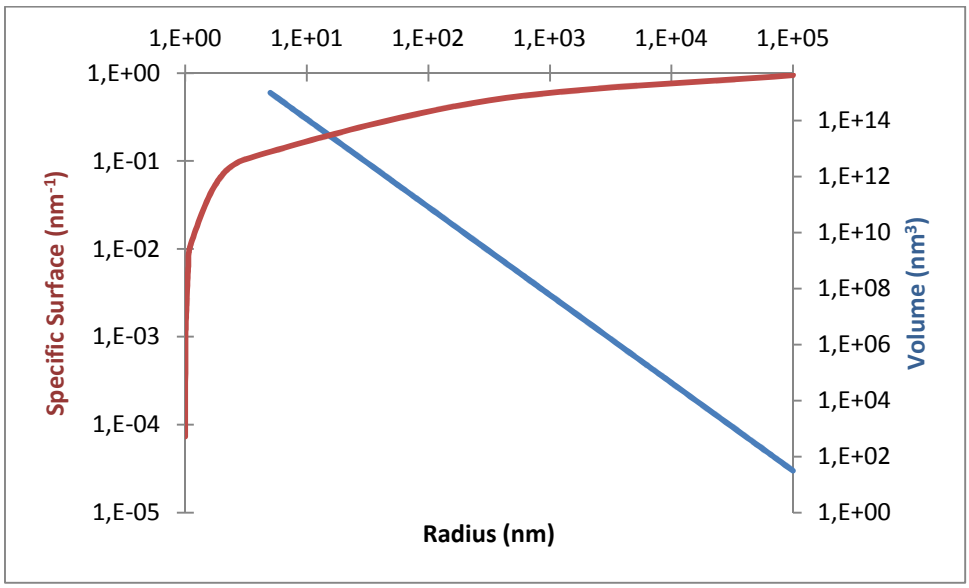

Figure 1.1: Evolution of the specific surface (blue) and of the volume (red) vs radius in the case of spherical particles

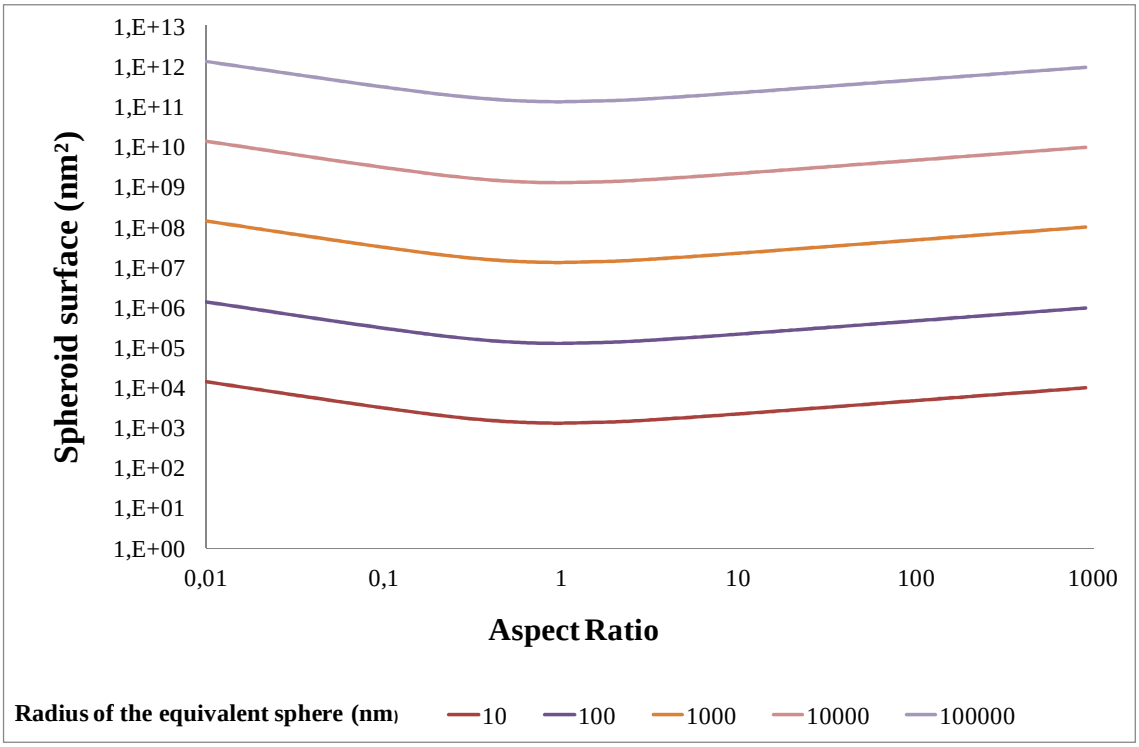

Figure 1.2: Total surface of particles of different shapes. Each curve represents a series of particles of different shapes but with the same volume.

Size effects are pretty well known (although their effects are sometimes underestimated in practice). However, the influence of shape on volume and surface forces was much less considered so far. Changing the shape of the particles and maintaining their volume constant will affect the surface of the particles and so most of the forces applied on it. As shown in Figure 1.2 (log-log scale) in the case of spheroids with varying elongation but with a constant volume, a divergence of the aspect ratio from the sphere geometry to ovoid shapes leads to an increase of the specific surface, which can rapidly reach ten folds or more. This can considerably affect surface forces.

1.1.1. Particle displacement in fluids

In most targeting applications, suspensions of drug loaded nanoparticles are injected in the blood stream, where they are rapidly diluted and distributed to the whole body thanks to the vascular system. For reaching target sites (e.g. a specific cell type) the particles need to cross the vessel walls and further migrate in the interstitial fluids before finally meeting their target. Further, these vectors should either unload their cargo in the vicinity of specific cells or even enter the cell, migrate within the cell and finally unload their cargo at a specific subcellular organite. Hence it is of importance to understand how particles motion in liquids occurs for a better understanding of their *in vivo* fate. First we will give an insight on the displacement of particles in motionless fluids (e.g. interstitial or intracellular fluids). Then we will review the knowledge on particle displacement in liquids in motion and especially in blood.

1.1.1.1. Motionless fluids

In motionless fluids particles are submitted to the Brownian movement. It has been described as the diffusion of the particle in a liquid and it has been thoroughly studied. For spherical particles, due to their symmetry, this movement is isotropic in the space. However for non spherical particles, this movement is more complex[6]. A non spherical particle will first "remember" its original position and diffuse more rapidly along its longer axis. After a certain time, depending on the particle geometry, the rotation of the particle will result in a diffusion becoming isotropic. This is a very interesting piece of information that may have consequences on how non spherical particles will move in motionless liquids, for example in extra or intracellular media.

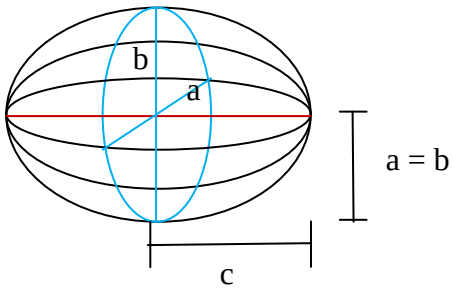

Figure 1.3: Spheroïdal particle

From these data it is possible to envision the movement of spheroïdal particles in motionless fluids. It can be imagined that spheroïdal particles will first translocate through the endothelium which would be favored by anisotropic movement and then explore the space they arrive in by isotropic diffusion. Each time the particles will encounter an obstacle (e.g. a cell membrane or extracellular matrix network) without adhering to it, they will keep a defined orientation as they move away from the obstacle. On the contrary, spherical particles will always explore space in an isotropic manner. So it can be assumed that spheroïdal particles are likely to explore biological fluids differently from spherical particles. When in the interstitial space, this exploration may be more efficient for elongated spheroids than for spherical particles in order to "meet" a cell.

However data on these displacements (such as size of the particles vs obstacles, typical distances, intracellular spaces…) were not easily available.

1.1.1.2. Fluids in motion

After injection and dilution of the nanoparticles in the bloodstream, the particles should be extravasated across the vascular endothelium wall to reach the interstitial space. So it is critical to understand which parameters can be affected by changes in the shape of the carrier. These movements have been examined quite in detail in the literature. Figure 1.4 depicts how the movement of the particles in an idealized blood flow can be decomposed, according to their position in the vessel at a given time.

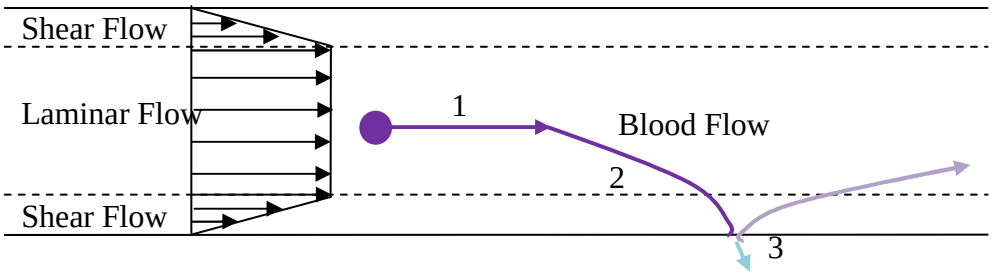

Figure 1.4: Schematic decomposition of the blood flow (1) Particles will follow the blood stream (2) Particles will marginate (3) Particles will either extravasate, stick to the wall, or rejoin the blood flow.

It is suggested that particles in the blood flow will be submitted either to a laminar or a shear flow. They will move in the blood stream and eventually migrate towards an endothelial wall by a phenomenon called “margination”. If the particle interacts efficiently with the endothelial wall it can attach to it and then either stay attached to it, or detach from the wall and either come back to the blood stream or extravasate.

i. Laminar flow

Blood flow is laminar except near the heart and in the close vicinity of the walls. Particles displacement in laminar fluids has been exhaustively described by Jeffery et al[7]. Spheres simply follow the main lines of current. On the contrary the movement of non spherical particles is much more complicated. To illustrate the complexity of movements that can be achieved by changing the shape of the particles, we will treat here the particular case of spheroïdal particles (a = b ≠ c, see figure 1.3).

To understand the movement of such spheroïdal particles in blood, they have to be divided into two families of particles, as shown on figure 1.5: (1) prolate spheroïdal particles which have a polar axis greater than the diameter of the equatorial circle whose plane bisects it (a = b < c), and (2) oblate spheroïdal particles which have a polar axis shorter than the diameter of the equatorial circle whose plane bisects it (a = b > c).

$\Gamma = \frac{c}{a}$ is the aspect ratio and will help us describe how elongated or flat the particle is.

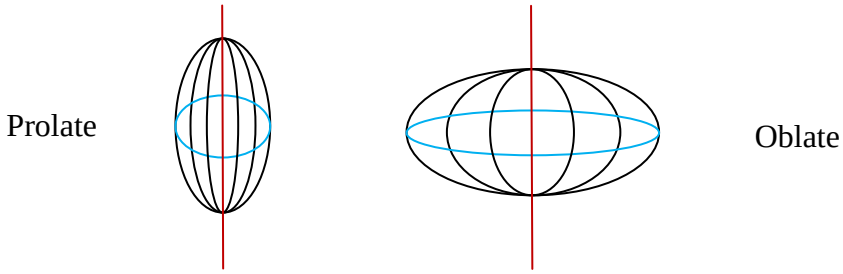

Figure 1.5: Two specific kinds of spheroïdal particles: prolate and oblate particles

Concerning their motion in laminar flow, it has been shown that prolate spheroïdal particles will tend to align their polar axis perpendicularly to the plane of undisturbed motion of the fluid. Meanwhile the particles will rotate around this axis at a constant speed (Figure 1.6). Oblate spheroïdal particles will align along an equatorial diameter perpendicularly to the

plane of undisturbed motion of the fluid. In this case, the particle will rotate around this axis at a periodic speed[7] (No information was given on the rotation speed value).

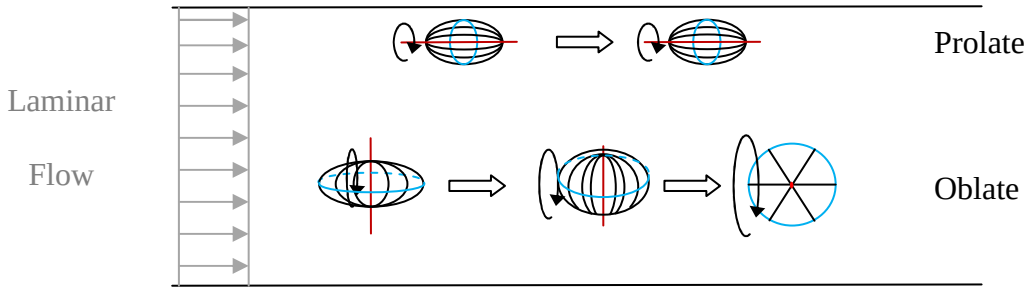

Figure 1.6: Spheroïdal particles movement in a laminar flow (most probable orientation)

In a capillary tube (cylindrical symmetry), particles tend to concentrate along the axis of the tube[7]. But the blood flow is not an ideal infinite laminar flow[8] and for pharmaceutical applications, vectors need to explore the vessel walls in order to extravasate out of the blood stream, via the EPR effect or other mechanisms. When particles are injected in the blood stream, they will be submitted to different forces. These forces will act either mainly on the volume of the particle or upon its surface depending on their nature, making necessary to describe these forces in order to foresee possible behavioral differences between spherical and non spherical particles.

There are four main forces that have to be taken into account when one wants to understand the motion of non spherical particles in the blood flow[9-10], volume forces, including hemodynamic forces and the steric repulsive interaction, and surface forces, including the Van der Waals interactions and the Electrostatic Double Layer interactions.

Hemodynamic forces: The blood flow (viscosity and shear rate) will have an influence on the particles depending on their diameter, density and position. This force is a volume force. The particle size will determine its ability to explore smaller vessels. Moreover, if the particle density is higher than blood density, then the particle will tend to diffuse towards the walls. Shear rate effects should also be considered and will be detailed later.

Van der Waals interactions: These interactions depend on the relative dielectric constant of the blood (ε_b), of the endothelial cells (ε_e) and of the particles (ε_p). If $\varepsilon_p > \varepsilon_b > \varepsilon_e$ then the particle will move towards the cell walls. This force depends on the shape of the particles.

Electrostatic Double Layer (EDL) interactions: This surface interaction characterizes the force due to the variations of the electric potentials close to the edge of the particle. This force can be repulsive if the electric potentials of the cells, which usually are negative, and of the particle (negative or positive) are of the same sign or can be attractive when they are of opposite signs.

Steric repulsive interactions: This volume interaction results from the fact that the particles occupy a certain volume. This is especially important when particles are covered by polymer chains floating in solution which occupy an additional space.

As seen previously (Figure 1.1), with size, specific surface and volume will change. Consequently all these forces will be modified. With shape, the surface of particles changes: all the surface forces will be impacted by a change of morphology. Even the steric repulsive interaction can be impacted, because a change in morphology will change the space occupied by the particle.

Therefore it can be expected that not only the particle size but also their shape will have a major influence on the displacement of particles in fluids.

ii. Margination dynamics

Margination is a phenomenon that usually describes the adhesion of white blood cells to the endothelial cells lining blood vessels and that occurs at the site of an injury during early phases of inflammation. This term will be used here to describe the migration of the particles towards the endothelial wall.

Decuzzi et al. have studied these effects[10] and have come up with certain characteristics that allow us to understand which parameters can be used to tune nanoparticles for different applications. (i) These authors have shown that there is an optimal size (around 100nm) for nanoparticles to stay in the blood flow before jumping to the endothelium wall. (ii) Margination dynamics is also dependant on the particle density. Surprisingly if the particle density is lower than water, the particle will not marginate; but if the particle has a higher density than water it will marginate in proportion of density. (iii) The dielectric constant of the particle will also have an influence on the margination dynamics, but only for particles of submicrometric size. (iv) Finally the surface of the particles also plays a role in margination

through surface potential and surface (bio)chemical functionalization (e.g.: PEG chains, functional groups…), which will have an influence on short distance interactions.

All these considerations suggests that shape will play an essential role in the margination dynamics, leading to the conclusion that two particles with the same volume but characterized by different shapes will have different surfaces and behave differently in space. Hence the Van der Waals interaction, the EDL interaction and the steric repulsion will be modified.

We therefore suggest that particles shape should be viewed as a tuning factor to help controlling the margination dynamics, whether margination is desired or not. For example the difference of displacement between spherical and ellipsoidal particles has been simulated in idealized capillary[11-12]. The ratio between the spherical particle and the tube diameter is 5; the ratio between the minor axis of the ellipsoidal particle and the tube diameter is 10 and the ellipsoidal particle has an aspect ratio $\Gamma = 2$.

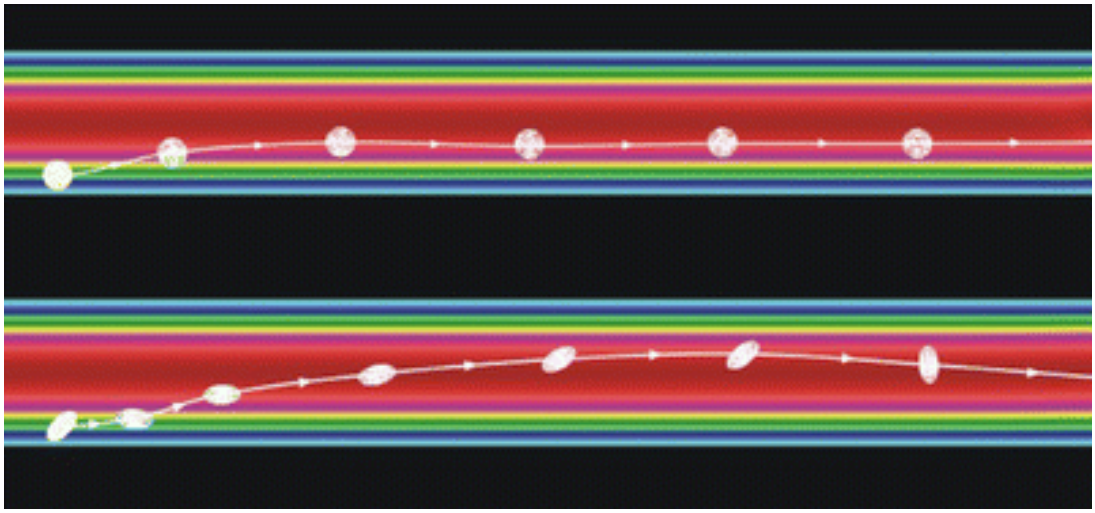

Figure 1.7: Trajectories of a neutrally buoyant spherical and ellipsoidal particle in a straight tube mimicking a capillary: the spherical particle will move to an equilibrium distance from the wall and move alongside a stream line while a disc tends to rotate and drift from one side of the capillary to the other. Hence one can easily see that non spherical particles will tend to explore more space in the capillary tube and thus have more chance to explore the walls[10]

In this situation modeling (Figure 1.7) suggests that spherical particles tend to stabilize at a definite distance from the wall and to follow a definite stream line, whereas a disc tends to rotate and drift from one side of the capillary to the other. Hence, one can easily see that non-

spherical particles will tend to explore more space in the capillary tube and thus have more chance to explore and interact with the endothelium[11-12].

In a practical study[13] R. Toy et al. have compared the behavior of two series of gold nanoparticles coated with PEG of different shapes: 60nm nanospheres and nanorods 56nm in length and 25nm in diameter (Γ=2.2) in PDMS microchannels (175µm in width x 100µm in height) intended to simulate the circulation and the physiologic flow rates expected in tumor microcirculation. They have found that the rods showed a deposition on the microchannels eight times higher than the sphere, which is a considerable difference.

Thus, considering only margination dynamics, if a slow release of the active molecule in the blood for extended period of time is looked for, one should use spherical particles. On the contrary organ targeting will necessitate extravasation of the particles from the blood flow, which could be tuned by the shape of the carrier.

1.1.2. Adhesion/Detachment of the particles

Particles displacement behavior in motionless fluids, laminar and shear flow are probably important determinants of the margination dynamics of particles. But margination dynamics are not the only component regulating the extravasation of the particles from the blood flow. Preliminary adhesion to endothelial cells will also play a crucial role for this mechanism. As a general rule, nanoparticles interaction with cells requires preliminary adhesion to the cell surface, which is the reason why we will now envision the impact of shape on adhesion in the particular case of particles in the vicinity of the endothelial cells or any cellular wall.

Once the particles come in contact with the endothelial wall, two opposite effects will challenge each other. Following a contact, the particle will try to adhere to the cellular wall either through non specific or specific (ligand-mediated) interactions. However, simultaneously, the particle will also be subjected to shearing forces e.g. due to blood flow or cell deformation motions, that will tend to detach the particle from the membrane.

1.1.2.1. Forces applied on a particle near a wall in a shear flow: Particle Detachment

The case of particles adherent to vascular endothelium is first considered. The forces applied to a particle near a wall subjected to a shear flow are described in figure 1.8. The conditions near the wall are as follow:

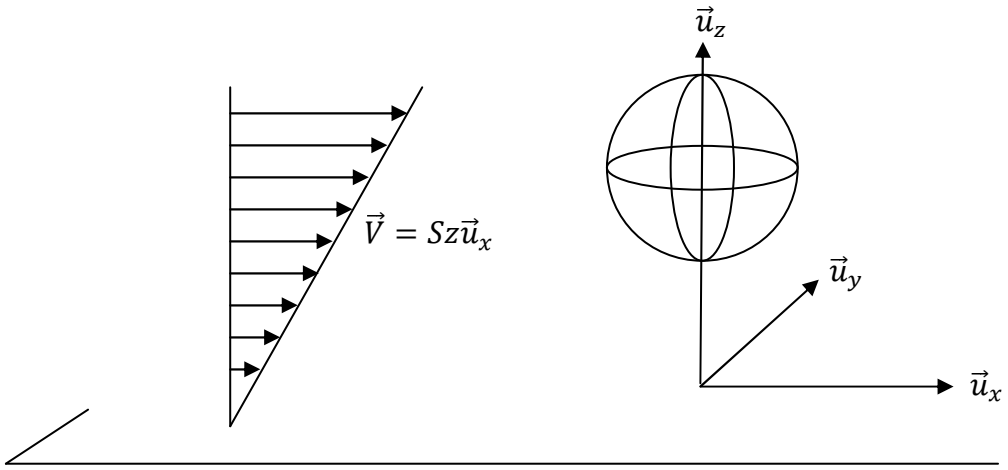

Figure 1.8 : Fluid and particle near a wall

where S is the shear rate of the laminar flow close to the walls of the blood vessel[14-16].

The force ($\vec{F}$) and the torque ($\vec{T}$) applied by the blood flow on the particle can be calculated.

$$\vec{F} = \iint dS.\vec{P} \text{ and } \vec{T} = \iint \vec{r} \wedge dS.\vec{P}$$

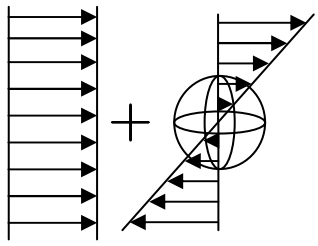

Figure 1.9: Decomposition of the pressure applied by a shear flow on a particle.

$\vec{P}$ is the pressure applied by the fluid on the particle. We can divide it in different components: in the referential of the particle. The pressure has three components: the pressure

due to the presence of a fluid surrounding the particle, this term is isotropic, the pressure due to the moving fluid which is responsible for $\vec{F}$ and $\vec{T}$ (Figure 1.9), and the pressure due to the shear stress on the particle which is responsible for the torque $\vec{T}$. The force and the torque depend only on the section of the particle presented to the fluid.

Figure 1.10 presents the sections in the cases of a sphere, an oblate spheroid and a prolate spheroid.

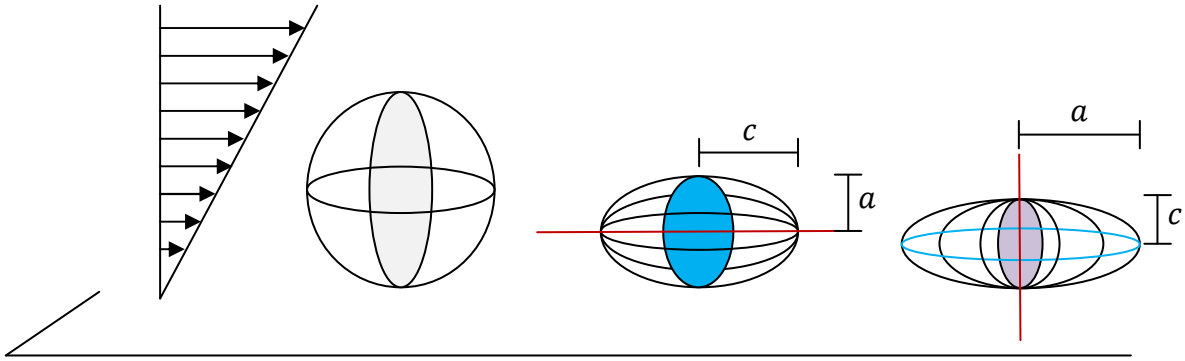

$S_{prolat} = \Pi R^2$ $S_{prolat} = \Pi a^2$ $S_{oblat} = \Pi ac$

Figure 1.10: Sections of the sphere, prolate and oblate particles

In the case of particles of same volume: $V = \frac{4}{3}\Pi * R^3 = \frac{4}{3}\Pi * a^2 * c$

$$R^3 = a^2 * c$$

$\frac{S_{prolat}}{S_{sphère}} = \frac{a^2}{R^2} = \frac{R}{c}$ with $R < c$ et $\frac{S_{oblat}}{S_{sphère}} = \frac{a*c}{R^2} = \frac{R}{b}$ with $R < a$

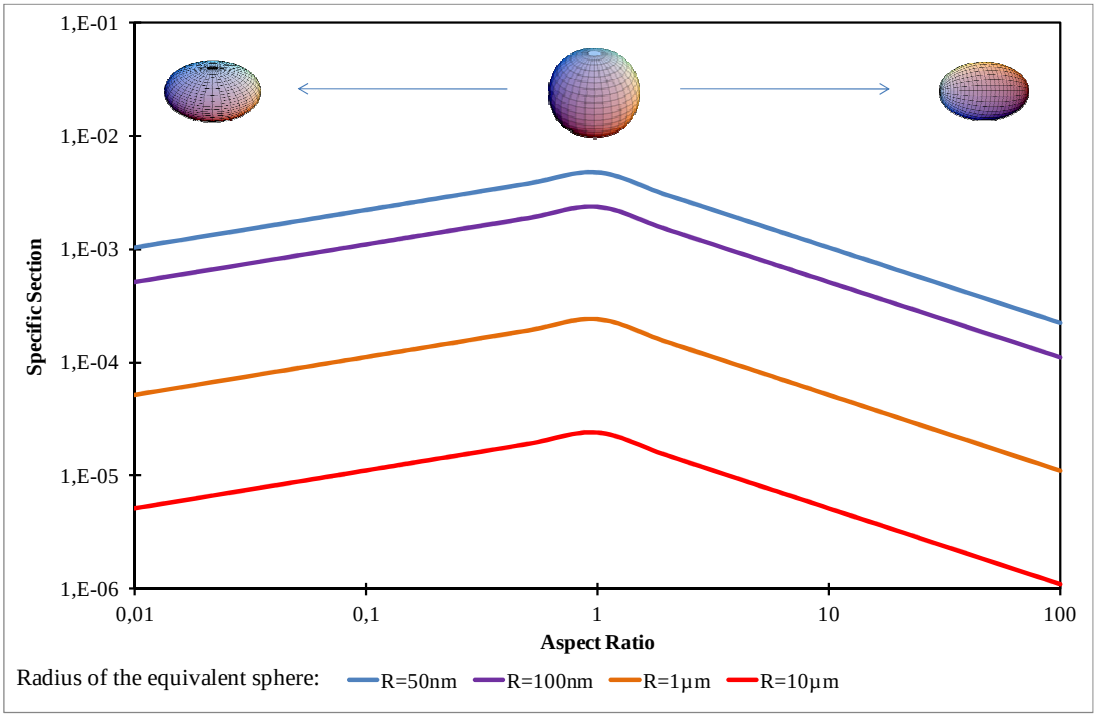

Figure 1.11 Specific surface implicated in the detachment of the particles

As shown on figure 1.11, the shape factor describing the elongation of the spheroid will have only a moderate influence on the detachment force because a variation of 10 folds of the aspect ratio results only in 5 fold modification of the specific section, provided that the particles are adherent along their greatest surface. In any case the force and the torque applied to the particle will be maximal in the case of the sphere[17-18]. Of course the situation would prove to be different in the case of an adhesion by the tip/side of the particles (smallest surface) and for establishing permanent adhesion, this force would have to be less than the binding forces of the particle on the wall.

1.1.2.2. Ligand-Receptor interaction: Particle Adhesion

In the case of particles intended to interact with cells by the mean of specific ligands, the modalities of adhesion are quite different since, as an approximation, when the particle reaches the wall and “locks on”, the force required to break all the ligand-receptor bonds will depend on the number of bonds which have been created.

In some cases, ligand-receptor interactions are well defined and can be assessed by a range of experimental techniques, including calorimetry, surface plasmon resonance and quartz balances; even bond forces can be determined by atomic force microscopy. However the interpretation of data can be difficult in some situations due to the complexity of these interactions, especially in the case of multivalent particles, bearing simultaneously several ligands per particle.

In fact, in this latter case, multiple phenomena have to be taken into account, including the total number of interactions created and a possible cooperation between bonds when a detachment force is applied to the adherent particle. In the case of multiple ligands binding on a single receptor site, it has been suggested that the strength of the bond was not linear with the number of interactions. In many systems, it has been shown that a few interactions could increase the magnitude of the dissociation constant (K_D) by several orders of magnitude. For example in the case of the NTA / Ni^{2+} / His-Tag interaction, from a mono to a bis interaction, there are two orders of magnitude in terms of K_D and the K_D of the system gains another order of magnitude when adding another ligand-receptor interaction.[19]

However, in the case of one ligand for each receptor (1:1 binding model), the problem is getting simpler. In this situation, the force of the bond is proportional to the dissociation constant (K_D) and the number of bonds. Different parameters have been evaluated in the literature[20-22], including the ligand and receptor concentration, pH, ionic strength, contact area, dissociation constant, but not the shape.. Decuzzi et al.[23] have studied this phenomenon in the case of a sphere. The effect of the shape on the strength of the bonding can be evaluated for a same ligand-receptor system

One can wonder how the force of the bond will be impacted by shape. We present in chapter 4.1 a model to compare the detachment forces as a function of particles shape. In this model, it was considered that the ligand and the receptor are springs and that they can interact until a critical distance H. Hence, the force is proportional to the surface of the particle between the surface plane and the particle plane (ligands are considered to be homogeneously distributed on the particle surface). When dealing with spheroids, two distinct cases can be considered, which correspond to different geometries of attachment to the wall. In the first case the particle will present its axis of symmetry perpendicularly to the wall, while in the second case this axis will be parallel to the wall. Both cases represent valid approaches for the

different types of particles. In the case of the sphere both cases are equivalent. Obviously, the number of bonds which can be created and thus the overall intensity of interactions will depend considerably on the geometry of the interaction.

1.1.3. Biodistribution and particle internalization in cells

The biodistribution[24-25] of particles in the body and their interactions with cells[26-27] have been thoroughly studied. These phenomena have been described to be influenced by the nature of the material constituting the particle (e.g. polymer, metal…), its size and more importantly its surface properties, understood at molecular scale. Although there are few experimental studies describing the effect of shape on the interaction of particles with cells, there are actually only very scarce experimental data at the nanometric level.

We will present here the different studies that have been performed concerning the influence of shape *in vivo* and *in vitro*. First we will detail the interactions of non spherical particles with cells and then we will present the existing biodistribution studies investigating the influence of shape.

1.1.3.1. Non spherical particles interactions with cells:

Champion et al.[28] have performed a study of the effect of shape on the phagocytosis of microparticles. Polystyrene particles of various shapes (aspect ratio from 1 to 6) were prepared through deformation of microparticles (diameters = 1-12.5µm) in a polymer film (see 1.2.1.3). Particles were incubated with NR8383 and J774 macrophage cells from 2h to 12h and their behavior was followed by time lapse video microscopy.

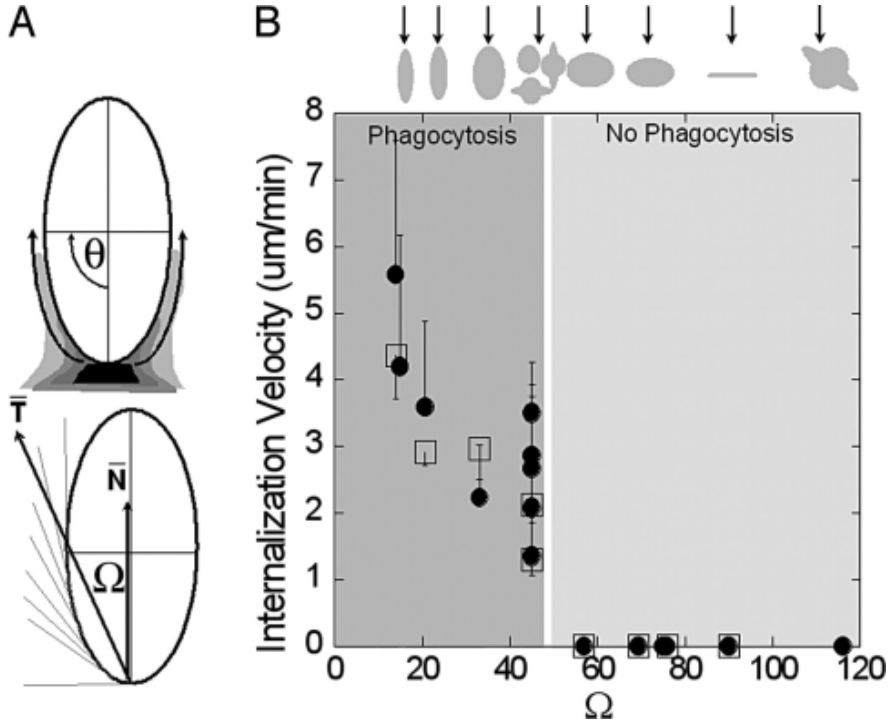

Figure 1.12: Internalization rates for particles of different shapes depending on the contact site between the particle and the cell[28]

As can be seen on figure 1.12, outside of size effects, it was shown that the polystyrene particle morphology had a severe impact on the rate of internalization and could even hinder the phagocytosis completely. In fact endocytosis necessitates a deformation of the cell membrane, which should form first a cup and then a ring around the point of attachment of the particle. For very flat surfaces, this deformation of the membrane requires too much energy, which prevents the phagocytosis from happening. However this study has been performed on microspheres ranging between 1µm and 20µm in diameter and one can wonder how it translates for nanoparticle and what would be the impact of morphology on internalization rate?

Gratton et al.[29] have performed a study on the effects of size, shape, and surface chemistry on cellular internalization. For this purpose they prepared particles by using the particle replication in non-wetting template method (see 1.2.1.2). These particles were prepared by polymerization of trimethyloylpropane ethoxylate triacrylate in presence of poly(ethylene glycol) monomethylether monomethacrylate and fluorescently labelled with fluorescein .Two types of particles were prepared (see figure 1.13), including cubes (A-F) and cylinders (G-K). Their sizes ranged from 150nm to 5µm while their length/width ratios varied from 1 to 3.

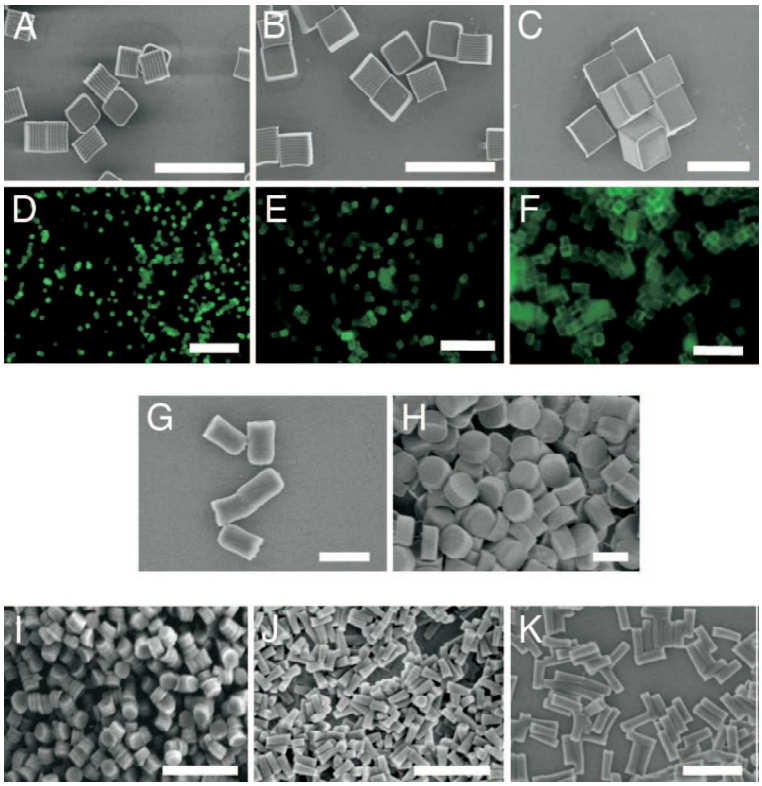

Figure 1.13: Micrographs of PRINT particles varying in both size and shape. (A–C) Scanning electron micrograph of the cubic particles (A) 2µm, (B) 3µm, and (C) 5µm in diameter. (D–F) Fluorescence micrographs of the cubic particles (D) 2µm, (E) 3µm, and (F) 5µm in diameter. (G–K) Scanning electron micrographs of the cylindrical particles (G) diameter = 0.5µm, height = 1µm; (H) diameter = 1µm, height = 1µm; (I) diameter = 200nm, height= 200 nm; (J) diameter = 100 nm, height = 300nm; and (K) diameter = 150 nm, height = 450 nm. (Scale bars: A–F, 20 µm; G–K, 1 µm.)[29]

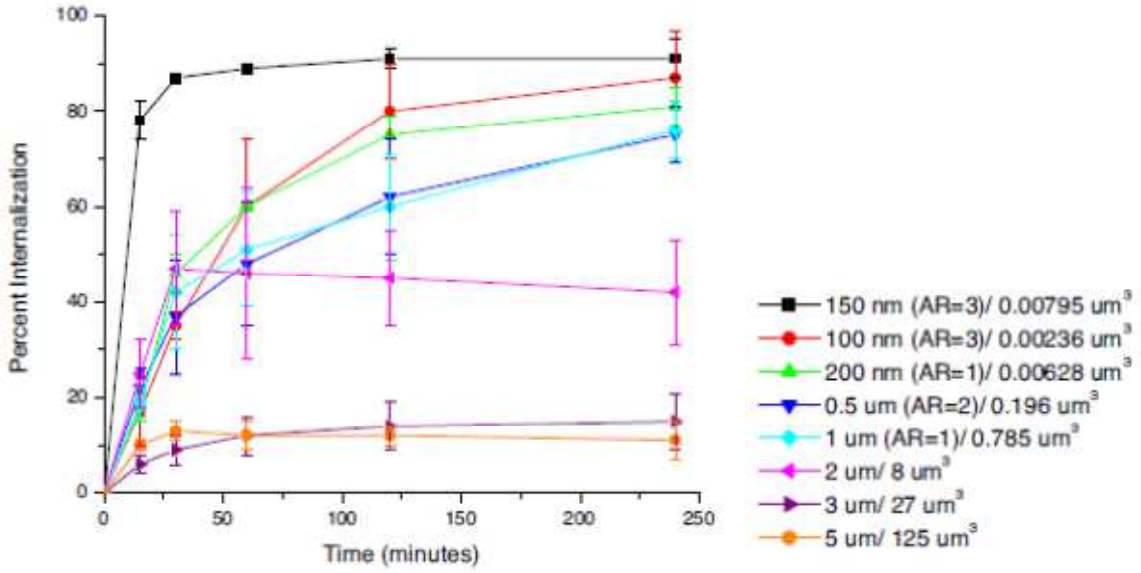

Figure 1.14: Internalization profile of PRINT particles with HeLa cells over a 4h incubation period at 37°C. Legend depicts the particle diameter (the aspect ratio) / and the particle volume.[29]

These particles were further incubated with HeLa cells over a 4h incubation period at 37°C. Figure 1.14 shows that 150nm nanoparticles (black squares) were 9 times more internalized than 5µm microparticles (orange circles). Furthermore the relevance of shape is also demonstrated with particles with different aspect ratios ranging from 1 (green triangles) to 3 (black squares) but with the same volume (0.007µm3) and which shows 4 folds difference in terms of rates of internalization.

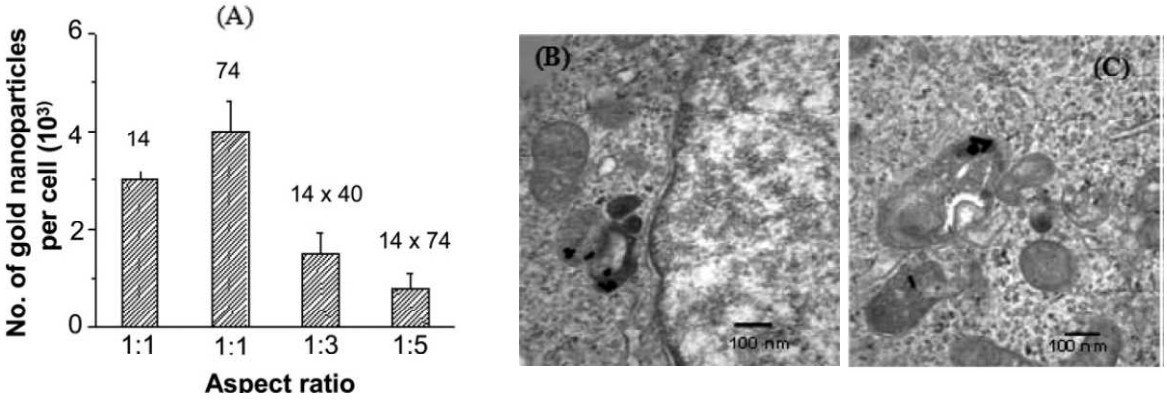

Figure 1.15: The effect of shape of the nanoparticles on cellular uptake and transmission electron microscopy images of rod-shaped gold nanoparticles internalized within the cells. (A) Comparison of uptake of rod-shaped nanoparticles (with aspect ratio 1:3 and 1:5) and spherical shaped nanoparticles, the transmission electron microscopy images of

rod-shaped gold nanoparticles with aspect ratio 1:3 (B) and 1:5 (C) internalized inside vesicles of Hela cells.[30]

In another study Chithrani et al.[30] have studied the influence of the shape of gold nanoparticles on their endocytosis. Figure 1.15 depicts the effect of shape on cellular uptake. TEM images of rod shaped gold nanoparticles (synthesized in presence of CTAB, a cationic surfactant, which may be somewhat toxic for cells) internalized within the cells show a clear effect of shape. Entry into Hela cells was 2-5 folds smaller for particles with an elongation ratio of 5 compared to spherical particles. Therefore, these authors concluded that shape had to be taken into account when designing particles.

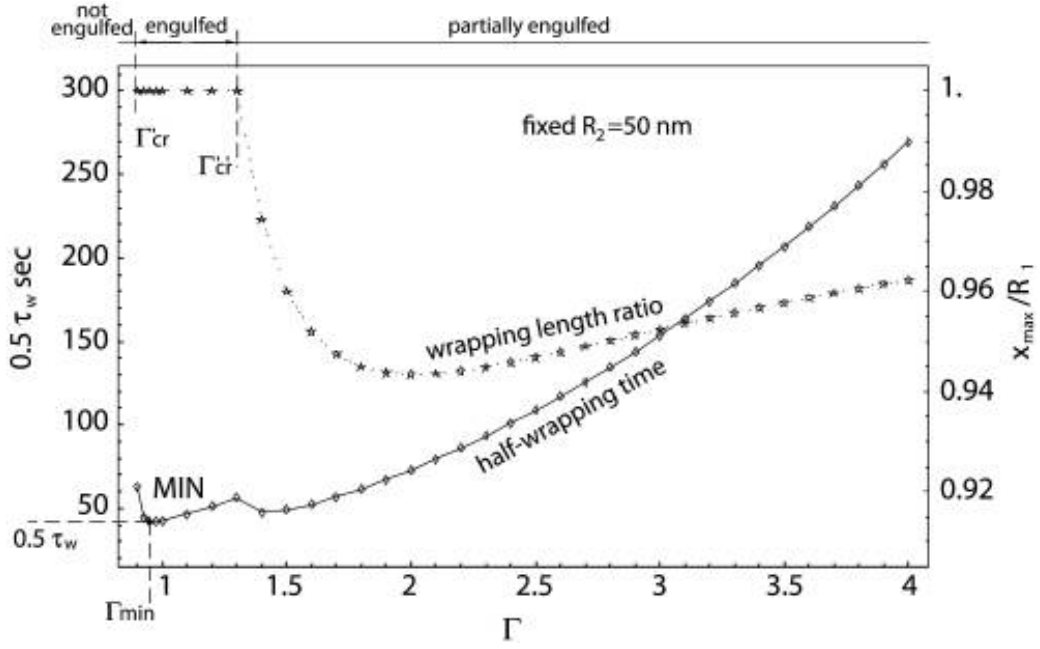

Figure 1.16: Simulated endocytosis of spheroidal particle[31]: Influence of the aspect ratio on the half wrapping time and the wrapping over length ratio.

Decuzzi and Ferrari[31] gave recently a theoretical insight on the influence of shape on endocytosis. They have developed a model for the endocytosis of spheroïdal particles (We refer the reader to article 31 for the details of the model). According to their work, there is a critical aspect ratio Γ_{cr} under which (e.g. for certain oblate spheroids) the particle will not be internalized. Furthermore, with the deformation of particles (aspect ratios smaller or larger than 1) the internalization rate will decrease. From an aspect ratio comprised between 1 and 4 the internalization rate was decreased 7 times.

All these experimental data only partially answer to the question of the influence of shape on endocytosis. Experimental studies diverge in terms of results, either elongated particles enter the cell faster[28-29] of slower[30]. This may be due to the nature and differences in the surface of the particles used in these studies. Either way shape matters dramatically for endocytosis. It is not the purpose of this review to discuss in detail the biophysics of cell membranes. However, it can be pointed out that an invagination of cell membrane in contact with particles is requested for endocytosis and necessitates a deformation of the membrane which may be costly for the cell in term of energy. Thus, not surprisingly, the degree of curvature of the surface requested would depend on the shape of the particles (interaction by the tip of a needle or through contact of the flat surface). In this scheme the rate of internalization not only depends on the shape but also on how is operated the contact point.

1.1.3.2. Biodistribution

Only very few biodistribution studies have been conducted so far on non spherical particles. Although much more experimental data would be necessary for gaining a better understanding, the review of these studies leads quite strongly to the conclusion that the shape of particles can result in considerable differences in organs distribution.

When reviewing available data, one should take into account any possible alterations of the shape of the particles following their delivery in the body. As an example of this situation, Y.Geng & al. have performed a a pioneering study on the distribution of filomicelles[32], which are flexible cylindrical objects measuring around 50nm in diameters and 2-20µm in length.

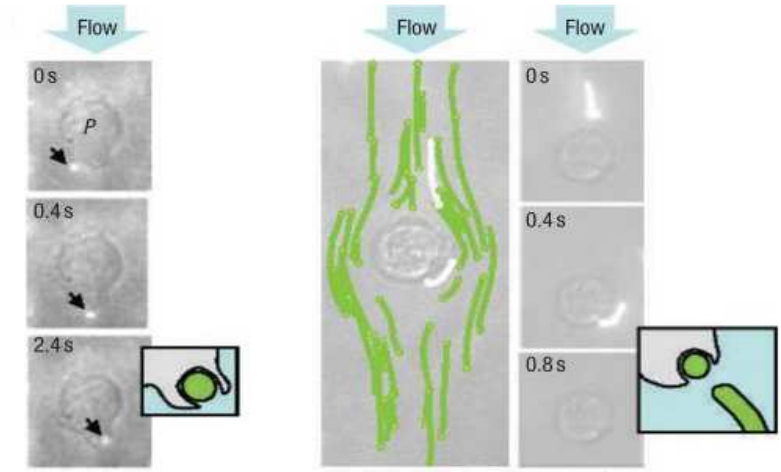

Figure 1.17 In vitro interactions between filomicelles and phagocytes (P).

These authors have shown that the IV injection of 0.5mL of filomicelles solution at 5mg.mL^{-1} in the vein tail of Sprague-Dawley rats resulted in a prolonged presence of the particles in the blood flow, which could last between 4 days for 2µm particles to 7 days for 18µm particles. However concerning shape effects, this study is quite questionable because of the instability of these silica particles in plasma and their rupture in multiple smaller micelles (see figure 1.17), until reaching a spherical geometry.

A much more conclusive study of morphology effects on biodistribution[33] has been conducted using silica microparticles. Different geometries of silica microparticles have been injected subcutaneously in an orthotropic tumor model using MDA-MB-231 breast cancer cells in female nude (nu/nu) mice. Mice were injected with silica particles suspensions(10^7-10^8 particles) in saline via tail vein (4 mice per group). After two to six hours, mice were sacrificed and the organs (liver, spleen, heart, lungs, kidneys and brain) were excised and weight. Silica biodistribution was obtained by elemental analysis of Si and histological evaluation.

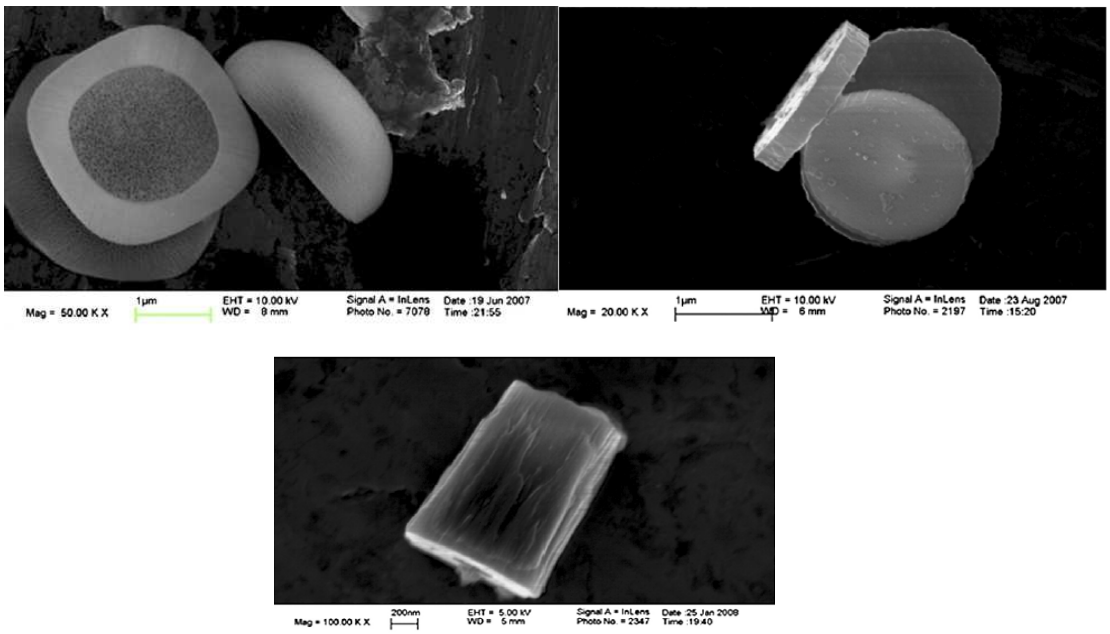

Figure 1.18: SEM images of the (A) quasi-hemispherical silica particles (B) discoïdal silica particles (C) cylindrical silica particles[33] Scale bars (A-B) 1µm (C) 200nm

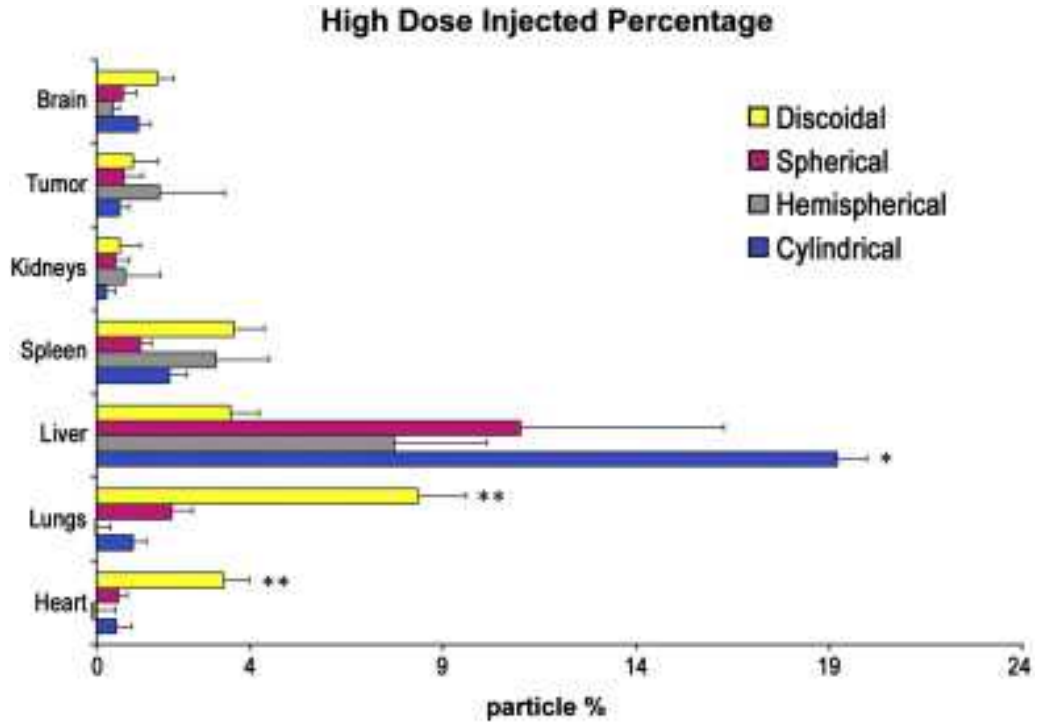

Figure 1.19: Biodistribution of the Si particles of different shapes shown in Figure 1.18[33]. Different geometries of silica microparticles were injected subcutaneously in an orthotropic tumor model using MDA-MB-231 breast cancer cells in female nude (nu/nu) mice. Mice were injected with silica particles suspensions(107-108 particles) in saline via tail vein (4 mice per group). After two to six hours, mice were sacrificed and the organs (liver, spleen, heart, lungs, kidneys and brain) were excised and weight. Silica biodistribution was obtained by elemental analysis of Si and histological evaluation.

As can be seen on Figure 1.19, spherical, hemispherical and cylindrical particles were captured to a large extent by the liver (respectively around 50%, 50% and 65% of the recovered particles, as the mass balance is often not experimentally determined in such studies), discoïdal particles tended to accumulate in the lungs (around 40% of the recovered particles). It was noticeable that the shape parameter did not only affect the percentage of total particles reaching the organs, but also their relative mass distribution in organs. For example hemispherical particles that might seem uninteresting apparently never reached the heart and the lungs. Such data are of practical interest in view of selecting potential targeting carrier for drug delivery to specific organs, while avoiding others because of potential toxicities. For

instance hemispherical particles would decrease the exposure of the heart or the lungs, which can be important for some drugs, while discoïdal particles could be used to enhance drug delivery to the lungs. Alternatively, it is obvious that distribution data are also of paramount importance in nanotoxicology for gaining in safety.

1.2. Producing non spherical micro- and nano- particles of pharmaceutical interest

Now that some of the potentialities of non spherical particles have been highlighted, we will present here different methods to produce non spherical micro and nanoparticles. While reviewing these methods we will be keeping in mind the pharmaceutical constraints, including mainly the selection of the different materials composing these particles, the control of their surface properties and the problem of the association/controlled release of an active ingredient.

1.2.1. Preparation of non spherical nanoparticles

There are numerous methods for producing micro and nanoparticles, which depend on the material to be used, metals, metal oxides, polymers and generally speaking, organic molecules. When polymers are used for their preparation, it appears that most techniques lead to spherical or at least round-shaped particles, either in the micro or nanometer range.

Basically the reasons for this is that for minimizing the energy of the system, nano and microobjects naturally tend to minimize their surface tension by reducing their surface thus adopting the geometry of a sphere (see 1.1). Furthermore, in general, the polymers used as building blocks to create nanoparticles adopt mainly random coil conformations due to their flexibility. Whatever the method of preparation, aggregates composed of a discrete number of polymers chains are formed, in which chains reorganization lead to spherical geometries, which presents the lowest surface energy for a given amount of material. The principle remains the same for other methods of preparation of spherical particles.

Therefore, to create non spherical particles one has to find a way to stop the isotropic association of the building blocks, which leads to form spheres. In the literature different approaches to solve this problem have been described so far. Two types of techniques leading to non spherical particles have been proposed so far. A first strategy consists to auto-assemble specifically conformed building-blocks able to aggregate anisotropically and to form non spherical particles. The second strategy consists in applying external constraints on the particle either during its formation or after.

From a practical point of view, these techniques can also be divided in one step approaches (auto assembly and preparation through constraint) and two steps approaches (preparation through deformation and preparation through fusion).

The first approach that will be presented is the auto assembly. The particles can be prepared by commonly used techniques in liquids, such as the nanoprecipitation technique or its variations. The material used to prepare them has specific properties which will impose the final aspect of the particles. The materials used in this approach can be polymers, peptides, or even spherical particles, which all are prone to form non spherical aggregates.

The second approach consists in imposing constraints to the material, which can be achieved in placing the material in a confined space, which does not allow the formation of spheres. The particles take the form of the space they are confined in. An alternative approach is to prepare spherical particles in a first stage, and then to deform these particles to obtain a definite form.

1.2.1.1. Auto assembly methods

The easiest method to prepare non spherical particles is the autoassembly method. Easiest because this method presents little difficulty, once a specific object: polymer, molecule, etc… used to form non spherical particles has been obtained. This method is based on the principle that if the building blocks that form the particle have a definite structure they can assemble in a structured way that can lead to specific geometrical forms. Here we will present different autoassembly methods that are based on different types of building blocks: peptides, polymers, amphiphilic molecules and crystals.

i. Peptide based structure

Using peptides is a route for creating non spherical particles, which is widely used in the living world. It is well known that peptides often exist as secondary structures such as α-helices and β-sheets. These structures are then folded and lead to tertiary structures, which are a specific three-dimensional conformation of the protein. The unique shape of the protein determines its function in vivo. Depending on their properties, these 3D conformations can further arrange themselves into supramolecular assemblies, leading to various nanostructures, which are one of the bases of life. As an example, tubulin is a major 100kDa protein leading to the formation of microtubules (25nm in diameter) after a polymerization process, which results in the formation of the cytoskeleton of cells and is mandatory for cell division.

Spheroid nanoparticles:

In some circumstances, non spherical micro and nanoparticles can be obtained from the use of proteins or polypeptidic materials. These molecules can be found in nature, for example amelogenin, a protein which is suspected to be a key factor in the biomineralization of dental enamel[34], has the ability to form prolate nanoparticles. Polypeptides, which consist in a controlled repeat of a L- or D- amino acid, may adopt α-helices or β-sheets conformations, which can be used to obtain definite three dimensional arrangements. An example is given by the potential of poly(γ-benzyl-L-glutamate) (PBLG) to lead to ovoid nanoparticles with an aspect ratio (Γ = length/width) varying from 1 (sphere) to 4 (ovoid) as shown in figure 1.20 (see chapter 3). These particles can be quite easily prepared through a nanoprecipitation technique consisting in diluting an organic solution of the protein in a water miscible solvent in a water solution. The potential of this strategy is developed in the present dissertation.

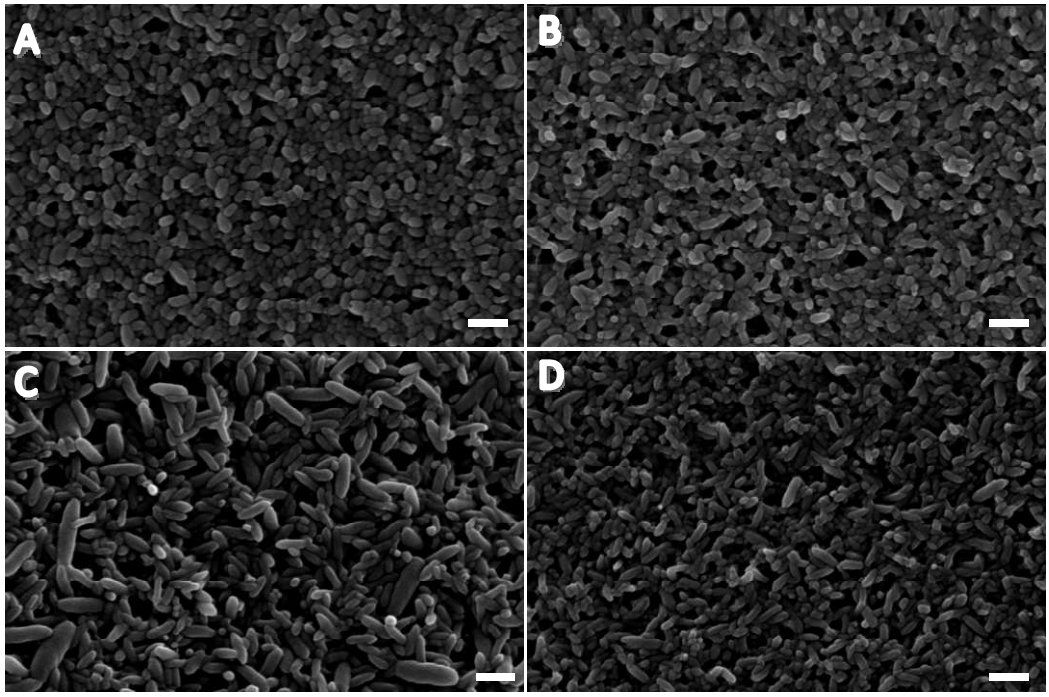

Figure 1.20 Scanning Electron Microscopy (SEM) microphotographs of nanoparticles prepared from PBLG with varying molecular weights. (A) 28kg.mol^{-1} (B) 45kg.mol^{-1} (C) 70kg.mol^{-1} (D) 85kg.mol^{-1} Scale bar = 200 nm.

For example, figure 1.20 shows PBLG nanoparticles with a varying aspect ratio depending on the molecular weight of the polypeptide 1.8 for the PBLG of 28kg.mol^{-1}, 2.0 for the polymer of 45kg.mol^{-1}, 2.8 for the PBLG of 70kg.mol^{-1}and 3.0 for the polymer of 85kg.mol^{-1}.

As will be shown in this dissertation, this is a simple and controllable way to produce spheroïdal nanoparticles. It only allows the production of one kind of shape but elongations can be varied to some extent.

Nanotubes :[35-48]

Peptide nanotubes are another family of structures which results from the intrinsic ability of peptides to self-assemble. Many different structures of nanotubes have been identified.

A first example shows that structures very similar to the one of carbon nanotubes can be obtained. Some dipeptides like Alzheimer's disease β-amyloid peptide diphenylalanine motifs[42,48] are able in solution to form single or multi walled nanotubes (80-300nm x 1µm). These nanotubes can be prepared by solubilization of the peptide in water. They are stable

under extreme conditions (stable at 150°C, but destroyed at temperatures higher than 200°C). They present a high stiffness (160N.m^{-1}) and their Young's modulus is comprised between 19 and 27GPa[41,47]. This structure has been used for oligonucleotide delivery as a proof of concept for gene and drug delivery[49]. Briefly a cationic dipeptide was nanoprecipitated in an aqueous solution. ss-DNA or oligonucleotides were then added to the nanoparticles and finally these complexes were tested on HeLa cells, as shown on figure 1.21.

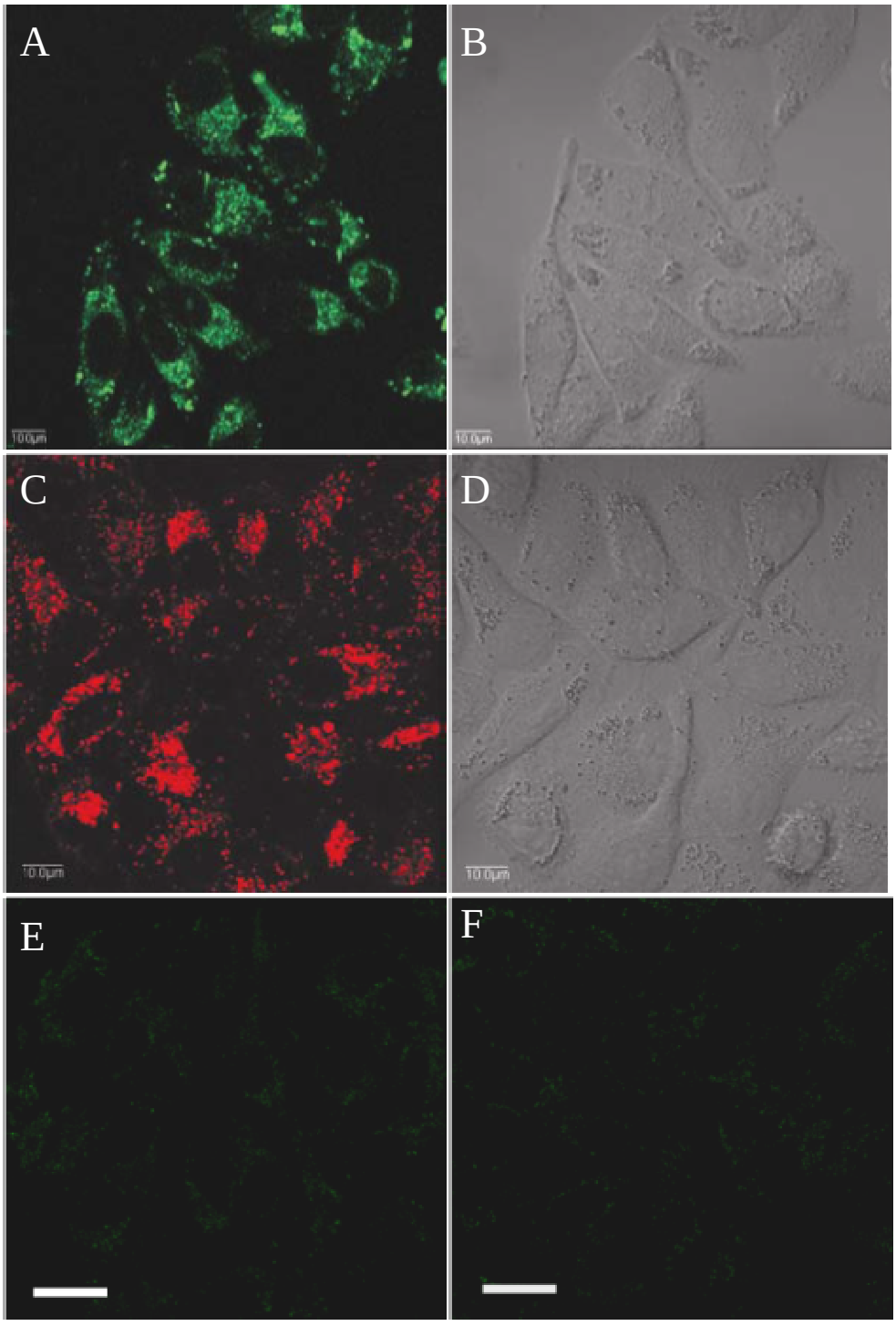

Figure 1.21 Confocal laser scanning microscopy images of (A-B) HeLa cells (B bright field image) after 24h incubation with the complexes of carbon dipeptides nanotubes and fluorescently labeled ss-DNA (green), (C-D) positive control cells (D bright field image) after 24h incubation with the carbon dipeptides nanotubes labeled by Congo red, (E) cells after 24h incubation with fluorescently labeled ss-DNA (green) alone and (F) cells

after after 24 h incubation with zwitterionic dipeptide(prepared via dissolving diphenylalanine in pH 4 ~ 5 HCl solution). (E-F) serve as the negative controls[49]

As second example, auto assembling of peptidic surfactant molecules of 2-3nm in length with a hydrophobic head (1 or 2 amino acid or AA amongst R,H,K,D,E) and a hydrophilic tail (more than 4 AA chosen amongst A,I,L,M,F,W,Y,V) has been shown to provide nanotubes. Many examples can be found in the literature[39-40,50] with different compositions, such as A_6D, V_6D, L_6D_2, V_6D_2, KL_6, V_6K, KV. Their association results in the production of 30-50nm nanotubes. The nanotubes walls are composed of a peptide surfactant bilayer and their ends are opened. These structures are very sensitive to dilution. At high concentration they form a network (figure 1.22) due to the creation of three-way junctions but at low concentrations this networks breaks into smaller vesicles.

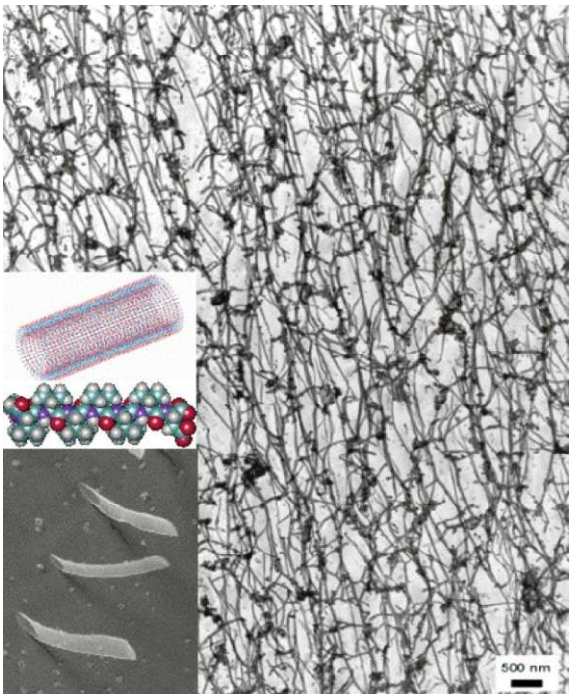

Figure 1.22 Example of self assembling peptide nanotubes obtained from the dissolution of V_6D peptide in water[40]

Interestingly, chemical modifications of the secondary structure of the polypeptides can lead to new quaternary structures which may form various kinds of nanotubes. For instance β-sheets can be modified to form β-sheets hybrids leading to β-barrels, β-helices or stacked ring[37] (see figure 1.23).

As a practical example Schlick et al.[51] have developed derivatives of the capsid peptide of the tobacco mosaic virus that can lead to the formation of peptide nanotubes through the stacking of disks. Figure 1.24 shows that under different conditions, this peptide can yield either 18nm disks or extended tube like structures with the same diameter.

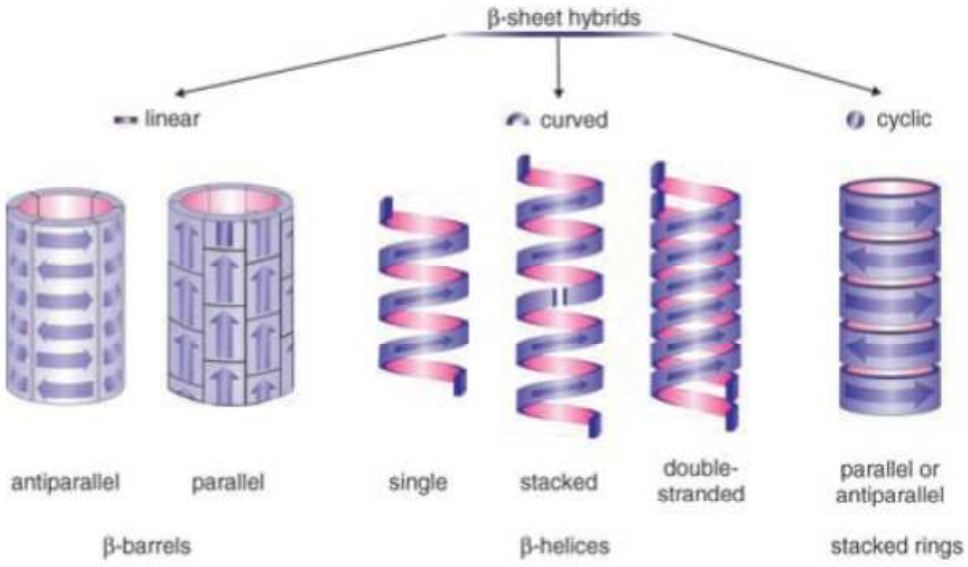

Figure 1.23: Tubular structures derived from the b-sheet hydrogen-bonding motif present in linear, curved, or cyclic form[37].

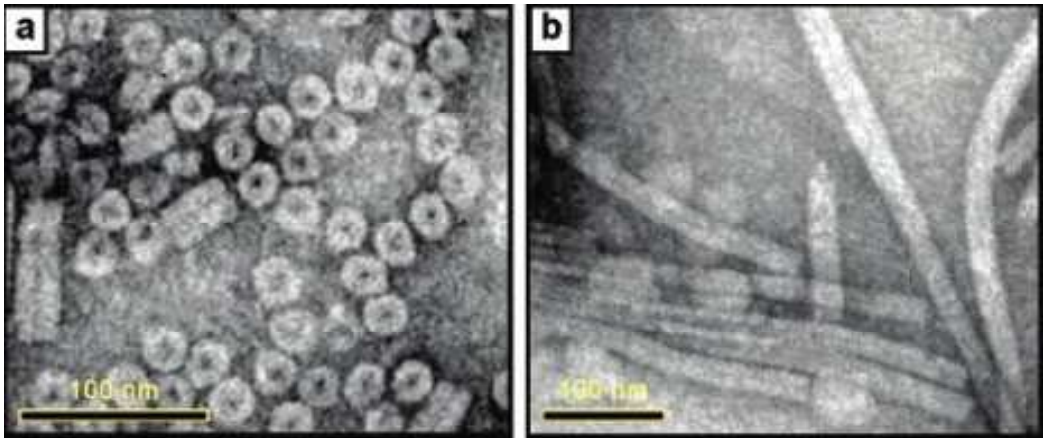

Figure 1.24 Reassembly of a modified tobacco mosaic virus conjugate. After capsid disassembly, refolding of the protein, and (a) dialysis into pH 7.0 phosphate buffer (47 mM), TEM analysis indicated the formation of 18 nm disk aggregates. (b) alternatively, dialysis against pH 5.5 acetate buffer (100 mM) yielded extended tube like structures that were microns in length[51].

A third structure that is worth mentioning is peptide nanoribbons. Y.Lim et al.[52] have created a molecule (Glu-KW) that can form β-sheets (due to the presence of a glutamic acid).

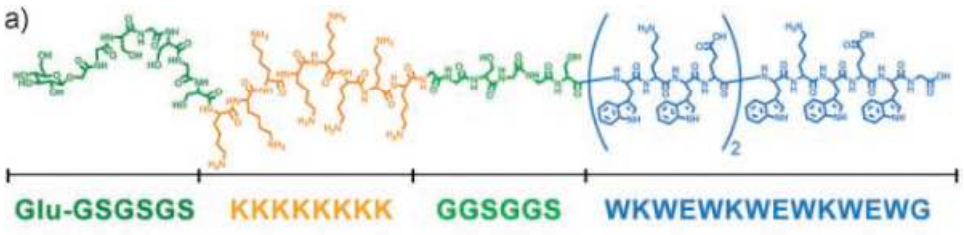

Figure 1.25 Structure of Glu-KW[52] a peptide that auto assembles into nanoribbons

These Glu-KW peptides auto assemble to form nanoribbons. Other molecules designed through the same concept by this group lead to the formation of nanoribbons with characteristic sizes of 5nm in width, 2nm in height and a length comprised between 20 and 200nm[53]. These objects have been used for testing their efficiency for siRNA transfection on HeLa cells and have shown an activity comparable to that of Lipofectamine 2000[52], a common transfection reagent.

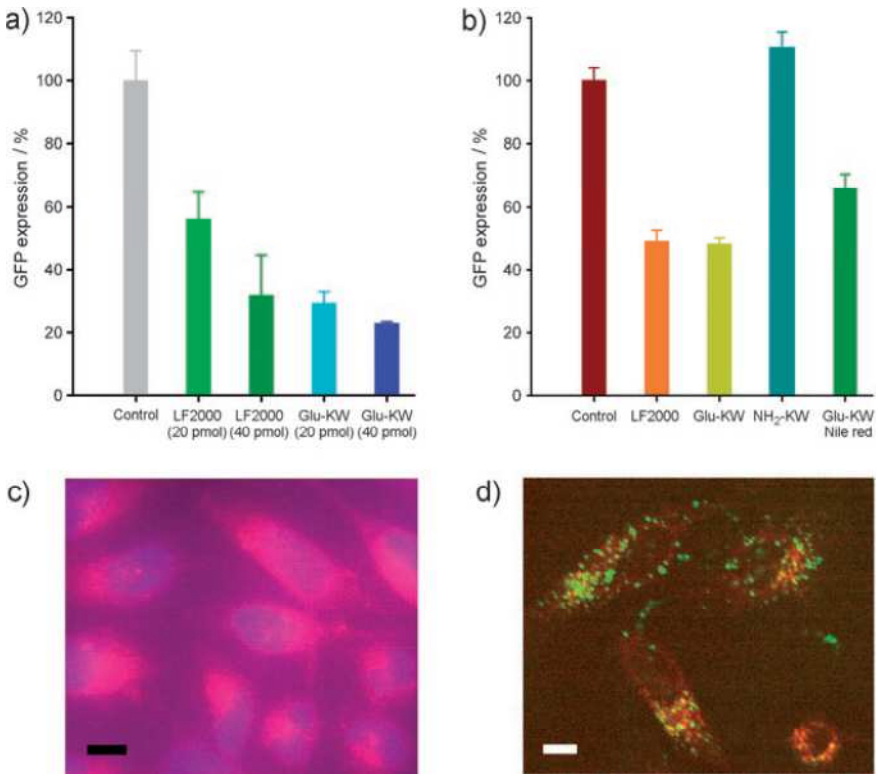

Figure 1.26 Intracellular deliveries of siRNA and hydrophobic guest molecules. (a-b) Knockdown of GFP expression in HeLa cells. (a)in the absence of serum (GFP siRNA concentration under the chart) (b) with 10% serum(40 pmol GFP siRNA) The nanorribons show a better efficiency than the traditional for intracellular delivery. (c-d) Intracellular distribution studies by confocal laser scanning microscopy Scale bar: 50 mm. (c) of nile red (red) delivered by the ternary complex of [Glu-KW, nile red, and GFP siRNA] The nucleus was stained with 4'-6-diamidino-2-phenylindole (blue).(d) The Glu-KW/FAM-KW (100:1) β ribbon and LysoTracker Red DND-99 are shown in green and red, respectively.[52]

Those examples, which are not comprehensive of all the possibilities of peptide nanotubes, intend to show the potential of peptides to create non spherical objects, likely to be used in biological applications. There is no doubt that the production of peptides themselves can be really costly. However, the methods for preparing these nano objects would be generally quite easy to scale-up in order to produce large amounts of drug carriers for various applications. This being said it is clear that this approach needs further development in certain areas. For example, there is still no control over length for the nanotubes; controlled

functionalization of interior and exterior surfaces has to be thought of to give these systems interesting targeting properties while maintaining shape integrity.

From a pharmaceutical point of view, the autoassembly of peptide and/or peptide derivatives is interesting because even if the building blocks are not always easily obtained, there is very little or no solvent and heating used, for the formation of the carriers, which are stable and could be easily mass produced. Depending on the method, size and shape can be very well controlled. Different active ingredients for gene therapy (oligonucteotides, siRNA) have been loaded in these structures and do not seem to impact shape.

ii. Amphiphilic Molecules: Worm Micelles and Niosomes and Nanoribbons

Auto assembly of amphiphilic molecules is another example of strategy leading to micelles, which in some conditions behave like non spherical nanoparticles. Worm micelles are a first example of such a possibility. As indicated by their name, these particles are a few micrometers long while only a few nanometers wide. They have been described as early as 1975 by Israelachvili et al[54]. They can be produced from carefully engineered block copolymers, for which one has finely tuned the respective weight fractions of the copolymer. The ratio of the polar head to lipophilic tail volume has to be comprised between $1/3 < v/a_0l_c < 1/2$ where v is the volume occupied by the hydrocarbon chain, a_0 the area of the head group and l_c the length of the hydrocarbon chain. Polymers such as diblock copolymer can form worm micelles. Poly(ethylene oxide) is the most commonly used hydrophilic block, because it has been thoroughly studied and is biocompatible. Whereas poly(epsilon caprolactone) and poly(lactic acid) are the most commonly used hydrophobic blocks due to their degradability.

Once the polymer is obtained, preparation of worm micelles is simple through cosolvent/evaporation[55]. In some cases: worm micelles can spontaneously form under hydration for 16h at 50-60°C[56].

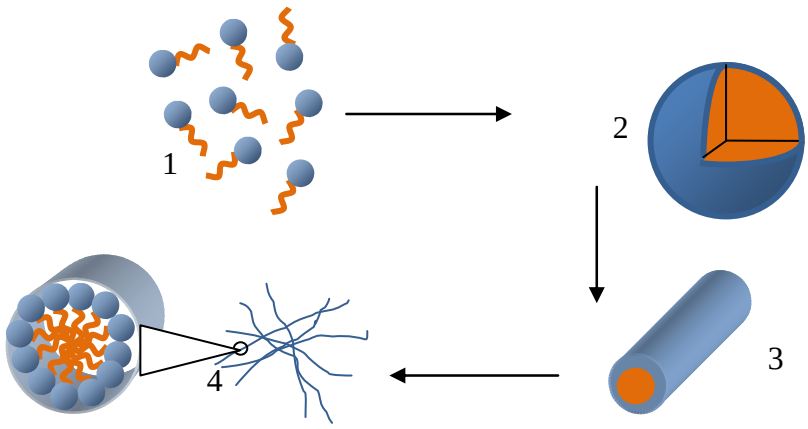

Figure 1.27: Formation of worm micelles as the concentration of amphiphilic molecules increases 1. Amphiphilic molecules 2. Micelles 3. Worm micelles 4. Worm micelles network

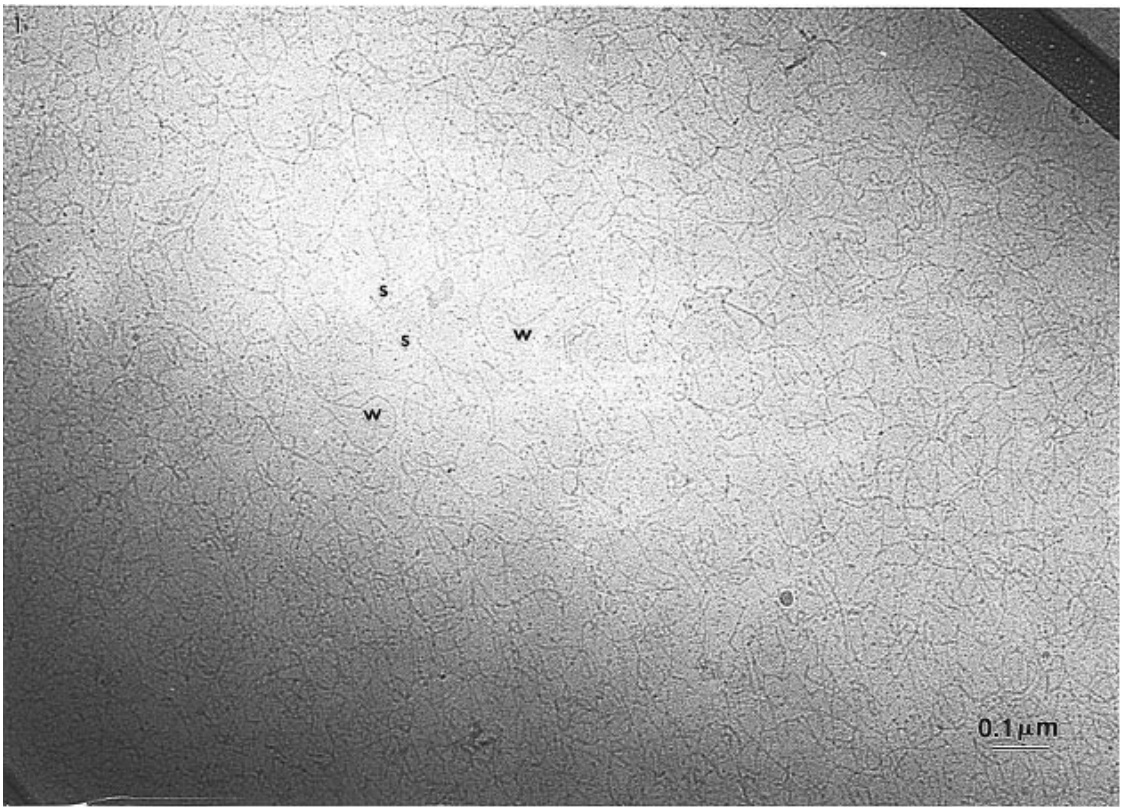

Figure 1.28: Cryo-TEM image of a typical worm micelles solution. Despite the inadequacy of the magnification, this picture shows that worm-like micelles (w) and spherical micelles (s) coexist in solution[57].

Worm micelles seem to possess all the requirements to be excellent drug carriers. Since they are a specific kind of micelles, they benefit from all the knowledge accumulated on micellar systems, and are consequently easily tunable for mandatory properties such as stealthness, targeting…

Worm micelles have already been tested for taxol[58] delivery, for which loading were in the range of 4 to 7%w/w and for triamterene[56] which have already been loaded in these systems. Promising results were obtained in terms of controlled-release, as these systems exhibited only a reasonable initial burst release (20%-40%) and kinetics as extended drug delivery lasted on a period of days, while permeation studies suggested effectiveness for delivery deep into tissues.

Unfortunately any parameter that changes the v/a_0l_c ratio will affect the stability of worm micelles. For example they are easily broken or splitted in smaller spherical micelles under mechanical stress, ionic, pH or temperature modification and even dilution.

In fact despite its interest due to its lack of stability and high flexibility, can it be considered as non spherical? It is definitely non spherical during transportation processes, but once worm micelles reach the cell vicinity they are likely to be strongly diluted and would have a tendency to break into smaller spherical micelles. Then for cell entry and cell trafficking, they probably behave mostly like spheres.

Furthermore, even though they are used for their interesting rheological behavior (especially fine tuning the viscosity) in various field of application such as petrol oil extraction, cooling fluids, home care products and personal care products[59], to our knowledge, there were no study so far on the effect of the shape of worm micelles on the delivery of drugs.

Niosomes[60-62] or non-ionic surfactant-based liposome, are another kind of micelles. They distinguish themselves from regular liposomes because of the cholesterol added in their composition. These microparticles can be either spherical or non spherical depending on their formulation. For example Uchegbu et al[63] have prepared niosomes from hexadecyl glycerol ether ($C_{16}G_2$) non-ionic surfactant, cholesterol and cholesteryl poly-24-oxyethylene ether (Solutan C24), and they have shown that by tuning the concentration of each molecule the niosome obtained had different morphology (see figure 1.29).

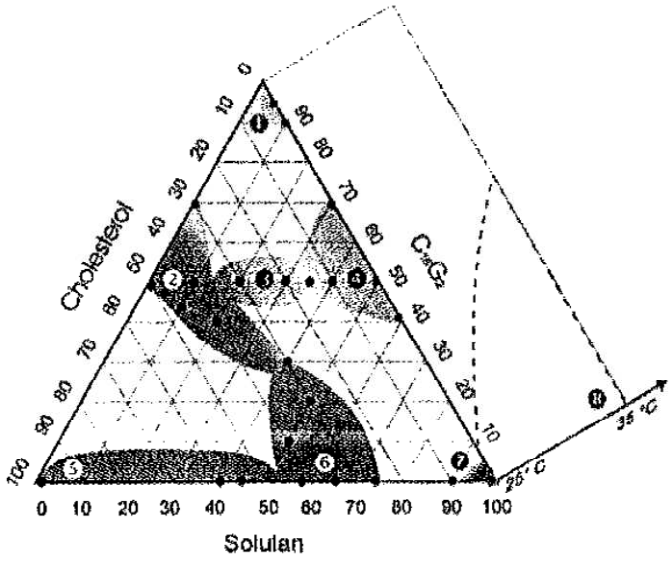

Figure 1.29: Regions of the $C_{16}G_2$/cholesterol/solutan C24 ternary phase diagram: 1: polygonal vesicles; 2: spherical, helical and tubular vesicles; 3: discosomes large vesicles, small spherical vesicles and helical vesicles; 4: discosomes and possibly Solutan C24 micelles; 5: cholesterol crystals; 6: spherical vesicles; 7: probably SolutanC24 micelles; and 8: mixed micelles formed on elevation of the temperature[63]

There exist other examples of amphiphilic surfactant molecules forming non spherical objects. For example derivatives of bis-ureido surfactant molecules (figure 1.30) can interact strongly due to strong hydrogen bonding interactions and allow the formation of nanoribbons[64].

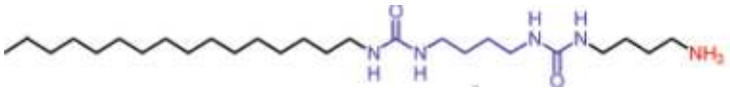

Figure 1.30: Example of a bis-ureido surfactant molecule

These molecules form highly ordered ribbon-like bilayers upon heating of as little as a 0.5wt% aqueous dispersion to 70°C and after cooling to room temperature. They can be easily functionalized, e.g. with a biotin or an azobenzene group[64].

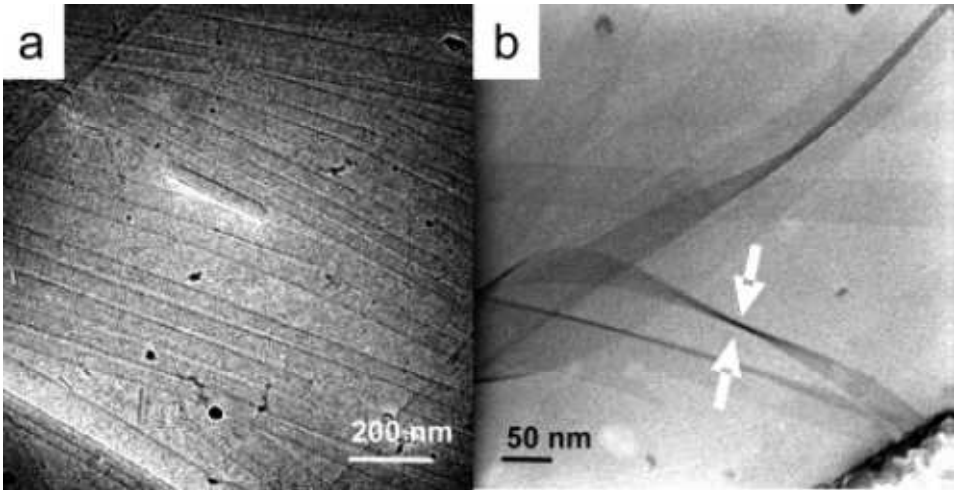

Figure 1.31: Cryo-TEM image of an aqueous dispersion of 1 (0.5 wt %) showing (a) ribbons with a homogeneous width distribution and (b) a twist point (arrows) from which the thickness of the ribbon can be determined[64].

All those examples show the versatility of amphiphilic molecules and their propensity to be used as building blocks in the engineering of non spherical micro or nano-objects.. A wide range of shapes, sizes, composition, surfaces may be quite accessible and they may be of interest for the preparation of interesting drug carriers. However, the potential toxicity of these molecules should not be forgotten. Further, the stability of the auto-assembled objects in biological fluids, all along the travel of the particles from their site of administration to their target may be a real concern, because the stability of these assemblies is often dependant on the surfactant concentration, and the temperature, the shearing in the body, interactions with cells surfaces, leading to a possible early breakage of the particles. Thus their potential should deserve many further investigations, especially under physiological conditions, to assess their potential as drug carriers.

iii. Dendritic molecules

Dendrimers are highly branched synthetic molecules. When exhibiting low water solubility, some dendrimers can self-assemble. Their 3D arrangement is usually spherical and can under certain conditions form spherical micelles. However, it is possible to create asymmetrical dendrimers[65-66], these dendrimers have a degree of branching well below that observed for spherical architecture[67] (figure 1.32).

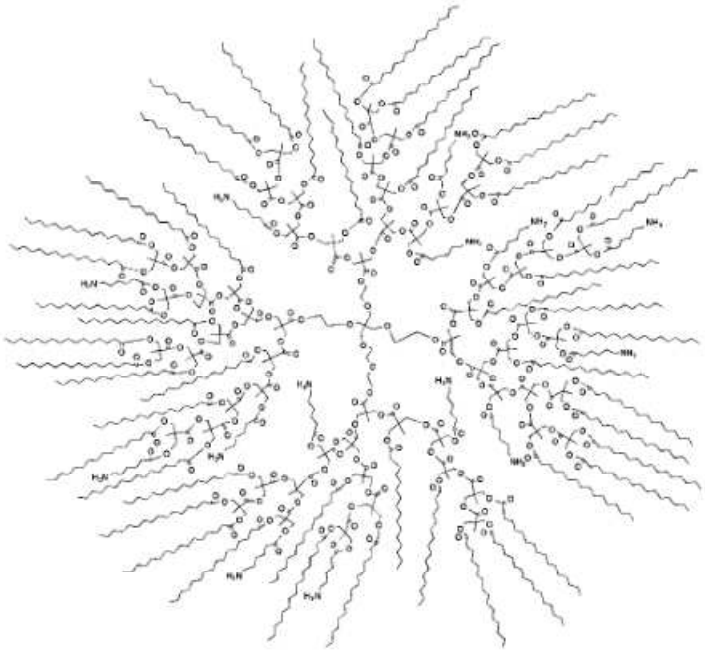

Figure 1.32 Structural formula of the amphiphilic hyperbranched polyester with a degree of branching of 40%, modified with terminal alkyl and amino groups[66]

This type of dendrimer can self-assemble and form asymmetrical nanoobjects such as rods, fibers, ribbons and helices. These structures are only a few nanometers in width and can reach up to a few centimeters in length, as exemplified in figures 1.33 and 1.34.

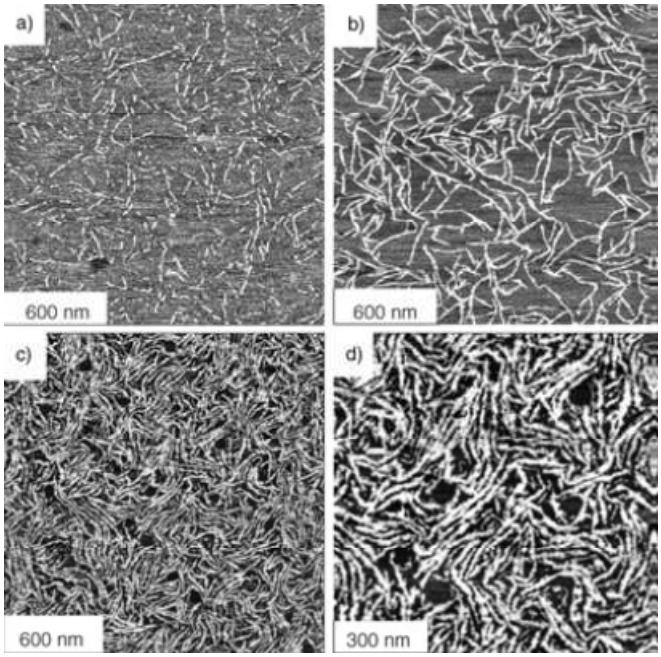

Figure 1.33 AFM phase images of nanofibrillar structures formed on a water air interface at different pressures from average dendritic molecules (~50 hydrophobic C_{16} alkyl tails, at different surface pressures, 14amino-terminated groups, and 1-2hydroxy-terminated groups, see Figure 1.32). (a) 0.2mN.m^{-1} yielded 2nm*500nm particles; (b) 5 mN.m^{-1} yielded 2nm*1µm particles (c, d) 30mN.m^{-1}, different scales yielded 3-4nm*several µm particles. [66]

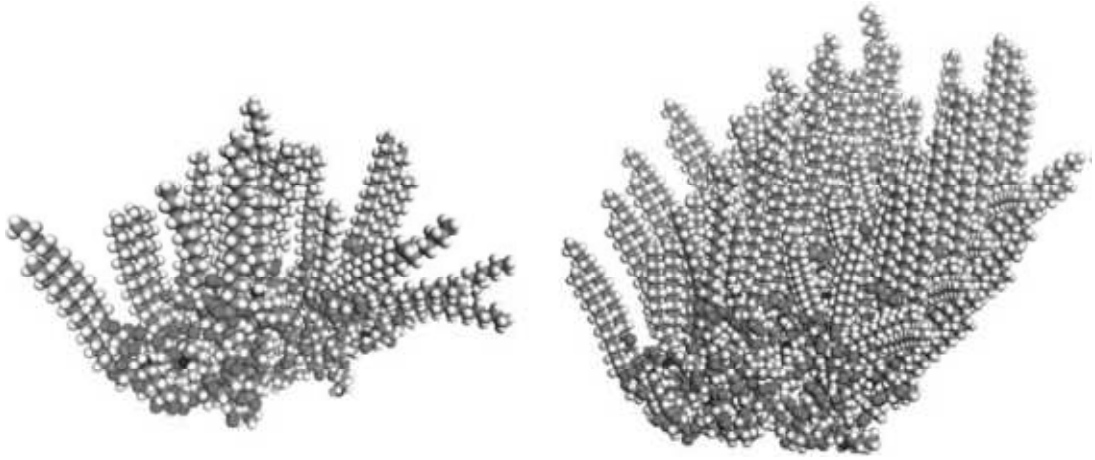

Figure 1.34: Molecular graphics representation of the suggested conformation of a single amphiphilic hyperbranched molecule on a solid hydrophilic surface (left) and their aggregation in the one-dimensional supramolecular structure (right)[66].

As for peptide based structures, the difficulty that arises during the preparation of dendritic nanoobjects from amphiphilic hyperbranched molecules comes from the synthesis of chemically well defined molecules, with purity considerations and the need for monodisperse molecular weights. But once the molecule/polymer is obtained the preparation of nanoparticles is fairly easy because nanoprecipitation techniques described earlier can be easily employed.

Dendritic particles have already been tested as carriers for different drugs, including cisplatin, doxorubicin, adriamycin and methotrexate[68-70], with varying successes. Drug loading could be high and increased with every generation of the dendritic molecule, as well as with chain length, but release profiles were less satisfactory, as they were characterized by slow kinetics in aqueous solutions but fast release in isotonic media.

iv. Crystal based structure

Crystals are found in nature under non spherical shapes. These shapes derive from the inner arrangement of atoms (dependant on the nature of the atoms); these arrangements have been described by Kepler as soon as 1611. But we have only been able to use this property to form nanocrystals for the last fifty years. Most common particles created by assembling atoms are metal particles (gold, silver, platinium…), carbon nanotubes, graphen and nanodiamonds.

In this area, bottom up and top down approaches are the two major techniques presently described in the literature[71] for building non spherical objects. Bottom up techniques consist in assembling atoms in order to generate nanostructures. These techniques regroup various procedures, including nanosphere litography, templating, chemical, electrochemical, sonochemical, thermal and photochemical reduction techniques, seeding technique, two-phase reactions, and inverse micelles. Top down methods consist in breaking bulk materials to obtain the desired nanostructure. This group of techniques comprises photolithography and electron beam lithography procedures.

Nanospheres litography[72] is a simple and inexpensive method to produce metal nanoparticles. In details, polystyrene spheres (hundreds of µm) are densely packed to form a monolayer template. Thermal evaporation is then used to deposit metal atoms in gazeous

phase on and in between the particles. After dissolution in organic solvent of the polystyrene particles the triangular shaped metal particles are recovered (see figure 1.37).

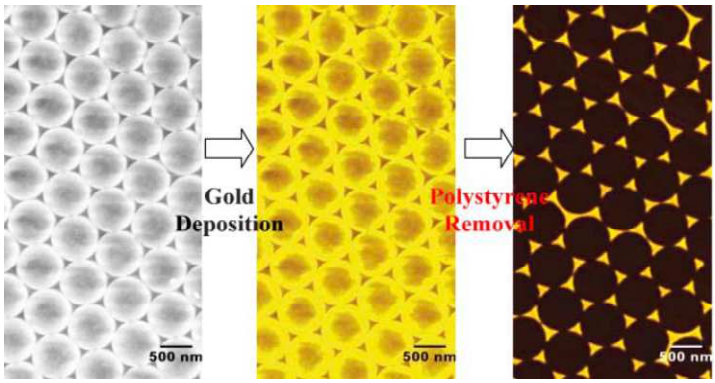

Figure 1.35: Nanosphere lithography[72]: A) deposition of a monolayer of PS particles on a substrate, B)Gold deposition and C)polystyrene removal via solubilization to produce triangular gold nanoparticles.

Templating[73], chemical, electrochemical, sonochemical and thermal and photochemical reduction techniques can generate particles of various morphologies, including spheres, rods, disks, cubes, wires, tubes... The control of the shape is achieved by the choice of reagents: metallic atoms are obtained by the action of a reducing agent on metal oxides in the presence of a capping material to prevent material re-oxydation[74] (cetyl trimethyl ammonium bromide (CTAB). Citrate, cysteine, glucose, biotin…). These capping materials can orient the crystal growth.

The seeding technique[75] consists in using spherical nanoparticles called seeds (~4nm diameter), which are created in a first step by reducing an oxidized gold compound (e.g. $HAuCl_3$) in solution (e.g. by $NaBH_4$). Then, in a second step these particles are added to a solution containing both metal ions and surfactant to induce an anisotropic growth.

In some cases two phase reactions[75] are used, in which metal salts are transferred in a organic phase by addition of a specific surfactant. Then, on addition of sodium borohydrate to the solution, very small metal nanoparticles (1-5 nm) are formed. Temperature and metal to surfactant ratio are the critical parameters to obtain monodisperse suspensions. Widely used gold nanoparticles suspensions are often prepared by such techniques.

Metal particles can also be prepared by using inverse micelles as nano reactors. In this case, the size of the formed metal particle will be regulated by the size of the inverse micelle.

Photolithography and electron beam lithography are carving techniques using a laser beam. However, they are limited by the size of the laser and can only create two-dimensional structures in a single step.

These metal nanocrystals can also be grown by two other mechanisms: cluster growth in vacuum and specific growth in solution. The difficulty arising during the formation of such nanocrystals consists in retaining the crystalline shape as the particle grows to a nanoscopic scale while keeping the narrowest size distribution.

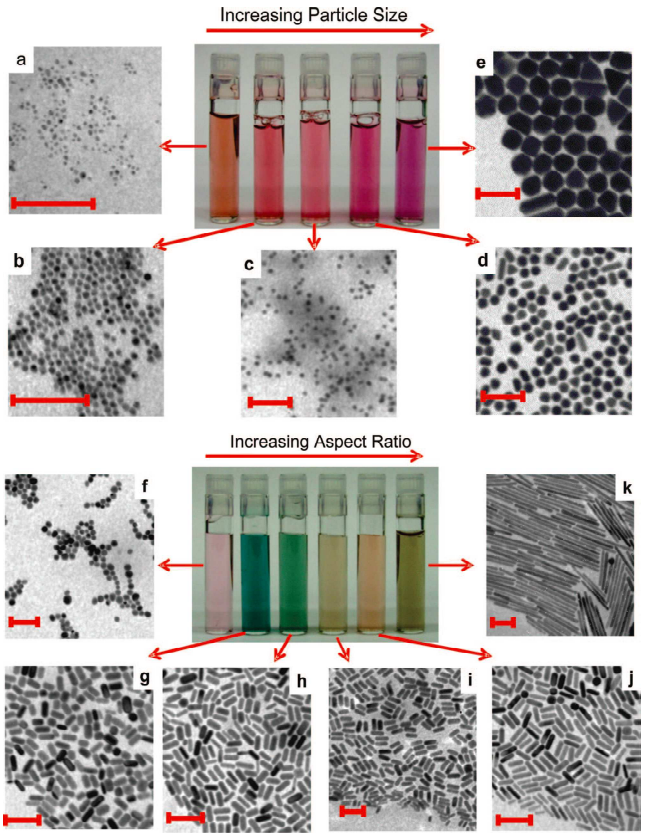

Figure 1.36: Photographs of aqueous solutions of gold nanospheres (upper panels) and gold nanorods (lower panels) as a function of increasing dimensions. Corresponding transmission electron microscopy images of the nanoparticles are shown (all scale bars 100 nm). For spheres, the size varies from 4 to 40 nm (TEMs a-e), whereas for rods, the aspect ratio varies from 1.3 to 5 for short rods (TEMs f-j) and 20 (TEM k) for long rods.[76]

Cluster growth in vacuum is performed by the chemical vapor deposition (CVD) method. A supersaturation regime is needed to produce highly crystalline nanoparticles. This method produces very little material amounts with a mix of sizes and shapes. This is why specific growth in solution (soft chemistry) is now favored. Not only is it easier to scale up, but also this technique can be conducted at room temperature in solution in presence or absence of various organic molecules, polymers, and/or surfactants. These additives in solution may be used to control the shape during the crystal growth. With this method, shapes such as cubes, polyhedral, nanodisks, rods, prisms, plates, and spheres have been produced. The bottleneck of this technique is to maintain ultrapure solutions, which is mandatory for obtaining well defined shapes and sizes. Finally, due to inherent potential toxicity, the use of metals for delivery applications is probably restrained only to very specific applications, such as imaging and/or thermotherapy as shown by the recent development of iron oxides ultra small particles (USPIOs).

Other methods to grow crystals that may be used to make nanoparticles of interest may be found in other research areas like electronics. For example Indium Phosphide (InP) nanowires were prepared through laser assisted growth. 10nm particles in diameter were produced with tens of micrometers in length[77]. Morales et al. have developed a method combining laser ablation cluster formation and vapor liquid solid growth for the synthesis of nanowires[78]. They have produced Si and Ge nanowires of 10nm in diameter and hundreds of nm in length. Tanase et al. have fabricated Ni magnetic nanowires functionalized with porphyrins by electrochemical deposition on templates[79]. These particles are 180nm in diameter and 5-25µm in length and have been used to separate NIH-3T3 cells[80]. Finally Chen et al. decribed a method to form twisted nanoribbons using a Fe-based alloy under a magnetic field[81].

Carbon Nanotubes (CNT) and fullerenes represent the third allotropic crystalline form of carbon. They represent potentially interesting particles of controlled shape with a few nanometer in diameter and up to tens of microns long. CNTs are classified into two families: Single Wall NanoTubes (SWNT) and MultiWall NanoTubes (MWNT). SWNT are composed of a rolled monolayered graphene sheet whereas MWNT are comprised of several layers of concentric graphene sheets. These particles are a few nanometers wide for several hundred nanometers long. Since their discovery in 1991, CNTs preparation has been thoroughly described in the literature[82-84]. Three main methods are used to produce CNT, including arc-discharge, laser ablation, and chemical vapor deposition (CVD). Arc-discharge and laser

ablation are based on vaporization of a solid carbon source at high temperatures (>1000°C) to grow nanotubes. The synthesized nanotubes are very well controlled in terms of size distribution. Unfortunately, these methods produce a lot of byproducts. CVD is a slightly gentler method. In this technique, CNTs are grown on metal particles from a hydrocarbon gas at 500-1000°C. This method allows the production of a selective type of CNT (SWNT or MWNT) with few byproducts and a high control over the size.

In order to use these CNTs in drug delivery strategies, they would need obviously to be functionalized. Many research efforts were oriented in this direction[85-86]. Many ligands have been already attached to CNTs such as drugs including amphotericin B, methroxate, ligands such as immunogenic peptides, PEG, fluorophores… Applications for these particles regroup nanocontainment, diagnostics, gene and drug delivery, vaccination…

All these methods demonstrate a high potential for varying the obtainable shapes because these techniques are manipulating the arrangement of atoms in crystals or at least are crystal based. The main particles described so far in the literature with such structures are gold and silver particles, iron oxides, nanodiamonds, and carbon nanotubes. They are thoroughly studied for their applications including for pharmaceutical applications. but very rarely is the shape described as an important parameter. Moreover, their potential toxicity in the body should also be considered, depending on their application, doses, etc.

1.2.1.2. Preparation through constraint

An alternative strategy for preparing non spherical nanoparticles consists in applying orientated constraints on a certain amount of material. Three major methods can be regrouped under this category, including electrospinning, particle replication in non-wetting templates (PRINT^{TM}), and micro/nanofluidics. Basically in these methods the particle material, generally polymer, either in a melt state or as a solution in a solvent, is subjected to physical constraints. Therefore it requires an external device able to impose the form of the nanoparticles. Then the polymer must undergo a stimulus which causes solidification or solvent evaporation and finally the nanoparticles have to be retrieved.

i. Jet spinning/Electrospinning

Jet spinning, or electrospinning is a modified extrusion method that allows the formation of nanofibers, nanoribbons and nanowires from an electrically charged jet of melt polymer or polymer solution[87-88]. Figure 1.37 shows the principle of the method. Every soluble or fusible polymer is eligible for this method. E.g., poly lactic acid (PLA), polyethylene co-vinyl acetate (PEVA), polyethylene oxide (PEO), poly vinyl phenol (PVP), polyvinyl alcool (PVA), poly lactic co-glycolic acid (PLGA) have already been jet spun and tested for biomedical or drug delivery applications[89]. However, for these applications the fibers were only a few tens of nanometer in diameter and do not seem to have a maximal length. These techniques allow an adjustment of fibers length. As for their structure the fibers can be plain, hollow or porous, and can even be woven together.

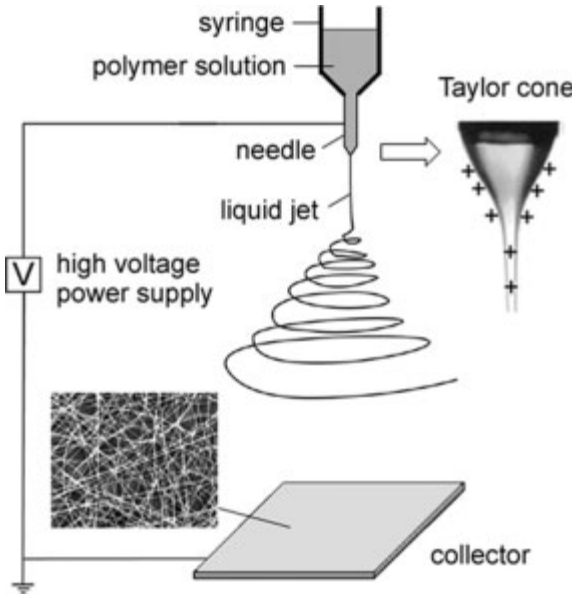

Figure 1.37: Schematic illustration for the basic setup of electrospinning. The SEM picture shows poly(vinyl pyrrolidone) deposited on the collectors[87]

Electrospinning does not necessitate an expensive setup and is easy to use. This process depends on several molecular, processing, and technical parameters that can be tuned in order to modify the properties of the spun fibers. Further, encapsulation during the formation of the fibers necessitates the drugs to be really stable under the fabrication conditions.

ii. PRINT™

The PRINT method is a molding technique based on the use of a positive master mold obtained through photolithography. Then a perfluoropolyether (PFPE) negative mold is imprinted on the master mold with nanometric features. Then a polymer is casted in the PFPE mold under pressure. The nanoparticles are removed by sticking them on an adhesive layer. Finally dissolution of the adhesive layer allows the retrieval of the nanoparticles (figure 1.38).

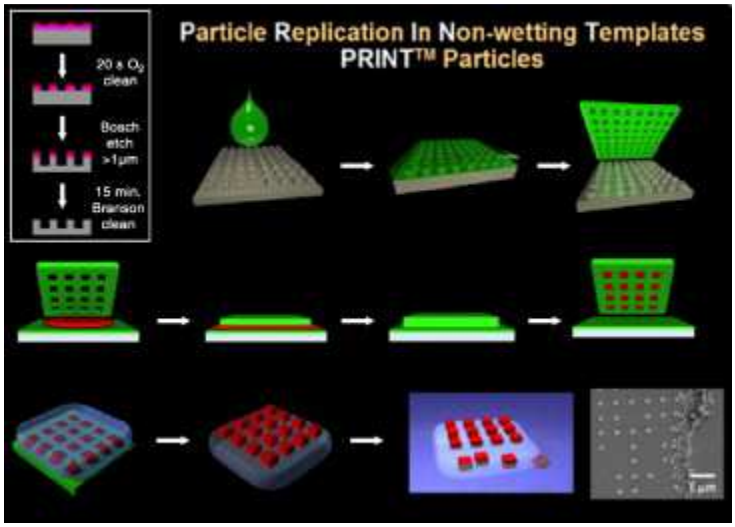

Figure 1.38: Illustration of PRINT[90] Fabrication of the silicon master template (box, upper left); Wetting of the silicon master with (green) liquid fluoropolymer, followed by curing (top row); PFPE elastomeric mold produced with nanoscale features from the master (upper right); Confining (red) organic liquid to cavities by applying pressure between mold and a PFPE surface (middle row); Removal of organic particles from mold with adhesive layer (bottom left); Dissolution of adhesive layer producing free particles (bottom right)

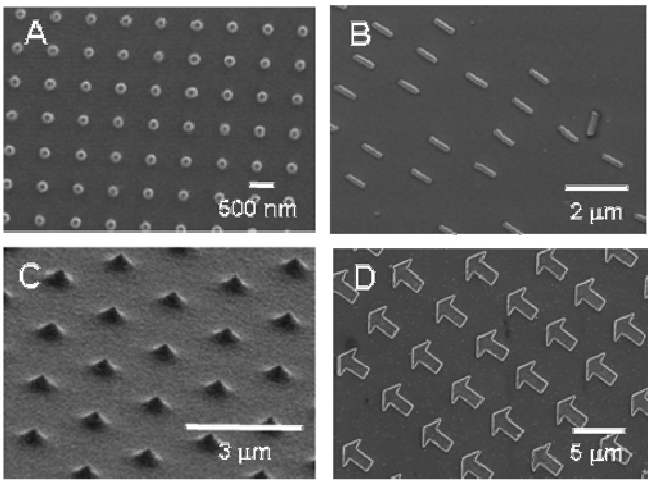

Figure 1.39: Micro and Nanoparticles of complex shape prepared by PRINT process[91] (A) 200nm trapezoidal PEG particles; (B) 200nm x 800nm bar PEG particles; (C) 500nm conical PEG particles that are <50nm at the tip; (D) 3µm arrow PEG particles.

As for electrospinning, any solvent soluble or fusible polymer is eligible for the PRINT process. For example PEG[91], PLA[92] and PLGA[92] particles have been already fabricated. This method offers the advantage of providing a wide variety of shapes (see figure 1.39) despite the fact that all shapes must present a flat surface (air contact) and be removable from the mold. Furthermore filling of the molds in steps allows the creation of particles with multiple layers[93] or anisotropic particles[94].

These particles are able to load cargo (drug, protein, fluorophore…) with the same restrictions as jet spun particles, mostly stability under operating conditions.

This process allows the mass production of particles with dimensions as small as 20nm. Only the fabrication of the master mold imposes limitation to the obtainable shapes. This process is very smooth for the loading of a drug, because it requires no heating and no solvent out of the dissolution of the adhesive layer. However, a potential drawback of the method may result from the difficulty, if not the impossibility, to control and to functionalize the surface properties of the particles. If ligands are linked to the polymers before molding, their presentation at the surface of the particles is not guaranteed. A functionalization post particles fabrication is problematic because of the necessity of a chemical reaction, potentially harmful to the active ingredient (nature and concentration).

iii. Micro/NanoFluidics

Micro-nanofluidics[95] methods are based on the use of micro or nanochannels to form the particles either from a liquid polymer solution or in the melted state. By forcing polymer drops slightly bigger than the size of the channel, it is possible to strain each drop, one by one, in the channel. The drop is solidified in the channel and then the nanoparticles are retrieved at the end of the system as a suspension[96].

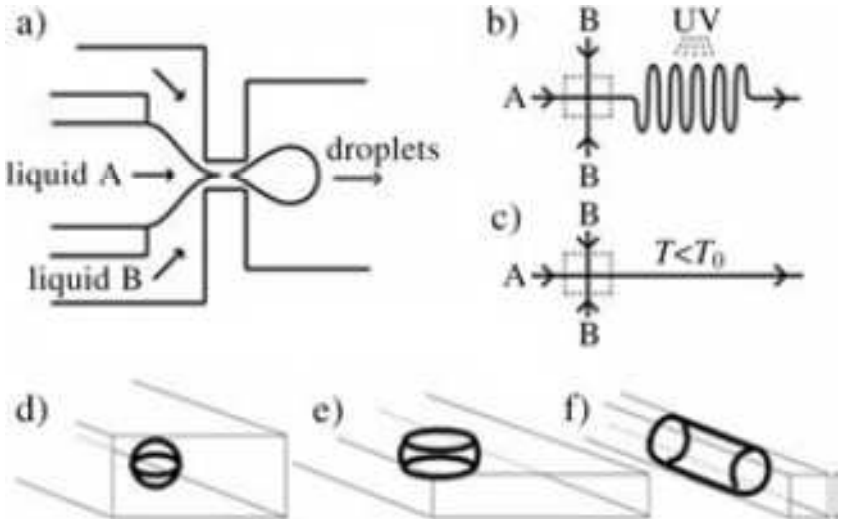

Figure 1.40: Formation of nanoparticles of complex shape through microfluidics[97]: (a) A representation of the flow focusing geometry used in the microfluidics droplet generator. The two immiscible liquids A and B are forced into the narrow orifice where the inner liquid core breaks to release monodisperse droplet into the outlet channel (b-c) Representations of the devices used for producing photochemically and thermally solidified particles. The dashed rectangles mark the flow-focusing device shown in part (a). The channels used for photochemical cross-linking were elongated to allow longer durations or exposure of the droplets to UV light. For thermal settings experiments, the flow focusing region was kept at a temperature exceeding the gelling (or solid-liquid phase transition) temperature (T_0). The outlet channel was cooled to a temperature below T_0, and the droplets solidified as they traveled down the channel (d-f) Representations of the shape of drops in the microfluidic channel. If the volume of the droplet exceeds that of the largest sphere which could be accommodated in the channel, the droplet is deformed into a disk (e) or an ellipsoid or a rod (f).

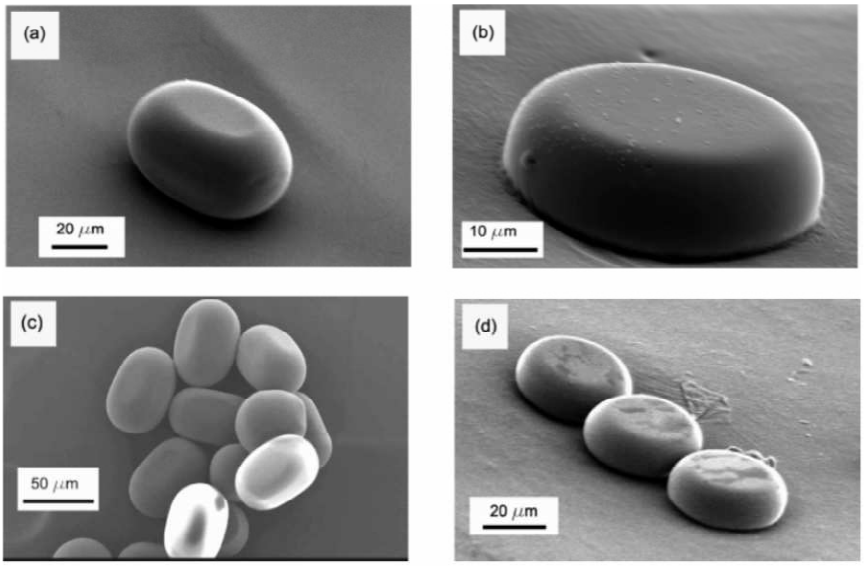

Figure 1.41: SEM images of non spherical colloids[96]: (a) plug; (b) disk; (c) collection of plugs; and (d) collection of disks.

Figure 1.41 illustrates some of the attainable geometries via microfluidics, such as plugs and discs. Even if the geometries are simple, the particles can be easily and quickly mass produced in very smooth conditions. A possible drawback of the method is that the size of particles depends on the size of the channels. For now, size of the channels is still in the micrometers range and only microparticles can be produced, but with the development of nanofluidics we can expect the production of nanoparticles in the years to come. Another problem may arise from the need for an extreme purity of the materials to be treated, in order not to obstruct the channels during production.

1.2.1.3. Preparation through deformation

Formation of non-spherical nanoparticles can be conducted using a two step method consisting in: (i) preparing spherical particles and then (ii) deforming these nanoparticles. A possible technique to deform the particles consists in enclosing the particles in a polymer film[98] or a gel[99]. Before or after liquefaction of the particles either by the action of a solvent or through melting by heating, this film/gel is stretched after being mounted on a frame. After

deformation, the nanoparticles are solidified and retrieved trough film solubilization and elimination. Figure 1.42 shows the principle of this technique.

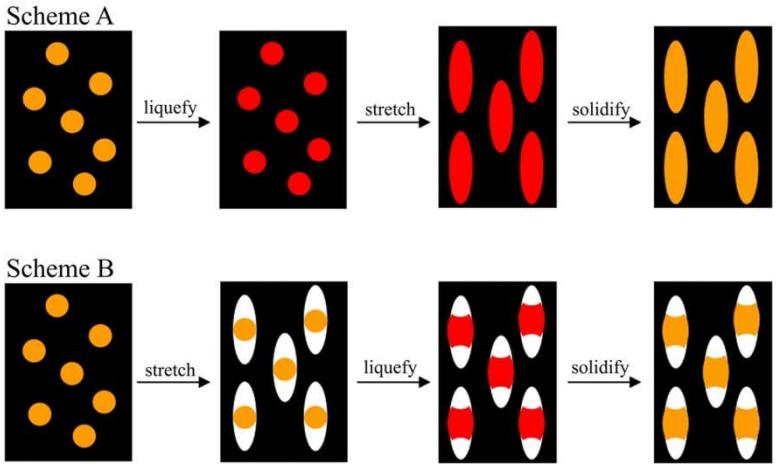

Figure 1.42: Methods used for making particles with different shapes can be categorized into two general schemes. (Upper) Scheme A involves liquefaction of particles by using heat or toluene, stretching the film in one or two dimensions and solidifying the particles by extracting toluene or cooling. The example shown here produces elliptical disks. (Lower) Scheme B involves stretching the film in air to create voids around the particle, followed by liquefaction using heat or toluene and solidification. The example shown here produces barrels [98]

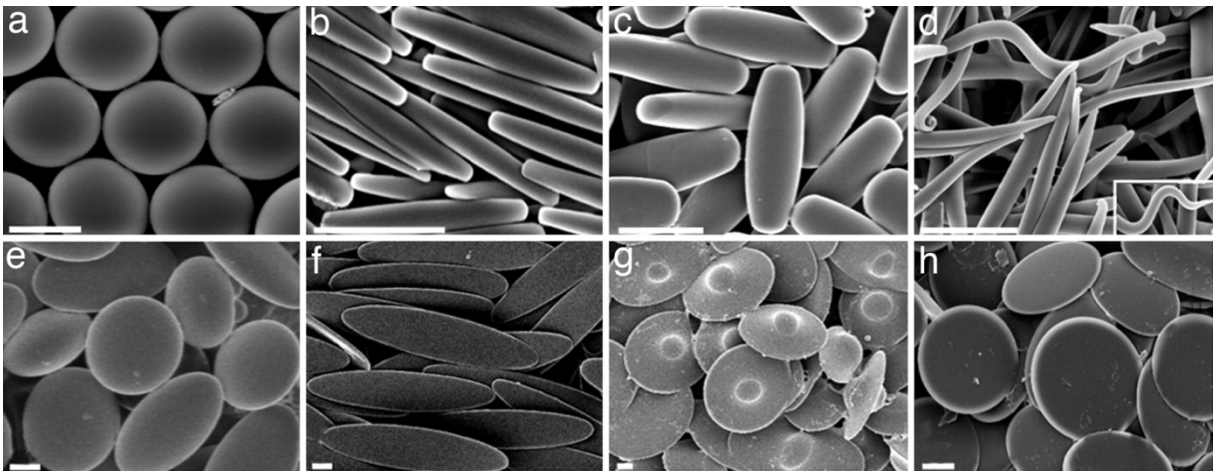

Figure 1.43: Micrographs of shapes made by using scheme A. (a) Spheres. (b) Rectangular disks. (c) Rods. (d) Worms. (e) Oblate ellipses. (f) Elliptical disks. (g) UFOs. (h) Circular disks. (Scale bars: 2µm.) [98]

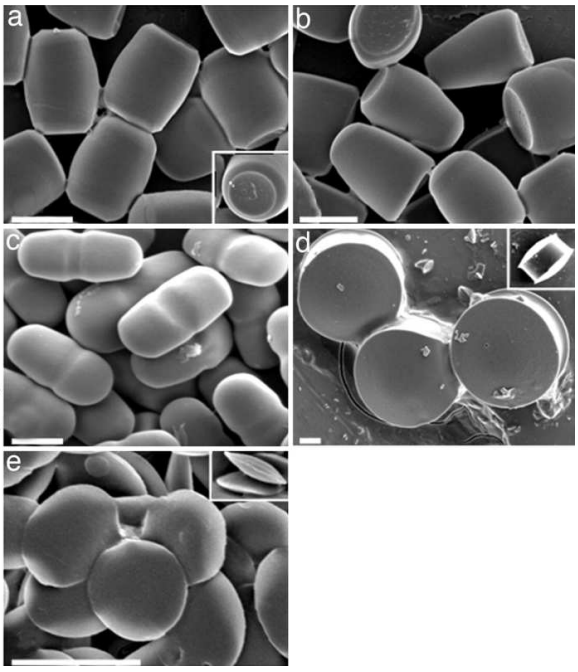

Figure 1.44: Micrographs of shapes made by using scheme B. (a) Barrels. (b) Bullets. (c) Pills. (d) Pulleys. (e) Biconvex lenses. (Scale bars: 2 µm) [98]

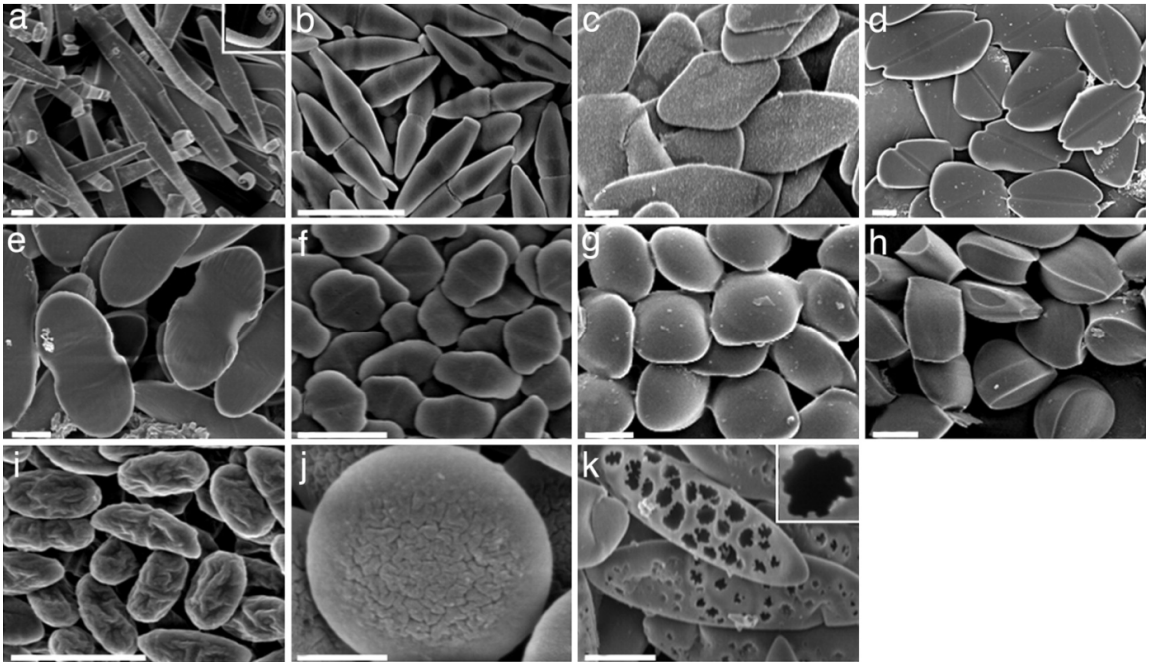

Figure 1.45: Micrographs of shapes made by using combinations of schemes A and B. (a) Ribbons with curled ends (b) Bicones (c) Diamond disks (d) Emarginate disks (e) Flat pills (f) Elongated hexagonal disks (g) Ravioli (h) Tacos (i) Wrinkled prolate ellipsoids (j) Wrinkled oblate ellipses (k) Porous elliptical disks. Scale bars: (a–i, k) 2 µm; j 400 nm[98]

This method is very interesting in terms of nanoparticle analysis. Not only does it provide a wide variety of shape (Figures 1.43, 1.44 and 1.45), but particles, either nano or micro, are all of the same volume, which allows the comparison for cellular interactions. The two main problems of this method are the use of a solvent for particles liquefaction and the use of a polymer film which is very hard to completely eliminate. So far this method has only been used for deforming polystyrene particles (microspheres), but virtually any polymer that can be melted and could be deformed by this method. Whatever, as in other deformation techniques, the control of surface properties at a molecular level (controlled grafting of ligands) may be a difficult, if not impossible, task.

1.2.1.4. Preparation through fusion

The last approach that will be tackled is the formation of non-spherical particles through fusion. In this method spherical nanoparticles are grouped in clusters either via synthesis or through aggregation.

Different modus operandi have been described in the literature, but they are all based on the same principle. A suspension of spherical particles is previously prepared and those particles are further aggregated via emulsion evaporation[100-101] as shown on figure 1.46 or by covalent bonding[100], which leads to particles sintering. In the case of emulsion-evaporation aggregation, this method is applicable to any kind of particles, contrary to the aggregation via covalent bonding which requires the action of a chemical linker on the surface of the particles.

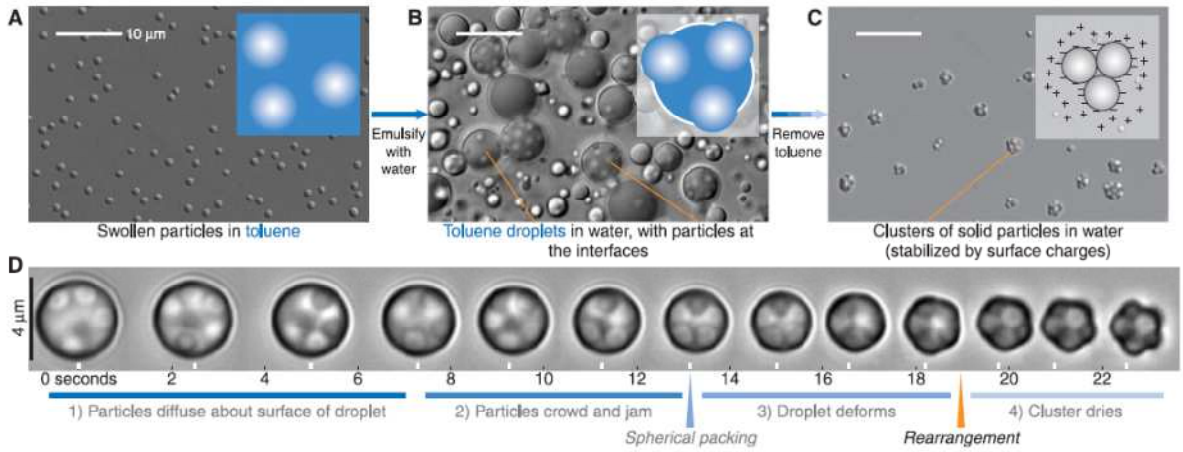

Figure 1.46: Optical micrographs and diagrams (insets) of the packing process. (A) Polymer particles swollen and dispersed in toluene (shown in blue). (B) Emulsion of toluene droplets with particles, still swollen, bound to the interfaces. (C) Clusters after toluene evaporation. These are stabilized against further aggregation by the dissociation of charged groups on the surfaces of the particles. (D) A time series of micrographs taken during evaporation of the toluene, showing the evolution of the system between (B) and (C). Particles freely diffuse about the surface of the droplet until, as more toluene evaporates, they touch one another, forming a spherical packing (blue arrowhead). Deformation of the interface then leads to a rapid rearrangement (orange arrowhead) to a cluster. The final configuration of this seven-sphere cluster is also shown in figure 1.47. [101]

Figure 1.47 shows different possible arrangements when associating particles. The geometry of the aggregated particles is regulated by the minimisation of the second moment of the mass distribution. As can be seen on these electron microscopy images, the aggregates are globally close to a sphere but with a very rough surface.

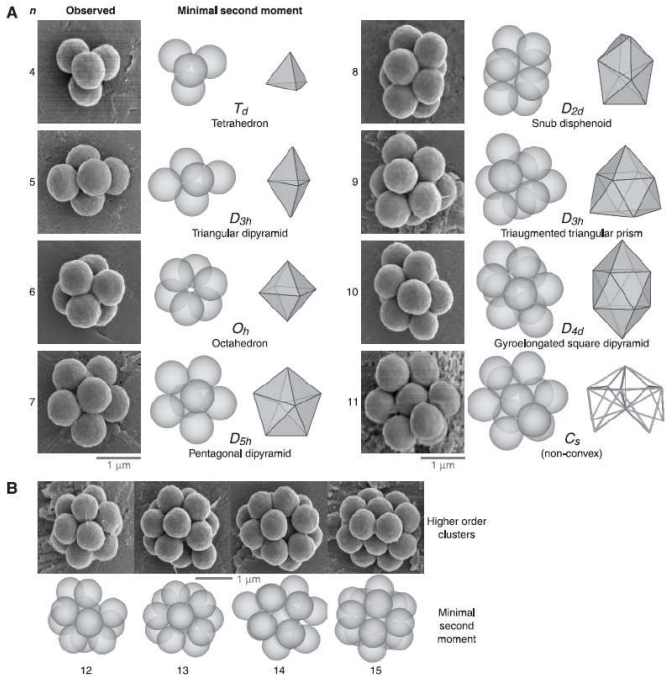

Figure 1.47: Cluster configurations at each n, as determined by optical and electron microscopy. Some shrinkage and deformation of the spheres occur during drying and exposure to the electron beam, but the configurations of particles remain the same as those observed in situ optically. (A) Left columns show electron micrographs of the clusters. All clusters of a given n have identical structures. Right columns illustrate the polyhedral formed by drawing lines from the center of each particle to its neighbors. Middle columns show computer renderings of sphere configurations that minimize the second moment of the mass distribution, which match the packings.[101]

This method produces particles almost spherical and would be better suited to study the effect of the roughness of the particles themselves than to study the effect of the aspect ratio on the interactions with cells and on biodistribution. A difficulty with this method stems also from the necessity to produce primary particles of different volume in order to be able to obtain aggregates of comparable volume, to be able to compare shape or roughness effects.

We have described here all the methods we could find in the literature and that allow the production of non spherical particles. As it has been shown, they can be classified into two categories, one step methods based on auto assembly of e.g; hydrophobic polymers, peptides, amphiphilic molecules, atoms… and preparation through constraint methods. In these latter methods, constraints can be applied by various means, including molding, extrusion processes, e.g; in microfluidic channels; deformation in films or gels, and aggregation and sintering. All these methods have specific advantages and drawbacks. Clearly, auto assembling techniques necessitate the selection and the production of suitable molecular or atomic materials able to induce particle anisotropy. They probably offer the opportunity of a smart tuning of the surface of the particles at the molecular scale. On the contrary, deformation techniques may suffer from a lack of control of surface properties but can be envisionned for a large variety of commonly used materials.

Conclusion

This review shows that, despite the fairly little amount of available experimental data, there are nowadays many evidences that the behavior of particles in the body can be considerably affected by their morphology. Because nanoparticles are often regarded as promising carriers for drug targeting applications, it is thus important to understand shape effects when non spherical particles are used instead of classical spherical particles. As far as the aim of drug targeting is to replace an inadequate drug distribution by the distribution of the carrier itself once loaded with the molecule of interest (small molecule, protein, DNA…) this is a very important task.

However such studies and further developments cannot be foreseen in the absence of a suitable method making possible to prepare particles of pharmaceutical interest. This is probably a key point in this area, as it is not a trivial task.

Indeed these methods should be able to respect some key parameters for these particles, as they would be prepared from non toxic materials and their size, surface and shape should be tunable.

So far, within the different methods reviewed, the auto assembly method meets probably most of the requirements above, provided that the material chosen as the building block is biodegradable. Finding and choosing the right building blocks for the size and biodegradability properties is probably the more difficult part of the job, making metals and crystal particles unfitting in most circumstances. Once this step is achieved, it offers the opportunity for surface modifications. Further, there are different ways to load a cargo in these particles (covalent bond or physical encapsulation). However these modifications may alter the shape of the particles.

Other preparation methods rely on physical constraints and could offer also viable options for the preparation of non-spherical particles. Interestingly, the size polydispersity is very low but access to very small particles (10-100nm) can be a problem. The PRINT process allows the use for biodegradable polymer, and drug loading seems feasible even if the use of heat and solvent could damage the drug. Probably the major limitation of these methods stems from the fact that surface control may be difficult (if not impossible) to ensure, especially when surface

engineering must be envisioned at the molecular scale with precise presentation of ligands able to control simultaneously particle recognition and to escape non specific capture phenomena. Deformation techniques using films or gels are quite interesting as they offer an easy access to many geometries, but similarly surface control may be a real trap. Furthermore, the scale up of these processes may be problematic except for the jet spinning and microfluidic techniques.

Whatever their respective limitations, it is our belief, that material (polymers) auto assembly, the PRINT process as well as the deformation techniques are the most relevant methods for preparing non spherical particles. The choice of one or the other should be considered case by case depending on the applications. Even if they are not so easily handled, they are powerful enough to allow further studies on the effect of particle shape on their fate *in vivo* after their delivery in the body. Obviously major information can be expected not only in toxicological studies in case of accidental exposition to such particles, but more importantly for improving drug targeting strategies.

References

1. Hillaireau, H. & Couvreur, P.
Nanocarriers' entry into the cell: relevance to drug delivery,
Cellular and Molecular Life Sciences, 66, 2873-2896, **2009**.

2. Lleo, M.M., Canepari, P. & Satta, G.
Bacterial cell shape regulation: testing of additional predictions unique to the two-competing-sites model for peptidoglycan assembly and isolation of conditional rod-shaped mutants from some wild-type cocci,
J. Bacteriol., 172, 3758-3771, **1990**.

3. Young, K.D.
The Selective Value of Bacterial Shape,
Microbiol. Mol. Biol. Rev., 70, 660-703, **2006**.

4. Young, K.D.
Bacterial shape,
Molecular Microbiology, 49, 571-580, **2003**.

5. Matsumura, Y. & Maeda, H.
A New Concept for Macromolecular Therapeutics in Cancer Chemotherapy: Mechanism of Tumoritropic Accumulation of Proteins and the Antitumor Agent Smancs,
Cancer Research, 46, 6387-6392, **1986**.

6. Han, Y., Alsayed, A.M., Nobili, M., Zhang, J., Lubensky, T.C. & Yodh, A.G.
Brownian Motion of an Ellipsoid,
Science, 314, 626-630, **2006**.

7. Jeffery, G.B.
The Motion of Ellipsoidal Particles Immersed in a Viscous Fluid,
Proceedings of the Royal Society of London. Series A, 102, 161-179, **1922**.

8. Ku, D.N.
Blood flow in arteries,
Annual Review of Fluid Mechanics, 29, 399-434, **1997**.

9. Gentile, F., Chiappini, C., Fine, D., Bhavane, R.C., Peluccio, M.S., Cheng, M.M.-C., Liu, X., Ferrari, M. & Decuzzi, P.
The effect of shape on the margination dynamics of non-neutrally buoyant particles in two-dimensional shear flows,
Journal of biomechanics, 41, 2312-2318, **2008**.

10. Decuzzi, P., Lee, S., Bhushan, B. & Ferrari, M.
A Theoretical Model for the Margination of Particles within Blood Vessels,
Annals of Biomedical Engineering, 33, 179-190, **2005**.

11. Decuzzi, P., Pasqualini, R., Arap, W. & Ferrari, M.
Intravascular Delivery of Particulate Systems: Does Geometry Really Matter?,
Pharmaceutical Research, 26, 235-243, **2009**.

12. Broday, D., Fichman, M., Shapiro, M. & Gutfinger, C.
Motion of spheroidal particles in vertical shear flows,
American Institute of Physics, **1998**.

13. Toy, R., Hayden, E., Shoup, C., Baskaran, H. & Karathanasis, E.
The effects of particle size, density and shape on margination of nanoparticles in microcirculation,
Nanotechnology, 22, 115101, **2011**.

14. Goldman, A.J., Cox, R.G. & Brenner, H.
Slow viscous motion of a sphere parallel to a plane wall--II Couette flow,
Chemical Engineering Science, 22, 653-660, **1967**.

15. Gavze, E. & Shapiro, M.
Motion of inertial spheroidal particles in a shear flow near a solid wall with special application to aerosol transport in microgravity,
Journal of Fluid Mechanics, 371, 59-79, **1998**.

16. Lee, S.-Y., Ferrari, M. & Decuzzi, P.
Design of bio-mimetic particles with enhanced vascular interaction,
Journal of biomechanics, 42, 1885-1890, **2009**.

17. Gavze, E. & Shapiro, M.
Particles in a shear flow near a solid wall: Effect of nonsphericity on forces and velocities,
International Journal of Multiphase Flow, 23, 155-182, **1997**.

18. O'Neill, M.E.
A sphere in contact with a plane wall in a slow linear shear flow,
Chemical Engineering Science, 23, 1293-1298, **1968**.

19. Lata, S., Reichel, A., Brock, R., Tampé, R. & Piehler, J.
High-Affinity Adaptors for Switchable Recognition of Histidine-Tagged Proteins,
Journal of the American Chemical Society, 127, 10205-10215, **2005**.

20. Cozens-Roberts, C., Quinn, J.A. & Lauffenberger, D.A.
Receptor-mediated adhesion phenomena. Model studies with the Radical-Flow Detachment Assay,
Biophysical Journal, 58, 107-125, **1990**.

21. Kuo, S.C., Hammer, D.A. & Lauffenburger, D.A.
Simulation of detachment of specifically bound particles from surfaces by shear flow,
Biophysical Journal, 73, 517-531, **1997**.

22. Kuo, S.C. & Lauffenburger, D.A.
Relationship between receptor/ligand binding affinity and adhesion strength,
Biophysical Journal, 65, 2191-2200, **1993**.

23. Decuzzi, P. & Ferrari, M.
Design maps for nanoparticles targeting the diseased microvasculature,
Biomaterials, 29, 377-384, **2008**.

24. Sakamoto, J.H., van de Ven, A.L., Godin, B., Blanco, E., Serda, R.E., Grattoni, A., Ziemys, A., Bouamrani, A., Hu, T., Ranganathan, S.I., De Rosa, E., Martinez, J.O., Smid, C.A., Buchanan, R.M., Lee, S.-Y., Srinivasan, S., Landry, M., Meyn, A., Tasciotti, E., Liu, X., Decuzzi, P. & Ferrari, M.
Enabling individualized therapy through nanotechnology,
Pharmacological Research, 62, 57-89, **2010**.

25. Godin, B., P. Driessen, W.H., Proneth, B., Lee, S.-Y., Srinivasan, S., Rumbaut, R., Arap, W., Pasqualini, R., Ferrari, M. & Decuzzi, P.
Advances in Genetics, *2 - An Integrated Approach for the Rational Design of Nanovectors for Biomedical Imaging and Therapy,*
Academic Press, **2010**.

26. Mailänder, V. & Landfester, K.
Interaction of Nanoparticles with Cells,
Biomacromolecules, 10, 2379-2400, **2009**.

27. Gratton, S., Napier, M., Ropp, P., Tian, S. & DeSimone, J.
Microfabricated Particles for Engineered Drug Therapies: Elucidation into the Mechanisms of Cellular Internalization of PRINT Particles,
Pharmaceutical Research, 25, 2845-2852, **2008**.

28. Champion, J.A. & Mitragotri, S.
Role of target geometry in phagocytosis,
Proceedings of the National Academy of Sciences of the United States of America, 103, 4930-4934, **2006**.

29. Gratton, S.E.A., Ropp, P.A., Pohlhaus, P.D., Luft, J.C., Madden, V.J., Napier, M.E. & DeSimone, J.M.
The effect of particle design on cellular internalization pathways,
Proceedings of the National Academy of Sciences, 105, 11613-11618, **2008**.

30. Chithrani, B.D., Ghazani, A.A. & Chan, W.C.W.
Determining the Size and Shape Dependence of Gold Nanoparticle Uptake into Mammalian Cells,
Nano Letters, 6, 662-668, **2006**.

31. Decuzzi, P. & Ferrari, M.
The Receptor-Mediated Endocytosis of Nonspherical Particles,

Cell Press, **2008**.

32. Geng, Y., Dalhaimer, P., Cai, S., Tsai, R., Tewari, M., Minko, T. & Discher, D.E. *Shape effects of filaments versus spherical particles in flow and drug delivery,* Nat Nano, 2, 249-255, **2007**.

33. Decuzzi, P., Godin, B., Tanaka, T., Lee, S.Y., Chiappini, C., Liu, X. & Ferrari, M. *Size and shape effects in the biodistribution of intravascularly injected particles,* Journal of Controlled Release, 141, 320-327, **2010**.

34. Aichmayer, B., Wiedemann-Bidlack, F.B., Gilow, C., Simmer, J.P., Yamakoshi, Y., Emmerling, F., Margolis, H.C. & Fratzl, P. *Amelogenin Nanoparticles in Suspension: Deviations from Spherical Shape and pH-Dependent Aggregation,* Biomacromolecules, 11, 369-376, **2009**.

35. Scanlon, S. & Aggeli, A. *Self-assembling peptide nanotubes,* Nano Today, 3, 22-30, **2008**.

36. Toksöz, S. & Guler, M.O. *Self-assembled peptidic nanostructures,* Nano Today, 4, 458-469, **2009**.

37. Balbo, B.M.A. & Stefan, H. *Wrapping peptide tubes : Merging biological self-assembly and polymer synthesis,* Angewandte Chemie. International edition, 44, 4, **2005**.

38. Hartgerink, J.D., Granja, J.R., Milligan, R.A. & Ghadiri, M.R. *Self-Assembling Peptide Nanotubes,* Journal of the American Chemical Society, 118, 43-50, **1996**.

39. Vauthey, S., Santoso, S., Gong, H., Watson, N. & Zhang, S. *Molecular self-assembly of surfactant-like peptides to form nanotubes and nanovesicles,* Proceedings of the National Academy of Sciences of the United States of America, 99, 5355-5360, **2002**.

40. Zhang, S. & Zhao, X. *Design of molecular biological materials using peptide motifs,* Journal of Materials Chemistry, 14, 2082-2086, **2004**.

41. Kol, N., Adler-Abramovich, L., Barlam, D., Shneck, R.Z., Gazit, E. & Rousso, I. *Self-Assembled Peptide Nanotubes Are Uniquely Rigid Bioinspired Supramolecular Structures,* Nano Letters, 5, 1343-1346, **2005**.

42. Reches, M. & Gazit, E.

Designed aromatic homo-dipeptides: formation of ordered nanostructures and potential nanotechnological applications,
Physical Biology, S10, **2006**.

43. Elgersma, R.C., Meijneke, T., Posthuma, G., Rijkers, D.T.S. & Liskamp, R.M.J.
Self-Assembly of Amylin(20-29) Amide-Bond Derivatives into Helical Ribbons and Peptide Nanotubes rather than Fibrils,
Chemistry - A European Journal, 12, 3714-3725, **2006**.

44. Marsden, H.R., Korobko, A.V., van Leeuwen, E.N.M., Pouget, E.M., Veen, S.J., Sommerdijk, N.A.J.M. & Kros, A.
Noncovalent Triblock Copolymers Based on a Coiled-Coil Peptide Motif,
Journal of the American Chemical Society, 130, 9386-9393, **2008**.

45. Zhang, S.
Fabrication of novel biomaterials through molecular self-assembly,
Nature, 21, 8, **2003**.

46. Seebach, D., Beck, A.K. & Bierbaum, D.J.
The World of β- and γ-Peptides Comprised of Homologated Proteinogenic Amino Acids and Other Components,
Chemistry & Biodiversity, 1, 1111-1239, **2004**.

47. Niu, L., Chen, X., Allen, S. & Tendler, S.J.B.
Using the Bending Beam Model to Estimate the Elasticity of Diphenylalanine Nanotubes,
Langmuir, 23, 7443-7446, **2007**.

48. Adler-Abramovich, L., Reches, M., Sedman, V.L., Allen, S., Tendler, S.J.B. & Gazit, E.
Thermal and Chemical Stability of Diphenylalanine Peptide Nanotubes: Implications for Nanotechnological Applications,
Langmuir, 22, 1313-1320, **2006**.

49. Yan, X., He, Q., Wang, K., Duan, L., Cui, Y. & Li, J.
Transition of Cationic Dipeptide Nanotubes into Vesicles and Oligonucleotide Delivery,
Angewandte Chemie International Edition, 46, 2431-2434, **2007**.

50. Zhao, X. & Zhang, S.
Self-assembling nanopeptides become a new type of biomaterial,
Advances in Polymer Sciences, 203, 145-170, **2006**.

51. Schlick, T.L., Ding, Z., Kovacs, E.W. & Francis, M.B.
Dual-Surface Modification of the Tobacco Mosaic Virus,
Journal of the American Chemical Society, 127, 3718-3723, **2005**.

52. Lim, Y.-b., Lee, E., Yoon, Y.-R., Lee, Myeong S. & Lee, M.
Filamentous Artificial Virus from a Self-Assembled Discrete Nanoribbon,

Angewandte Chemie International Edition, 47, 4525-4528, **2008**.

53. Lim, Y.-b., Park, S., Lee, E., Jeong, H., Ryu, J.-H., Lee, M.S. & Lee, M.
Glycoconjugate Nanoribbons from the Self-Assembly of Carbohydrate−Peptide Block Molecules for Controllable Bacterial Cell Cluster Formation,
Biomacromolecules, 8, 1404-1408, **2007**.

54. Jacob N. Israelachvili, Mitchell, D.J. & Ninham, B.W.
Theory of self-assembly of hydrocarbon amphiphiles into micelles and bilayers,
J. Chem. Soc., Faraday Trans. 2, 72, 1525 - 1568, **1976**.

55. Geng, Y. & Discher, D.E.
Hydrolytic Degradation of Poly(ethylene oxide)-block-Polycaprolactone Worm Micelles,
Journal of the American Chemical Society, 127, 12780-12781, **2005**.

56. Kim, Y., Dalhaimer, P., Christian, D.A. & Dische, D.E.
Polymeric worm micelles as nano-carriers for drug delivery,
Nanotechnology, 16, S484, **2005**.

57. Lin, Z.
Branched Worm-like Micelles and Their Networks,
Langmuir, 12, 1729-1737, **1996**.

58. Geng, Y. & Discher, D.E.
Visualization of degradable worm micelle breakdown in relation to drug release,
Polymer, 47, 2519-2525, **2006**.

59. Yang, J.
Viscoelastic wormlike micelles and their applications,
Current Opinion in Colloid & Interface Science, 7, 276-281, **2002**.

60. Arunothayanun, P., Uchegbu, I.F., Craig, D.Q.M., Turton, J.A. & Florence, A.T.
Investigations into the in-vitro/in-vivo behaviour of polyhedral niosomes,
Journal of Pharmacy and Pharmacology, 50, 169-169, **1998**.

61. Arunothayanun, P., Uchegbu, I.F. & Florence, A.T.
Osmotic Behaviour of Polyhedral Non-ionic Surfactant Vesicles (Niosomes),
Journal of Pharmacy and Pharmacology, 51, 651-657, **1999**.

62. Uchegbu, I.F. & Vyas, S.P.
Non-ionic surfactant based vesicles (niosomes) in drug delivery,
International Journal of Pharmaceutics, 172, 33-70, **1998**.

63. Uchegbu, I.F., Mccarthy, D., Schatzlein, A. & Florence, A.T.

Phase transitions in aqueous dispersions of the hexadecyl diglycerol ether (C[16]G[2]) non-ionic surfactant, cholesterol and cholesteryl poly-24-oxyethylene ether : vesicles, tubules, discomes and micelles,
STP pharma sciences, 6, 1157-1489, **1996**.

64. Vos, M.R.J., Jardl, G.E., Pallas, A.L., Breurken, M., Van Asselen, O.L.J., Bomans, P.H.H., Leclere, P.E.L.G., Frederik, P.M., Nolte, R.J.M. & Sommerdijk, N.A.J.M.
The Bis-urea Motif as a Tool To Functionalize Self-Assembled Nanoribbons,
Journal of the American Chemical Society, 127, 16768-16769, **2005**.

65. Ornatska, M., Peleshanko, S., Genson, K.L., Rybak, B., Bergman, K.N. & Tsukruk, V.V.
Assembling of Amphiphilic Highly Branched Molecules in Supramolecular Nanofibers,
Journal of the American Chemical Society, 126, 9675-9684, **2004**.

66. Ornatska, M., Bergman, K.N., Rybak, B., Peleshanko, S. & Tsukruk, V.V.
Nanofibers from Functionalized Dendritic Molecules,
Angewandte Chemie International Edition, 43, 5246-5249, **2004**.

67. Fréchet, J.M.J., Hawker, C.J., Gitsov, I. & Leon, J.W.
Dendrimers and Hyperbranched Polymers: Two Families of Three-Dimensional Macromolecules with Similar but Clearly Distinct Properties,
Journal of Macromolecular Science, Part A: Pure and Applied Chemistry, 33, 1399 - 1425, **1996**.

68. Patri, A.K., Majoros, I.J. & Baker, J.R.
Dendritic polymer macromolecular carriers for drug delivery,
Current Opinion in Chemical Biology, 6, 466-471, **2002**.

69. Gillies, E.R. & Fréchet, J.M.J.
Dendrimers and dendritic polymers in drug delivery,
Drug Discovery Today, 10, 35-43, **2005**.

70. Ihre, H.R., Padilla De Jesús, O.L., Szoka, F.C. & Fréchet, J.M.J.
Polyester Dendritic Systems for Drug Delivery Applications: Design, Synthesis, and Characterization,
Bioconjugate Chemistry, 13, 443-452, **2002**.

71. Eustis, S. & El-Sayed, M.A.
Why gold nanoparticles are more precious than pretty gold : Noble metal surface plasmon resonance and its enhancement of the radiative and nonradiative properties of nanocrystals of different shapes,
Royal Society of Chemistry, **2006**.

72. Huang, W., Qian, W. & El-Sayed, M.A.
The Optically Detected Coherent Lattice Oscillations in Silver and Gold Monolayer Periodic Nanoprism Arrays: The Effect of Interparticle Coupling,
The Journal of Physical Chemistry B, 109, 18881-18888, **2005**.

73. Hasan, W., Lee, J., Henzie, J. & Odom, T.W.
Selective Functionalization and Spectral Identification of Gold Nanopyramids,
The Journal of Physical Chemistry C, 111, 17176-17179, **2007**.

74. Demortière, A., Launois, P., Goubet, N., Albouy, P.A. & Petit, C.
Shape-Controlled Platinum Nanocubes and Their Assembly into Two-Dimensional and Three-Dimensional Superlattices†,
The Journal of Physical Chemistry B, 112, 14583-14592, **2008**.

75. Murphy, C.J., Sau, T.K., Gole, A.M., Orendorff, C.J., Gao, J., Gou, L., Hunyadi, S.E. & Li, T.
Anisotropic Metal Nanoparticles: Synthesis, Assembly, and Optical Applications,
The Journal of Physical Chemistry B, 109, 13857-13870, **2005**.

76. Murphy, C.J., Gole, A.M., Stone, J.W., Sisco, P.N., Alkilany, A.M., Goldsmith, E.C. & Baxter, S.C.
Gold Nanoparticles in Biology: Beyond Toxicity to Cellular Imaging,
Accounts of Chemical Research, 41, 1721-1730, **2008**.

77. Duan, X., Huang, Y., Cui, Y., Wang, J. & Lieber, C.M.
Indium phosphide nanowires as building blocks for nanoscale electronic and optoelectronic devices,
Nature, 409, 66-69, **2001**.

78. Morales, A.M. & Lieber, C.M.
A Laser Ablation Method for the Synthesis of Crystalline Semiconductor Nanowires,
Science, 279, 208-211, **1998**.

79. Tanase, M., Bauer, L.A., Hultgren, A., Silevitch, D.M., Sun, L., Reich, D.H., Searson, P.C. & Meyer, G.J.
Magnetic Alignment of Fluorescent Nanowires,
Nano Letters, 1, 155-158, **2001**.

80. Hultgren, A., Tanase, M., Chen, C.S., Meyer, G.J. & Reich, D.H.
Cell manipulation using magnetic nanowires,
Journal of Applied Physics, 93, 7554-7556, **2003**.

81. Chen, X., Yang, S., Motojima, S. & Ichihara, M.
Morphology and microstructure of twisting nano-ribbons prepared using sputter-coated Fe-base alloy catalysts on glass substrates,
Materials letters, 59, 854-858, **2005**.

82. Kolosnjaj, J., Szwarc, H. & Moussa, F.
Bio-Applications of Nanoparticles, *Toxicity Studies of Carbon Nanotubes,*
Springer New York, **2007**.

83. Dai, H.
Carbon Nanotubes: Synthesis, Integration, and Properties,

Accounts of Chemical Research, 35, 1035-1044, **2002**.

84. Thostenson, E.T., Ren, Z. & Chou, T.-W.
Advances in the science and technology of carbon nanotubes and their composites: a review,
Composites Science and Technology, 61, 1899-1912, **2001**.

85. Bianco, A., Kostarelos, K., Partidos, C.D. & Prato, M.
Biomedical applications of functionalised carbon nanotubes,
Chemical Communications, 571-577, **2005**.

86. Prato, M., Kostarelos, K. & Bianco, A.
Functionalized Carbon Nanotubes in Drug Design and Discovery,
Accounts of Chemical Research, 41, 60-68, **2007**.

87. Li, D. & Xia, Y.
Electrospinning of Nanofibers: Reinventing the Wheel?,
Advanced Materials, 16, 1151-1170, **2004**.

88. Garg, K. & Bowlin, G.L.
Electrospinning jets and nanofibrous structures,
Biomicrofluidics, 5, 013403-013419, **2011**.

89. Huang, Z.-M., Zhang, Y.-Z., Kotaki, M. & Ramakrishna, S.
A review on polymer nanofibers by electrospinning and their applications in nanocomposites,
Composites science and technology, 63, 31, **2003**.

90. Gratton, S.E.A., Pohlhaus, P.D., Lee, J., Guo, J., Cho, M.J. & DeSimone, J.M.
Nanofabricated particles for engineered drug therapies: A preliminary biodistribution study of PRINT(TM) nanoparticles,
Journal of Controlled Release, 121, 10-18, **2007**.

91. Rolland, J.P., Maynor, B.W., Euliss, L.E., Exner, A.E., Denison, G.M. & DeSimone, J.M.
Direct Fabrication and Harvesting of Monodisperse, Shape-Specific Nanobiomaterials,
Journal of the American Chemical Society, 127, 10096-10100, **2005**.

92. Euliss, L.E., DuPont, J.A., Gratton, S. & DeSimone, J.
Imparting Size, Shape, and Composition Control of Materials for Nanomedicine,
ChemInform, 38, **2007**.

93. Hernandez, C.J. & Mason, T.G.
Colloidal Alphabet Soup: Monodisperse Dispersions of Shape-Designed LithoParticles,
The Journal of Physical Chemistry C, 111, 4477-4480, **2007**.

94. Zhang, H., Nunes, J.K., Gratton, S.E.A., Herlihy, K.P., Pohlhaus, P.D. & DeSimone, J.M.

Fabrication of multiphasic and regio-specifically functionalized PRINT particles of controlled size and shape,
New Journal of Physics, 075018, **2009**.

95. Kleinstreuer, C., Li, J. & Koo, J.
Microfluidics of nano-drug delivery,
International Journal of Heat and Mass Transfer, 51, 5590-5597, **2008**.

96. Dendukuri, D., Tsoi, K., Hatton, T.A. & Doyle, P.S.
Controlled Synthesis of Nonspherical Microparticles Using Microfluidics,
Langmuir, 21, 2113-2116, **2005**.

97. Xu, S., Nie, Z., Seo, M., Lewis, P., Kumacheva, E., Stone, H.A., Garstecki, P., Weibel, D.B., Gitlin, I. & Whitesides, G.M.
Generation of Monodisperse Particles by Using Microfluidics: Control over Size, Shape, and Composition,
Angewandte Chemie International Edition, 44, 3799, **2005**.

98. Champion, J.A., Katare, Y.K. & Mitragotri, S.
From the Cover: Making polymeric micro- and nanoparticles of complex shapes,
Proceedings of the National Academy of Sciences, 104, 11901-11904, **2007**.

99. Lu, Y., Yin, Y. & Xia, Y.
Preparation and Characterization of Micrometer-Sized ldquoEgg Shellsrdquo,
Advanced Materials, 13, 271-274, **2001**.

100. He, T., Adams, D.J., Butler, M.F., Cooper, A.I. & Rannard, S.P.
Polymer Nanoparticles: Shape-Directed Monomer-to-Particle Synthesis,
Journal of the American Chemical Society, 131, 1495-1501, **2009**.

101. Manoharan, V.N., Elsesser, M.T. & Pine, D.J.
Dense Packing and Symmetry in Small Clusters of Microspheres,
Science, 301, 483-487, **2003**.

Chapter II

Manufacture of polymeric non spherical micro and nanoparticles through the film stretching technique: conditions and limitations

Chapter 2. Manufacture of polymeric non spherical micro and nanoparticles through the film stretching technique: conditions and limitations.

Introduction

Whether it is for rockets, cars, bullets, cells... when displacement is involved, at every size level, shape has always been a major parameter in the creation of new systems. In pharmaceutical technology, only some systems at the macroscopic scale, such as patches for transdermal skin delivery, oros tablets for the oral route, take advantage of a complex morphology. However, at the micro and nano scale, most of the particulate carriers intended for targeting applications are spheres. Drug targeting consists in replacing the unfavorable biodistribution properties of a drug by those of a carrier in which the drug is encapsulated. For being successful this strategy necessitates the carriers to present simultaneously a desired set of physico-chemical characteristics. Among them, classical parameters that are used to tune this biodistribution are size, nature of the materials used for their preparation and surface properties. Indeed size effects have been extensively studied but only few groups have been studying the influence of shape on the biodistribution.

Recent advances in micro and nanotechnologies offer us more and more control, among other things, over the shape of micro and nanoparticles. Many techniques have been described to modulate the shape of particles: autoassembly (peptides[1-3], amphiphilic molecules[4-6], dendritic molecules[7-8]), molding[9-12] or deformation[13]. Yet all these techniques are not ideal for pharmaceutical applications, some use solvents or heat which can degrade the active ingredient and/or induce toxicity, some other necessitate polymers or solvents that are hard to prepare and/or to purify.

Some interesting studies of the interaction of non spherical particles with cells[10,13-15] biodistribution[15] have been conducted recently and suggest unanimously that shape is an essential parameter to consider when preparing carriers.

The present chapter aims to describe the film stretching technique[16] for the preparation of micro and nanoparticles suitable for pharmaceutical applications.

The film stretching technique[16] has been previously proposed by the group of Mitragotri, using polystyrene as a model. The principle of this method is as follows (Figure 2.1). First, previously prepared polymeric particles are casted in a polymer film. This film is mounted on a frame making possible to stretch it at a defined rate and temperature, making possible to soften the particles before stretching, which is achieved either by liquefaction of the particles through the action of a solvent or by heating. After deformation, the particles are solidified and retrieved trough film dissolution in a non solvent of the particles and elimination of the polymer forming the film.

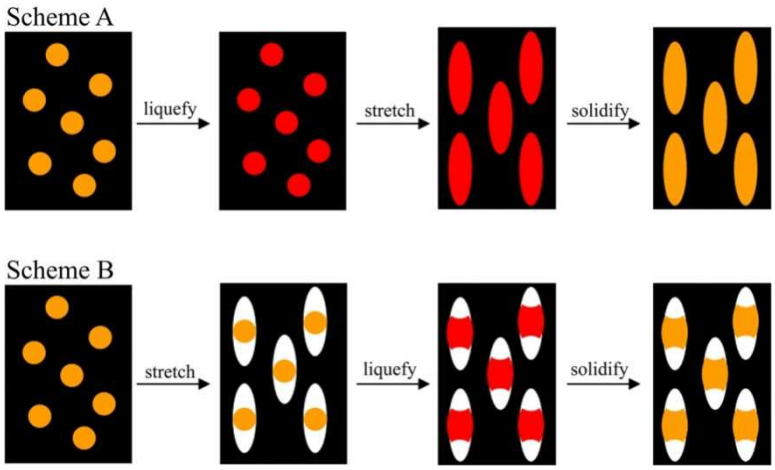

Figure 2.1 Methods used for making particles with different shapes can be categorized into two general schemes. (Upper) Scheme A involves liquefaction of particles by using heat or toluene, stretching the film in one or two dimensions and solidifying the particles by extracting toluene or cooling. The example showed here produces elliptical disks. (Lower) Scheme B involves stretching the film in air to create voids around the particle, followed by liquefaction using heat or toluene and solidification. The example shown here produces barrels[16] Reproduced after Mitragotri et al.

The film stretching method looks attractive when foreseeing the preparation of non spherical particles. Not only does it provide a wide variety of shape, but deformed particles, either nano or micro, are made of the same volume of material whatever their shape after deformation, which allows to study only the shape factor in biodistribution or cells interactions studies. However, when addressing pharmaceutical applications, the film

stretching method presents two main problems, which are the use of heat (or a solvent such as toluene in the case of polystyrene) for particles liquefaction and the use of a water soluble polymer film (such as poly(vinyl alcohol) (PVA), which is very hard to completely eliminate during the recovery process. Furthermore the control of the surface of the particles may be difficult, for example when the grafting of PEG chains or recognition ligands at the surface of the particles is foreseen, due to possible interactions of these macromolecules with PVA chains. So far this method has only been developed for polystyrene (PS) particles, but in theory any polymer that can be melted could be used for this method. Further, there are only very few data concerning the feasibility of this method for the preparation of non spherical nanoparticles by this technique.

Here we will present the adaptation of this method for pharmaceutical applications. First the elongation system will be described, then the choice of the film forming materials will be discussed and finally results of micro and nanoparticles elongation experiments will be presented.

2.1. Material and Methods

2.1.1. Elongation system

A proper elongation system able to heat and stretch simultaneously polymeric films tightened between two jaws has been developed. This protoptypic apparatus was conceived to be adjustable and will be detailed in the results section.

2.1.2. Preparation of water soluble films

Two polymers were investigated for preparing water soluble films, suitable for the technique.

- PVA formulation: 1g (5% w/w) polyvinylalcool (PVA) and 0.2g (1% w/w) glycerol were dissolved in 18.8mL of milli-Q water at 85°C under magnetic stirring until total dissolution of the PVA.
- Eudragit formulation: 3.33g polymethacrylate polymer (Eudragit® FS 30D) 30% w/w and 0.2g triethylcitreate (TEC) were mixed in 17.47mL of milli-Q water.

2.1.3. Nanoparticles preparation

Different polymers were used for preparing nanoparticles. Briefly, 15mg of poly-ε-caprolactone (PECL), or poly lactic acid (PLA) or poly-gamma-benzyl-L-glutamate (PBLG) were dissolved in 5mL tetrahydrofuran (THF) at 30°C for 18h. These solutions were added dropwise to 10mL of milli-Q water under magnetic stirring. The mixtures were left under magnetic stirring for 15min and then transferred in a Teflon coated recipient. The solvent was gently evaporated under a light air flow. In order to eliminate residual solvent, nanoparticles were washed with 5mL of milli-Q water and evaporation was carried out to yield 10mL of nanoparticles suspensions.

Alternatively, polystyrene particles (Polybead®) of 1µm and 100nm in diameter were bought from Polyscience (France).

2.1.4. Film stretching experiments

2.1.4.1. Preparation of the filmogen solutions

Different filmogen solutions were prepared and the nanoparticles were dispersed in these solutions before film casting. The respective compositions of these suspensions are given in Table 2.1.

Table 2.1: Filmogen preparation composition

	PVA based film	PVA based film	Eudragit based film
Filmogen	1g PVA	1g PVA	3.33g Eudragit® FS 30D (30% w/w)
Plastifier	0.2g Glycerol	0.2g Glycerol	0.2g TEC
Deionised Water	18.4mL	Ø	Ø
PS particles	0.4mL	Ø	Ø
PECL or PLA particles	Ø	18.8mL	17.47mL

2.1.4.2. Film casting

Films containing dispersed particles were obtained as follows. 1mL of the different filmogen suspensions deposited on a freshly washed glass slide (5x3cm). Samples were left to dry at room temperature for 24h.

2.1.4.3. Film stretching

In a typical experiment, after removal from the glass plate, the film was clipped between the two fasteners and elongated to a specific length at a specific rate and temperature (See Figure 2.4).

2.1.4.4. Particle recovery and film elimination

After stretching the film, particles had to be recovered to be characterized. For this purpose, the film was dissolved in aqueous solutions. Eudragit based film were put in 10mL of milli-Q water. Upon addition of NaOH (2.5mol/L) the film dissolved. Similarly, PVA based films were dissolved in a solution of 30% isopropanol and 70% water at 65°C for 2h.

2.1.4.5. Purification of the recovered nanoparticles suspensions

After dissolution of the film, a suspension of the particles was obtained in which the water dissolved polymer composing the film had to be eliminated. For this purpose the particle suspension underwent an ultracentrifugation. Nanoparticles were centrifuged at 40,000rpm for 1h at 20°C while microparticles were centrifuged at 10,800rpm for 15min at room temperature. The residue composed of aggregated particles was re-suspended in the dissolution medium. Then it was sonicated and vortexed until total disappearance of the residue.

2.1.5. Transition Electron Microscopy (TEM) observations

Nano and microparticles shape and size were further analyzed through TEM (Transmission electron microscope, Philips EM208) at 60 kV. 3µl of particles suspension, after suitable dilution of bulk suspensions in milli-Q water, were placed on a formvar-carbon film previously coated on a copper grid (400 meshes). After 5 minutes of deposition, a drop of phosphotungstic acid (1%) or uranyle acetate was placed on the copper grid, on top of the sample. After 30s, the liquid was drained and the sample was placed inside the EM208 and pictures were taken. Particles measurements were obtained through Gimp© software.

2.1.6. Size and shape analysis

Particles suspensions from TEM pictures were diluted to a suitable concentration and after deposition the particles were supposed to be flat on the grid. For each sample, the dimensions of the particles were individually measured on different TEM pictures on an average of 30 nanoparticles (total). On each particle, the smallest and the longest size were measured and were respectively named width and length. The model chosen for shape analysis was that the obtained form of the nanoparticles was an ovoid. To assess the evolution of volumes with a parameter easily understandable the diameter of the sphere of equivalent volume was calculated using the formula on figure 2.2.

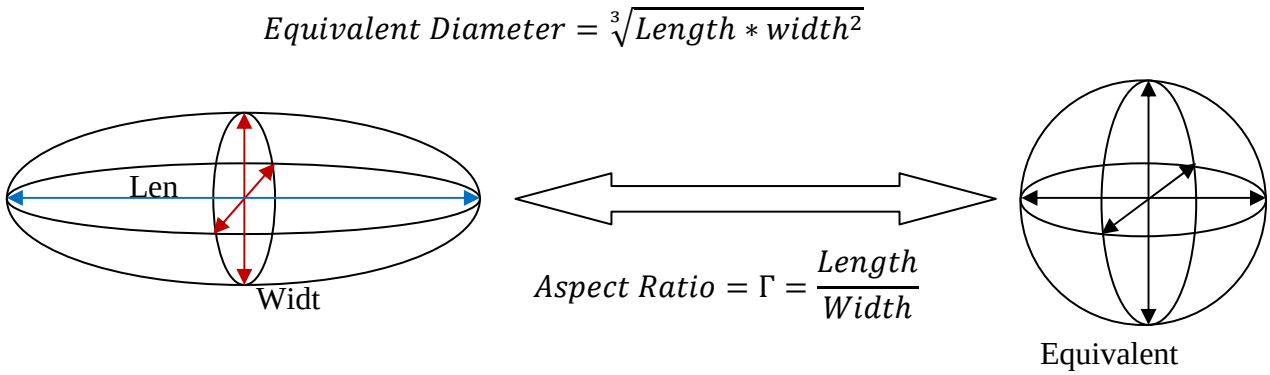

Figure 2.2: Nanoparticles size and shape analysis parameters

2.2. Results & Discussion

The goal of this study was to investigate the potential of the film stretching method to elongate particles, especially nanoparticles, in order to modify their shape in a controlled way and by using degradable polymers. Many articles have presented this technique and its promising results[16-17], but the study by Champion et al.[16] from the group of Mitragotri gave the wider array of shapes. So we tried to replicate their results in order to adapt this technology to pharmaceutically acceptable polymers. In the first part of this study we will describe the prototype used for film stretching, and the necessary steps to reproduce nano and microparticles elongation, then reproducibility problems will be tackled and finally the assays to adapt this technology for pharmaceutical applications will be detailed.

2.2.1. Reproducing Elongation Experiments

The first objective of our study was to reproduce the experiments undertaken by Champion et al[16]. for the manufacture of nano and microparticles of complex shapes. To do so we needed to recreate a prototypic apparatus for film stretching, with a control over stretching rate and temperature.

To achieve these experiments an oven was coupled with a stretching system. This system was composed of an electric engine which regulates the stretching speed (1 to 500mm/min), and of two fasteners, one that is fixed and one that is mobile. The film to be elongated can be placed between the two fasteners. The motor will stretch the film by moving the mobile fastener until it makes contact with the limit stop.

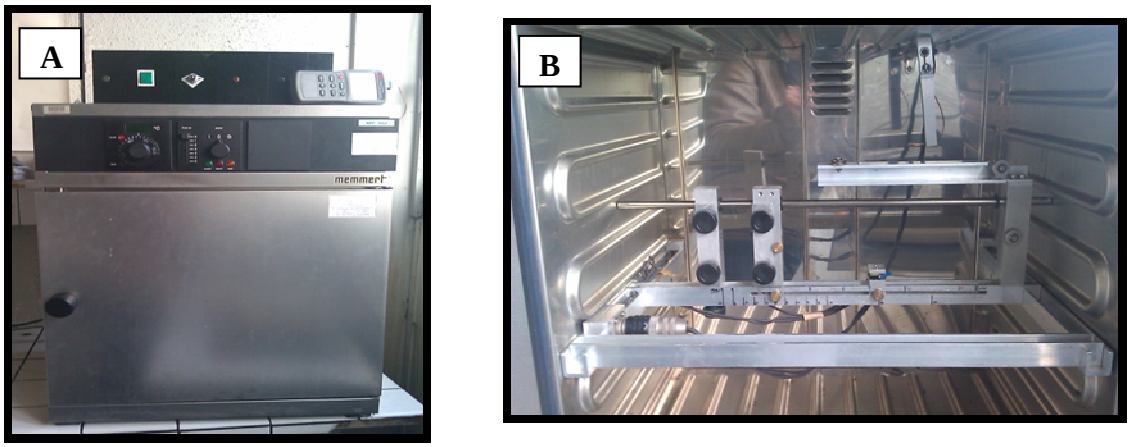

Figure 2.3 Photographs of the elongation prototype (A) Exterior of the oven with the motor on top (B) Interior of the prototype with the elongation system

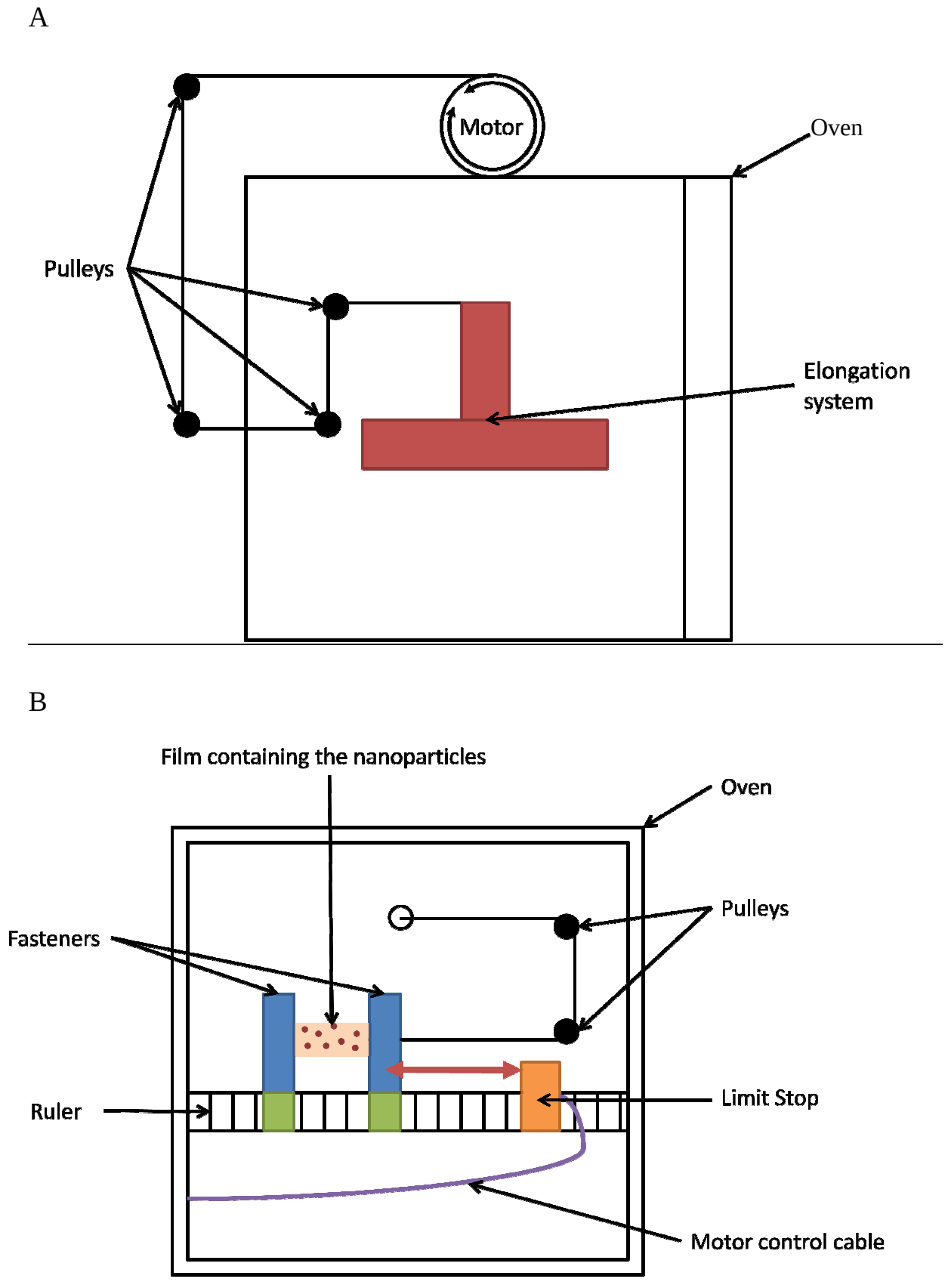

Figure 2.4: Elongation prototype (A) Side view showing the motor and the connections to the elongation system (B) Front view showing a film being elongated

This system made it possible to stretch a film to a controlled size, heat it and cool it in a row, and in any order. Recreating most of the non spherical particles presented in Champion et al.[16] was then possible.

The filmogen solutions were prepared as detailed in Champion et al.[16]. These solutions were casted either on Teflon or glass. Both surfaces allowed the manufacture of films. However and surprisingly Teflon surface interacted with the filmogen preparation and the film formed on this surface turned brown instead of transparent. Due to this interaction films were only prepared on glass surfaces.

Furthermore we tried to determine what the ideal volume was to prepare films that could be stretched the farthest without tearing. To do so different volumes of filmogen preparation were plated on 2.5cm x 5cm glass slides, namely 0.3mL, 0.5mL, 1mL, 1.5mL and 2mL. Under 0.3mL there was not enough liquid to cover the whole glass slide. 0.3mL and 0.5mL films tear at a smaller elongation than 1mL, 1.5mL and 2mL films. These latter films had excellent elongation properties, but the more the liquid plated on the glass, the stiffer the film was and the harder it was to elongate. Thus it was decided to work with films made from 1mL of filmogen preparation plated on 2.5cm x 5cm glass slides.

Different techniques were tested for drying: in an oven at different temperature (30°C, 40°C, 50°C), in a vacuum chamber at different temperatures (room temperature, 30°C, 40°C, 50°C), and on the bench at room temperature.

It was clear from these experiments that the higher the temperature, the quicker the film was ready. However, defaults appeared at the same time: in the oven and in the vacuum chamber, holes and uneven surfaces appeared. These defaults created weakness points in the film leading to an early tearing when the film was elongated. Furthermore, drying films at high temperature rendered them drier and consequently more breakable. The only method allowing the formation of film regular enough was by letting them dry slowly on the bench at room temperature. Spin coating the film would have lead to the formation of thickness controlled films, but this technology was not available in our facilities.

The dissolution of the films was ensured in a mix of 30% isopropanol and 70% milliQ water. After heating at 65°C under magnetic stirring for 2h the obtained solution was clear. Different volumes of the mixture were used to evaluate the minimum volume for achieving

the complete dissolution of the film (in order to recover the highest amount of particles). The optimal dissolution volume was determined to be 10mL for 7.5cm^2. These solutions were centrifuged and the residue was re-dispersed in the isopropanol/water mix and heated at 65°C for 2h under magnetic stirring.

2.2.2. Making non spherical particles

In a first step, attempts were made with the system to modify the shape of polystyrene particles. As in Champion et al. study[16], microparticles (1µm) were dispersed in PVA/TEC films. Furthermore, polystyrene nanoparticles (100nm) were also studied in the same conditions. The films were elongated to different final length. The final elongation ratios of the films were 1, 1.3, 1.6, 2, 2.6 and 3. After suitable recovery and purification, the particles were observed by transmission electron microscopy (TEM).

TEM microphotographs of the nano and microparticles before and after insertion in films and heating at 150°C without elongation are shown in figure 2.5 and 2.6, respectively.

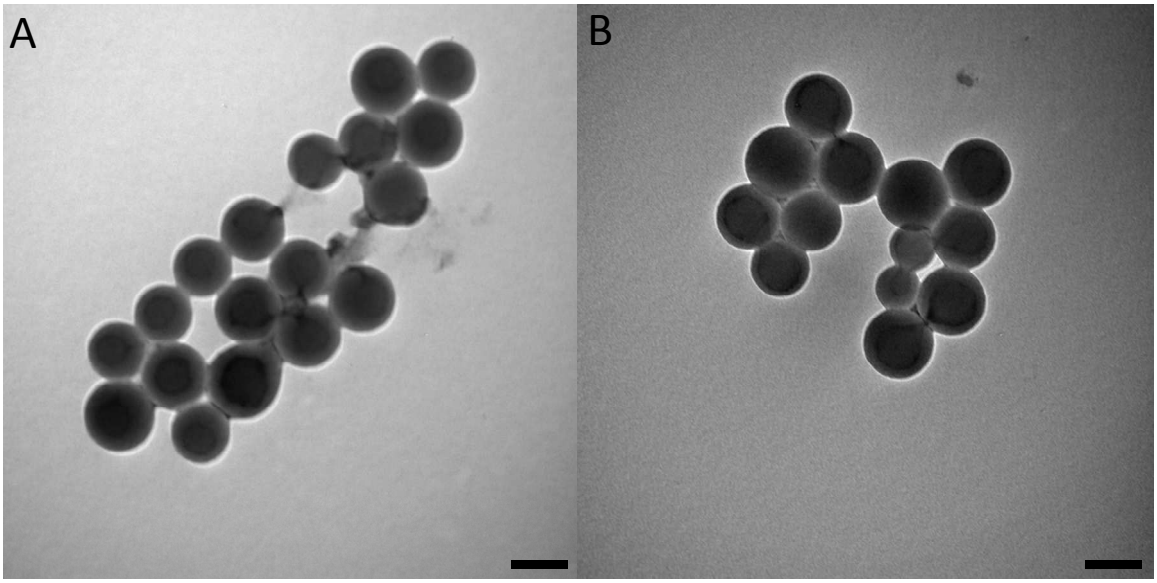

Figure 2.5: TEM micrographs of nanoparticles before (A) and after (B) insertion in films and heating at 150°C (Scale bars = 100nm)

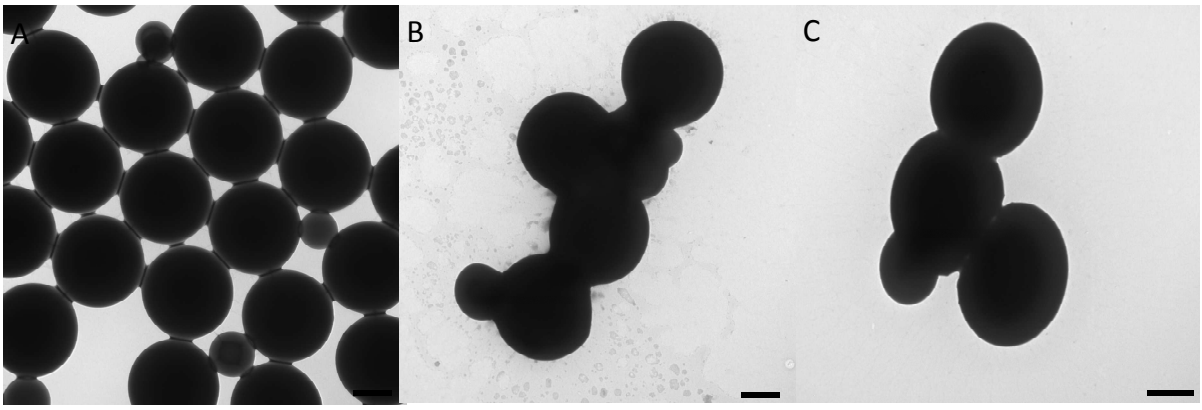

Figure 2.6: TEM micrographs of microparticles before (A) and after (B, C) insertion in films and heating at 150°C (Scale bars = 500nm)

Figures 2.5A and 2.6A show respectively nano and microparticles before elongation. They were spherical and their size was regular. The nanoparticles had a mean diameter of 114nm, whereas the microparticles a mean diameter of 1144nm. Their mean aspect ratios were respectively 1.04 ± 0.04 and 1.01 ± 0.02.

As a control a film for each kind of particles was not elongated, but underwent the same heating procedure at 150°C as for the other films which were intended to be stretched.

For nanoparticles, as shown on figure 2.5B, which is representative of the sample, the elongation did not vary the aspect ratio, which was 1.02 ± 0.02. However, the diameter of the nanoparticles was slightly increased from 114nm to 138nm.

For microparticles, as shown on Figure 2.6B and C, only moderate modifications of their morphologies were observed in these conditions and the aspect ratio of the particles ranged between 1 and 1.3. As for the nanoparticles, the size was slightly increased, as the mean microparticle diameter grew from 1.05µm to 1.27µm.

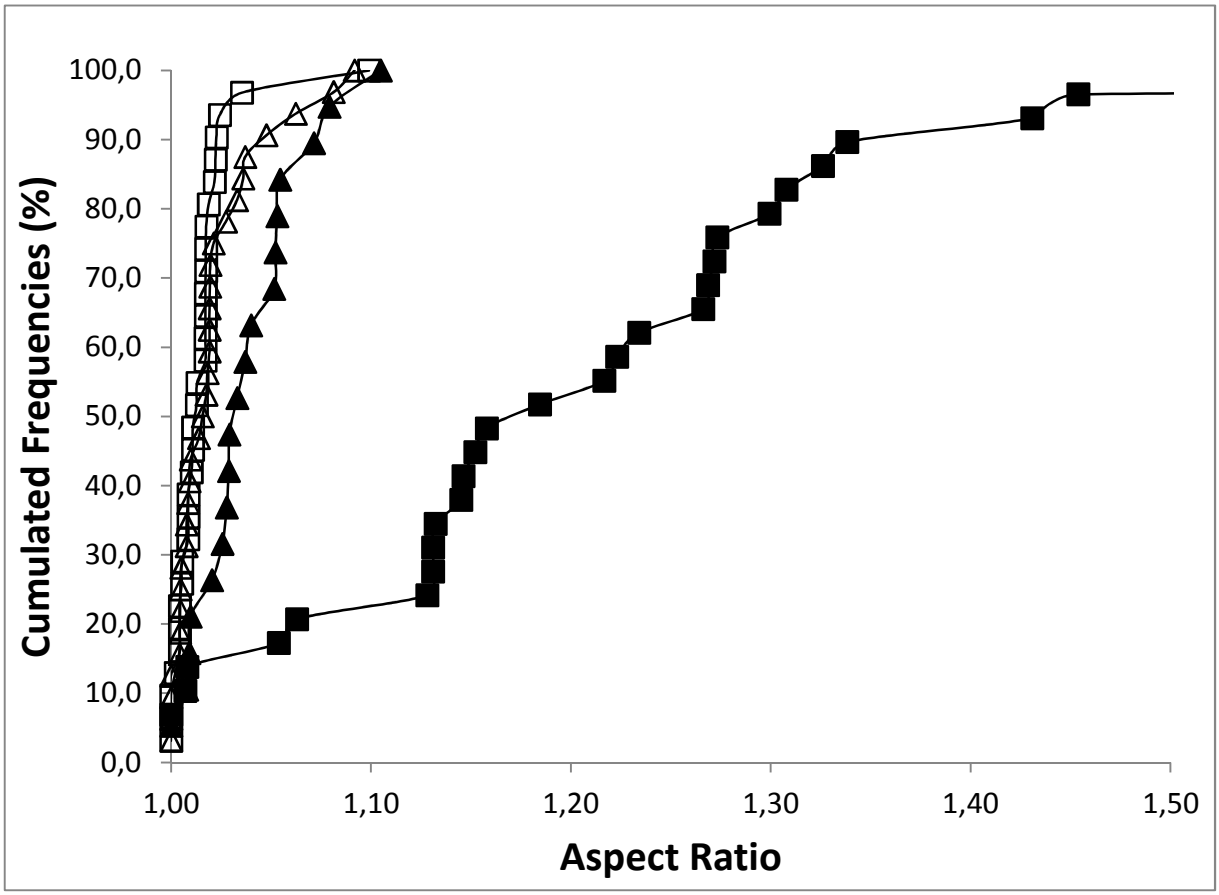

Figure 2.7: Microparticles and nanoparticles aspect ratios before (empty boxes and empty triangles, respectively) and after encapsulation in PVA based films, heating at 150°C and dissolution of the film (full boxes and full triangles, respectively)

Figure 2.7 shows the distribution of particles aspect ratio (length/width) for approximately 30 particles per sample (each symbol represents one particle). This shows that the impact of the encapsulation of the particles in film was low. Moderate deformations of microparticles were noticed, but almost not in the case of nanoparticles.

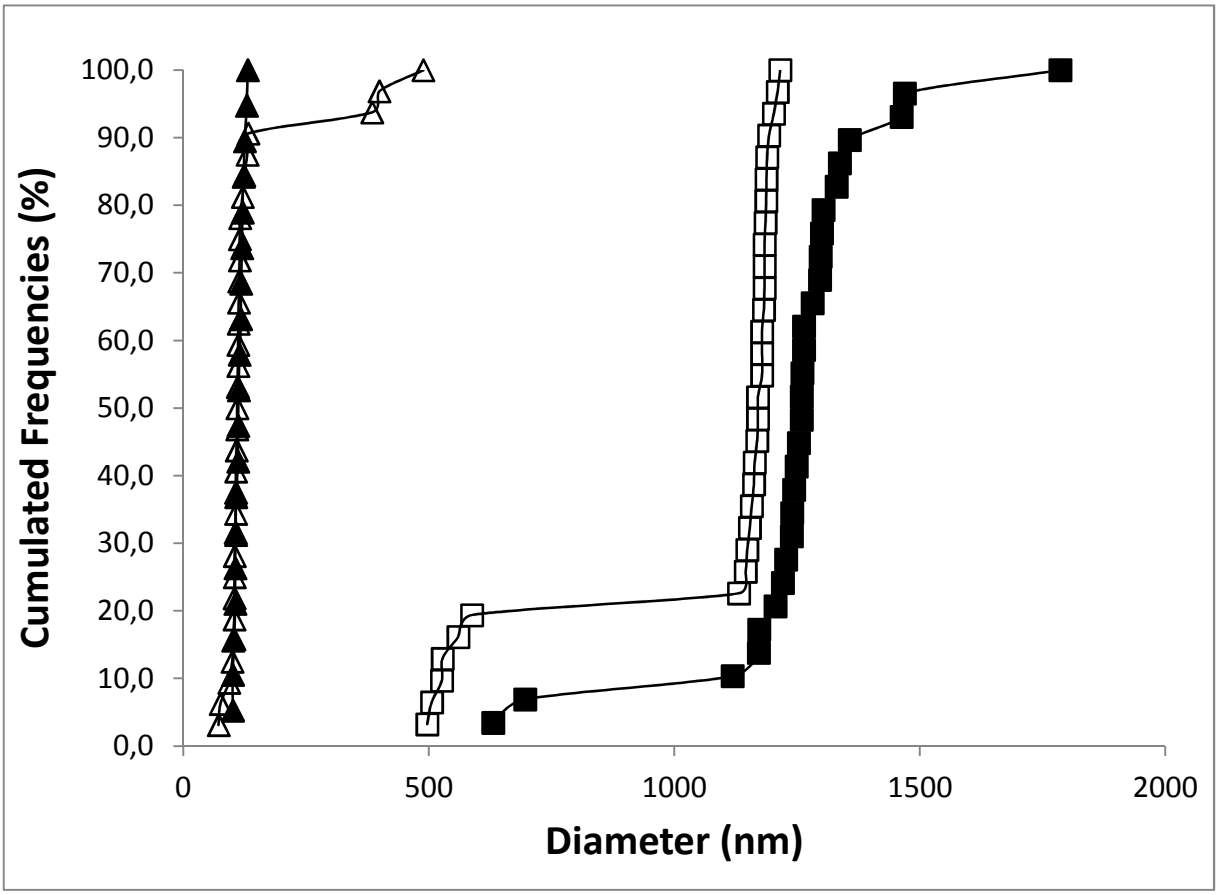

Figure 2.8: Distribution of sphere equivalent diameters of nano- and microsphere before (empty boxes and triangles, respectively) and after encapsulation in PVA based films, heating at 150°C and dissolution of the film (full boxes and triangles, respectively)

Figure 2.8 points out the impact of the dispersion of the particles in films on the size of particles. As can be seen the volume of the microparticles increased, while almost no increase occured for nanoparticles. Two phenomena can explain this increase in diameter: (i) either the film was not thoroughly eliminated (ii) or/and the particles have fused. If the film was not thoroughly eliminated we should observe a shift in the curve to the higher sizes, this shift can be of any value, and the TEM photograph can confirm the presence of residues of film. If the particles fused together another shift should appear, but this shift would present characteristic incremental values. Indeed if two particles fuse together, the volume of the fused particle is twice that of a single particle, which means that the diameter should be $\sqrt[3]{2} \approx 1.25$ times higher that of a single particle. Here the film encapsulation step makes the mean microparticle diameter increase from 1.05µm to 1.27µm. The ratio of these sizes was 1.21. The TEM pictures did not suggest the presence of film on the particles. The edges of the nanoparticles

were well defined, there was no shift in transparency of the particles, making most likely that microparticles may have fused two by two. The nanoparticles also presented such a phenomenon. Their mean diameter increased from 114nm to 138nm and no trace of film appeared on the surface of the particles. The ratio of the sizes before and after was 1.21 which suggests the same amount of fusion between nanoparticles.

This fusion problem could probably be solved by reducing the number of particles in the filmogen preparation. However, since the number of observable particles in a sample was already low, we decided to continue with these concentrations.

The second step of the study was to observe a controlled change in shape of the particles through a series of experiments covering a range of elongations of the films from 1 to 3 by steps of 1/3.

Figures 2.9 and 2.10 present some of the non spherical polystyrene particles that we were able to obtain. These TEM pictures show that non spherical, and considerably elongated, nano and microparticles could be obtained although the polydispersity in each sample was high and secondly the particles.

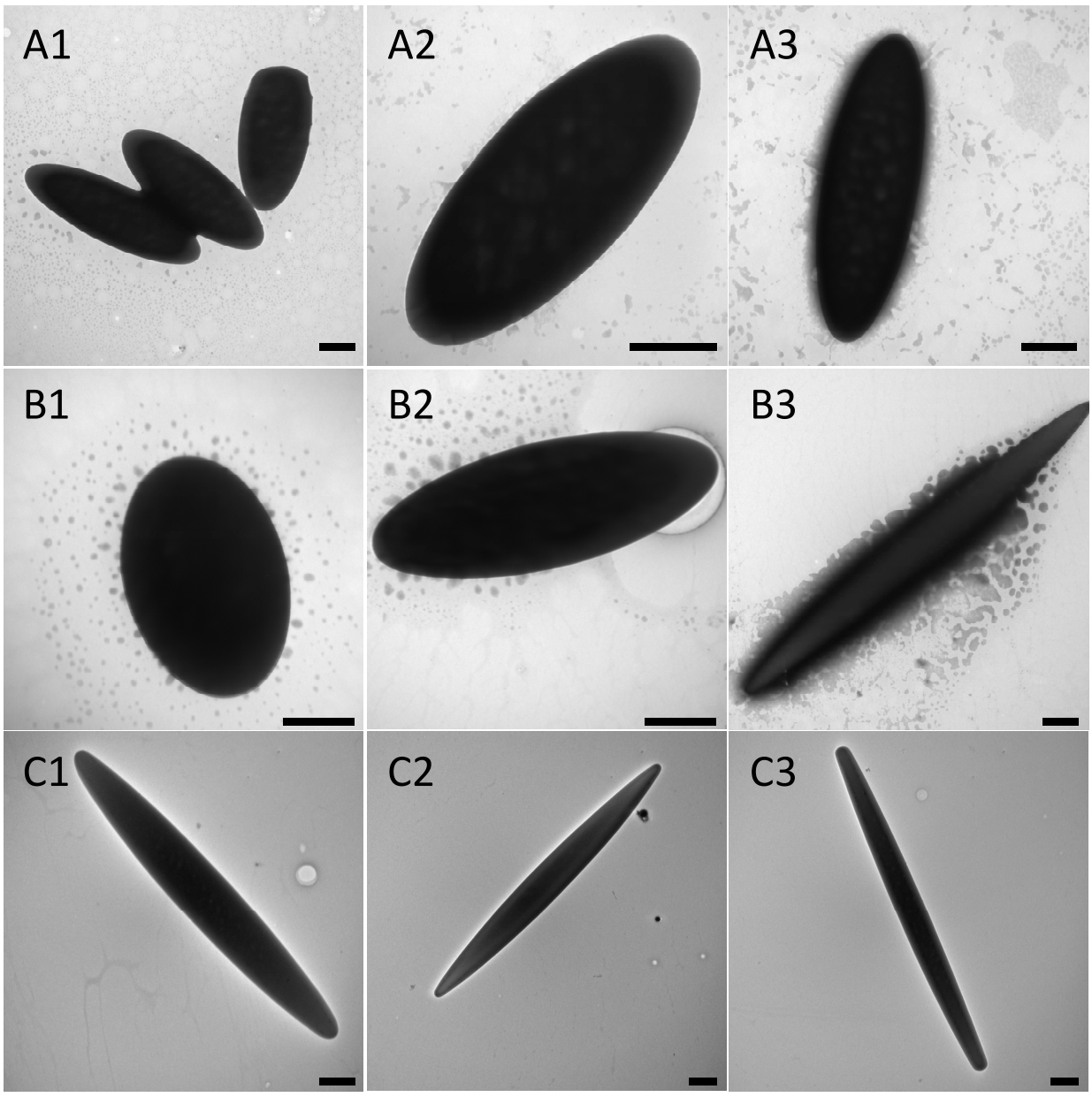

Figure 2.9: Non spherical polystyrene microparticles obtained by stretching of a film at 150°C (A) 1.6x (B) 2.3x (C) 3x . Scale bar = 500nm

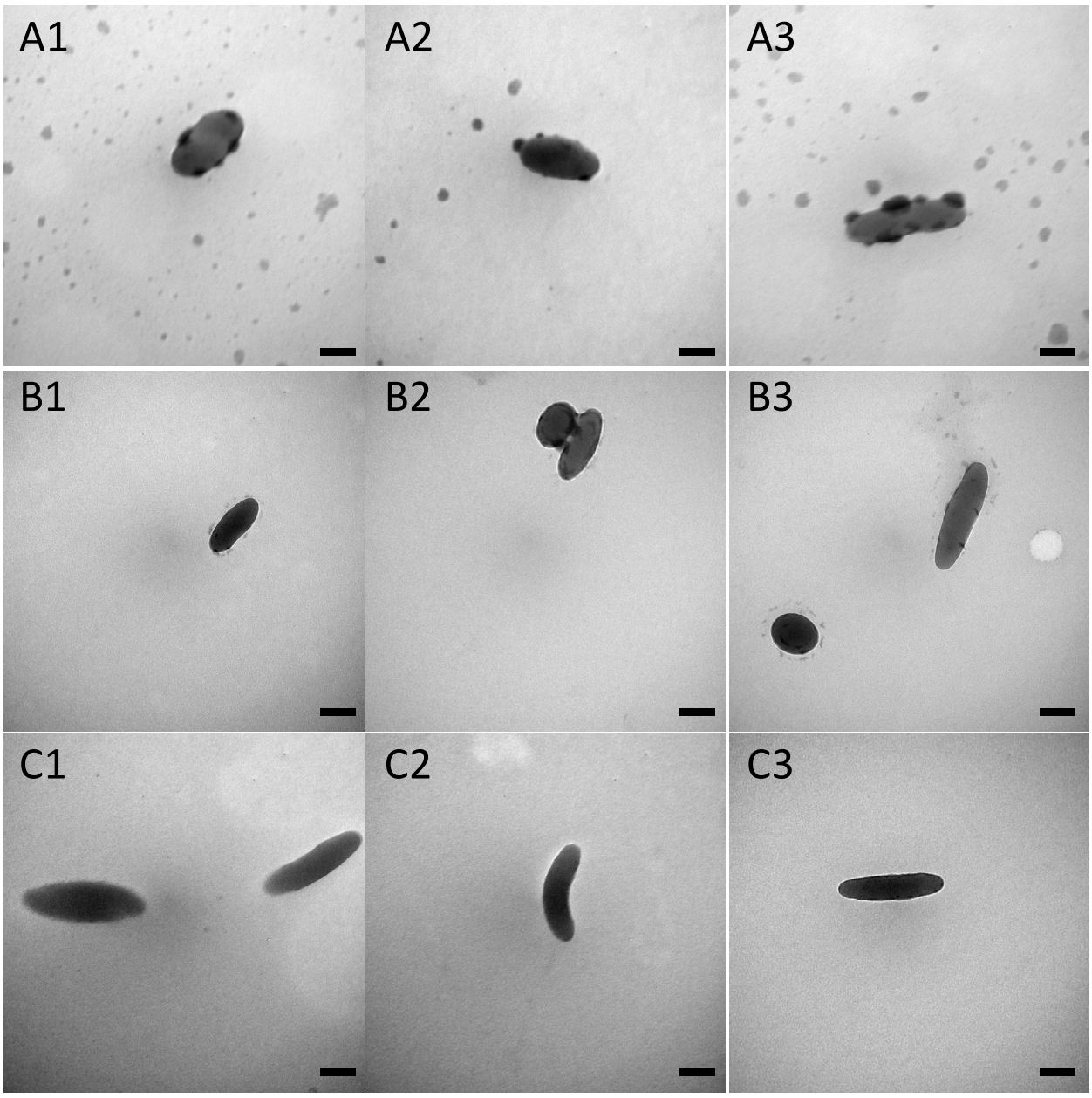

Figure 2.10: Non spherical polystyrene nanoparticles obtained by stretching of a film at 150°C (A) 1.6x (B) 2x (C) 3x . Scale bar = 100nm

The next figures 2.11 and 2.12 present the distribution of the aspect ratios for the nano and microparticles obtained for different elongations of the film

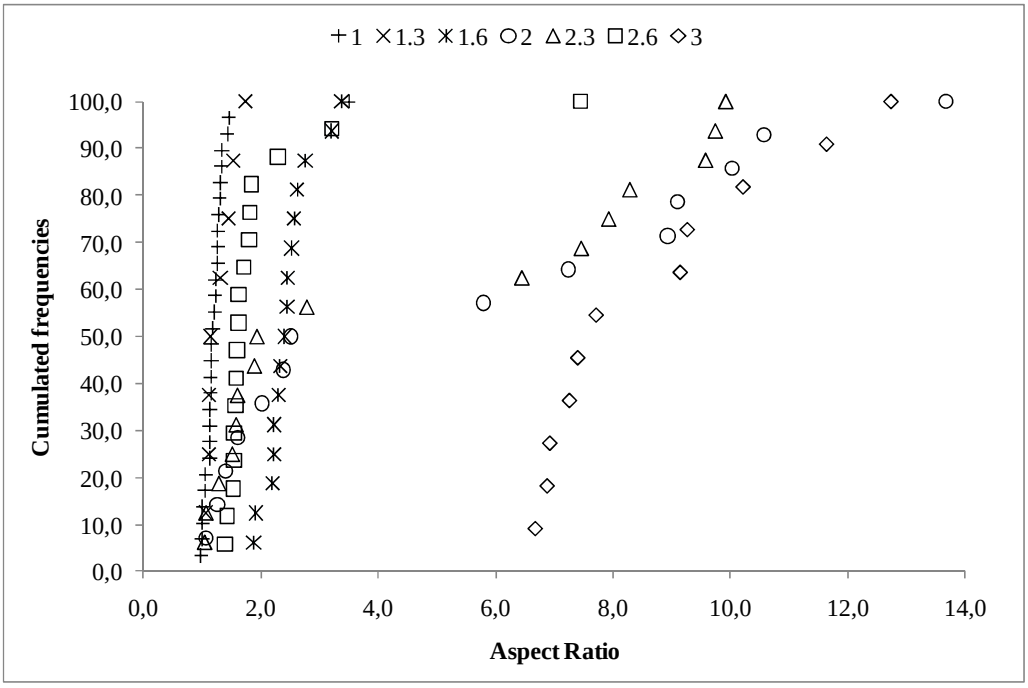

Figure 2.11: Aspect ratios of the microparticles after encapsulation in PVA based films, heating at 150°C, stretching at different elongations (see legend) and dissolution of the film

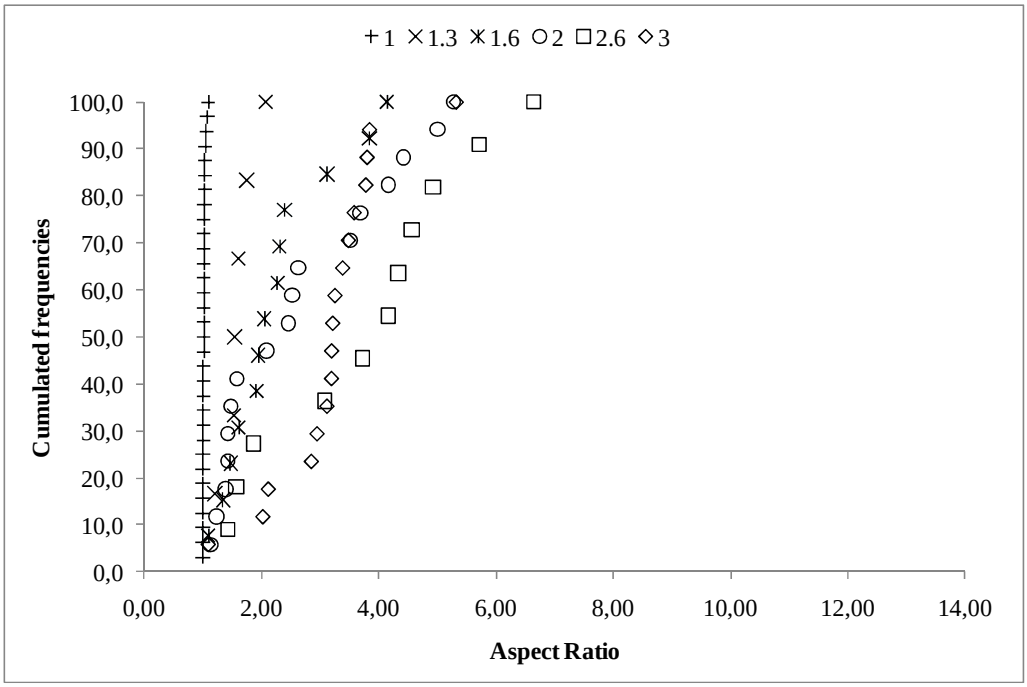

Figure 2.12: Aspect ratios of the nanoparticles after encapsulation in PVA based films, heating at 150°C, stretching at different elongations (see legend) and dissolution of the

film. Data at a film stretching of 2.3 was not shown because no particle could be recovered in the sample.

Figures 2.11 and 2.12 show that the elongation of the film at a temperature over the glass transition temperature of polystyrene effectively allowed the formation of non spherical micro- and nanoparticles. However, there was a wide variety of particle shapes for each elongation of the film.

Attempts were made to correlate both for the nanometric and micrometric levels the film elongation and the mean aspect ratio of the particles as shown on figure 2.13**.** It appears that the microparticles shape was more impacted by the elongation of the film than nanoparticles shape. The elongation of the film $E_{film} = \left(\frac{L_f}{L_i}\right)_{film}$ (L_i and L_f are respectively the initial and final length of the film) was not directly proportional to the aspect ratio of the particle $\Gamma = \left(\frac{L_f}{w_f}\right)_{particle}$. (l and L are respectively the initial (i) or final (f) width and length of the particle)

We were expecting the relation described as follows:

We expected that the volume remained the same during deformation of the particles: $V_f = V_i$ and that the elongation of the particles was equal to that of the film: $\left(\frac{L_f}{L_i}\right)_{particle} = E_{film}$

For the particles: $V_i = \frac{4}{3}\Pi \left(\frac{L_i}{2}\right)^3$ *and* $V_f = \frac{4}{3}\Pi \frac{L_f}{2} * \left(\frac{w_f}{2}\right)^2$

$$V_f = \frac{4}{3}\Pi \frac{L_f}{2} * \left(\frac{L_f}{2 * \Gamma}\right)^2 = \frac{4}{3}\Pi * \frac{1}{\Gamma^2} * \left(\frac{L_f}{2}\right)^3$$

$$\frac{V_f}{V_i} = 1 = \frac{1}{\Gamma^2}\left(\frac{L_f}{L_i}\right)^3 = \frac{E^3}{\Gamma^2}$$

$$\boxed{\Gamma = E^{(3/2)}}$$

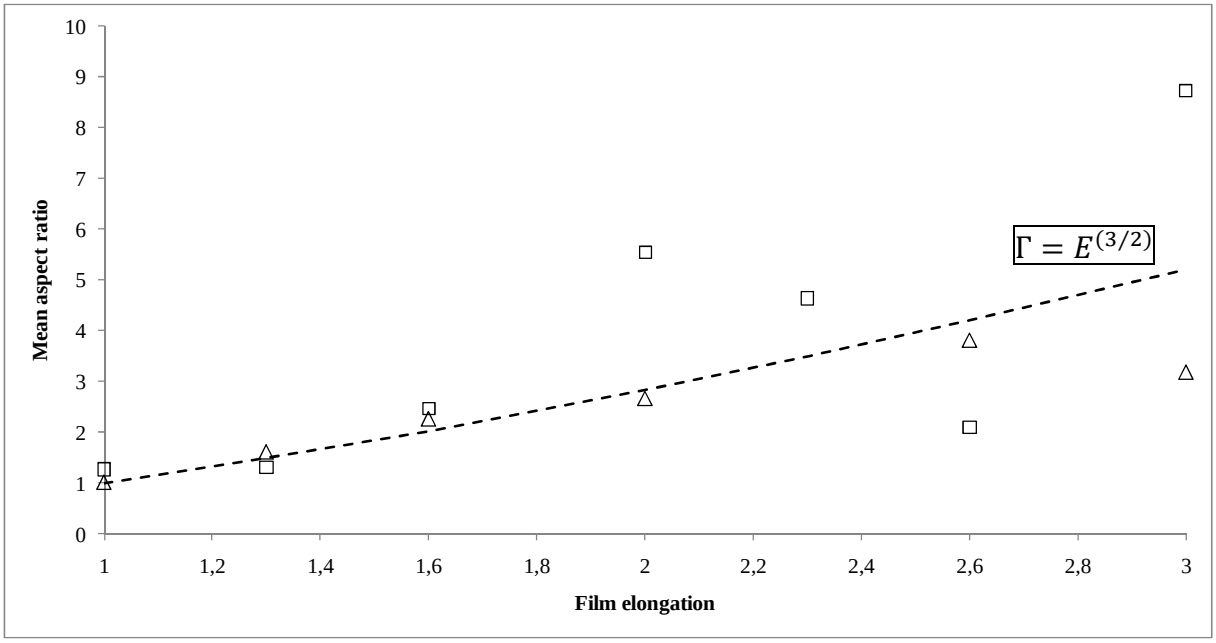

Figure 2.13 Mean aspect ratio of the nano (triangles) and microparticles (squares) and the theoretical aspect ratio.

This relationship was verified only in the region of low film elongations for micro and nanoparticles. However at higher film elongations (above 2 for microparticles and 2.6 for nanoparticles) the deformations were not as expected. Still because of the high variability for those elongations in these samples of a few particles, the relationship might be respected. Experiments should be repeated on a higher number of particles.

Figures 2.14 and 2.15 present the distribution of the sphere equivalent diameters of the micro- or nanospheres were plotted. They depict the evolution of the particles volume.

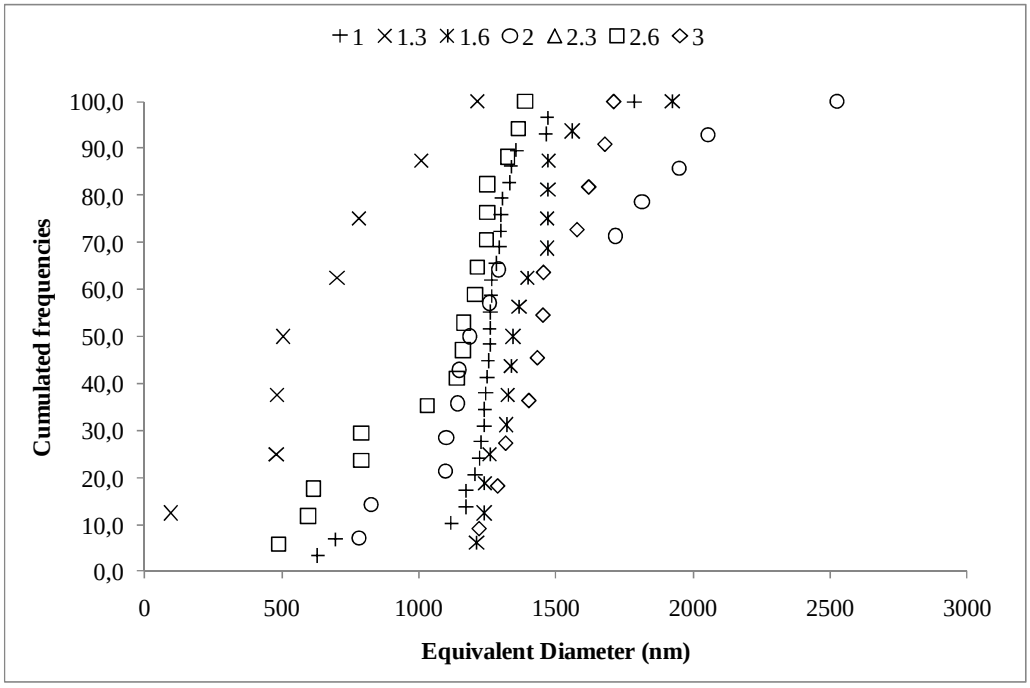

Figure 2.14: Sphere equivalent diameters of microspheres after encapsulation in PVA based films, heating at 150°C, stretching at different elongations (see legend) and recovery by dissolution of the film

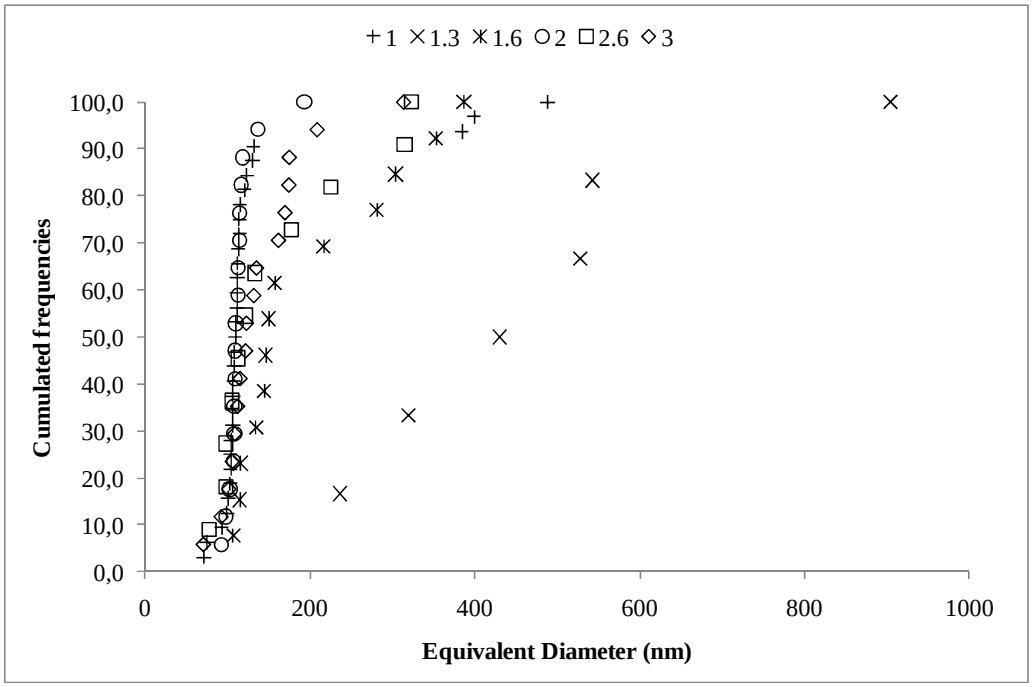

Figure 2.15: Sphere equivalent diameters of nanospheres after encapsulation in PVA based films, heating at 150°C, stretching at different elongations (see legend) and recovery by dissolution of the film

On figures 2.14 and 2.15 the cumulated frequencies of the sphere equivalent diameter of the non spherical particles are plotted. For both nano and microparticles more or less important shift in the distribution compared to the industrial sample were observed. However, no obvious relationship between the elongation of the films and the fusion of particles appeared.

2.2.3. Understanding the reasons behind the variability

In order to understand the phenomenon causing variability in particle elongation, the experiments previously described were repeated. For better understanding the mode of stretching of the film, a grid of 5mm squares was drawn on it before elongation. The film was scanned before and after elongation as shown on figure 2.16.

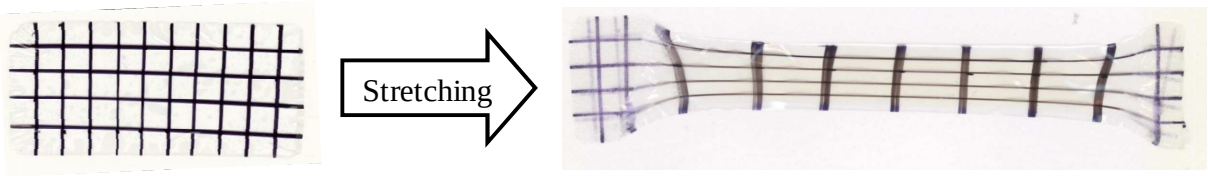

Figure 2.16: PVA film and its grid before and after stretching. Squares of 5mmx5mm

As can be seen on figure 2.16 the grid on the film before stretching was uniform, but after stretching the squares were not all elongated to the same ratio. The extremities of the film that were not stretched corresponded to the part of the film that was contained in the fasteners.

For better understanding, each square was measured before and after stretching. From these measurements we calculated the elongation (L_f/L_i) and the aspect ratio (L_f/l_f) of each square, which were tabulated in table 2.2 and 2.3 for two film samples.

Table 2.2: Example of grid elongation patterns for different stretching on films containing microparticles

Film stretched x1										
1.05	1.04	0.92	1.07	1.17	1.19	1.24	1.21	1.11	1.1	1.00
1.02	1.02	1.04	1.07	1.23	1.44	1.32	1.29	1.26	0.92	1.00
1.00	1.00	1.04	1.03	1.12	1.39	1.50	1.35	1.15	0.91	1.00
1.00	0.94	1.23	0.94	1.14	1.36	1.47	1.28	1.25	0.98	1.00
1.00	0.93	1.00	1.16	1.25	1.15	1.18	1.15	1.22	1.04	1.00
Film stretched x1.5										
1.00	1.22	1.57	1.57	1.60	1.60	1.74	1.95	2.06	1.09	1.02
1.00	1.14	1.39	1.56	1.73	1.75	1.76	1.66	1.88	1.08	1.02
0.96	1.17	1.43	1.60	1.83	1.78	1.68	1.49	1.92	0.98	0.98
1.00	1.19	1.46	1.62	1.85	1.88	1.75	1.68	1.66	0.98	1.00
1.00	1.27	1.4	1.54	1.73	1.7	1.74	2.21	1.46	0.98	1.00
Film stretched x2										
0.80	1.32	1.89	2.45	3.19	3.85	4.02	3.00	0.98	1.02	1.04
0.83	1.35	1.63	2.44	3.59	3.99	3.87	2.34	1.00	1.00	1.25
0.88	1.39	1.69	2.53	3.53	4.19	3.88	2.59	1.02	0.98	1.48
0.98	1.52	1.97	2.75	3.81	4.04	4,00	2.88	1.00	1.00	1.98
1.05	1.42	2.65	2.66	3.66	3.79	3.87	3.00	1.00	1.17	NA
Film stretched x2.5										
1.00	1.38	3.31	3.50	3.64	3.84	3.95	3.87	4.04	2.71	1.20
0.89	1.34	2.43	3.13	3.35	3.83	4.04	3.50	3.16	2.17	1.16
0.96	1.58	2.51	3.41	3.76	3.71	4.11	3.65	3.01	2.42	1.09
1.15	1.60	3.12	3.68	4.01	4.02	4.02	4.33	3.86	2.19	0.89
1.11	1.36	3.38	3.63	3.74	4.11	4.00	4.58	5.12	1.62	0.97
Film stretched x3										
1.00	1.31	NA	7.94	7.11	7.49	7.24	7.16	7.04	NA	1.17
0.98	1.02	NA	4.25	5.86	6.93	6.15	5.08	3.97	NA	1.02
1.02	1.05	NA	3.65	5.77	7.15	5.73	5.24	3.85	NA	1.02
1.02	1.16	NA	4.16	5.23	6.93	5.83	5.67	3.94	NA	1.00
1.00	NA	NA	3.66	4.66	5.40	5.14	5.27	4.32	NA	0.90
Film stretched x3.5										
0.95	3.06	3.65	5.15	6.49	7.32	7.47	7.71	9.44	NA	1.10
0.87	3.00	3.22	5.35	6.77	7.19	7.07	6.20	7.18	NA	1.00
0.93	2.44	3.32	4.57	6.77	6.42	6.36	5.59	7.22	NA	1.05
0.92	2.30	3.78	4.43	6.78	6.74	6.82	6.21	8.07	NA	1.02
1.01	2.51	3.07	4.66	5.32	5.91	6.65	6.78	7.06	NA	1.11

Table 2.3: Example of grid elongation patterns for different stretching on films containing nanoparticles

Film stretched x1										
1.07	0.98	0.98	1.02	1.19	1.15	1.10	1.33	1.28	1.07	1.00
0.96	0.94	0.96	1.05	1.22	1.12	1.15	1.33	1.28	0.96	0.96
0.98	0.96	0.94	0.98	1.28	1.15	1.10	1.20	1.31	0.98	0.96
1.00	0.98	1.02	1.05	1.23	1.13	1.07	1.21	1.26	1.00	0.98
1.00	0.92	1.07	1.02	1.11	1.05	1.05	1.18	1.23	1.00	0.96
Film stretched x2										
1.07	2.67	5.68	4.04	3.24	2.34	2.18	1.78	1.67	1.11	1.13
0.96	2.25	4.79	3.38	2.73	2.03	2.15	1.50	1.90	1.11	1.08
0.98	2.56	4.33	3.41	2.77	2.13	1.95	1.40	1.82	1.00	1.08
1.00	2.12	3.88	3.40	2.67	2.00	1.89	1.24	2.00	1.02	1.08
1.00	3.78	6.00	4.07	2.59	1.97	2.03	1.59	2.34	1.02	1.10
Film stretched x3										
1.07	1.00	6.21	6.45	5.52	5.67	5.41	4.75	4.12	1.67	1.00
0.96	0.96	4.81	5.04	5.21	5.54	4.42	4.23	3.27	1.90	0.96
0.98	0.96	4.73	4.93	4.56	4.72	4.15	3.89	3.10	1.82	0.96
1.00	0.98	5.15	5.35	4.77	4.50	4.42	4.00	2.94	2.00	0.98
1.00	0.96	6.83	6.17	5.25	4.88	4.42	4.29	3.73	2.34	0.98
Film stretched x3.3										
1.07	1.02	1.29	2.68	3.11	2.93	4.38	7.70	12.18	NA	NA
0.96	1.08	1.59	2.52	2.79	3.14	4.58	6.18	10.05	NA	NA
0.98	1.06	1.72	2.53	2.75	2.93	4.38	5.17	8.38	NA	NA
1.00	1.06	1.86	2.75	2.40	3.14	4.38	4.83	7.36	NA	NA
1.00	1.08	1.74	2.73	2.83	3.36	4.64	5.13	6.38	NA	NA

Table 2.3 presents the elongation of the grids. Firstly the deformations of the films were not uniform. Furthermore when comparing films undergoing the same stretching but containing different kinds of particles, differences could be pointed out, which means that the stretching of films was not repeatable. This may result from soft and hard regions in the films.

In these experiments each film was cut in regions of different aspect ratio and each region of the film was dissolved and purified separately to recover the particles.

Analysis of size and shape of the particles by TEM is presented on figure 2.17.

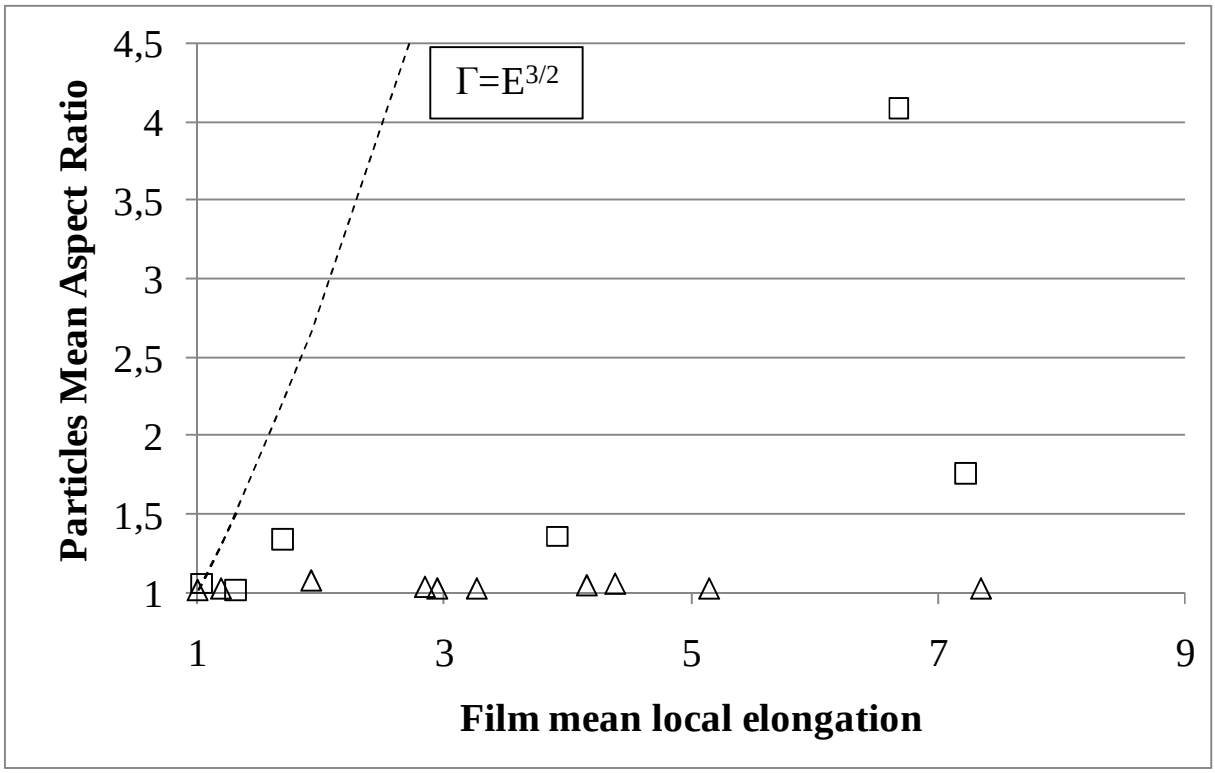

Figure 2.17 Mean aspect ratio of polystyrene nano (triangles) and microparticles (squares) and the theoretical aspect ratio (dashed line).

As can be seen on figure 2.17, and as was observed for the first series of experiments, nanoparticles were less deformed than microparticles. Furthermore, when comparing particles aspect ratio to the local elongation of the film, it appeared that the particles, whatever their size range, were less deformed than expected.

We have elements to understand the differences in aspect ratios of the particles. At a macroscopic level we observe differences in elongation of the squares of the grid, rationally at

a microscopic level and even more at a nanoscopic level these differences are even more important. It is only logical to find these differences in the deformation of the particles (e.g. nanoparticles could be located in a zone free of elongation, but in a square that is deformed at a macroscopic level).

Once more nanoparticles were harder to deform, in this case they were even not deformed. This might stem from the fact that to deform the liquid particles the film must apply a force stronger than the surface tension of the particles. The surface tension force is proportional to a surface and requires contact of the particle with the film, whereas the force applied to the particle by the film is proportional to a length (modelisation of the particle as a spring). So the ratio of the deformation against the surface tension is inversely proportional to a length. It is 10^3 times harder to deform a nanoparticle than a microparticle. This could explain what we observed in these experiments. Furthermore only specific regions of the film were observed; nanoparticles may have been deformed elsewhere in the film.

2.2.4. Adapting the system to degradable polymers

To adapt this technology for pharmaceutical applications, such as drug targeting, a few modifications had to be made. First the type of filmogen preparation had to be changed, then other degradable polymers were used instead of polystyrene.

2.2.4.1. Film material

Champion et al.[16] used PVA for their filmogen preparation. However PVA was difficult to completely eliminate, especially for particles covered with PEG chains (for stealth). PVA in surface would change the biological properties of the particles. Therefore, in order to use this technology for pharmaceutical applications, other filmogen preparations were evaluated using filmogen preparations currently used in the pharmaceutical industry.

Opadry®II, a hydroxypropyl methylcellulose film, can be dissolved by addition of a base in aqueous solution (here a NaOH solution, for a final pH=7-8). This film was easily stretched. Still after 24h, during TEM observation, the film was found not to be completely dissolved.

Kollicoat IR® is a PEG-PVA copolymer. It is water soluble and is announced to yield 105% elongation before rupturing. Dissolution tests revealed fast elimination of the film

(<1min), but in practice the stretching properties were never over 25% elongation before rupture even with a plasticizer.

Finally Eudragit®FS 30D with TEC as a plasticizer presented the best properties, for a formulation of 5% w/w Eudragit®FS 30D with 20% w/w TEC the film could easily be stretched up to 1000% and dissolution was done by addition of NaOH.

Observation in TEM with phosphotungstic acid revealed precipitation of the Eudragit®FS 30D. Thus, we used uranyle acetate for the observation of the particles deformed with this film. This revealed the necessity of a thorough purification. Regular and ultracentrifugation step have been optimized to completely eliminate film residues. Nanoparticles were centrifuged at 40,000rpm for 1h at 20°C while microparticles were centrifuged at 10,800rpm for 15min at room temperature. The residue was re-suspended in the dissolution medium. Then, it was sonicated and vortexed until total disappearance of any residue.

Eudragit®FS 30D could be a viable option for pharmaceutical applications, especially because it is already used as a coating agent for tablets. Further experiments were made with this film composition.

2.2.4.2. Nanoparticles

Different types of nanoparticles prepared from degradable polymers were selected to be tested for deformation through film stretching.

First, poly(gamma-benzyl-L-glutamate) (PBLG) nanoparticles were tested. However after several attempts no deformation was observed. This was not really surprising as PBLG chains form quite rigid rods which may organize the internal structure of the PBLG nanoparticles (see Chapter3), making them harder to deform.

Further attempts were made with poly(lactic acid) (PLA) nanoparticles. For this purpose, PLA nanoparticles of 94±23nm with an aspect ratio of 1.1±0.1 were used. The film containing these nanoparticles were stretched 1.6, 2.4 and 4.9 times at 150°C in the elongation prototype. To complete this study, we tried an alternative way of deforming the particles by first stretching 1.6 times the film and then heating the film to 150°C. This last trial was supposed to form barrels or bullets according to Champion et al.[16]. Figure 2.18 presents the non

spherical nanoparticles which were obtained with this method. As for previous experiments, these pictures illustrate both the deformability of the PLA nanoparticles and the polydispersity of the samples.

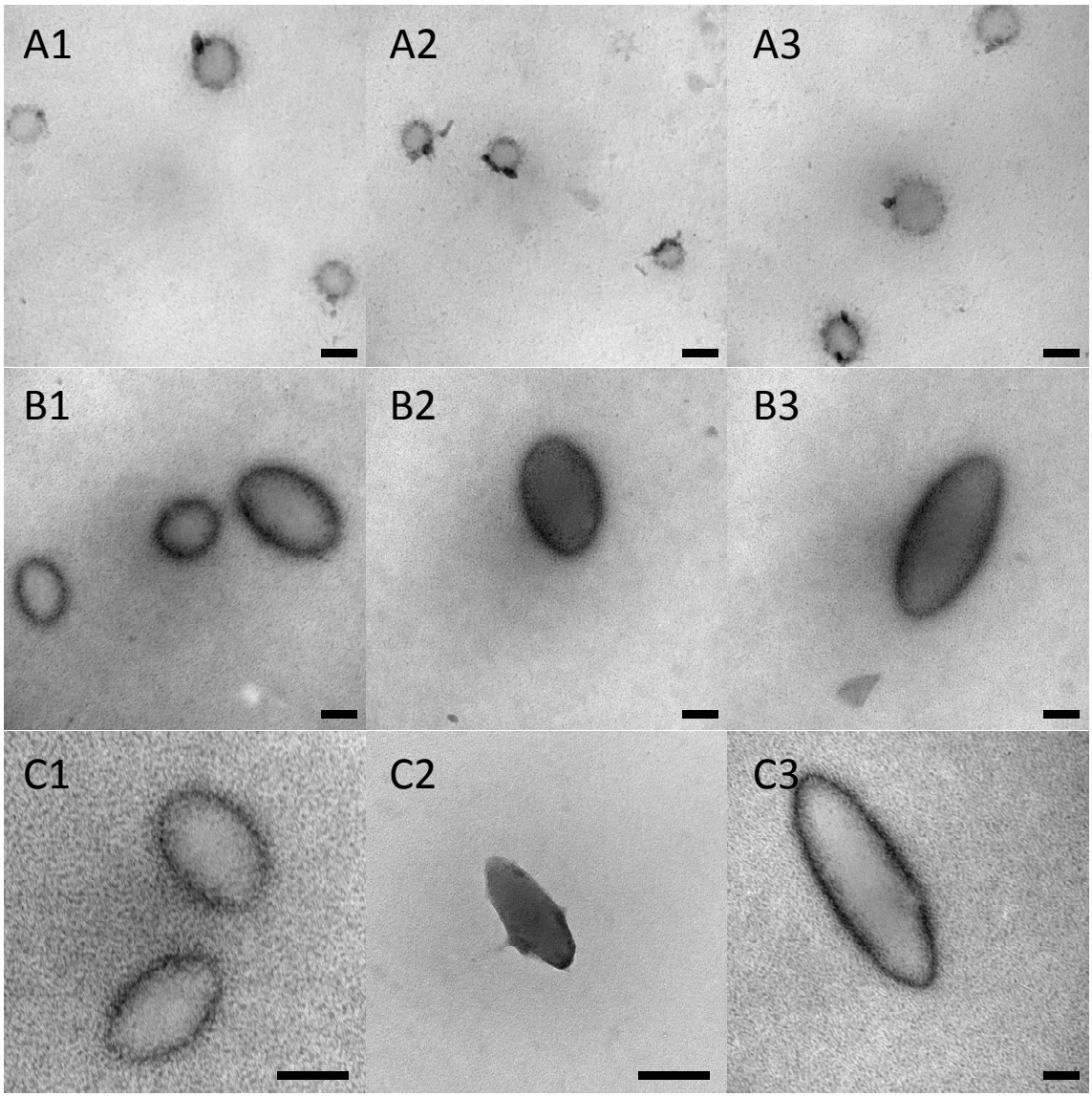

Figure 2.18: PLA nanoparticles deformed by the elongation technique. Film stretched after heating:(A) 1x (B) 1.6x (C) 2.4x. Scale bar = 100nm

Figure 2.19 presents the results of the adaptation of the non spherical particle production through the film elongation technique. We obtain here spheroïdal particles. The nanoparticles that were obtained by the alternative method (not shown here) present the same profile as those made with the regular method at the same elongation. We find here the same limitations as before, that is to say high sample variability in shapes, and the difficulty to completely

eliminate the film residues, even if this film is more efficiently eliminated than PVA (see figure 2.10).

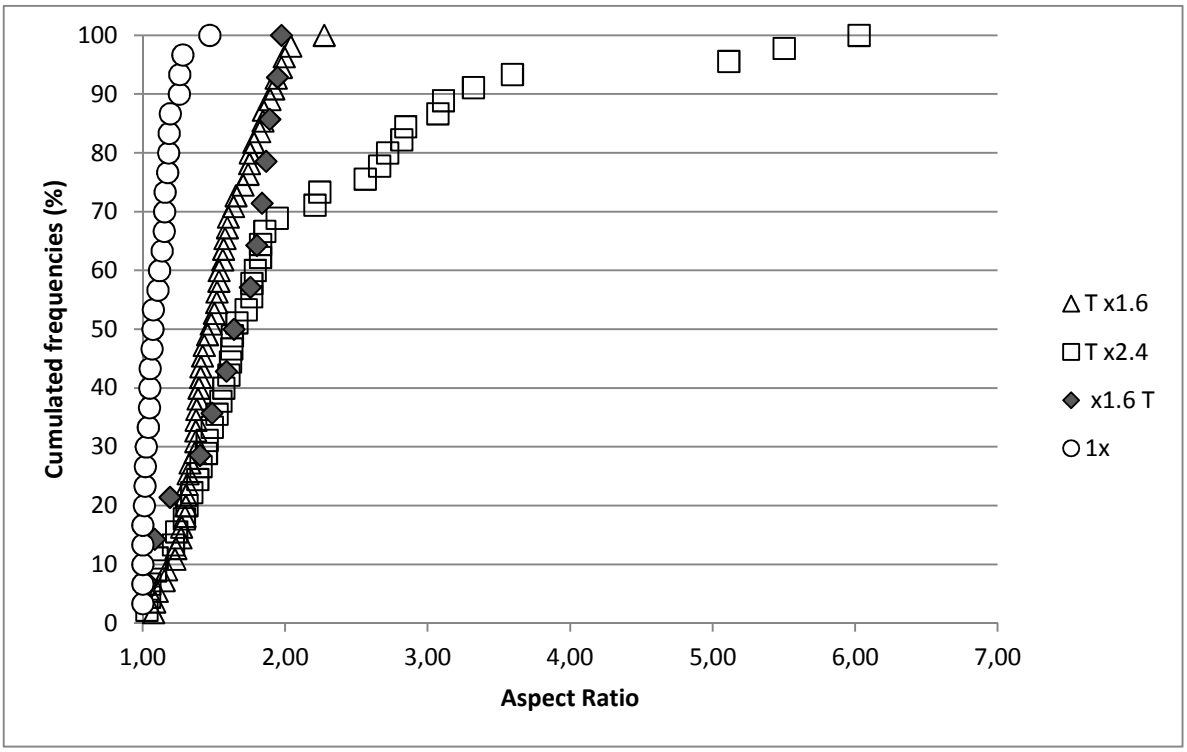

Figure 2.19 PLA Nanoparticles aspect ratio for different film elongation at 150°C. (○)x1 (△,◆)x1.6 (□)x2.4. ○, △ and □ particles were first heated, then elongated whereas ◆ particles were first elongated and then heated.

Figure 2.19 represents the PLA nanoparticles aspect ratio for different elongations of the film and modus operandi. Up to an elongation of 1.6 the variability of the aspect ratio of the samples was low, which confirmed that the stretching method yields once again not uniformly deformed particles.

Moreover we noticed a variability of the particles sizes during the TEM observations.

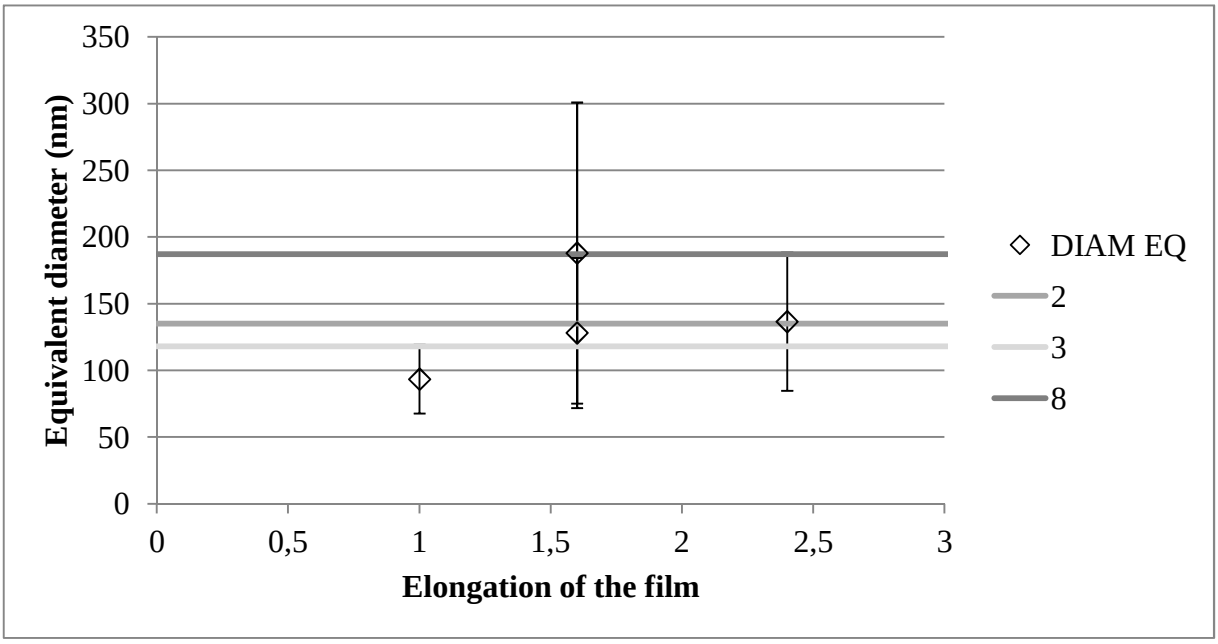

Figure 2.20: Mean equivalent diameter of the PLA nanoparticles for different film elongation at 150°C. The gray lines represent the equivalent diameter of 2, 3 and 8 nanoparticles fused together.

Figure 2.20 suggests that several nanoparticles have fused together during the deformation process. This study shows that it is effectively possible to adapt this technique for other polymers than polystyrene, by changing the nature of the filmogen preparation.

Conclusion

The results shown here do not aim to present a perfect manufacturing technique to produce non spherical nanoparticles. Rather our aim was to investigate the possibility to develop this technique in the case of nanoparticles and using other polymers than polystyrene. In fact these experiments underline the progresses that have to be made to ensure a repeatable and uniform process to produce non-spherical particles.

We have created a prototype from the data given in the publication presenting this method by Champion et al.[16]. Then we were able to reproduce some of their experiments by encapsulating polystyrene 1µm microparticles in polyvinylalcool films and stretching them at 150°C. These experiments were completed by their repetition with 100nm nanoparticles to assess the possibility of adapting this technology to nanoparticles. We achieved changing the shape of both micro and nanoparticles, even though a few technological bottle-necks were discovered, including: (i) the high variability of shapes in a sample obtained from one film; (ii) fusion takes place between particles and (iii) nanoparticles seemed to be less prone to be deformed by elongation. By studying these technological bottlenecks we have noted that the polydispersity of shapes in our sample may be caused by the polydispersity of stretching in different regions of the film. We also suggest that the difficulty to obtain very elongated nanoparticles may arise from the differences in specific forces at different volumes, and that it is difficult to obtain nanoparticles of high aspect ratios because it would require a lot of energy to drastically rearrange the chains inside the particles. Still we have tested the adaptability of this method by changing the nature of the stretching film. Eudragit® FS 30D proved to be interesting for this purpose. Finally, our results demonstrated the possibility to obtain non spherical poly(lactic acid) nanoparticles.

As a conclusion, the stretching film process to obtain non spherical nanoparticles looks promising, despite a series of drawbacks. Whatever, a lot of work is required to master this technology and obtain uniform samples before it could be used for preparing sufficient particles amounts in view of *in vitro* or *in vivo* studies.

Acknowledgements

We would like to thank Jean-Jacques Vachon for the realization of the elongation prototype. We also would like to thank Marion Santacreu, Cindy Roussard, and Naïla El Kechaï for their participation to this work.

We would like to thank Danielle Jaillard (CCME, Paris XI, Orsay) for her help with the TEM measurements.

References

1. Toksöz, S. & Guler, M.O.
Self-assembled peptidic nanostructures,
Nano Today, 4, 458-469, **2009**.

2. Scanlon, S. & Aggeli, A.
Self-assembling peptide nanotubes,
Nano Today, 3, 22-30, **2008**.

3. Balbo, B.M.A. & Stefan, H.
Wrapping peptide tubes : Merging biological self-assembly and polymer synthesis,
Angewandte Chemie. International edition, 44, 4, **2005**.

4. Dalhaimer, P., Engler, A.J., Parthasarathy, R. & Discher, D.E.
Targeted Worm Micelles,
Biomacromolecules, 5, 1714-1719, **2004**.

5. Kim, Y., Dalhaimer, P., Christian, D.A. & Dische, D.E.
Polymeric worm micelles as nano-carriers for drug delivery,
Nanotechnology, 16, S484, **2005**.

6. Jacob N. Israelachvili, D.J.M.a.B.W.N.
Theory of self-assembly of hydrocarbon amphiphiles into micelles and bilayers,
Journal of the Chemical Society., Faraday Trans. 2, 72, 1525 - 1568, **1976**.

7. Gillies, E.R. & Fréchet, J.M.J.
Dendrimers and dendritic polymers in drug delivery,
Drug Discovery Today, 10, 35-43, **2005**.

8. Ihre, H.R., Padilla De Jesús, O.L., Szoka, F.C. & Fréchet, J.M.J.
Polyester Dendritic Systems for Drug Delivery Applications: Design, Synthesis, and Characterization,
Bioconjugate Chemistry, 13, 443-452, **2002**.

9. Gratton, S., Napier, M., Ropp, P., Tian, S. & DeSimone, J.
Microfabricated Particles for Engineered Drug Therapies: Elucidation into the Mechanisms of Cellular Internalization of PRINT Particles,
Pharmaceutical Research, 25, 2845-2852, **2008**.

10. Gratton, S.E.A., Ropp, P.A., Pohlhaus, P.D., Luft, J.C., Madden, V.J., Napier, M.E. & DeSimone, J.M.
The effect of particle design on cellular internalization pathways,
Proceedings of the National Academy of Sciences, 105, 11613-11618, **2008**.

11. Rolland, J.P., Maynor, B.W., Euliss, L.E., Exner, A.E., Denison, G.M. & DeSimone, J.M.
Direct Fabrication and Harvesting of Monodisperse, Shape-Specific Nanobiomaterials,
Journal of the American Chemical Society, 127, 10096-10100, **2005**.

12. Zhang, H., Nunes, J.K., Gratton, S.E.A., Herlihy, K.P., Pohlhaus, P.D. & DeSimone, J.M.
Fabrication of multiphasic and regio-specifically functionalized PRINT particles of controlled size and shape,
New Journal of Physics, 075018, **2009**.

13. Champion, J.A. & Mitragotri, S.
Role of target geometry in phagocytosis,
Proceedings of the National Academy of Sciences of the United States of America, 103, 4930-4934, **2006**.

14. Chithrani, B.D., Ghazani, A.A. & Chan, W.C.W.
Determining the Size and Shape Dependence of Gold Nanoparticle Uptake into Mammalian Cells,
Nano Letters, 6, 662-668, **2006**.

15. Decuzzi, P., Godin, B., Tanaka, T., Lee, S.Y., Chiappini, C., Liu, X. & Ferrari, M.
Size and shape effects in the biodistribution of intravascularly injected particles,
Journal of Controlled Release, 141, 320-327, **2010**.

16. Champion, J.A., Katare, Y.K. & Mitragotri, S.
Making polymeric micro- and nanoparticles of complex shapes,
Proceedings of the National Academy of Sciences, 104, 11901-11904, **2007**.

17. Lu, Y., Yin, Y. & Xia, Y.
Preparation and Characterization of Micrometer-Sized ldquoEgg Shellsrdquo,
Advanced Materials, 13, 271-274, **2001**.

Chapter III

Controlling the elongation of degradable poly(γ-benzyl-L-glutamate) nanoparticles

Chapter 3. Controlling the elongation of degradable poly(γ-benzyl-L-glutamate) nanoparticles

By *Olivier Cauchois, Freimar Segura-Sanchez,* and *Gilles Ponchel**

Keywords: Nanoparticles, shape, oblates, PBLG, self-assembly, morphology

Abstract

It is well known that poly(gamma-benzyl-L-glutamate), a degradable polymer forms α-helices rods. These rods can be easily self-assembled by nanoprecipitation, which leads to oblates, i.e. non spherical nanoparticles. We show that their elongation ratio is controlled by the molecular weight of the polymer (28 to 85 $kg.mol^{-1}$) at least in a range of 1.5 to 3.5, which likely results from a liquid crystal-like self organization of PBLG rods with varying lengths. Since morphology is emerging as an important parameter modulating nanoparticle behaviour in biological fluids and their interactions with cells, it is believed that these elongated nanoparticles may be a valuable tool for gaining a better understanding of the influence of shape on *in vivo* distribution for drug targeting applications.

Introduction

In pharmacy, drug targeting is a promising strategy aiming not only to reduce the amount of drugs administered, but also to improve the benefit/risk ratio for the patient. Specific delivery in target organs or cells is raised while toxic effects caused by non specific delivery in other tissues are weakened. To be fully efficient various vectors have been proposed which should be able not only to encapsulate the therapeutic molecules, but also to interact efficiently with target cells. From this point of view, polymeric nanoparticles are interesting objects for active targeting of organs or cells in the body because of a unique combination of their nanometric size and the possibility to considerably modulate their physico-chemical properties, which governs their biodistribution and thus the one of the therapeutic molecule encapsulated within.

The fate of micro and nanoparticles in the body, including their interactions with cells, depends on many parameters which have been thoroughly investigated, including size and surface effects. However, there are only very few investigations looking into the effect of their morphology on these interactions[1], on biodistribution[2-3] and kinetics[4]. Indeed, in the micron range, it is known for long that the morphology of microorganisms has a great influence over their phagocytosis by macrophages. Recently, it was shown that the morphology of polystyrene microparticles had more influence on phagocytosis than the particle size[5]. Inhibition of phagocytosis by macrophages was even attained by modulations of particles morphology[1]. At the nanoparticle level, there are also evidences that many biological structures necessitate specifically-shaped building blocks. For example, the aggregation of amelogenin, a protein involved in the constitution of enamel in vertebrate, has been shown to form oblate-shaped nanoparticles, which structure is mandatory for an highly ordered crystallization of hydroxyapatite in enamel[6].

However, morphology effects have been much less investigated in the case of nanoparticles of pharmaceutical interest, probably because available preparation methods lead to spherical or round-shaped objects so far. Understanding the influence of the morphology over nanoparticles-cells interactions is the next challenge for creating new vectors for improved targeting. Today various non-spherical nanoparticles and their methods of production have been described in the literature. However, these are mostly suitable for metals and inorganic materials, making them of limited interest for pharmaceutical applications. For polymers, molding[7-10] or deformation[5] techniques have been recently proposed for producing various shapes using polystyrene. Furthermore, some peptides[11-13], amphiphilic molecules[14-16], and dendritic molecules[17-18] have been shown to auto-assemble and to produce non spherical objects.

Here we report a novel method to produce elongation controlled oblate shaped nanoparticles by self-assembly of poly(gamma-benzyl-L-glutamate) (PBLG). This degradable polymer is well known for its ability to form α-helices rods[19]. Because it is water insoluble it can be easily nanoprecipitated in water to form nanoparticles. Moreover, amphiphilic copolymers of PBLG can be prepared and assembled to form ligand decorated multifunctional nanoparticles intended for targeting purposes[20]. The purpose of this work was to investigate the possibility of controlling the shape and the aspect ratio of these particles by self-assembling PBLG rods of varying molecular weights.

3.1. Experimental

3.1.1. Reagents

N,N-dimethylformamide (DMF; Acros, 99%) and benzylamine (Janssen Chimica) were distilled under reduced pressure over BaO and KOH, respectively, and stored under argon atmosphere at room temperature. γ-benzyl-L-glutamate N-carboxyanhydride (BLG-NCA) (ISOCHEM-SNPE, stored at -18°C), and THF (Carlo Erba, HPLC grade) were used as received.

Water was purified by reverse osmosis (MilliQ, Millipore). Diethyl ether, tetrahydrofuran, methanol and other solvents, of analytical grade, and all other chemicals, of commercially available reagent grade, were used as received unless otherwise stated.

3.1.2. Polymer Synthesis

Poly(γ-benzyl-L-glutamate) (PBLG) of different molecular weights were synthesized in anhydrous DMF by ring-opening polymerization of γ-benzyl-L-glutamate N-carboxyanhydride (BLG-NCA) using benzylamine as initiator according to a slightly modified method described elsewhere[21]. The theoretical molecular weights of samples were adjusted by adjusting the initiator/BLG-NCA ratio.

Briefly, BLG-NCA was weighted under argon atmosphere in a degassed three-necked round bottomed flask equipped with a thermometer, mechanical stirring, a refrigerant with a silica gel guard and a bubble detector. BLG-NCA was dissolved in DMF (volume was adjusted to obtain a 0.5M BLG-NCA final concentration) at room temperature under mechanical stirring and argon flux. After about 10 min, the argon flux was stopped, the solution was heated at 30°C and the initiator solution was added. Immediately after the addition, CO_2 emission was observed in the bubble detector. Absence of BLG-NCA auto-

polymerization was checked by FTIR spectroscopy of the BLG-NCA solution before addition of the initiator. The reaction mixture was stirred at 30°C until the characteristic BLG-NCA bands disappeared from the FTIR spectrum. The mixture was precipitated in an excess of cold diethyl ether to give a white solid. The precipitate was filtered and washed with diethyl ether. The polymers were again washed with diethyl ether and dried under vacuum at room temperature for at least 12h. A second precipitation, purification and drying procedure was performed for polymers of all molecular weights. FTIR spectra were recorded to analyze BLG-NCA auto-polymerization and to follow the reaction using a Brüker Vector 22 spectrometer.

3.1.3. Polymers analysis

Molecular weights of synthesized PBLG were determined by capillary viscosimetry and MALDI-TOF. Helicity of PBLG chains was determined by circular dichroïsm and FTIR.

3.1.4. Capillary viscosimetry analysis

Solutions of the polymers samples were prepared in DMF at 4 different concentrations (typically ranging from 1 to 10g.L^{-1}). 5mL of these solutions were poured into a µ-Ubbelohde microtube (type 53710/I, Schott Geräte). The microtube was then placed into a thermostated bath (CT1450 and CK100, Schott Geräte), and the flow rates were automatically measured (AVS400, Schott Geräte). Each determination was repeated three times. Molecular weights of the different polymers were calculated from the flow rates using a method described elsewhere[22].

3.1.5. Matrix assisted laser desorption/ionization time of flight mass spectroscopy (MALDI-TOF-MS)

Matrix-assisted Laser Desorption/Ionization-Time of Flight-Mass Spectrometry (MALDI-TOF-MS) analysis was carried out in positive-ion mode on a Voyager DE-STR MALDI-TOF

mass spectrometer (Perseptive Applied Biosystems, Framingham, MA, USA) equipped with a 337nm nitrogen laser. DCTB or 2-[(2E)-3-(4-tert-Butylphenyl)-2-methylprop-2-enylidene] malononitrile (40mg.mL^{-1} in dichloromethane) and potassium trifluoroacetate (5mg.mL^{-1} in water) were used respectively as matrix and cationic ionization agent. The polymer: matrix molar concentration ratio was comprised between 40:1 (for the lowest molecular weight) and 1:1000 (for the highest molecular weight). 1.5µL of this premix were deposited onto the sample plate and allowed to dry at room temperature. Spectra of PBLG were acquired with the default calibration (accuracy ca. 0.1%) under the same condition as those described in Sicard-Roselli et al.[23].

3.1.6. Circular Dichroïsm

The CD spectra were recorded in THF with a Jasco J-810 dichrograph and expressed as ellipticity (bandwidth 1nm, scanning speed 50nm.min^{-1}). Quartz cuvette (Hellma) had a 0.1 or 0.5cm optical pathlength.

3.1.7. Nanoparticles Preparation

PBLG nanoparticles were prepared using a modified nanoprecipitation method described elsewhere[24]. Briefly, 15mg of polymer were dissolved in 5mL of THF at 30°C during 18h, without stirring. This solution was added dropwise to 10mL of milli-Q water under magnetic stirring. The mixture was left under magnetic stirring for 15min and then transferred in a Teflon coated recipient. The solvent was gently evaporated, at 30°C, under a light air flow. In order to eliminate residual solvent, nanoparticles were washed with 5mL of milli-Q water and evaporation was carried out to yield 10mL of nanoparticles suspension.

3.1.8. Nanoparticles Characterization

Helicity of the PBLG chains in the nanoparticles was checked using circular dichroïsm and FTIR spectroscopy. FTIR spectra were recorded using a Brüker Vector 22 spectrometer either on purified polymers following their synthesis or on lyophilized nanoparticles.

3.1.9. Transmission Electron Microscopy

Nanoparticles shape and size were determined from TEM images. TEM was performed on a transmission electron microscope (Philips EM208) at 60kV. After suitable dilution of bulk suspensions in milli-Q water, 3µl of nanoparticles suspension were placed on a formvar-carbon film previously coated on a copper grid (400 meshes). After 5min of deposition, a drop of phosphotungstic acid was placed on the copper grid, on top of the sample. After 30s, the liquid was drained and the sample was placed inside the EM208 and pictures were taken. Nanoparticles measurements were obtained thanks to The Gimp© software.

3.1.10. Scanning Electron Microscopy

Nanoparticles shape and size were analyzed through SEM (Scanning electron microscopy). SEM was performed using a LEO 1530 (LEO Electron Microscopy Inc, Thornwood, NY) operating between 1kV and 3kV with a filament current of about 0.5mA. Sample suspensions were deposited on carbon conductive double-sided tape (Euromedex, France) and dried at room temperature. Nanoparticles were then coated with a palladium-platinum layer of about 4nm using a Cressington sputter-coater 208HR with a rotary-planetary-tilt stage, equipped with a MTM-20 thickness controller.

3.1.11. Size and Shape Analysis

Only nanoparticles from TEM pictures were analyzed for determining the size and shape of the particles. SEM pictures showed that nanoparticles could be deposited in various manners on the double-sided tape and with varying angles of the long axis making impossible to obtain a reliable determination of nanoparticle sizes. On the contrary, TEM pictures were obtained from very diluted suspensions and the particles appeared flattened on the grid

surface. Sample variability was checked on the 28kg.mol^{-1} polymer and showed no significant difference. For each PBLG, nanoparticles dimensions were measured on different TEM pictures and on a population of 200 nanoparticles. For each particle, the smallest and the longest dimensions were measured and were named width and length, respectively. For analysis the shape of the nanoparticles was assumed to be ovoid. From these data the diameter of the equivalent volume sphere was calculated using the formula below:

Eq.1

$$Aspect\ Ratio = \Gamma = \frac{Length}{Width}$$

Eq.2

$$Equivalent\ Diameter = \sqrt[3]{Length * width^2}$$

3.2. Results and Discussion

Polymeric nanoparticles for drug targeting are envisioned as a very promising mean for improving an inadequate natural drug distribution pattern in the body, in view of enhancing their efficacy as well as decreasing side-effects. In order to be efficient, these carriers must comprise simultaneously different functionalities, including the capacity to carry and control the release of a sufficient drug payload, to be able to traffic efficiently in the body and possibly within cells following their endocytosis, which depends on an adequate decoration of their surface by various ligands aimed to ensure simultaneously an high affinity to target cells and low non specific recognition in other non-targeted tissues.

Obviously, the shape of nanoparticles can be an important determinant of their distribution in the body after administration. Indeed non spherical particles exhibit higher specific surfaces, varying curvature radius and their surface charges and surface decoration can be locally varied at the molecular scale. The shape parameter has long been neglected in the field of drug targeting, although it has already been shown that elongation could play a role in the ability of particles to interact with cells. For instance shape effects have been well documented not only for asbestos inorganic fibers in the micron range, but also for carbon nanotubes at the nanoscale, which have been suggested to penetrate easily cell membranes as shown by atomic force microscopy (AFM) experiments[25].

Most of nanoparticles prepared so far for drug targeting applications are round-shaped nanoparticles. These particles can be conveniently prepared from sufficiently water insoluble polymers, in presence of surfactants or directly from tailored amphiphilic copolymers, which aggregate to form round-shaped objects. The flexible random coil conformation of the polymers chains, often polyesters, allow the physical entanglement of the disordered

statistical chains and finally leads to spherical geometries characterized by the lowest surface energy. Thus, not surprisingly, whatever the method of fabrication, these nanoparticles adopt round-shaped morphologies, with hydrodynamic diameters ranging from a few tenths to a few hundredths of nanometers.

Different approaches have been recently described to form non spherical polymeric nanoparticles. A first approach consists in the preparation of spherical nanoparticles as a first step, which can be aggregated under various conditions and further consolidated during an emulsion/solvent evaporation process[26] or by chemical binding[27]. A second approach consists in molding an amount of random coiled polymer chains in a confined space, which can exhibit various morphologies. Following unmolding, nanoparticles keep the form of the mold they are confined in[7,9-10]. A variation of this approach consists in deforming previously prepared spherical nanoparticles, which have been softened by heating and moltening the polymer. Depending on the geometry of deformations, these nanoparticles can adopt various non spherical morphologies, which can be blocked by decreasing the temperature[1,5,28]. This approach has been developed for micro and nanoparticles by Champion et al.[1] who obtained various shapes by deforming molten polystyrene micro and nanoparticles incorporated in a water-soluble polymeric film.

An alternative approach for obtaining non-spherical nano-objects consists in using ordered self-orientated macromolecules adopting ordered secondary chains conformations and able to interact together, such as certain polymers or peptides. Jet-spinning represents an example of a technique exploiting such polymers characteristics as well as combining mechanical constraints to produce fibers, needle-like or elongated particles[29].

In the present work a self-assembling strategy has been preferred mostly because: (i) it does not necessitate heating, (ii) it avoids any contamination of the surface by residual materials forming the deformation film and thus would allow an efficient control of the surface characteristics of the particles and (iii) because of the easiness of large scale production necessitated for envisioning *in vivo* experiments. The self-assembling strategy necessitates selecting a material with specific molecular conformational properties which could impose the morphology of the nanoparticles[15,30-31]. For this purpose, poly(γ-benzyl-L-glutamate) (PBLG), which is well known for its ability to form α-helices rods has been used to prepare nanoparticles by the mean of a nanoprecipitation method. These α-helices structures can supra-organize themselves inside the nanoparticles which may fight the forces leading to sphericity.

3.2.1. Synthesis and characterization of PBLG

As previously demonstrated PBLG can easily self-associate and form nanoparticles. In this work it was postulated that an increase in the length of PBLG chains and thus in the molecular weight would result in varying morphologies. For this purpose polymers with molecular weights ranging from 28 to 85 $kg.mol^{-1}$ were synthesized by ring-opening polymerization of the corresponding N-carboxy anhydride[32]. The primary amine route for PBLG polymerization has been chosen because of easiness and conducted accordingly to a method described elsewhere[21,33].

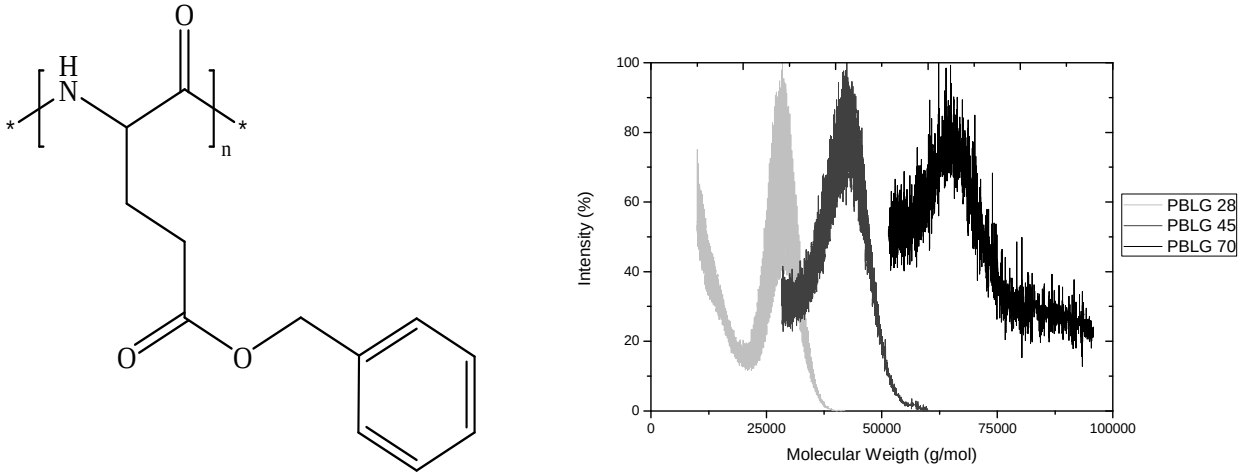

Figure 3.1: PBLG Formula and MALDI-TOF spectra of different PBLG samples with varying molecular weights.

Molecular weights were experimentally determined by Matrix-Assisted Laser Desorption/Ionization-Time of Flight. MALDI-TOF spectra (figure 3.1) exhibited peaks with a mean distance characteristic corresponding to the monomer unit of PBLG (219 $g.mol^{-1}$). The means and the standard deviation of the peaks are gathered in Table 3.1. Capillary viscosimetry measurements gave results consistent with the MALDI-TOF-MS analysis, although some discrepancies could be noted for PBLG 70. Further, the different polymer samples were named accordingly to their experimental molecular weights.

Table 1: Molecular weights of PBLG samples obtained from MALDI-TOF MS and viscosimetry determinations. Standard deviation was determined from the molecular weights distribution.

	PBLG28	PBLG45	PBLG70	PBLG85
MALDI ToF MS ($kg.mol^{-1}$)	28 ± 2.5	42 ± 3.5	66 ± 7.2	84± 20.2
Viscosimetry ($kg.mol^{-1}$)	27	54	84	90

Very long PBLG chains were difficult to synthesize because the reaction was slow. The synthesis of the highest molecular weight was stopped after three weeks during which deactivation of growing chains could have occurred, which might explain the high polydispersity compared to other molecular weights.

3.2.2. Morphology and aspect ratio of elongated nanoparticles

Stable nanoparticles suspensions in water could be easily produced via nanoprecipitation of a THF solution of PBLG in water and were further characterized.

Morphology was determined through SEM (figure 3.2) and TEM (figure 3.3) experiments. As can be seen, elongated, oblate-shaped, nanoparticles were obtained. Similar images have been obtained before by others for PBLG nanoparticles[22,34].

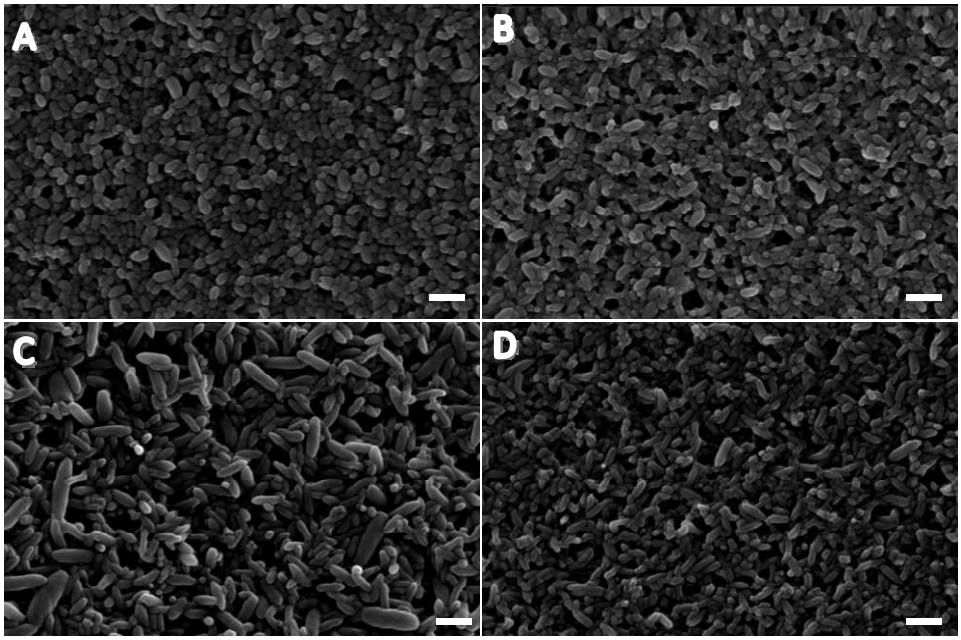

Figure 3.2: SEM microphotographs of nanoparticles prepared from PBLG with varying molecular weights. (A) PBLG 28 (B) PBLG 45 (C) PBLG 70 (D) PBLG 85. Scale bar = 200 nm.

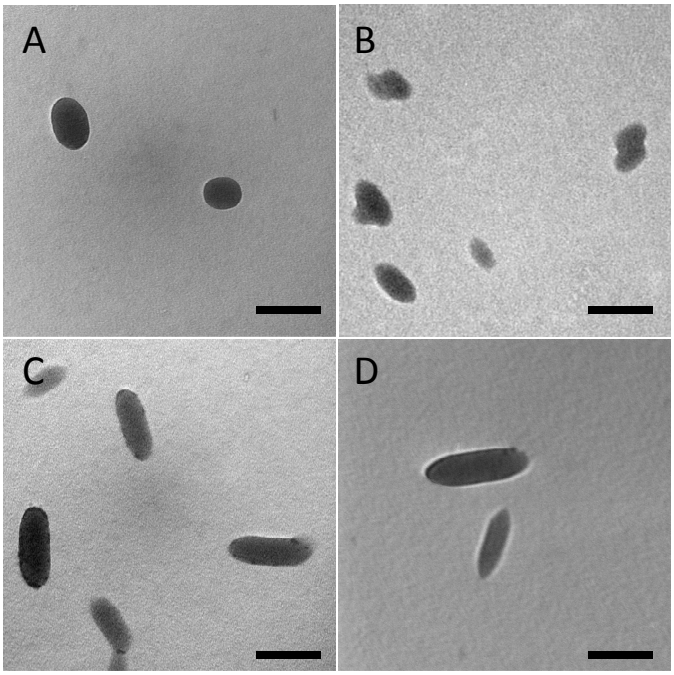

Figure 3.3: TEM microphotographs of nanoparticles prepared from PBLG with varying molecular weights. (A) PBLG 28 (B) PBLG 45 (C) PBLG 70 (D) PBLG85. Scale bar = 100 nm

However, TEM microphotographs showed that elongation depended on the molecular weight, which has not been investigated in depth yet. Although dynamic light scattering (DLS) can be used for evaluating dimensional parameters, it was preferred to analyze directly TEM images as explained in Chapter 2.1.6 for obtaining the distribution frequencies of widths (figure 3.4) and lengths (figure 3.5) for the different types of nanoparticles. It is noteworthy that the different population distributions depended on the molecular weight of the polymer used for their preparation. The length and width distributions were unimodal suggesting that there was only one population of nanoparticles per polymer of a given molecular weight, except for nanoparticles made from PBLG 85 where two length populations appeared. Although the lengths of nanoparticles (50 to 250 nm) was comparable to the ones commonly obtained by nanoprecipitation of various polymers, the average widths of nanoparticles ranged only from 30 to 50 nm. Furthermore, except in the case of PBLG 85, it could be noted that the higher the molecular weight used to prepare the nanoparticles, the longest and the narrowest were these nanoparticles.

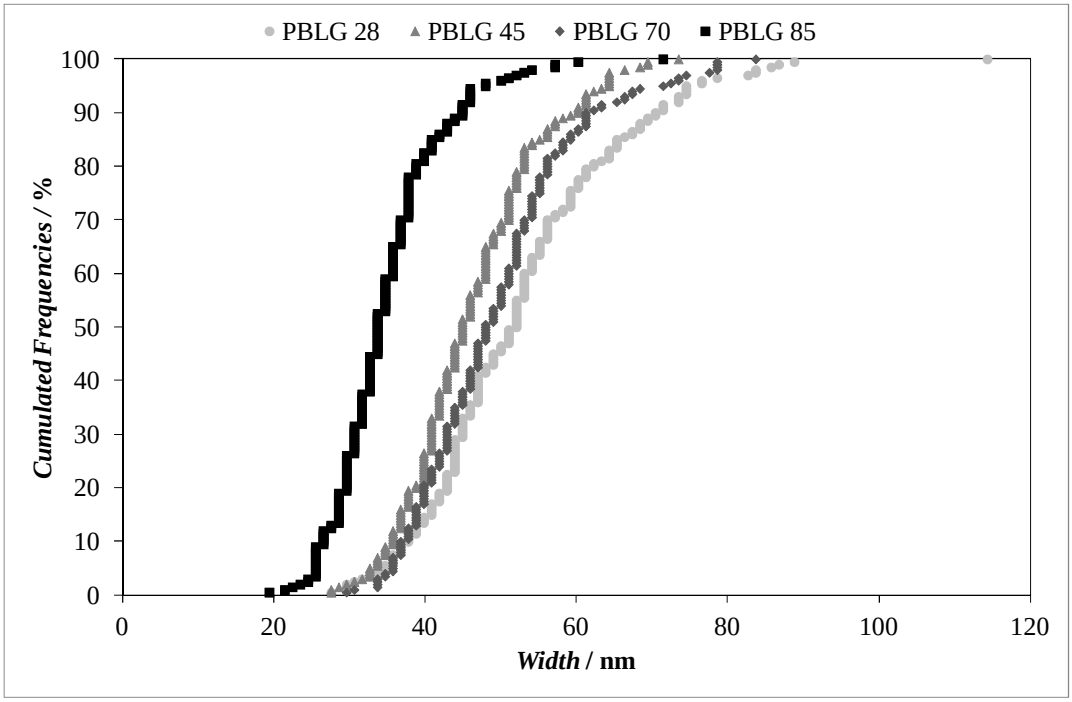

Figure 3.4: Cumulated width frequencies for nanoparticles populations obtained from PBLG polymers with varying molecular weights.

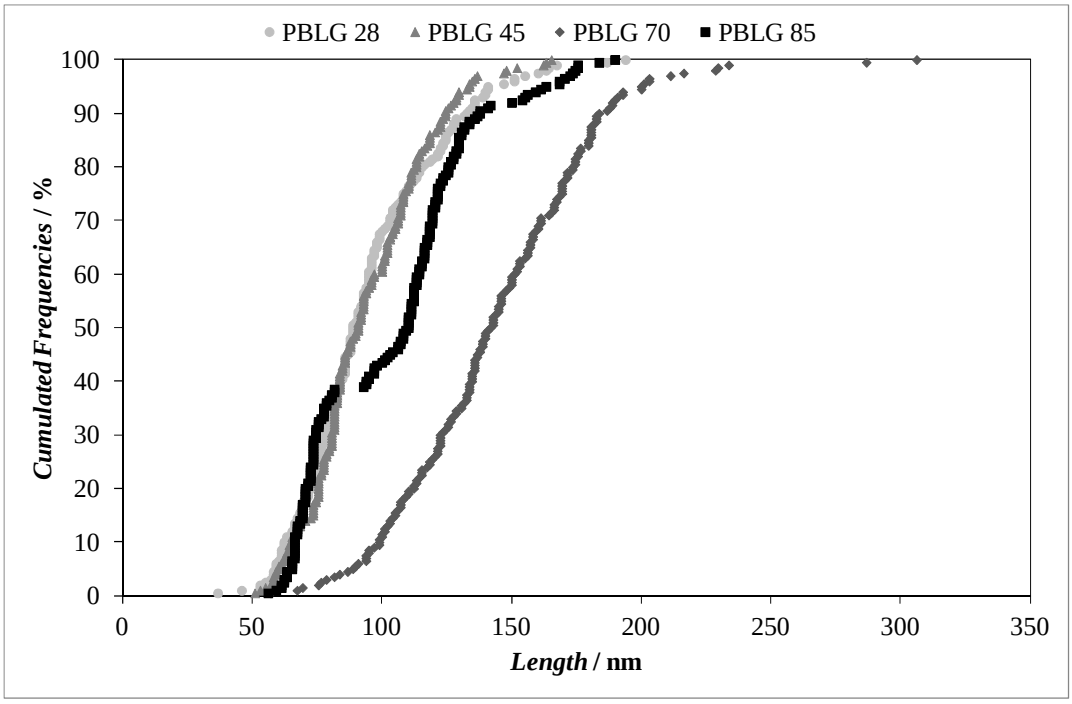

Figure 3.5: Cumulated length frequencies for nanoparticles populations obtained from PBLG polymers with varying molecular weights

The aspect ratio and the diameter of the equivalent sphere of the nanoparticles were derived from these data and were gathered in table 3.2. While the diameter of the volume equivalent sphere was not much affected by the increase in molecular weight, the aspect ratio increased from 1.8 to 3.0 with the molecular weight of PBLG. It suggests that the nanoparticles were made approximately from the same volume of material, whatever the molecular weight, but that the length of PBLG chains could control their elongation ratio.

Table 3.2: Morphological characteristics of nanoparticles prepared from PBLG samples with varying molecular weights. Primary data were obtained from individual determinations of the long and small axis of particles from TEM microphotographs (n = 200).

Polymer Samples	**PBLG 28**	**PBLG 45**	**PBLG 70**	**PBLG 85**
Aspect Ratio (nm)	1.79 ± 0.23	2.03 ± 0.26	2.92 ± 0.51	2.98 ± 0.72
Length (nm)	94 ± 27	94 ± 23	144 ± 37	103 ± 31
Width (nm)	53 ± 13	46 ± 9	49 ± 10	35 ± 7
Equivalent Diameter (nm)	64 ± 16	58 ± 12	70 ± 15	50 ± 11

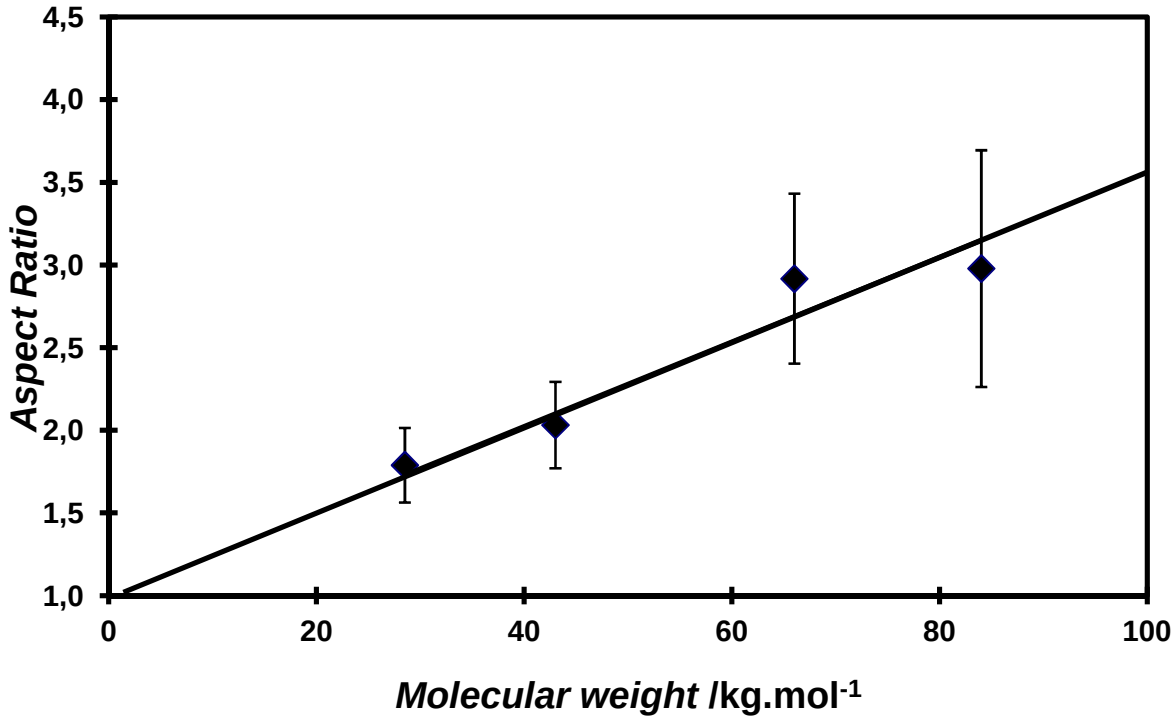

Figure 3.6: Aspect ratio of nanoparticles prepared from PBLG with varying molecular weights.

Figure 3.6 shows that there was a linear relationship between the aspect ratio of the nanoparticles and the molecular weight of the polymer. An aspect ratio of 1 was assumed when the molecular weight tended towards zero while drawing the tendency line, which was probable since the nanoparticles tended to be rounder when the molecular weight decreased. Indeed, for a minimal degree of polymerization PBLG chains would rather exist in random-coil conformation form, thus aggregating as round-shaped nanoparticles.

This stretching of the nanoparticles when using longer PBLG chains could be related to the internal organization of the α-helix rods after the nanoprecipitation in presence of THF, which has been confirmed by circular dichroïsm and FT-IR on the precipitated nanoparticles.

2.3 Post-nanoprecipitation characterization of chain conformation of PBLG by circular dichroïsm and FTIR spectroscopy

Dichroïsm spectra of the purified polymer powders as well as after dissolution of the nanoparticles in THF revealed a negative peak around 222nm, which was characteristic of α-helices (figure 3.7). This was expected as THF is known as a helicogenic solvent of PBLG. Random coil chains presented a positive characteristic peak at 218nm. The graph suggests that most of the chains were in the α-helix right-handed conformation even if some chains could still exist under the random coil conformation.

FTIR spectra of polymers powders obtained after synthesis and purification (data not shown) presented peaks located near 1656$cm^{-1}$and 1548cm^{-1}, which respectively corresponded to the amide I and II bands for a polypeptide in α-helix conformation[21,33,35]. They also presented a band located near 1260cm^{-1} corresponding to the amide III band for a polypeptide in α-helix conformation[21].

The same characteristic peaks were found for lyophilized nanoparticles obtained by nanoprecipitation of these polymers of different molecular weights. Together with circular dichroïsm data, these data suggests that PBLG chains existed in the conformation of alpha-helices. Indeed, PBLG chains have often been described as nanorods, which are able to associate and form hexagonal lattices[36]. Despite the fact that the persistence length of these α-helices, which has been estimated by Papadopoulos et al.[37], has been shown to depend on the environment, it was likely that α-helices could comprise helical defects inducing local breaks of the rods.

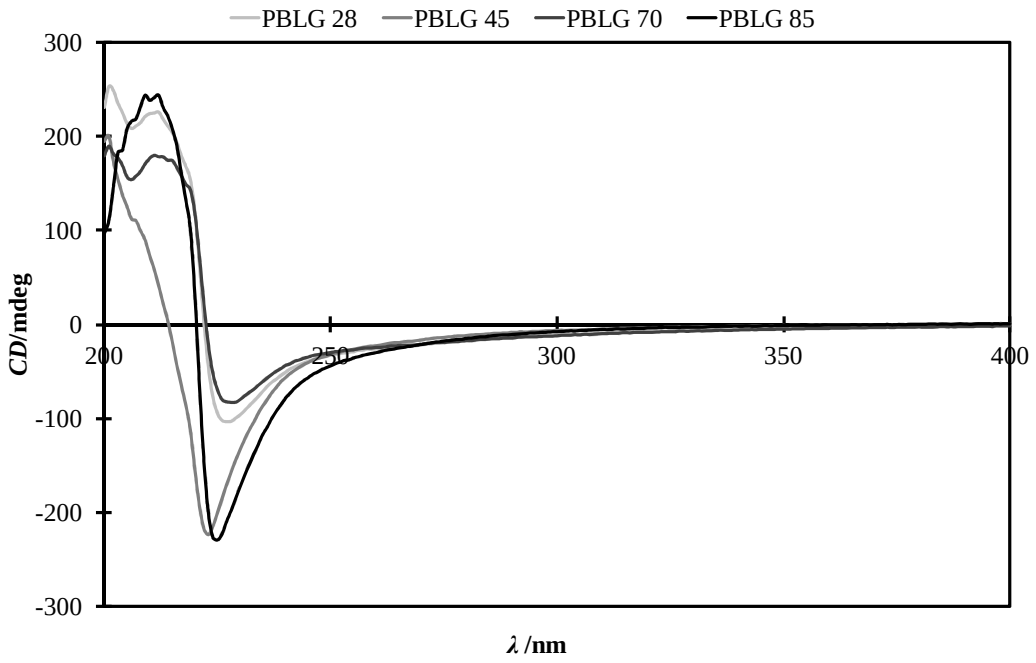

Figure 3.7: Circular dichroïsm of PBLG polymers with varying molecular weights in THF and 25 °C.

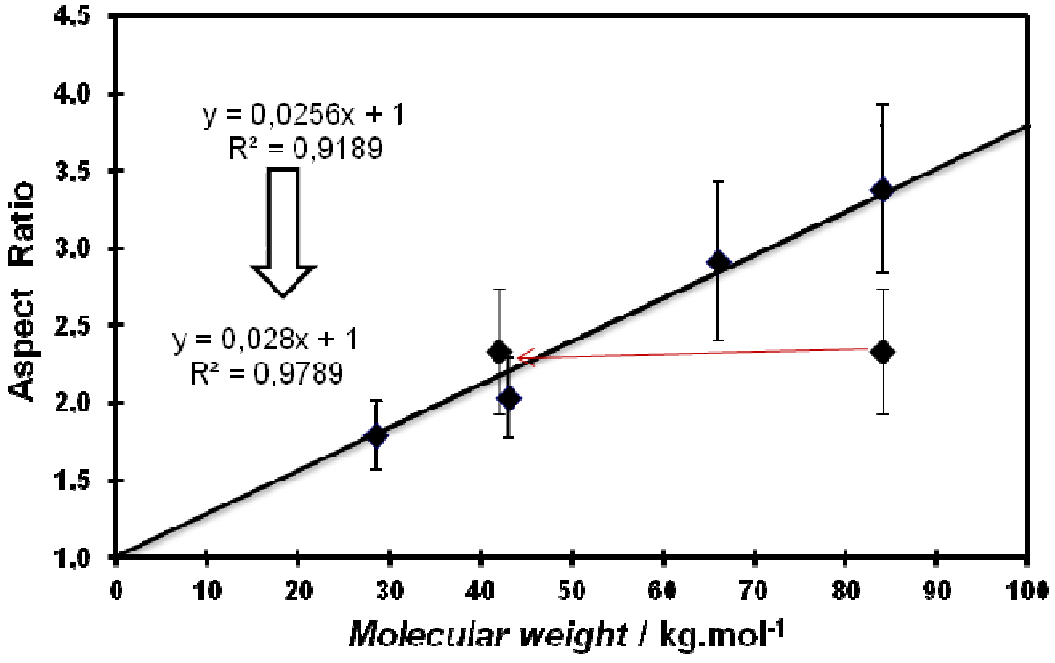

Figure 3.8: Aspect ratio of nanoparticles prepared from PBLG with varying molecular weights including the two aspect ratios values issued from the bimodal distribution observed for PBLG85 nanoparticles

Thanks to this analysis, figure 3.8 shows an attempt to reinterpret the data concerning the nanoparticles prepared from the 84kg.mol^{-1} PBLG. Clearly, two populations of nanoparticles were observed when looking at the bimodal distribution of the length for 84kg.mol^{-1} nanoparticles (figure 3.5). It can be hypothesized that long enough polymer chains α-helix, instead of forming a single nanorod, could exist as a mixture of either straight or folded α-helices. For investigating this possibility, the two populations were analyzed separately (length cutoff was 90nm). Doing so, two statistically different populations characterized by two different aspect ratios could be calculated to be respectively 2.3 and 3.4. When plotted on figure 3.8, these two populations corresponded to theoretical molecular weights of 84 kg.mol^{-1} (straight α-helix) and 42kg.mol^{-1}, respectively, which would be consistent with a partial folding of the α-helices for the higher PBLG molecular weight.

Conclusions

Small oblate-shaped nanoparticles could be conveniently obtained from nanoprecipitation in water of poly(gamma-benzyl-L-glutamate) solutions in THF, an helicogenic solvent. Their aspect ratio depended linearly on the molecular weight of the polymer, which is believed to stem from an ordered association of rod-like α-helices PBLG chains as shown by FTIR and circular dichroïsm. Although the inner structure of the particles and chains organization within the particles should be more in depth investigated, this result is also of practical interest in view of designing non spherical degradable nanocarriers with varying elongation ratios for drug targeting applications. Indeed there are now growing experimental evidences that nanoparticles elongation can affect their distribution in the body as well as their interactions with cells. It is believed that these nanoparticles could be fruitfully used for investigating the effect of the shape parameter in targeting applications.

Acknowledgements

Dr Monique Cheron-Francke is acknowledged for performing circular dichroïsm experiments and Nicolas Tsapis for performing the SEM measurements.

We would like to thank Danielle Jaillard (CCME, Paris XI, Orsay) for her help with the TEM measurements.

References

1. Champion, J.A., Katare, Y.K. & Mitragotri, S.
Particle shape: A new design parameter for micro- and nanoscale drug delivery carriers,
Journal of Controlled Release, 121, 3-9, **2007**.

2. Chithrani, B.D., Ghazani, A.A. & Chan, W.C.W.
Determining the Size and Shape Dependence of Gold Nanoparticle Uptake into Mammalian Cells,
Nano Letters, 6, 662-668, **2006**.

3. Murphy, C.J., Gole, A.M., Stone, J.W., Sisco, P.N., Alkilany, A.M., Goldsmith, E.C. & Baxter, S.C.
Gold Nanoparticles in Biology: Beyond Toxicity to Cellular Imaging,
Accounts of Chemical Research, 41, 1721-1730, **2008**.

4. Lee, S.-Y., Ferrari, M. & Decuzzi, P.
Shaping nano-/micro-particles for enhanced vascular interaction in laminar flows,
Nanotechnology, 495101, **2009**.

5. Champion, J.A. & Mitragotri, S.
Role of target geometry in phagocytosis,
Proceedings of the National Academy of Sciences of the United States of America, 103, 4930-4934, **2006**.

6. Aichmayer, B., Wiedemann-Bidlack, F.B., Gilow, C., Simmer, J.P., Yamakoshi, Y., Emmerling, F., Margolis, H.C. & Fratzl, P.
Amelogenin Nanoparticles in Suspension: Deviations from Spherical Shape and pH-Dependent Aggregation,
Biomacromolecules, 11, 369-376, **2009**.

7. Gratton, S., Napier, M., Ropp, P., Tian, S. & DeSimone, J.
Microfabricated Particles for Engineered Drug Therapies: Elucidation into the Mechanisms of Cellular Internalization of PRINT Particles,
Pharmaceutical Research, 25, 2845-2852, **2008**.

8. Gratton, S.E.A., Ropp, P.A., Pohlhaus, P.D., Luft, J.C., Madden, V.J., Napier, M.E. & DeSimone, J.M.
The effect of particle design on cellular internalization pathways,
Proceedings of the National Academy of Sciences, 105, 11613-11618, **2008**.

9. Rolland, J.P., Maynor, B.W., Euliss, L.E., Exner, A.E., Denison, G.M. & DeSimone, J.M.
Direct Fabrication and Harvesting of Monodisperse, Shape-Specific Nanobiomaterials,
Journal of the American Chemical Society, 127, 10096-10100, **2005**.

10. Zhang, H., Nunes, J.K., Gratton, S.E.A., Herlihy, K.P., Pohlhaus, P.D. & DeSimone, J.M.
Fabrication of multiphasic and regio-specifically functionalized PRINT particles of controlled size and shape,
New Journal of Physics, 075018, **2009**.

11. Scanlon, S. & Aggeli, A.
Self-assembling peptide nanotubes,
Nano Today, 3, 22-30, **2008**.

12. Toksöz, S. & Guler, M.O.
Self-assembled peptidic nanostructures,
Nano Today, 4, 458-469, **2009**.

13. Balbo, B.M.A. & Stefan, H.
Wrapping peptide tubes : Merging biological self-assembly and polymer synthesis,
Angewandte Chemie. International edition, 44, 4, **2005**.

14. Dalhaimer, P., Engler, A.J., Parthasarathy, R. & Discher, D.E.
Targeted Worm Micelles,
Biomacromolecules, 5, 1714-1719, **2004**.

15. Kim, Y., Dalhaimer, P., Christian, D.A. & Dische, D.E.
Polymeric worm micelles as nano-carriers for drug delivery,
Nanotechnology, 16, S484, **2005**.

16. J. N. Israelachvili, Mitchell, D.J. & Ninham, B.W.
Theory of self-assembly of hydrocarbon amphiphiles into micelles and bilayers,
J. Chem. Soc., Faraday Trans. 2, 72, 1525 - 1568, **1976**.

17. Gillies, E.R. & Fréchet, J.M.J.
Dendrimers and dendritic polymers in drug delivery,
Drug Discovery Today, 10, 35-43, **2005**.

18. Ihre, H.R., Padilla De Jesús, O.L., Szoka, F.C. & Fréchet, J.M.J.
Polyester Dendritic Systems for Drug Delivery Applications: Design, Synthesis, and Characterization,
Bioconjugate Chemistry, 13, 443-452, **2002**.

19. Klok, H.-A., Langenwalter, J.F. & Lecommandoux, S.
Self-Assembly of Peptide-Based Diblock Oligomers,
Macromolecules, 33, 7819-7826, **2000**.

20. Vladimir P, T.
Multifunctional nanocarriers,
Advanced Drug Delivery Reviews, 58, 1532-1555, **2006**.

21. Barbosa, M.E.M., Montembault, V., Cammas-Marion, S., Ponchel, G. & Fontaine, L.
Synthesis and characterization of novel poly(gamma-benzyl-L-glutamate) derivatives tailored for the preparation of nanoparticles of pharmaceutical interest,
Polymer International, 56, 317-324, **2007**.

22. Segura-Sánchez, F., Montembault, V., Fontaine, L., Martínez-Barbosa, M.E., Bouchemal, K. & Ponchel, G.
Synthesis and characterization of functionalized poly([gamma]-benzyl-l-glutamate) derivates and corresponding nanoparticles preparation and characterization,
International Journal of Pharmaceutics, 387, 244-252, **2010**.

23. Sicard-Roselli, C., Lemaire, S., Jacquot, J.-P., Favaudon, V., Marchand, C. & Houée-Levin, C.
Thioredoxin Ch1 of Chlamydomonas reinhardtii displays an unusual resistance toward one-electron oxidation,
European Journal of Biochemistry, 271, 3481-3487, **2004**.

24. Thioune, O., Fessi, H., Devissaguet, J.P. & Puisieux, F.
Preparation of pseudolatex by nanoprecipitation: Influence of the solvent nature on intrinsic viscosity and interaction constant,
International Journal of Pharmaceutics, 146, 233-238, **1997**.

25. Chen, X., Kis, A., Zettl, A. & Bertozzi, C.R.
A cell nanoinjector based on carbon nanotubes,
Proceedings of the National Academy of Sciences, 104, 8218-8222, **2007**.

26. Manoharan, V.N., Elsesser, M.T. & Pine, D.J.
Dense Packing and Symmetry in Small Clusters of Microspheres,
Science, 301, 483-487, **2003**.

27. He, T., Adams, D.J., Butler, M.F., Cooper, A.I. & Rannard, S.P.
Polymer Nanoparticles: Shape-Directed Monomer-to-Particle Synthesis,
Journal of the American Chemical Society, 131, 1495-1501, **2009**.

28. Lu, Y., Yin, Y. & Xia, Y.
Preparation and Characterization of Micrometer-Sized ldquoEgg Shellsrdquo,
Advanced Materials, 13, 271-274, **2001**.

29. Minato, K.-I., Ohkawa, K. & Yamamoto, H.
Chain Conformations of Poly(γ-benzyl-L-glutamate) Pre and Post an Electrospinning Process,
Macromolecular Bioscience, 6, 487-495, **2006**.

30. Zhang, S. & Zhao, X.
Design of molecular biological materials using peptide motifs,
Journal of Materials Chemistry, 14, 2082-2086, **2004**.

31. Ornatska, M., Peleshanko, S., Genson, K.L., Rybak, B., Bergman, K.N. & Tsukruk, V.V.
Assembling of Amphiphilic Highly Branched Molecules in Supramolecular Nanofibers,
Journal of the American Chemical Society, 126, 9675-9684, **2004**.

32. Deming, T.J.
Facile synthesis of block copolypeptides of defined architecture,
Nature, 390, 386-389, **1997**.

33. Fontaine, L., Ménard, L., Brosse, J.-C., Sennyey, G. & Senet, J.-P.
New polyurethanes derived from amino acids: Synthesis and characterization of [alpha],[omega]-diaminooligopeptides by ring-opening polymerization of glutamate N-carboxyanhydrides,
Reactive and Functional Polymers, 47, 11-21, **2001**.

34. Zhu, G.-Q.

Micellization behavior comparision of polypeptide graft copolymer and block-graft copolymer in ethanol,
Journal of the Chilean Chemical Society, 55, 266-269, **2010**.

35. Miyazawa, T. & Blout, E.R.
The Infrared Spectra of Polypeptides in Various Conformations: Amide I and II Bands1,
Journal of the American Chemical Society, 83, 712-719, **1961**.

36. Klok, H.A. & Lecommandoux, S.
Supramolecular Materials via Block Copolymer Self-Assembly,
Advanced Materials, 13, 1217-1229, **2001**.

37. Papadopoulos, P., Floudas, G., Klok, H.A., Schnell, I. & Pakula, T.
Self-Assembly and Dynamics of Poly(γ-benzyl-l-glutamate) Peptides,
Biomacromolecules, 5, 81-91, **2003**.

Chapter IV

Specific interactions of non spherical particles: Theoretical approach and development of spheroïdal nanoparticles decorable on demand via the nitriloacetic acid-Nickel-His Tagged system

Chapter 4. Specific interactions of non spherical particles: Theoretical approach and development of spheroïdal nanoparticles decorable on demand via the nitriloacetic acid-Nickel-His Tagged system

Introduction

Drug targeting consists in replacing the unfavorable biodistribution of a drug by those of a carrier. The carrier is expected to be more specifically distributed in target organs or cells and less in the organs where it causes toxicity. To be fully efficient, a possible strategy is to cover the carriers with ligands that will recognize a specific target. These ligands can be small molecules e.g. folic acid, RGD sequences, or large molecules such as peptides or proteins. For every disease one or more specific receptor may be used as a target, for example folate receptors in certain cases of tumors[1]. The development of efficient systems requires each time to adapt the ligand to a new disease. Further, efficient attachment of the ligand to the carrier without damaging its structure and its recognition properties is a complex task.

In this chapter we will consider the influence of the shape of the nanoparticulate carriers on the process of recognition and attachment when these carriers are functionalized in surface. Then we will present an innovative all-purpose system for the drug targeting strategy that is able to attach different ligands or mix of ligands extemporaneously to a carrier.

Our aim was to understand the effect of the shape of nanoparticles on the specific interaction between a nanoparticle and its target.

For this purpose, we will present a theoretical study on the influence of the shape of nanoparticles on the adhesion on a plane surface. Then we will present preliminary results concerning the development of an innovative versatile carrier system, able to be functionalized on demand by attaching a desired his-tagged protein via the formation of a NTA/Ni^{2+}/His-Tagged protein complex. Some of the characteristics of this versatile carrier were finally evaluated by isothermal titration calorimetry and surface plasmon resonance.

4.1. Material and Methods

4.1.1. Polymer synthesis

Poly(γ-benzyl-L-glutamate), PBLG, were synthesized in anhydrous DMF by ring-opening polymerization of γ-benzyl-L-glutamate N-carboxy anhydrides (BLG-NCA, ISOCHEM-SNPE, stored at -18°C) using benzylamine (Janssen Chimica, distilled under reduced pressure over KOH and stored under argon atmosphere at room temperature) as initiator according to a slightly modified method described elsewhere[15].

Briefly, BLG-NCA was weighed under argon atmosphere in a degassed three-necked roundbottomed flask equipped with a thermometer, mechanical stirring, a refrigerant with a silica gel guard and a bubble detector. BLG-NCA was dissolved in DMF (volume was adjusted to obtain a BLG-NCA final concentration of 0.5M) at room temperature under mechanical stirring and argon flux. After about 10min, the argon flux was stopped, the solution was heated at 30°C and the initiator solution was added. Immediately after the addition, CO_2 emission was observed. Absence of BLG-NCA auto-polymerization was checked by FTIR spectroscopy of the BLG-NCA solution before addition of the initiator. The reaction mixture was stirred at 30°C until the characteristic BLG-NCA bands disappeared from the FTIR spectrum. The mixture was precipitated in an excess of cold diethyl ether to give a white solid. The precipitate was filtered and washed with diethyl ether. The polymers were again washed with diethyl ether and dried under vacuum at 35°C for at least 12 h. A second precipitation, purification and drying procedure was performed for all polymers. FTIR spectra were recorded to analyze BLG-NCA auto-polymerization and to follow the reaction using a Perkin-Elmer 1750 FTIR spectrometer.

4.1.2. Post-synthesis Modification

Polymers of different molecular weights were then used for post synthesis modification.

4.1.2.1. Peggylation

Coupling Metoxy-PEG(6000)-N-Hydroxysuccinimide to PBLG was done overnight in a mix of solvent. Briefly 500mg of PBLG was dissolved in 4mL of 25% THF, 25% DMF and 50% DMSO during 18h. 4mL of Metoxy-PEG(6000)-N-Hydroxysuccinimide was added to the mix for a final concentration of 1.5 equivalent. The reaction was heated at 30°C under magnetic stiring and under argon atmosphere during 24h.

4.1.2.2. Nitriloacetic acid-Peggylation

N_α-N_α-Bis(carboxymethyl)-L-lysine hydrate (>97% TLC, Sigma-Aldrich) was added to 70mg of N-Hydroxysuccinimide-PEG(6000)-N-Hydroxysuccinimide (Iris Biotech GmbH) for a final concentration of 1.5 equivalent in 20mL of DMSO. After 2h, 10mL of the resulting solution was mixed with 500mg of PBLG, dissolved in 20mL of 25% THF, 25% DMF and 50% DMSO, during 18h. The reaction was heated at 30°C under magnetic stiring and under argon atmosphere.

4.1.3. Nanoparticles preparation

Nanoparticles from PBLG were prepared using a modified nanoprecipitation method. Briefly, 15mg of polymer (1.5, 12 and 1.5mg of PBLG-rhodamine, PBLG-PEG and PBLG) were dissolved in 5mL of THF at 30°C during 18h, without stirring. This solution was added dropwise to 10mL of Poloxamer F68 at 0.1% under magnetic stirring (700rpm). The mixture was left under magnetic stirring for 10min and then transferred in a glass flask. The solvent was gently evaporated in a rotavapor (V850, R124, Buchi) at 40°C, first at 200mbar for 5min and then at 40mbar to yield 5mL of suspension. The pH of each preparation was measured, and the osmolarity of each preparation was adjusted to 9% by adding 200µl of NaCl solution with a concentration 225g.L^{-1}.

4.1.4. Matrix-assisted laser desorption/ionization time-of-flight mass spectroscopy

Matrix-assisted Laser Desorption/Ionization-Time of Flight-Mass Spectrometry (MALDI-TOF-MS) analysis was carried out in positive-ion mode on a Voyager DE-STR MALDI-TOF mass spectrometer (Perseptive Applied Biosystems, Framingham, MA,USA) equipped with a 337nm nitrogen laser. DCTB or 2-[(2E)-3-(4-tert-Butylphenyl)-2-methylprop-2-enylidene] malononitrile (40mg.mL^{-1} in THF) and potassium trifluoroacetate (50mg.mL^{-1} in THF) were used respectively as matrix and cationic ionization agent and polymer:matrix molar concentration ratio was adjusted between 40:1(for the lowest molecular weight) and 1:3600 (for the highest molecular weight). 20µL of this matrix, 1µL of polymer (at the adjusted concentrations) and 1µL of ionization agent were mixed and deposited onto the sample plate and allowed to dry at room temperature. Spectra of PBLG were acquired with the default calibration (accuracy ca. 0.1 %) under the same condition as those described in Sicard-Roselli et al.[2].

4.1.5. Nuclear Magnetic Resonance

^{1}H NMR spectra of the copolymers (PBLG-PEG, PBLG-PEG-NTA) were measured in solvent deuterated chloroform ($CDCl_3$) to estimate the copolymers composition and the molecular weight of PBLG blocks using a Bruker Advance 400 apparatus, operating at 400MHz. For molecular weight estimation, integration values of 1H NMR (δ, $CDCl_3$): 7.26 (br, s, 5H, Ph–) or 5.04 (br, s, 2H, –CH2–benzyl) for the PBLG segment, and 3.65 (br, s, 4H, $–OCH_2–CH_2O–$) for the PEG segment were used.

4.1.6. Transition Electron Microscopy (TEM) observations

Nanoparticles shape and size were further analyzed through TEM (Transmission electron microscope Philips EM208) at 60 kV. 3µl of nanoparticles suspension, after suitable dilution of bulk suspensions in milli-Q water, were placed on a formvar-carbon film previously coated on a copper grid (400 meshes). After 5min of deposition, a drop of phosphotungstic acid or uranyle acetate was placed on the copper grid, on top of the sample. After 30s, the liquid was drained and the sample was placed inside the EM208 and pictures were taken. Nanoparticles measurements were obtained through Gimp© software.

4.1.7. Size and shape analysis

Nanoparticles from TEM pictures were in very dilute solution and were supposed to be flat on the grid. For each sample particle dimensions were measured on different TEM pictures on an average of 30 nanoparticles (total). On each particle, the smallest and the longest size were measured and were named width and length respectively. The model chosen for the analysis was that the obtained form of the nanoparticles was an ovoid. To assess the evolution of volumes with a parameter easily understandable the diameter of the sphere of equivalent volume was calculated using the formula below

Eq.1

$$Aspect\ Ratio = \Gamma = \frac{Length}{Width}$$

Eq.2

$$Equivalent\ Diameter = \sqrt[3]{Length * width^2}$$

4.1.8. Isothermal Titration Microcalorimetry (ITC) studies

ITC experiments were carried out with a VP-ITC, Microcal-GE Healthcare. Interaction of His-TAG with the nanoparticles of PBLG of different molecular weight (inducing different shapes) and different surface coating was assessed at 25°C by simple comparison, and then fitting could be made according to the nanoparticle surface functionalization. Nanoparticles solutions at 3mg.mL^{-1} of polymers in water pH7 were placed in the sample cell of 1.44mL. They were "titrated" by the solution of His-TAG at 60µM (preactivated by Ni2+ ions) placed in the 298µL syringe, continuously rotating at 394rpm. Injections of 10µL of the HisTAG solution were made every 500s and the observed heat was registered by the software VPviewer. The data were then processed with Microcal-Origin.

4.1.9. Surface Plasmon Resonance (SPR) experiments

4.1.9.1. Chips preparation:

SPR studies were carried out with a BiacoreT100, Biacore-GE Healthcare. Preparation of C1 and CM5 Sensor chips (Biacore, GE Healthcare) were all prepared using the same protocol. Canal 1 and 3 were inactivated with ethanolamine at 10µL.s^{-1} for 400s and canal 2 and 4 were first treated with EDC/NHS at 10 µL.s^{-1} for 400s, then with His-Tag 125µg.mL^{-1} in acetate at 10µL.s^{-1} for 400s, and finally with ethanolamine at 10µL.s^{-1} for 400s.

4.1.9.2. Binding experiments:

Various nanoparticles were injected at 10µL.min^{-1} to flow over the chips surface according to the following sequence: (i) Ni^{2+} 2mM for activation of the surface for 60s (ii) Binding of nanoparticles 1.5mg.mL^{-1} in water for 300s (iii) Regeneration of the surfaces with EDTA 0.5M, pH=8, for 120s twice and for 300s once.

4.2. Results & Discussion

Following their delivery, there are many circumstances where nanoparticles are prone to adhere to biological surfaces. These interactions can be mediated either by “non specific” or “specific” (i.e. ligand-receptor interactions). Whatever the mechanisms, the control of these interaction processes is of utmost importance as it is one of the parameter which dictates the distribution of the particles in the body.

After intravenous delivery of a nanoparticle suspension in the bloodstream and dilution, the particles are distributed in the whole body through the vascular system. At this early step of the distribution there are already numerous possibilities of interactions e.g. with plasmatic proteins, red blood cells, endothelial cells lining the capillaries, reticulo-endothelial cells. Some of these interactions are favorable but others do not increase the specificity of distribution in target cells and/or internalization. This is the reason why a general strategy for targeting nanoparticles precisely to their site of action consists in modifying their surface by the attachment of molecules able to repulse unwanted interactions and simultaneously allow the desired one. The “quality” of the presentation needs to be especially considered at the molecular scale: nature of the molecule, density, spacing, flexibility.

Most of the nanoparticles investigated so far are spheres, but obviously if their shape diverges from sphericity, it is highly probable that considerable changes in recognition mechanisms will occur. For this reason, the aim of this chapter was first to model the effect of shape on the interactions of non spherical particles with a plan surface and secondly to develop a technique for decorating “on demand” non spherical particles with protein ligands, in order to investigate the mechanisms of attachment and detachment

4.2.1. Modeling the interactions of non spherical nanoparticles

A simple model of the interactions of non spherical nanoparticles has been developed in order to give some rules on how non spherical particles will interact with the surface of a “wall” bearing receptors able to recognize the ligands beared by the particles. If the particle is able to reach the wall and “locks on”, there will be an attachment and a certain force will be required to break all the ligand-receptor bonds.

Ligand-receptor interactions between two soluble species are discrete events, which can be quite easily assessed on populations by experimental techniques such as surface plasmon

resonance technique (Biacore) or calorimetric techniques such as isothermal titration calorimetry (ITC). However, for a multivalent particle (bearing several ligands per particle), two phenomena have to be taken into account: multi-interactions and the total number of interactions.

In the case of multiple ligands binding on a single receptor site (if possible), the strength of the bond is not linear with the number of interactions. In many systems, it has been shown that a few interactions could change the dissociation constant K_D by several orders of magnitude. For example the NTA/Ni^{2+}/His-Tag interaction falls in this category. This interaction is commonly used in biology for tagging proteins for detection purposes. In this system, from a mono to a bis interaction, there are two orders of magnitude in terms of K_D and the system gains another order of magnitude by adding another ligand-receptor interaction[3-4]

However in the case of one ligand for each receptor (1:1 binding model), the problem is simplified. The strength of the bond is proportional to the dissociation constant (K_D) and the number of bonds. The effects of different parameters have been extensively evaluated in the literature[5-7]: ligand and receptor concentration, pH, ionic strength, contact area, dissociation constant,…but not the shape. Still the effect of the shape on the strength of the bond can be evaluated for a same ligand-receptor system. Decuzzi et al. [8] have studied this phenomenon in the case of a sphere.

In the present case, we have evaluated the impact of the shape on the force of attachment occurring between a particle bearing ligands homogeneously distributed on the particle surface (see figures 4.5 and 4.7 for example). We present here a model to compare the force of interaction for different shapes. To simplify the problem it has been considered that each ligand and receptor is a spring and that it can interact up until a critical distance, H. Hence, the force is proportional to the surface of the particle between the plane and the plane particle.

4.2.1.1. Computer modeling

To be able to solve this problem, two cases corresponding to the different ways to attach the particles to the surface have been considered. In the first case, the particle will present its axis of symmetry perpendicular to the surface in the second case this axis will be parallel to the surface (figures 4.1 and 4.2).

First case:

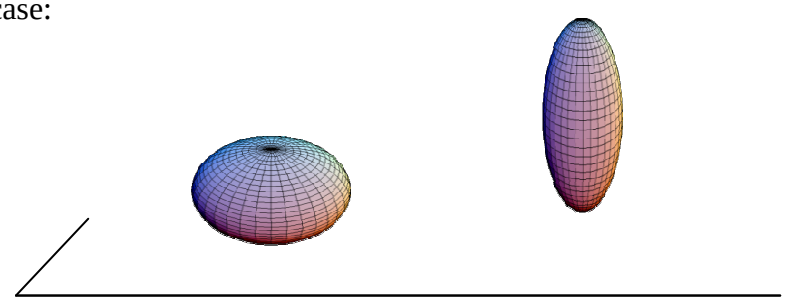

Figure 4.1: First case. Ellipsoidal nanoparticles attach to the plane perpendicularly to their equatorial axis

Second case:

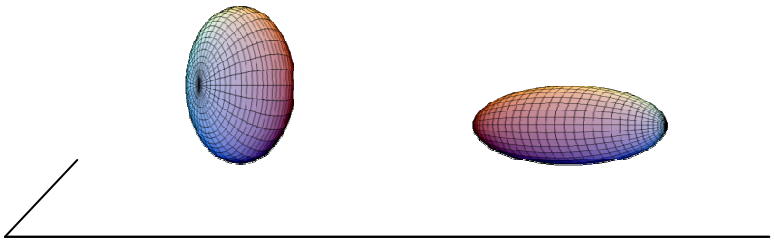

Figure 4.2: Second case. Ellipsoidal nanoparticles attach to the plane parallelly to their equatorial axis

Both cases represent valid approaches for the different types of particles. In the case of the sphere, both cases are equivalent. The equations making possible to calculate the surface of interactions have been derived in both cases.

First case : evaluation of the interacting surface (perpendicularly to the equatorial axis)

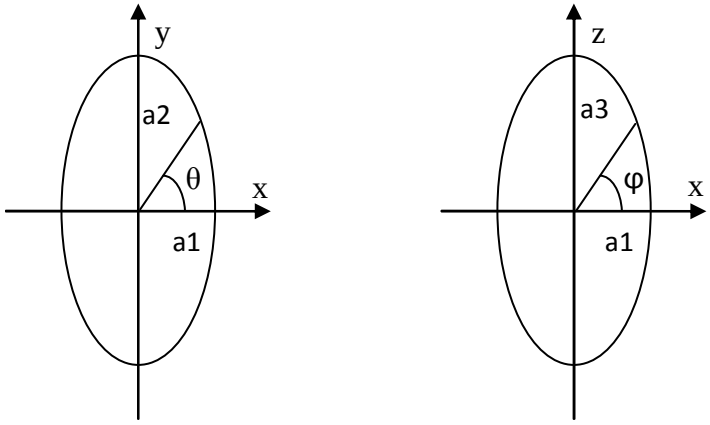

$$\theta \in [0; 2\pi];\ \varphi \in \left[-\frac{\pi}{2}; \frac{\pi}{2}\right]$$

Figure 4.3: Ellipsoid coordinates

The coordinates of an ellipsoid can be described as follow:

$$\begin{cases} x = a_1 \cos(\theta) \cos(\varphi) \\ y = a_2 \sin(\theta) \cos(\varphi) \\ z = a_3 \sin(\varphi) \end{cases}$$

From these coordinates we can calculate the surface of the ellipsoid:

$$\boldsymbol{T}_\theta = \begin{pmatrix} dx/d\theta \\ dy/d\theta \\ dz/d\theta \end{pmatrix} \text{ and } \boldsymbol{T}_{\boldsymbol{\varphi}} = \begin{pmatrix} dx/d\varphi \\ dy/d\varphi \\ dz/d\varphi \end{pmatrix}$$

$$S_{ellipsoid} = \iint_{\theta=\theta_i,\varphi=\varphi_i}^{\theta=\theta_f,\varphi=\varphi_f} \left\| \boldsymbol{T}_\theta \wedge \boldsymbol{T}_{\boldsymbol{\varphi}} \right\| d\theta d\varphi$$

$$\boldsymbol{T}_\theta \wedge \boldsymbol{T}_{\boldsymbol{\varphi}} = \begin{pmatrix} a_2 a_3 \cos(\theta)\cos^2(\varphi) \\ a_1 a_3 \sin(\theta)\cos^2(\varphi) \\ a_1 a_2 \sin(\varphi)\cos(\varphi) \end{pmatrix}$$

$$\left\| \boldsymbol{T}_\theta \wedge \boldsymbol{T}_{\boldsymbol{\varphi}} \right\|$$
$$= \sqrt{{a_2}^2 {a_3}^2 \cos^2(\theta)\cos^4(\varphi) + {a_1}^2 {a_3}^2 \sin^2(\theta)\cos^4(\varphi) + {a_1}^2 {a_2}^2 \sin^2(\varphi)\cos^2(\varphi)}$$

In our cases, we deal with spheroids which are a special kind of ellipsoid for which $a_1 = a_2$.

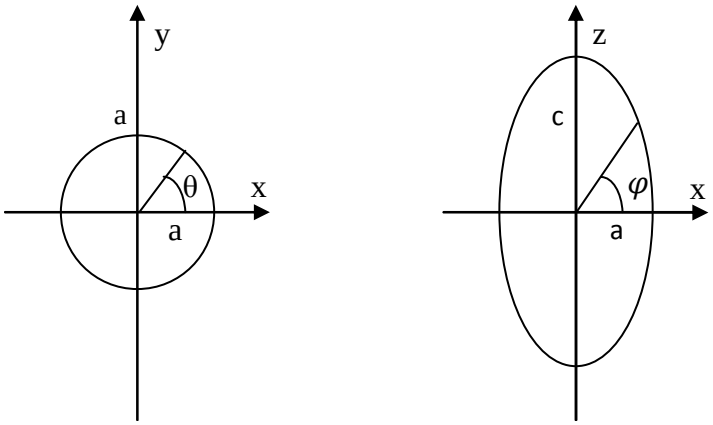

Figure 4.4: Spheroid coordinates

$$\left\|\boldsymbol{T}_{\theta} \wedge \boldsymbol{T}_{\boldsymbol{\varphi}}\right\| = \sqrt{{a_1}^2 {a_3}^2 \cos^2(\theta)\cos^4(\varphi) + {a_1}^2 {a_3}^2 \sin^2(\theta)\cos^4(\varphi) + {a_1}^4 \sin^2(\varphi)\cos^2(\varphi)}$$

$$\left\|\boldsymbol{T}_{\theta} \wedge \boldsymbol{T}_{\boldsymbol{\varphi}}\right\| = a_1 \cos(\varphi) \sqrt{{a_3}^2\cos^2(\varphi) + {a_1}^2 \sin^2(\varphi)}$$

$$S_{ellipsoid} = \iint_{\theta=\theta_i,\varphi=\varphi_i}^{\theta=\theta_f,\varphi=\varphi_f} a_1 \cos(\varphi) \sqrt{{a_3}^2\cos^2(\varphi) + {a_1}^2 \sin^2(\varphi)}\, d\theta d\varphi$$

$$\boxed{S_{ellipsoid} = a_1(\theta_f - \theta_i) \int_{\varphi=\varphi_i}^{\varphi=\varphi_f} \cos(\varphi) \sqrt{{a_3}^2\cos^2(\varphi) + {a_1}^2 \sin^2(\varphi)}\, d\varphi}$$

This integral cannot be mathematically solved except in the case of the sphere:

$$a_1 = a_3 \; ; \; \mathrm{S_{sphere}} = {a_1}^2\left(\theta_f - \theta_i\right) * (\sin(\varphi_f) - \sin(\varphi_i))$$

Furthermore $\theta_f, \theta_i, \varphi_f,$ and φ_i can be extracted from H the critical distance after which ligand and receptor cannot interact, and h_s the distance between the surface of the particle and the wall.

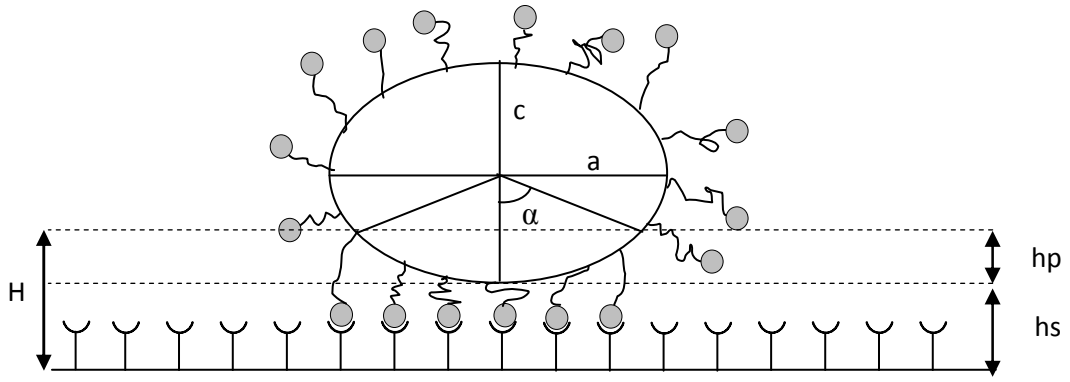

Figure 4.5: Attachment model

In the (yz) plan, the "critical" angle φ_f that characterizes the intersection of the spheroid with the plan can be calculated as follows:

$$\varphi_i = -\frac{\pi}{2} \quad \& \quad \varphi_f = -\frac{\pi}{2} - \alpha$$

$$cos(\alpha) = \frac{c - h_p}{r(\alpha)} = \frac{c + h_s - H}{r(\alpha)}$$

Where $r(\alpha)$ is the radius of the ellipse (a1 = c, a2 = a3 = a) at the angle α and can be calculated as follows:

$$r(\alpha) = \frac{ac}{\sqrt{a^2 cos^2(\alpha) + c^2 sin^2(\alpha)}}$$

$$\big(r(\alpha)\big)^2 cos^2(\alpha) = (c + h_s - H)^2$$

$$a^2 c^2 * cos^2(\alpha) = (c + h_s - H)^2 * [a^2 cos^2(\theta) + c^2 sin^2(\alpha)]$$

$$a^2 c^2 * cos^2(\alpha) = (c + h_s - H)^2 * [a^2 cos^2(\theta) + c^2 (1 - cos^2(\alpha))]$$

$$cos^2(\alpha) * (a^2 c^2 + (c + h_s - H)^2 * (c^2 - a^2)) = (c + h_s - H)^2 * c^2$$

$$cos(\alpha) = \frac{(c + h_s - H) * c}{\sqrt{a^2 c^2 + (c + h_s - H)^2 * (c^2 - a^2)}}$$

With α calculated, we can calculate φ_f. Furthermore, $\theta_i = 0$ & $\theta_f = 2\pi$.

From this we can evaluate the surface of the ellipsoid for different values of H and h_s.

Second case: evaluation of the interacting surface (parallelly to the equatorial axis)

To evaluate the surface in the second approach, we have to change the set of coordinates.

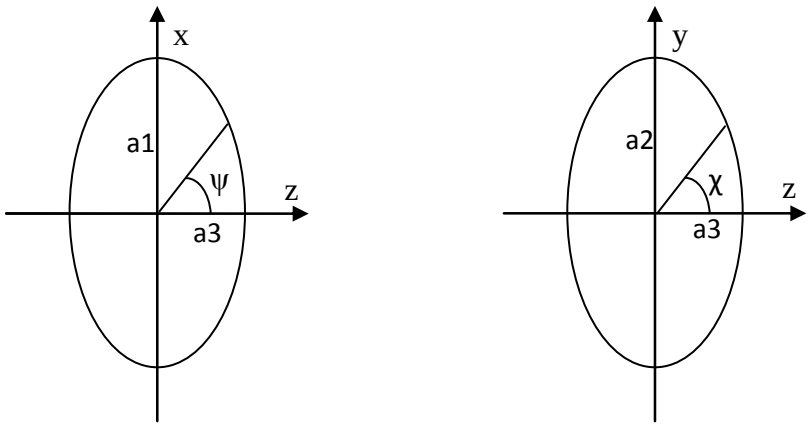

$$\psi \in [0; 2\pi];\ \chi \in \left[-\frac{\pi}{2}; \frac{\pi}{2}\right]$$

Figure 4.6: Ellipsoid coordinates

The coordinates of an ellipsoid can be described as follow:

$$\begin{cases} x = a_3 \cos(\chi) \cos(\psi) \\ y = a_2 \sin(\chi) \cos(\psi) \\ z = a_1 \sin(\psi) \end{cases}$$

From these coordinates we can calculate the surface of the ellipsoid:

$$\boldsymbol{T}_\chi = \begin{pmatrix} dx/d\chi \\ dy/d\chi \\ dz/d\chi \end{pmatrix} \text{ and } \boldsymbol{T}_\psi = \begin{pmatrix} dx/d\psi \\ dy/d\psi \\ dz/d\psi \end{pmatrix}$$

$$S_{ellipsoid} = \iint_{\chi=\chi_i,\psi=\psi_i}^{\chi=\chi_f,\psi=\psi_f} \left\| \boldsymbol{T}_\chi \wedge \boldsymbol{T}_\psi \right\| d\chi d\psi$$

$$\boldsymbol{T}_\chi \wedge \boldsymbol{T}_\psi = \begin{pmatrix} a_1 a_2 \cos(\chi)\cos^2(\psi) \\ a_1 a_3 \sin(\chi)\cos^2(\psi) \\ a_2 a_3 \sin(\psi)\cos(\psi) \end{pmatrix}$$

$$\|\boldsymbol{T}_\theta \wedge \boldsymbol{T}_{\boldsymbol{\varphi}}\| = \sqrt{{a_1}^2{a_2}^2\cos^2(\chi)\cos^4(\psi) + {a_1}^2{a_3}^2\sin^2(\chi)\cos^4(\psi) + {a_2}^2{a_3}^2\sin^2(\psi)\cos^2(\psi)}$$

In our cases, we deal with spheroids which are a special kind of ellipsoid for which $a_1 = a_2$.

$$\|\boldsymbol{T}_\theta \wedge \boldsymbol{T}_{\boldsymbol{\varphi}}\| = \sqrt{{a_1}^4\cos^2(\chi)\cos^4(\psi) + {a_1}^2{a_3}^2\sin^2(\chi)\cos^4(\psi) + {a_1}^2\,{a_3}^2\sin^2(\psi)\cos^2(\psi)}$$

$$\|\boldsymbol{T}_\theta \wedge \boldsymbol{T}_{\boldsymbol{\varphi}}\| = a_1\cos(\psi)\sqrt{{a_1}^2\cos^2(\chi)\cos^2(\psi) + {a_3}^2\sin^2(\chi)\cos^2(\psi) + {a_3}^2\sin^2(\psi)}$$

$$S_{spheroid} = \iint_{\chi=\chi_i,\psi=\psi_i}^{\chi=\chi_f,\psi=\psi_f} a_1\cos(\psi)\sqrt{{a_1}^2\cos^2(\chi)\cos^2(\psi) + {a_3}^2\sin^2(\chi)\cos^2(\psi) + {a_3}^2\sin^2(\psi)}\,d\psi d\chi$$

Furthermore $\chi_f, \chi_i, \psi_f,$ and ψ_i can be extracted from H the critical distance after which ligand and receptor cannot interact, and hs the distance between the surface of the particle and the wall.

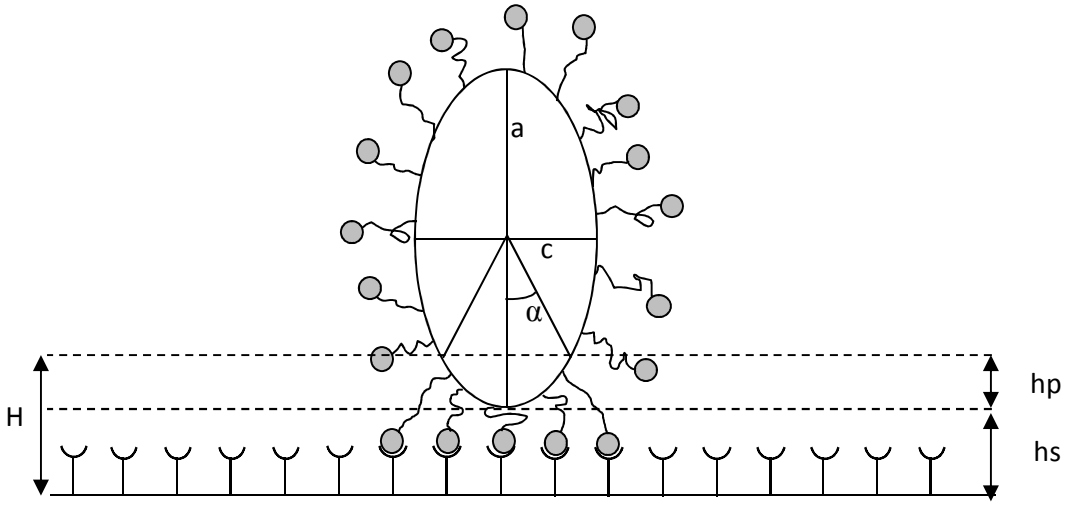

Figure 4.7: Attachment model

In the (xz) plan, the "critical" angle ψ_f that characterizes the intersection of the spheroid with the plan can be calculated as follows:

$$\psi_i = -\alpha \;\;\&\;\; \psi_f = \alpha$$

$$cos(\alpha) = \frac{a - h_p}{r(\alpha)} = \frac{a + h_s - H}{r(\alpha)}$$

Where $r(\alpha)$ is the radius of the ellipse (a1 = c, a2 = a3 = a) at the angle α and can be calculated as follows:

$$r(\alpha) = \frac{ab}{\sqrt{c^2 cos^2(\alpha) + a^2 sin^2(\alpha)}}$$

$$\big(r(\alpha)\big)^2 cos^2(\alpha) = (a + h_s - H)^2$$

$$a^2c^2 * cos^2(\alpha) = (a + h_s - H)^2 * [c^2 cos^2(\theta) + a^2 sin^2(\alpha)]$$

$$a^2c^2 * cos^2(\alpha) = (a + h_s - H)^2 * [c^2 cos^2(\theta) + a^2(1 - cos^2(\alpha))]$$

$$cos^2(\alpha) * (a^2c^2 + (a + h_s - H)^2 * (a^2 - c^2)) = (a + h_s - H)^2 * a^2$$

$$cos(\alpha) = \frac{(a + h_s - H) * a}{\sqrt{a^2c^2 + (a + h_s - H)^2 * (a^2 - c^2)}}$$

With α calculated, we can calculate ψ_f. Furthermore $\chi_i = 0$ & $\chi_f = 2\pi$.

4.2.1.2. Influence of the shape of ellipsoïds on the surface available for interactions

With those equations it is possible to calculate the surface of the ellipsoid available for interactions with the plane. This has been done for different values of H and hs using a specific Matlab routine (program available in appendix).

We chose here to present the results of the partial surface between a wall and a plan at a distance of H=20nm. This value has been considered to be representative of real situations. For instance when ligands are attached to the surface of the particles by a linear poly(ethylene glycol chain (M=5000g/mol) and that the ligand is interacting with a receptor directly on the wall. Moreover we assumed that the gap between the wall and the particle interacting surface is hs=10nm (for taking account of steric repulsion interactions).

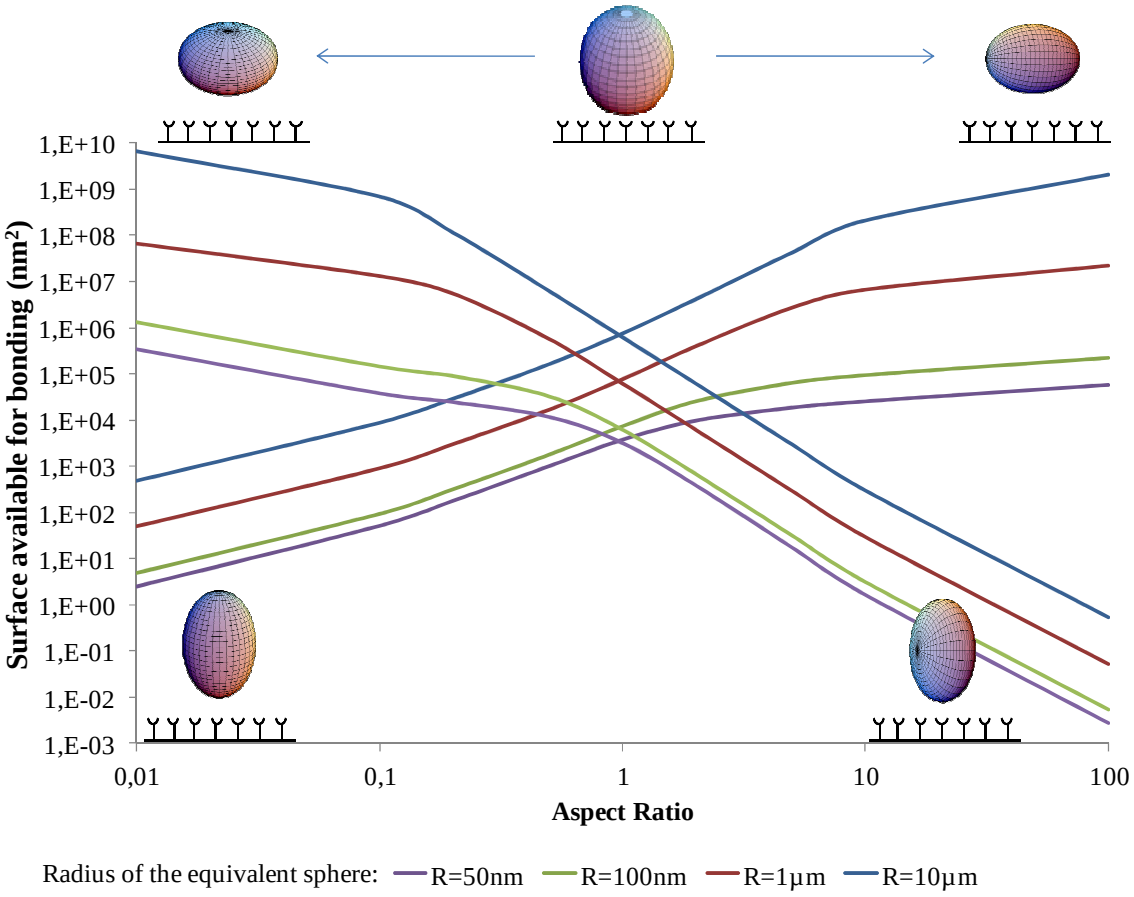

Figure 4.8: Available surface for interactions per nanoparticle according to the developed model. The calculated surface is expressed as nm^2 for a single particle (note the log scales). Different situations are presented for spheroids with different sphere equivalent volumes (i.e. different particle "sizes") and as a function of their shape.

As we mentioned at the start of this evaluation, the force of the bond between the particle and the wall was assumed to be proportional to the surface of the particle available for interactions. Figure 4.8 shows that the morphology of particles and the angle between the particle and the wall have a strong influence on the surface available for bonding. Assuming proportionality of the force to the number of bonds, the global binding strength of a particle to the surface is likely to vary up to 8 orders of magnitudes depending on the position of the particle on the wall for the less spherical particles. The shape also has a major influence on

the binding strength. Strikingly, with only a difference of a factor 10 in aspect ratio, the useful specific surface can vary by up to 4 orders of magnitude (bigger or smaller).

If the particle is in a motionless fluid, only the useful specific surface has to be taken into account to evaluate the strength of the bond. However in the case of fluids in motion, like blood, or under other external strengths, the probability for a stable attachment can be evaluated by comparing the available attachment surface of the particle (representing the strength of the bond) to the surface of its section (representing the force applied by the fluid on the particle). In doing so, we observed that shape will have an impact up to four orders of magnitude for an evolution in aspect ratio from 1 to 10. Decuzzi et al. have also studied this phenomenon[9]. They have shown that there is an optimal volume for each aspect ratio for which the adhesion strength will be maximal, depending on the shear stress at the wall and the ligand density at the wall. They even recommend the use of oblate spheroid particles to optimize both drug loading and interaction propensity.

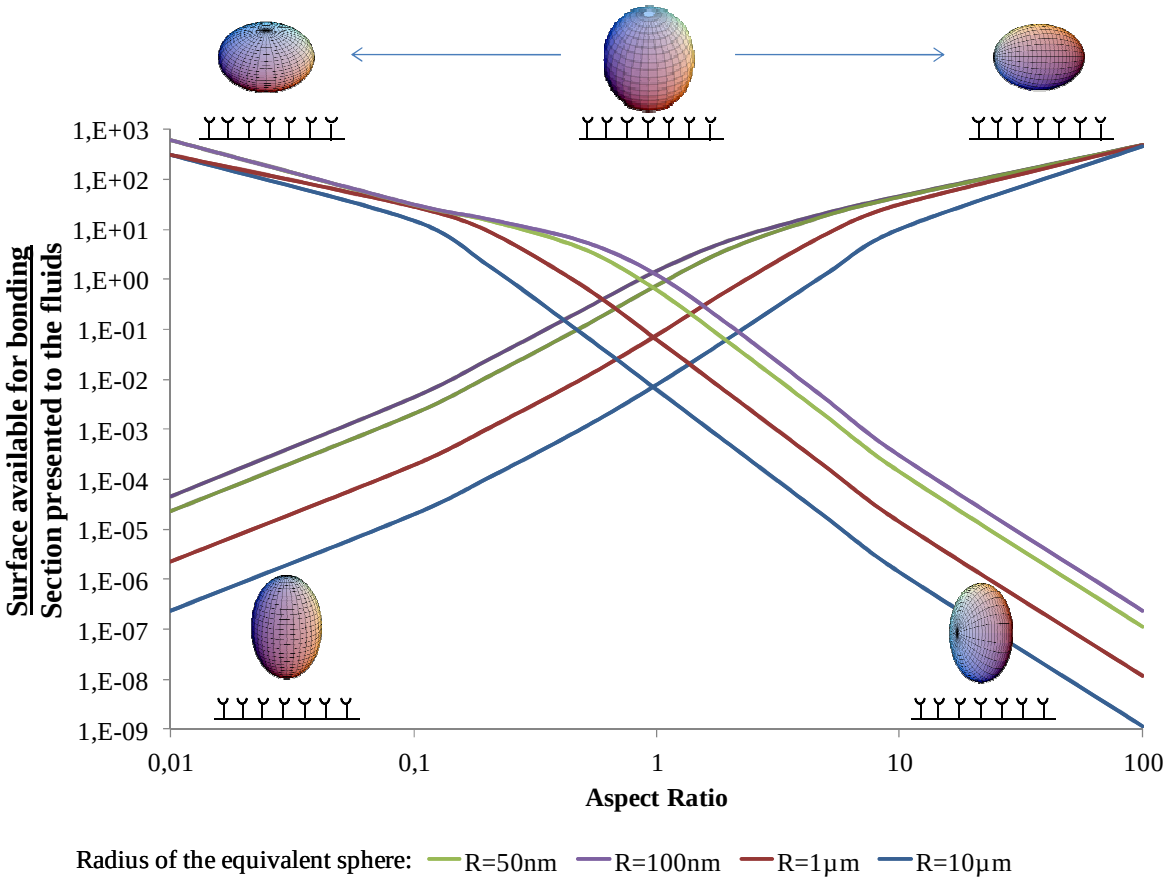

Figure 4.9: Probability for a stable attachment. Different situations are presented for spheroids with different sphere equivalent volumes (i.e. different particle "sizes") and as a function of their shape.

As shown on figure 4.9, and confirming intuition, the larger particles do not have a stronger probability of adhesion. On the contrary, smaller particles seem to have a higher chance of adhesion. However, we have looked at smaller particles as Decuzzi et al. did and we have not noticed the existence of an optimal size. Once more, we noticed that the non spherical particles have higher or lower probabilities to attach to the wall depending on their angle of approach.

Indeed, the present model does not take in account a series of conditions which should be encountered during in vivo. However, it can be concluded that a strong influence of particles shape can be expected on their capacity to escape the blood circulation and/or to adhere to biological surfaces, and/or detach from these surfaces. Therefore, even with particles made of the same material, variations in the biodistribution can be expected.

4.2.2. Preparation and characterization of model spheroïdal nanoparticles

This second part of the chapter presents preliminary experiments aiming to prepare functionalized spheroïdal nanoparticles and to characterize the influence of shape on their adhesive characteristics.

First was the necessity to produce nanoparticles of different shapes that possess the ability to be decorated "on demand" with ligands of interest. PBLG nanoparticles were used for this purpose because of their ability to form non spherical particles (see chapter 3). The ligand coupling strategy will be first presented and followed by a preliminary study of the adhesion of nanoparticles of different shapes.

4.2.2.1. Model spheroidal nanoparticles

Model spheroïdal nanoparticles able to be decorated "on demand" by proteins or peptides have been conceived by introducing nitriloacetic acid molecules at the surface of spheroïdal poly(γ-benzyl-L-glutamate) nanoparticles. The principle of the system is shown on figure 4.10. Attachment of his-tagged proteins at the surface of the particles can be performed under mild conditions after the manufacture of the particles by forming a NTA/Ni2+/His-Tag complex and the density of attachment could at least theoretically easily adjusted.

Nitriloacetic acid (or NTA) is a polyamino carboxylic acid that can be used as a chelating agent for metal ions such as Ca^{2+}, Cu^{2+}, Fe^{3+}… NTA is well known for its similarity to ethylenediaminetetraacetic acid EDTA, however NTA is not toxic to human. In biology, NTA has been used to purify solutions of proteins containing a His-Tag group, a chain of six histidine residues, through the use of a sephadex gel affinity column containing NTA groups. Indeed NTA is able to fix His-Tag groups via a Ni^{2+} ion as shown in figure 4.10.

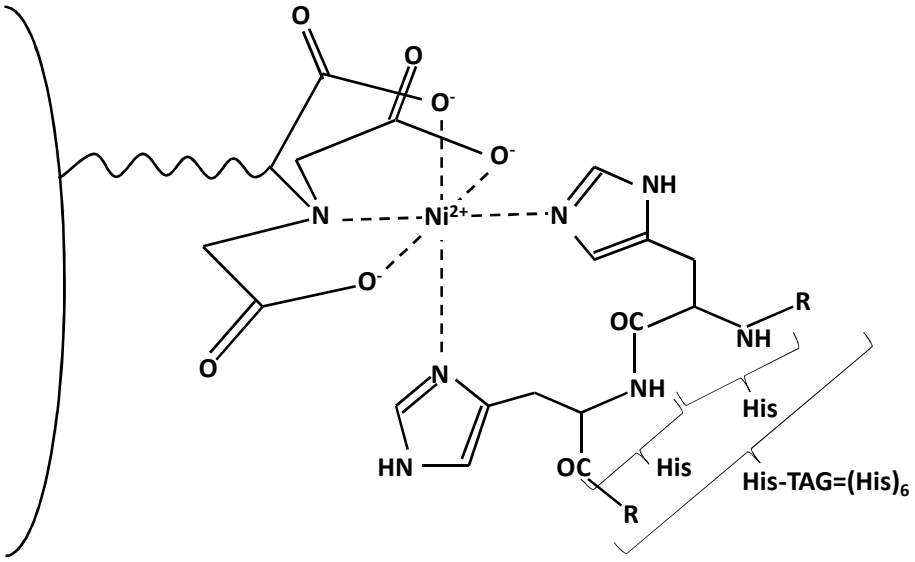

Figure 4.10: Principle for the attachment of his-tagged proteic ligands to spheroidal nanoparticles bearing in surface nitrilo acetic acid. Attachment of his-tagged proteins can be performed under mild conditions after the manufacture of the particles by forming a NTA/Ni2+/His-Tag complex

The NTA/Ni^{2+}/His-Tag system has been well studied. The affinities between Ni^{2+} and His-Tag[10], Ni^{2+} and NTA[11-12] and for the NTA/Ni^{2+}/His-Tag complex[13] have all been characterized in the literature.

This complexation system is not as powerful as the streptavidin-biotin system in term of affinity constant, however its size is a lot smaller. Indeed the streptavidin-biotin complex weights around 60kg/mol, whereas the NTA/Ni2+/His-Tag complex weights only 0.4kg/mol. In addition, this innovative system is more specific than the streptavidin-biotin system that tends to interfere non specifically with various proteins. Furthermore, NTA is also well known for fixing some radioactive markers such as ^{99}Tc, ^{111}In, and ^{44}Ca with high affinity constants[14]. Thus NTA as a ligand on the surface of carriers could be used for imaging the biodistribution and the *in vivo* fate of the carriers in real time.

4.2.2.2. Post synthesis modification of poly(gamma benzyle glutamate) (PBLG)

i. PEG coupling

PBLG polypeptidic chains were coupled post-synthesis to PEG chains. Results of the polymer synthesis and post synthesis modification are gathered in table 4.1. Polymers coupled with PEG chains could not be analyzed by MALDI-TOF. Thus, coupling was confirmed and measured through NMR analysis. 10 to 30% of the PBLG chains were coupled with PEG.

Since PEG coupling efficiency was low, and should not be sufficient for covering totally the surface of the particles, it was decided to use poloxamer F68® during the manufacturing process of the nanoparticles to maximize the coverage of the nanoparticles with hydrophilic PEG chains. Minimal concentration in the nanoprecipitation medium (water) was found to be 0.1% of poloxamer. This concentration is consistent with the literature dealing with nanoprecipitation.

ii. PEG-NTA coupling

NTA has been coupled to PEG before coupling this derivative to polypeptidic PBLG chains. NMR analysis also revealed 26% of PEG coupling for the PBLG-PEG-NTA. N_α-N_α-Bis(carboxymethyl)-L-lysine hydrate coupling to PEG was not evaluated since no method allowed its measurement.

Table 4.1 Characteristics of PBLG polymer and its derivatives after synthesis and post synthesis modifications (Molecular weights from MALDI-TOF experiments).

Polymer	Molecular Weight (kg/mol)
PBLG28	27.7
PBLG48	48.0
PBLG55	54.5
PBLG48-PEG(6000)-NTA	54.3

4.2.2.3. Preliminary characterization via isothermal titration calorimetry

Once the polymers of interest were obtained, proof-of-concept experiments were performed. First the N_α-N_α-Bis(carboxymethyl)-L-lysine hydrate/Ni^{2+}/His-Tag system was

characterized via isothermal titration calorimetry (ITC). Then composite nanoparticles (PBLG, PBLG-PEG and PBLG-PEG-NTA) were prepared and analyzed through ITC and Surface Plasmon Resonance (SPR) in which the effect of the presence of NTA groups on the surface of the nanoparticles and the effect of shape on the nanoparticles-NTA / Ni^{2+} / His-Tag were evaluated.

i. Nα-Nα-Bis(carboxymethyl)-L-lysine hydrate / Ni^{2+} / His-Tag system characterization by Isothermal Titration Calorimetry (ITC).

The first step of this project was to evaluate the strength of the binding of the N_α-N_α-Bis(carboxymethyl)-L-lysine hydrate / Ni^{2+} / His-Tag system. For this a series of assays were made by measuring the association of Ni^{2+} with His-Tag, and with N_α-N_α-Bis(carboxymethyl)-L-lysine hydrate.

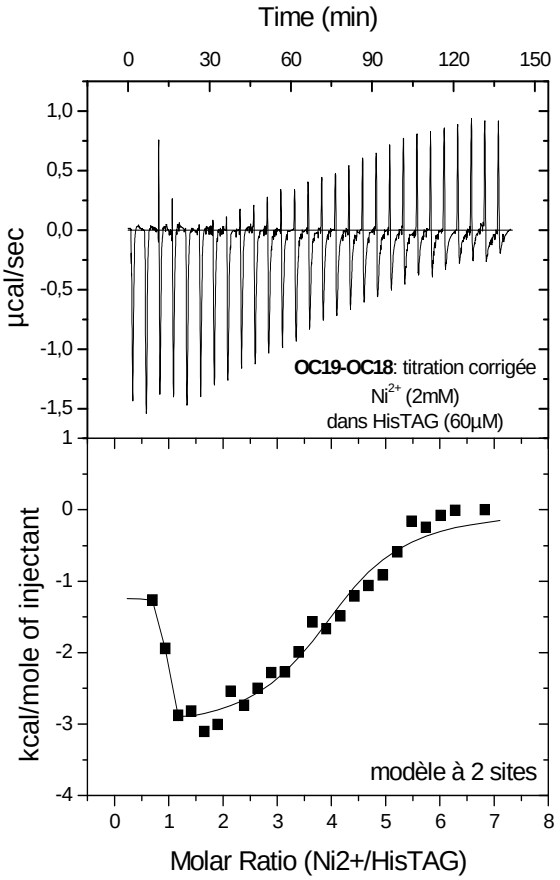

Figure 4.11: ITC characterization of the formation of the Ni^{2+}/His Tag complex

During the titration of Ni^{2+} in His-Tag, shown in figure 4.11, an exothermic reaction was highlighted, which was assumed to correspond to the formation of the Ni^{2+}/His Tag complex.

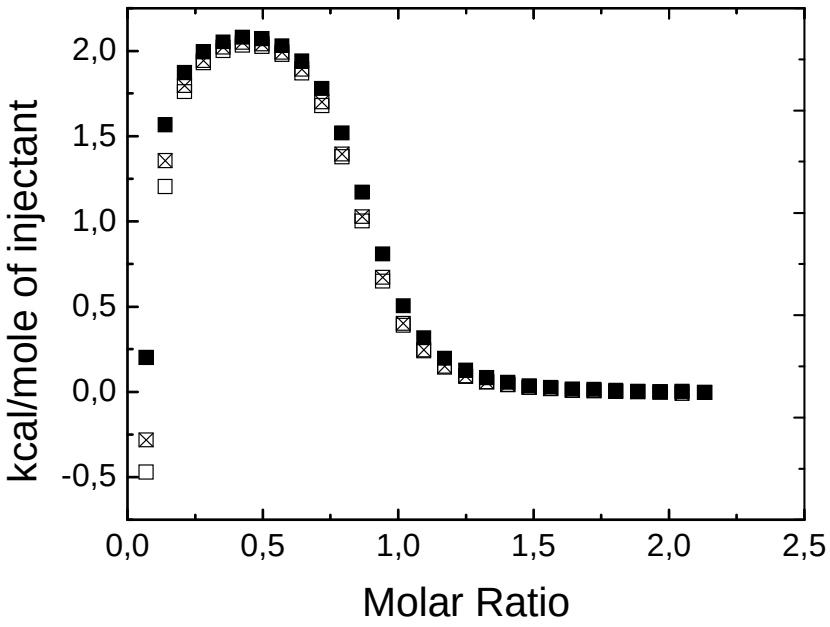

Figure 4.12: Titration of Ni^{2+} in Nα-Nα-Bis(carboxymethyl)-L-lysine hydrate by isothermal titration calorimetry (ITC) (n=3).

During the titration of Ni^{2+} in N_α-N_α-Bis(carboxymethyl)-L-lysine hydrate, shown in figure 4.12, an endothermic reaction was observed, corresponding to the Ni^{2+}/N_α-N_α-Bis(carboxymethyl)-L-lysine hydrate complex formation. This experiment was repeated three times and showed that the measurements were consistent.

ii. Preparation and characterization of PBLG-PEG-NTA nanoparticles

After the characterization of the NTA/Ni^{2+}/His-Tag complexation system, PBLG-NTA nanoparticles were prepared and evaluated. For this four types of nanoparticles with varying compositions in PEG and PEG-NTA were prepared according to table 4.2.

Table 4.2 Composition of the four types of nanoparticles studied

Polymer	PBLG28	PBLG28 PEG	PBLG55	PBLG55 PEG	PBLG48 PEG NTA	Aspect Ratio (Γ)
Formulation 1	80%	20%				1.3
Formulation 2	80%	10%			10%	1.3
Formulation 3			80%	20%		1.9
Formulation 4			80%	10%	10%	1.9

These formulations were used for the evaluation of the importance of the NTA groups on the nanoparticles and the evaluation of the impact of shape on specific and non-specific interactions.

First, a series of experiments were made by ITC to assess the presence of accessible NTA groups on the surface of the nanoparticles. For this purpose, nanoparticles were titrated by a solution containing the complex Ni^{2+} / His_6.

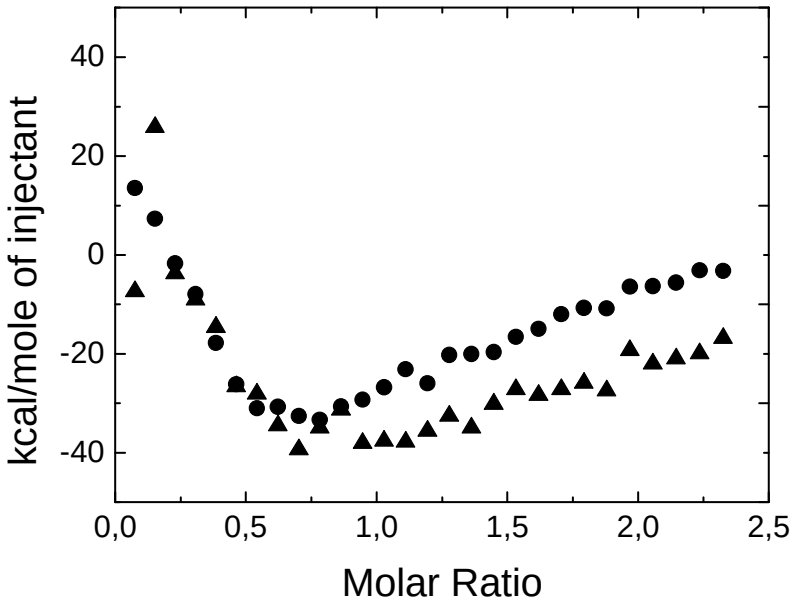

Figure 4.13 Titration of nanoparticles bearing NTA groups of different shapes (● Γ=1.30, ▲ Γ=1.88) in a His-Tag/Ni^{2+} solution

Figure 4.13 shows the titration profiles for nanoparticles of different shapes bearing NTA groups when titrated by a His-Tag/Ni^{2+} solution. An exothermic reaction occurred which could be attributed to the formation of the complex formation. There was no difference in molar ratio (His-Tag per PBLG-PEG-NTA) between the two types of particles. It suggests that NTA groups at the surface of these nanoparticles had probably comparable accessibility, which could be expected since all the nanoparticles have the same composition, and similar surfaces. In this situation, the shape modification had no influence on the particles interactions in solution and it can be expected that only the number of NTA groups per nanoparticle matters.

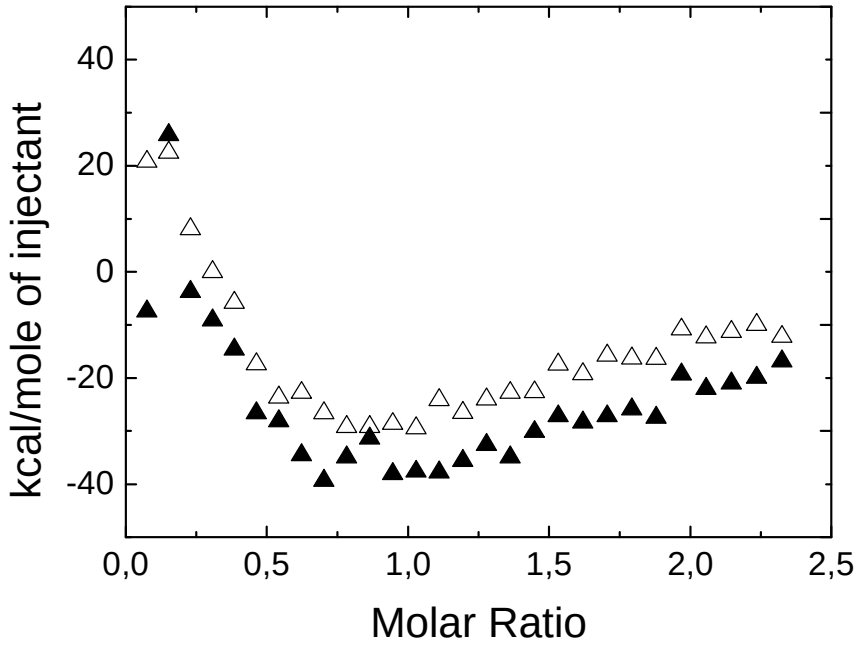

Figure 4.14 Titration of elongated nanoparticles (Γ=1.88) bearing NTA groups ▲ or not Δ in a His-Tag/Ni^{2+} solution

Figure 4.14 presents the impact of the presence of NTA groups on the formation of the NTA/Ni^{2+}/His-Tag complex. When the nanoparticles bear NTA groups, the formation of the complex was reinforced.

4.2.2.4. Surface Plasmon Resonance experiments

Surface Plasmon Resonance (SPR) experiments were performed to complete those results. First, two kinds of chips were tested for the analysis of the N_α-N_α-Bis(carboxymethyl)-L-lysine hydrate / Ni^{2+} / His-Tag system. Carboxylated gold chips, with varying surface structures were used for grafting purposes.

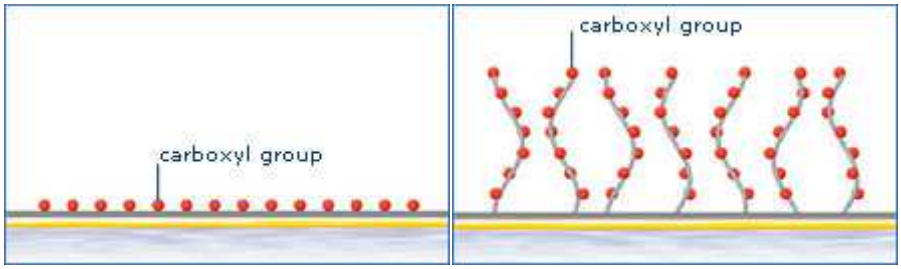

Figure 4.15 Schemes of the surface of C1 and CM5 chips. (Courtesy of Biacore, GE Healthcare)

C1 chips are composed of gold covered with carboxyl groups, whereas CM5 chips are composed of gold covered with a dextran matrix (with carboxyl groups). These two kinds of chips were tested, with the aim of finding optimal conditions for reducing dramatically the non specific interaction observed with C1 chips. However, if CM5 chips gave reliable results, C1 chips lead to only 10% of His-Tag immobilization which did not allow particles adhesion measurements.

The nanoparticles with different shapes with and without NTA groups in surface were tested on these chips.

In details, two channels were inactivated by addition of ethanolamine and two others were coupled with the His-Tag through EDC/NHS. Activated channel fixed respectively 472 and 382 RU of His-Tag. Then Ni^{2+} (2mM) was first passed on the CM5, and finally the nanoparticles suspensions (1.5mg.mL^{-1}).

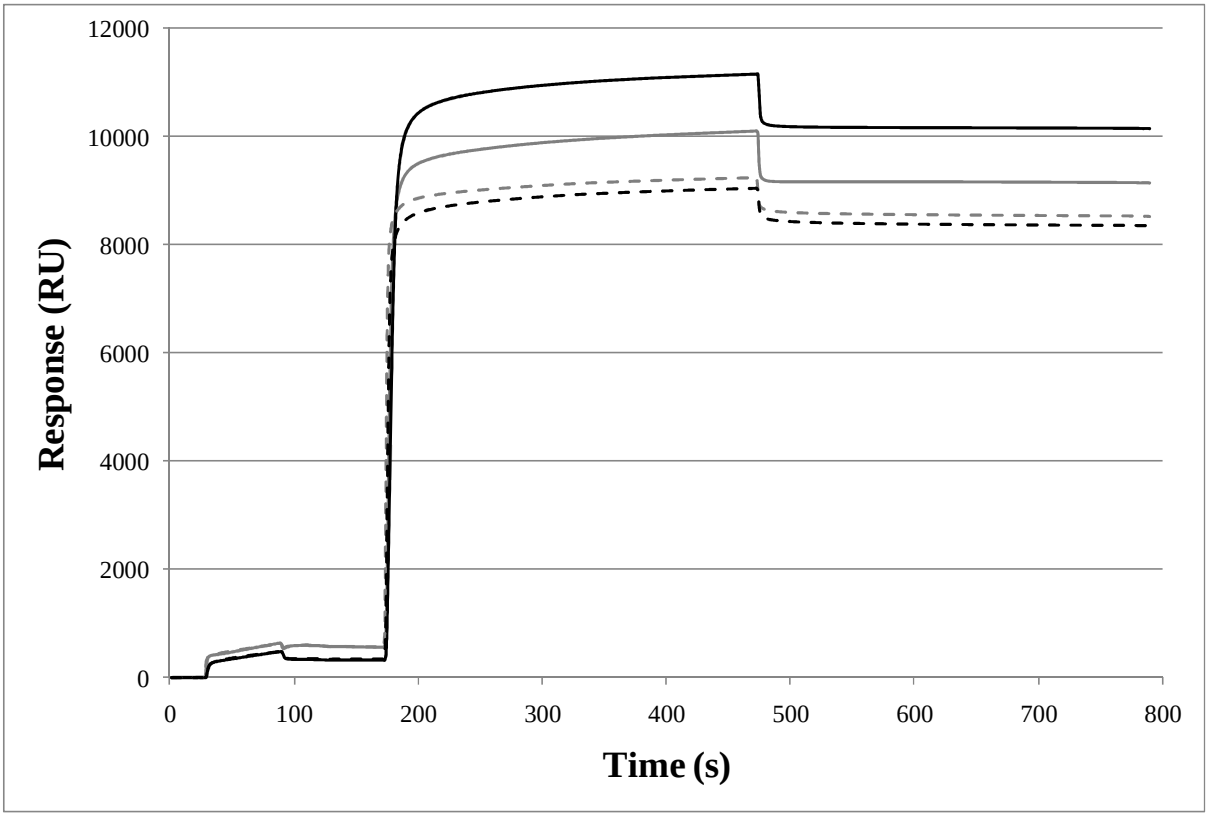

Figure 4.16 Interaction of spheroïdal nanoparticles (Γ=1.30) with NTA groups (lines) or without (dashes) on dextran surfaces with His-Tag (black) or without (gray).

Figure 4.16 presents the bonding of nanoparticles with an elongation ratio Γ=1.30 (corresponding to the PBLG28 formulations with or without 10% PBLG48-PEG-NTA, see table 4.2) to these channels. First it is important to note that the different kinds of particles adhere to all the surfaces. This reveals non specific interactions. They may be caused by the dextran matrix. This is confirmed by the results we obtained with the C1 chip that showed very low adhesion (5-15RU).

We can compare the behavior of the nanoparticles with NTA groups (formulation 2) and without them (formulation 1) for specific or non-specific interactions. First for the non-specific interactions, nanoparticles with and without NTA groups have similar adhesion on the non-specific (inactivated) channel, respectively 9150RU and 8530RU. The 7% of difference could be explained by the presence of NTA groups on the surface of the nanoparticles that change the particle surface charge. The particles without NTA on the specific channel (with His-Tag) show an adhesion of 8360RU, which is similar to the other non specific interactions.

Secondly the specific interaction with the chip: nanoparticles with NTA on the specific channel show an adhesion of 10160RU. This interaction has to be compared to the particles without NTA on the specific channel (8360RU): there is 18% difference between these channels. Two explanations can be proposed: (i) NTA groups on the surface of nanoparticles favor the attachment of the particles to the surface (ii) the difference is due to the difference in His-Tag immobilization.

Furthermore during the regeneration of the channels, we noticed that (i) Nanoparticles were hard to fully eliminate (ii) Particles with NTA groups were eliminated more completely than particles without NTA groups. This would suggest that the elimination of the particles by EDTA 0.5M during 10min is efficient for breaking specific interactions.

Then we studied PBLG55 formulations corresponding to more elongated particles (Γ=1.88) with or without 10% PBLG48-PEG-NTA (see table 4.2).

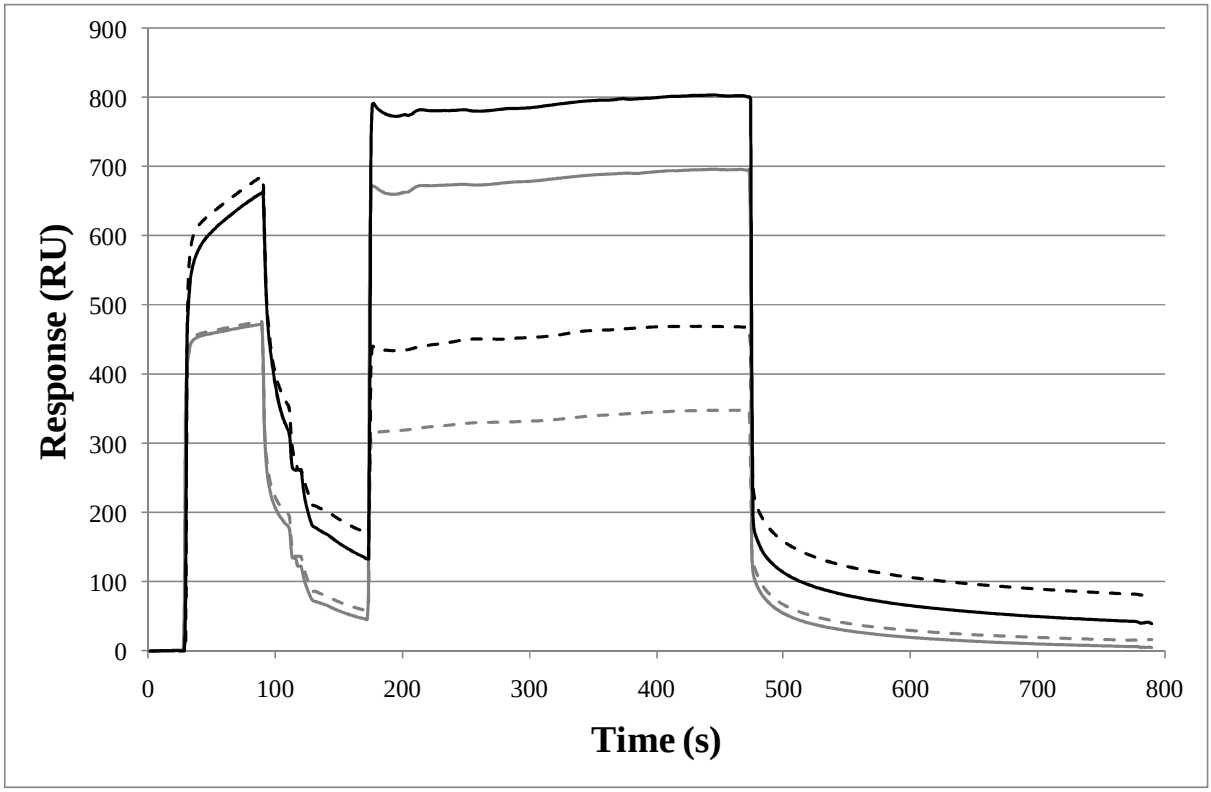

Figure 4.17 Interaction of elongated nanoparticles (Γ=1.88) with NTA groups (lines) or without (dashes) on dextran surfaces with His-Tag (black) or without (gray).

Figure 4.17 presents how nanoparticles corresponding to PBLG55 formulation bonded to these channels.

Contrary to previous results with formulations 3 and 4 there seems to be no adhesion of the particles on the channels. The fact that there is no non-specific interaction at all suggest that either there is a problem with this chip and the experiments need to be repeated, or that these formulations possess a shape that result in no approach of the walls.

Finally, a few conclusions can be drawn from these ITC and SPR experiments: (i) there is a specific interaction between nanoparticles with NTA groups and His-Tagged molecules, (ii) the particles shape has an influence on the binding to His-Tagged molecules, the closer the particle is to a sphere the stronger specific interactions and adhesion it will be. Obviously, these preliminary results would have to be further confirmed by a more complete study, including the use of other experimental techniques.

Conclusion

In this chapter we have tackled the subject of adhesion of spheroïdal nanoparticles to surfaces. We first envisioned from a theoretical point of view, what could be the influence of the geometry on these interactions. Strikingly, we highlighted the fact that depending on the scenario the interactions could be dramatically reinforced or weakened for non spherical particles compared to those of a sphere. Furthermore, when these interactions were compared to the forces of detachment that can be found in the blood stream or elsewhere in the body, the influence of shape was emphasized. The shape of the nanoparticles had an impact on the available surface for bonding up to 10^{10} by changing the approach of the same particle on a wall, up to 10^6 by changing the shape of a particle by a factor of 100, far stronger than the effect of the size, only up to 10^3 for a change in diameter by a factor of 100 (from 100nm to 10µm)

After pointing out the considerable incidence of shape on these interactions, we attempted to develop model spheroïdal nanoparticles likely to be functionalized “on demand”, after the manufacture of the particles. This attachment system was based on the use of the NTA/Ni^{2+}/His-Tag complex that could potentially be very interesting in drug targeting applications. Indeed this system is very interesting because it allows the extemporaneous preparation of decorated nanoparticles, with the possibility of introducing easily variable amounts of recognition ligands and/or to multifunctionalize the surface of the particles. Furthermore, the use of NTA groups in the surface of the particles may also offer the opportunity of introducing various metals either for diagnostic or even cancer treatment if using radioactive elements (Ca, Tc, In…).

Preliminary characterization attempts by isothermal titration calorimetry and surface plasmon resonance, although to be repeated, confirmed the validity of this approach for developing functionalized non spherical nanoparticles.

Acknowledgements

We would like to thank Danielle Jaillard (CCME, Paris XI, Orsay) for her help with the TEM measurements.

References

1. Stella, B., Arpicco, S., Peracchia, M.T., Desmaële, D., Hoebeke, J., Renoir, M., D'Angelo, J., Cattel, L. & Couvreur, P.
Design of folic acid-conjugated nanoparticles for drug targeting,
Journal of Pharmaceutical Sciences, 89, 1452-1464, **2000**.

2. Sicard-Roselli, C., Lemaire, S., Jacquot, J.-P., Favaudon, V., Marchand, C. & Houée-Levin, C.
Thioredoxin Ch1 of Chlamydomonas reinhardtii displays an unusual resistance toward one-electron oxidation,
European Journal of Biochemistry, 271, 3481-3487, **2004**.

3. Lata, S., Reichel, A., Brock, R., Tampé, R. & Piehler, J.
High-Affinity Adaptors for Switchable Recognition of Histidine-Tagged Proteins,
Journal of the American Chemical Society, 127, 10205-10215, **2005**.

4. Huang, Z., Hwang, P., Watson, D.S., Cao, L. & Szoka, F.C.
Tris-Nitrilotriacetic Acids of Subnanomolar Affinity Toward Hexahistidine Tagged Molecules,
Bioconjugate Chemistry, 20, 1667-1672, **2009**.

5. Cozens-Roberts, C., Quinn, J.A. & Lauffenberger, D.A.
Receptor-mediated adhesion phenomena. Model studies with the Radical-Flow Detachment Assay,
Biophysical Journal, 58, 107-125, **1990**.

6. Kuo, S.C. & Lauffenburger, D.A.
Relationship between receptor/ligand binding affinity and adhesion strength,
Biophysical Journal, 65, 2191-2200, **1993**.

7. Kuo, S.C., Hammer, D.A. & Lauffenburger, D.A.
Simulation of detachment of specifically bound particles from surfaces by shear flow,
Biophysical Journal, 73, 517-531, **1997**.

8. Decuzzi, P. & Ferrari, M.
Design maps for nanoparticles targeting the diseased microvasculature,
Biomaterials, 29, 377-384, **2008**.

9. Decuzzi, P. & Ferrari, M.
The adhesive strength of non-spherical particles mediated by specific interactions,
Biomaterials, 27, 5307-5314, **2006**.

10. Zhang, Y., Akilesh, S. & Wilcox, D.E.
Isothermal Titration Calorimetry Measurements of Ni(II) and Cu(II) Binding to His, GlyGlyHis, HisGlyHis, and Bovine Serum Albumin: A Critical Evaluation,
Inorganic Chemistry, 39, 3057-3064, **2000**.

11. Stora, T., Hovius, R., Dienes, Z., Pachoud, M. & Vogel, H.
Metal Ion Trace Detection by a Chelator-Modified Gold Electrode: A Comparison of Surface to Bulk Affinity,

Langmuir, 13, 5211-5214, **1997**.

12. Hull, J.A., Davies, R.H. & Staveley, L.A.K.
1033. Thermodynamics of the formation of complexes of nitrilotriacetic acid and bivalent cations,
Journal of the Chemical Society (Resumed), 5422-5425, **1964**.

13. Hart, B.R. & Shea, K.J.
Molecular Imprinting for the Recognition of N-Terminal Histidine Peptides in Aqueous Solution,
Macromolecules, 35, 6192-6201, **2002**.

14. Anderegg, G.
Critical survey of stability constants of NTA complexes,
Pure and Appl. Chem., 54, 2693-2758, **1982**.

15. Barbosa, M.E.M., Montembault, V., Cammas-Marion, S., Ponchel, G. & Fontaine, L.
Synthesis and characterization of novel poly(gamma-benzyl-L-glutamate) derivatives tailored for the preparation of nanoparticles of pharmaceutical interest,
Polymer International, 56, 317-324, **2007**.

Appendix: Matlab programming for calculating the surface of an ellipsoid between a wall and a plan at a definite distance:

Because calculating the angles theta and phi from hp involves resolving 2nd or 4th degree equations which may result in complex number hence complex angles which have no physical meaning we chose to calculate the surfaces or all phi values and calculate the corresponding hp.

Approach with the main axis parallel to the wall

```
global hp  a1 a3 r phi theta el re
% Definition of the different elongations of interest
el=[1/100 1/10 1/5 1/2 1 2 5 10 100];
% r can be changed to correspond to any particle
r=50;
% H can be tuned to correspond to any system
H=20;
%a1 and a3 are the parameters of the ellipse (a1=a2)
a1=r.*el.^(-1/3);
a3=r.*((el).^(2/3));
phi=(0:0.01*pi/2:pi/2);
j=size(el);
k=size(phi);
hp=zeros(j(1,2),k(1,2));
S=zeros(j(1,2),k(1,2));
theta=zeros(j(1,2),k(1,2));
for o=1:j(1,2)
    for p=1:k(1,2)
         %Calculus of the elliptic radius
         re(o,p)=a1(1,o).*a3(1,o)/(a3(1,o).^2.*(cos(phi(1,p))).^2.+a1(1,
   o).^2.*(sin(phi(1,p))).^2).^(1/2);
            % Calculus of hp
            hp(o,p)=a1(1,o)-(cos(phi(1,p)).*re(o,p));
    end
end
%Surface Calculus
for t=1:j(1,2)
    for u=1:k(1,2)
         F=@(alpha,psi)a1(1,t).*cos(psi).*(a1(1,t).^2.*cos(alpha).^2+a3(
   1,t).^2.*(cos(psi)^2.*sin(alpha).^2+sin(psi).^2)).^(1/2);
            S(t,u)=-4*dblquad(F,0,pi/2,pi/2,pi/2+phi(1,u));
```

```
        end
    end
```

Approach with the main axis perpendicular to the wall

```
    global hp  a1 a3 r phi theta el re
    % Definition of the different elongations of interest
    el=[1/100 1/10 1/5 1/2 1 2 5 10 100];
    % r can be changed to correspond to any particle
    r=50;
    % H can be tuned to correspond to any system
    H=20;
    %a1 and a3 are the parameters of the ellipse (a1=a2)
    a1=r.*el.^(-1/3);
    a3=r.*((el).^(2/3));
    phi=(0:0.01*pi/2:pi/2);
    j=size(el);
    k=size(phi);
    hp=zeros(j(1,2),k(1,2));
    S=zeros(j(1,2),k(1,2));
    theta=zeros(j(1,2),k(1,2));
    for o=1:j(1,2)
        for p=1:k(1,2)
             %Calculus of the elliptic radius
             re(o,p)=a1(1,o).*a3(1,o)/(a1(1,o).^2.*(cos(phi(1,p))).^2.+a3(1,
       o).^2.*(sin(phi(1,p))).^2).^(1/2);
                % Calculus of hp
                hp(o,p)=a3(1,o)-(cos(phi(1,p)).*re(o,p));
                %Symetry around the z axis
                theta(o,p)=2*pi;
        end
    end
    %Surface Calculus
    for t=1:j(1,2)
        for u=1:k(1,2)
      F=@(psi)cos(psi).*a1(1,t).*((a1(1,t)).^2*(sin(psi)).^2.+a3(1,t).^2*(c
os(psi)).^2).^(1/2);
          S(t,u)=2*pi*quad(F,-pi/2,-pi/2+phi(1,u));
        end
    end
```

Chapter V

In vitro preliminary study of the influence of the shape of nanoparticles on the internalization by HUVEC

Chapter 5. *In vitro* preliminary study of the influence of the shape of nanoparticles on the internalization by HUVEC

In recent years advances in nanotechnologies have allowed the production of nanoparticles of more and more complex shapes. However the question of the influence of the shape of nanoparticles on their *in vitro* and *in vivo* interactions remains unanswered and therefore, up to now, studies of the influence of shape on nanoparticles cell interactions are rare. In this work we will present preliminary investigations of the effect of shape using poly(γ-benzyl-L-glutamate) polymer non spherical nanoparticles on their interactions with cells.

However, prior to such a study, one must produce and label these nanoparticles. The process to manufacture non spherical nanoparticles has been presented before (see chapter 3). Here we have tested two different methods to label the nanoparticles, firstly by adding a fluorescent derivative of the polymer composing the nanoparticles and secondly by encapsulating quantum dots in the particles. After comparing the efficiency of these labeling methods and their effect on nanoparticles morphology, a study of the influence of shape on the *in vitro* fate of the nanoparticles has been undertaken. This study was performed on living cells: Human Umbilical Vein Endothelial Cells (HUVEC) by video and confocal microscopy to follow the capture and possible internalization in cells of nanoparticles of various shapes.

5.1. Material and methods

5.1.1. Polymer synthesis

Poly(γ-benzyl-L-glutamate) (PBLG) of different molecular weights were synthesized in anhydrous DMF by ring-opening polymerization of γ-benzyl-L-glutamate N-carboxy anhydride (BLG-NCA) using benzylamine as initiator according to a slightly modified method described elsewhere[1]. The theoretical molecular weights of samples were adjusted by adjusting the initiator/BLG-NCA ratio.

Briefly, BLG-NCA was weighted under argon atmosphere in a degassed three-necked round bottomed flask equipped with a thermometer, mechanical stirring, a refrigerant with a silica gel guard and a bubble detector. BLG-NCA was dissolved in DMF (volume was adjusted to obtain a 0.5M BLG-NCA final concentration) at room temperature under mechanical stirring and argon flux. After about 10min, the argon flux was stopped, the solution was heated at 30°C and the initiator solution was added. Immediately after the addition, CO_2 emission was observed in the bubble detector. Absence of BLG-NCA auto-polymerization was checked by FTIR spectroscopy of the BLG-NCA solution before addition of the initiator. The reaction mixture was stirred at 30°C until the characteristic BLG-NCA bands disappeared from the FTIR spectrum. The mixture was precipitated in an excess of cold diethyl ether to give a white solid. The precipitate was filtered and washed with diethyl ether. The polymers were again washed with diethyl ether and dried under vacuum at room temperature for at least 12h. A second precipitation, purification and drying procedure was performed for polymers of all molecular weights. FTIR spectra were recorded to analyze BLG-NCA auto-polymerization and to follow the reaction using a Brüker Vector 22 spectrometer.

5.1.2. PBLG-rhodamine synthesis

A PBLG rhodamine derivative was prepared with the same protocol as PBLG except a specific derivative of the rhodamine was used as an initiator. This derivative is shown in figure 5.1 and has been kindly provided by B. Ledroumaguet (UMR CNRS 8612).

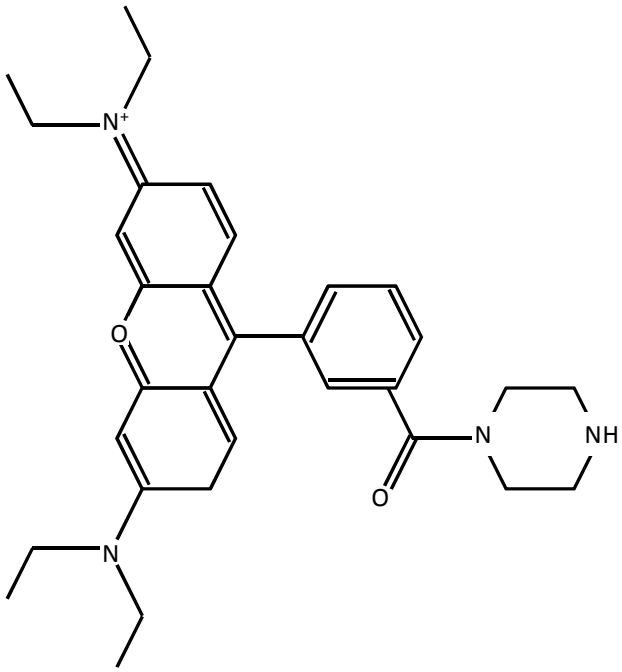

Figure 5.1: Rhodamine B derivative used as an initiator for the synthesis of PBLG-rhodamine

5.1.3. Post-synthesis coupling of PEG to PBLGs

PBLG polymers of different molecular weights were then coupled to PEG by a post synthesis modification procedure. Coupling methoxy-PEG(6000)-N-hydroxysuccinimide to PBLG was done overnight in a mix of solvent. Briefly 500mg of PBLG was dissolved in 4mL of 25% THF, 25% DMF and 50% DMSO during 18h. 4mL of methoxy-PEG(6000)-N-hydroxysuccinimide was added to the mix for a final concentration of 1.5 equivalent. The reaction was heated at 30°C under magnetic stirring and under argon atmosphere during 24h.

5.1.4. Matrix-assisted laser desorption/ionization time-of-flight mass spectroscopy

Matrix-assisted Laser Desorption/Ionization-Time of Flight-Mass Spectrometry (MALDI-TOF-MS) analysis was carried out in positive-ion mode on a Voyager DE-STR MALDI-TOF mass spectrometer (Perseptive Applied Biosystems, Framingham, MA, USA) equipped with a 337nm nitrogen laser. DCTB or 2-[(2E)-3-(4-tert-Butylphenyl)-2-methylprop-2-enylidene] malononitrile (40mg.mL-1 in dichloromethane) and potassium trifluoroacetate (5 mg.mL-1 in water) were used respectively as matrix and cationic ionization agent. The polymer:matrix

molar concentration ratio was comprised between 40:1 (for the lowest molecular weight) and 1:1000 (for the highest molecular weight). 1.5µL of this premix were deposited onto the sample plate and allowed to dry at room temperature. Spectra of PBLG were acquired with the default calibration (accuracy ca. 0.1%) under the same condition as those described in Sicard-Roselli et al.[2]

5.1.5. Quantum dots

5.1.5.1. Precursor preparation

$Cd(oleate)_2$ was prepared under argon atmosphere by degassing at 80°C a mixture of 0.5mmol of Cd with an excess of oleic acid and heating at 220°C until the mixture turned colourless. Then the solution was cooled down to 80°C and degassed for 30min. 0.5mmol of selenium (Se) in oleic acid was prepared by dissolving selenium pellets in oleic acid under magnetic stirring. 0.1M S(ODE) was prepared under argon atmosphere by heating at 180°C sulfur flakes in 1-octadecene (ODE).

5.1.5.2. CdSe core synthesis

CdSe nanocrystals were synthesized via modification of a previously reported procedure[3]. 0.5mmol $Cd(oleate)_2$ in 10mL ODE was introduced into a 50ml three-neck flask. The mixture was degassed at 70°C under vacuum for 30min. Under argon flux, the temperature was increased to 280°C before injecting a mixture of 0.5mmol Se in oleic acid. The temperature was maintained at 280°C for 5 to 10min. The resulting solution was then cooled in ice and the quantum dots were precipitated in ethanol. The supernatant was discarded and the pellet containing CdSe nanocrystals was suspended in hexane. This turbid solution was centrifuged for 5min at room temperature. The clear supernatant containing the QDs was precipitated one more time with ethanol and centrifuged. The pellet containing the QDs was suspended in hexane.

5.1.5.3. CdS shell synthesis

The shells were synthesized via modification of a previously reported procedure[4]. Cadmium stock solution was prepared by mixing 0.5M $Cd(oleate)_2$ in oleic acid with ODE to obtain a 0.1M cadmium solution. Sulphur stock solution was prepared by dissolving sulphur in ODE at 180°C under argon to obtain a 0.1M sulphur solution.

10ml ODE and 10ml CdSe core solution (2.99nm diameter, 2µM) in hexane were introduced into a 50ml three-neck flask. After removing the hexane under reduced pressure and degassing at 200°C for 30min, the flask was backfilled with argon and 0.33ml of the cadmium stock solution were injected before increasing the temperature to 230°C. After 10min at this temperature, the same amount of sulphur stock solution was added dropwise. Cadmium and sulphur stock solutions were then successively injected dropwise at 10 minute intervals. The volumes injected were respectively 0.48, 0.65, and 0.86mL. The last injection was carried out with the cadmium stock solution and was reacted for 20min before cooling in ice. The quantum dots were precipitated by centrifugation with ethanol and suspended in hexane.

5.1.6. Nanoparticles preparation

5.1.6.1. Nanoparticles labeled by rhodamine

Briefly, 15mg of polymer (1.5mg of PBLG-rhodamine, 1.5mg of PBLG-PEG and 12mg of PBLG) were dissolved in 5mL of THF at 30°C during 18h, without stirring. This solution was added dropwise to 10mL of Poloxamer F68 (0.1% w/v) under magnetic stirring (700rpm). The mixture was left under magnetic stirring for 10min and then transferred in a glass flask. The solvent was gently evaporated in a rotavapor (V850, R124, Buchi) at 40°C, first at 200mbar for 5min and then at 40mbar to yield 5mL of suspension. The pH of each preparation was measured, and the osmolarity of each preparation was adjusted to 0.9% by adding 200µl of NaCl solution with a concentration 225g.L^{-1}. The suspensions were kept at 4°C until use.

Table 5.1 presents the different formulations used in this study. These formulations have been prepared with polymers of different molecular weight:

Table 5.1 Nanoparticles formulations

Polymer	PBLG28	PBLG55	PBLG28-PEG	PBLG55 -PEG	PBLG-Rhodamine
Molecular weight	28kg/mol	54.5kg/mol			32kg/mol
Nano28	80%		10%		10%
Nano55		80%		10%	10%

5.1.6.2. Nanoparticles labeled with quantum dots

Encapsulating quantum dots in PBLG nanoparticles was done by modifying a previously described method. Briefly, 15mg of polymer were dissolved in 5mL of THF (minus the quantum dots solution volume) at 30°C during 18h, without stirring. Hexane from the quantum dots solution (0.2µM) was evaporated and replaced by the same volume of THF. 0, 10, 100, 500, or 1000µL of this quantum dots solution was added to the PBLG solution. This mix was added dropwise to 10mL of deionized water under magnetic stirring. The mixture was left under magnetic stirring for 10 min and then transferred in a glass flask. The solvent was gently evaporated in a rotavapor (V850, R124, Buchi) at 40°C, first at 200mbar for 5min and then at 40mbar to yield 5mL of suspension.

5.1.7. Transmission Electron Microscopy (Nanoparticles analysis)

Nanoparticles were further analyzed through TEM (Transmission electron microscope, Philips EM208) at 60kV. 3µl of nanoparticles suspension, after suitable dilution of bulk suspensions in milli-Q water, were placed on a formvar-carbon film previously coated on a copper grid (400 meshes). After 5min deposition, a drop of phosphotungstic acid solution (1%) was placed on the copper grid and on top of the sample. After 30s, the liquid was drained and the sample was placed inside the EM208 and pictures were taken. Nanoparticles measurements were obtained through The Gimp© software.

5.1.8. Size and shape analysis

For each type of nanoparticles, dimensions were measured on different TEM pictures through The Gimp© software. The smallest and the longest dimensions of individual nanoparticles taken from a series of microphotographs were measured and were named width and length, respectively. An average of 200 nanoparticles was measured. The nanoparticles

were assimilated to oblates and their elongation ratios, as well as their sphere equivalent diameters in volume, were calculated as follows:

Eq.1

$$Aspect\ Ratio = \Gamma = \frac{Length}{Width}$$

Eq.2

$$Equivalent\ Diameter = \sqrt[3]{Length * width^2}$$

5.1.9. Fluorescence analysis

Nanoparticles containing a fluorophore were analyzed with a spectrofluorimeter (PerkinElmer, California USA) at λ = 560nm for rhodamine based fluorescence and at the peak of emission for the quantum dots formulations.

5.1.10. Cell maintenance and cytotoxicity assays

HUVEC cells were maintained in DMEM with 10% FBS, and 0.5% Penn Strepp.Briefly, HUVEC cells were seeded in 96 well plates at $8x10^3$ cells per well. Cells were allowed to attach to the plate during 24h at 37°C. The next day, particles suspensions were deposited in the wells at concentrations ranging from 1 to 300mg.L^{-1}. After 72h, 20µL of 3-(4,5-Dimethylthiazol-2-yl)-2,5-diphenyltetrazolium bromide (MTT) were deposited in all wells. After 2hours, all wells were emptied and after addition of 200µL of DMSO in all the wells the plates were analyzed with a Labsystem Multiskan MS at 570nm.

5.1.11. Cell uptake and video and confocal microscopy

HUVEC cells were seeded in µ-Slide $VI^{0.4}$ (6 channel microslides, Ibidi) at 300 cells per channel. The cells were allowed to attach and to grow during 72h at 37°C. The day of the observations in videomicroscopy (AxioObserver Z1 Zeiss) or confocal microscopy (LSM 510 META Zeiss), the growth medium was replaced by a suspension of nanoparticles at 1.5mg.mL^{-1} in DMEM. Observations were directly performed on the living cells in the wells after 30min of incubation with calcein.

5.2. Results and Discussion:

5.2.1. Labeling the particles

Labeling of the nanoparticles was essential in order to investigate the influence of shape on the interactions between cells and nanoparticles. To that extent it was decided to fluorescently label the particles. This has been attempted by two approaches: firstly a fluorescent rhodamine derivative of PBLG composing the nanoparticles has been synthesized and secondly quantum dots have been prepared and encapsulated in the nanoparticles. Then their morphological properties have been evaluated by TEM for the sizes and shapes and by spectrofluorimetry for the fluorescence.

5.2.1.1. Rhodamine labeling

Rhodamine B is a fluorescent dye that belongs to the fluorine dyes family. This dye was modified in our laboratory to yield a molecule with a secondary amine that can be used as an initiator for the PBLG synthesis. The polymer obtained from this synthesis revealed a molecular weight of 32kg/mol through MALDI-TOF analysis.

It has been shown previously that the shape of PBLG nanoparticles is governed by the molecular weight of the polymer (see chapter 3). For this reason, in order not to modify drastically the shape of the nanoparticles, it was decided to prepare different batches of nanoparticles with different elongation ratios by using mixtures of PBLG (with varying molecular weights) and 10% of PBLG-rhodamine during the nanoprecipitation process.

After their manufacture, the nanoparticles were analyzed through TEM. Length and width were measured on individual particles, from which particles size and shape were characterized through the sphere equivalent diameter of the elongated nanosphere and through the aspect ratio Γ = length/width. Results are gathered in Table 5.2.

Table 5.2 Morphology of nanoparticles determined from TEM images

Molecular Weight ($kg.mol^{-1}$)	Width (nm)	Length (nm)	Aspect Ratio	Sphere Equivalent Diameter (nm)
28	56 ± 10	74±18	1.30 ± 0.14	62 ± 12
55	41± 8	78 ± 17	1.88 ± 0.27	51 ± 10

These data show that the nanoparticles, that have been prepared with the same composition but polymers of different molecular weights, had (i) similar surface charge -29.5 ± 4.2mV and -33.4 ± 3.1mV for the low molecular weight and the high molecular weight particles, respectively, (ii) the same volume which was evaluated through the sphere equivalent diameter of nanoparticles, and (iii) different elongations, which was evaluated through the aspect ratio. These particles were thus very similar in many aspects at the exception of the shape.

5.2.1.2. Quantum dots labeling

Quantum dots are spherical nanocrystals that measure a few nanometers in diameter. They possess a strong fluorescence due to the fact that their excitons are confined in all three dimensions. They are composed of a metallic core (e.g. cadmium and selenium) that can be coated by a passivation shell. Their fluorescence is specific and depends on the diameter of the core[5]. The smallest (around 2nm) will emit bluer light (down to 420nm) and the largest (around 8nm) will emit redder light (up to 850nm). These quantum dots can be prepared to emit at any wavelength in the visible light or for near infrared applications. The passivation shell protects the core from degradation and can boost the emissions and increase the lifetime of their fluorescence. These quantum dots can even present a continuous fluorescence without photobleaching[4].

Thus they present a series of advantages compared to molecular flurophores. However if such quantum dots open many possibilities in terms of particle tracking, they also require a precise preparation and extremely pure materials. Any polluting agent will create imperfections in the quantum dot and hinder the fluorescence.

Different core syntheses were performed with a nucleation time (time spent above 280°C) comprised between 5 and 10min. These reactions yielded cores that fluoresced between 539 and 580nm (between 2.8 and 3.8nm in diameter). After this, addition of a shell comprising two and four layers of Cd-S was deposited onto their surface to achieve passivation.

These quantum dots were then encapsulated in nanoparticles by conanoprecipitation. The size and shape of these particles was measured through TEM whereas their fluorescence was measured through spectroflurimetry.

The nanoparticles are shown in figure 5.2.

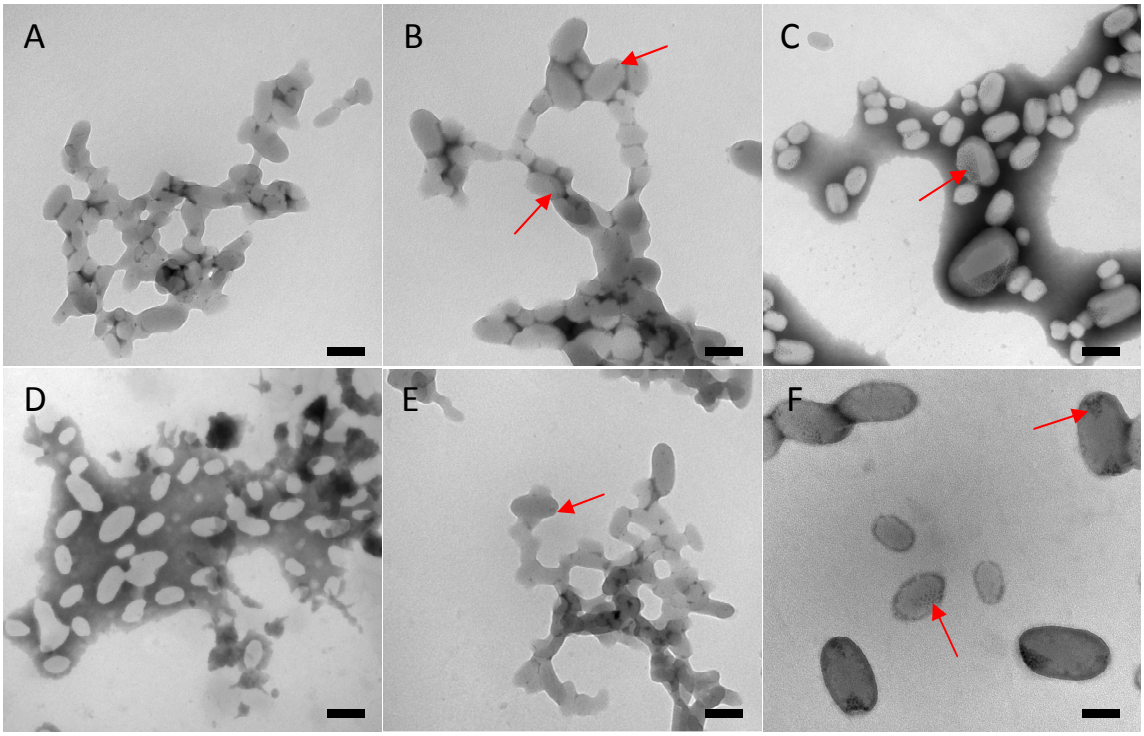

Figure 5.2: PBLG nanoparticles (A-C 30kg/mol; D-F 45kg/mol) containing quantum dots (A, D 0nmol ; B, E 10nmol ; C, F 20nmol). The arrows indicate regions with quantum dots. Scale bar 100nù

What clearly appears on these pictures is the presence of quantum dots inside the nanoparticles. Furthermore a shift in the size of the particles could be observed when the amount of QDs was increased during the preparation. There is a limit in quantum dots initial concentration not to exceed in order not to modify the size and shape of the nanoparticles.

For that purpose the size (length and width) of 200 particles were measured, for PBLG of different molecular weigths, from 10kg/mol to 85kg/mol.

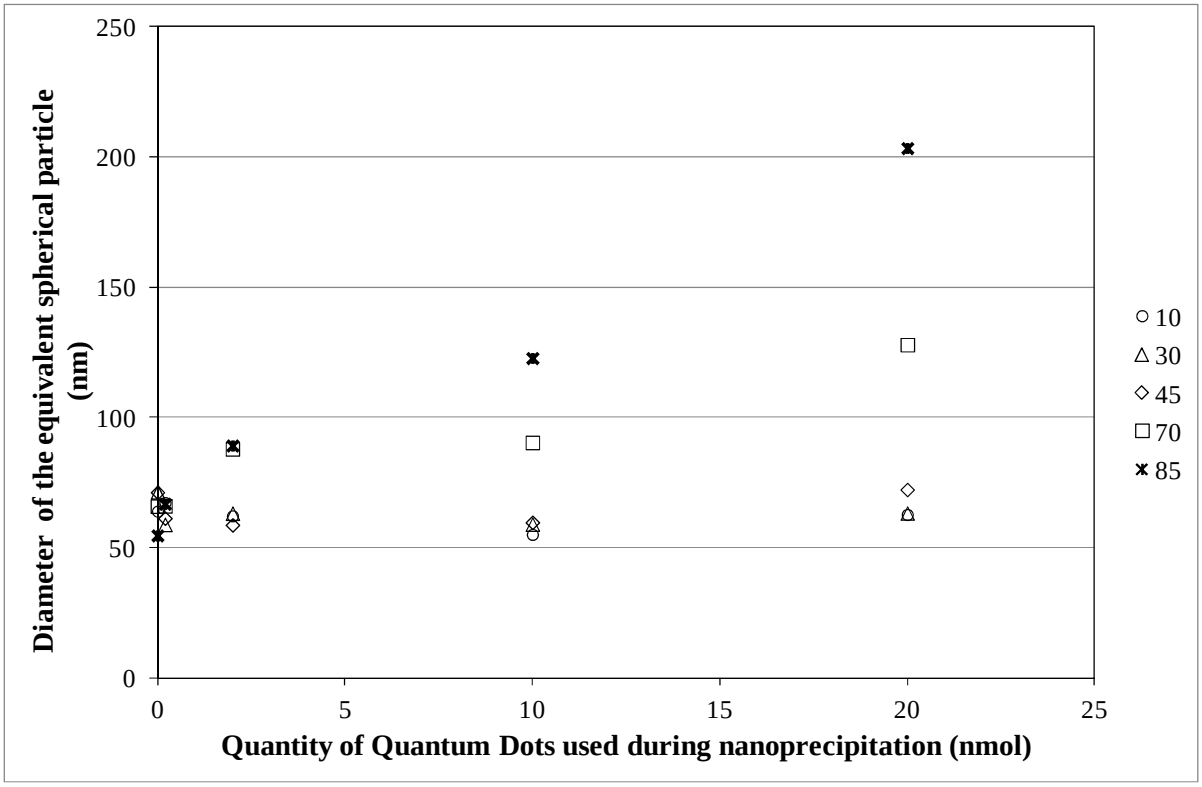

Figure 5.3: Sphere equivalent diameter of the nanoparticles, depending on the quantity of quantum dots used during the nanoprecipitation. Each series represents a set of nanoparticles made from a polymer of a different molecular weight (see legend for molecular weights in kg.mol^{-1}) leading to different shapes.

Although the diameter of the particles remained in the range of common sizes for nanoparticles obtained by nanoprecipitation, the effect of QDs on auto-assembly was not negligible. Quantum dots were a few nanometers in diameter, and self assembled PBLG nanoparticles in absence of QDs were around 60nm in diameter, that the addition of solid nanoparticles could modify the self assembly of these particles. Figure 5.3 shows that the volume of the particles was strongly impacted, especially for high molecular weight PBLG nanoparticles. Indeed, the longer the PBLG polymer chain, the more the particle were elongated (see chapter 3), and the more the particle were organized. It can be hypothesized that the insertion of QDs, with sizes comparable to the diameter of α-helices of PBLG chains would disrupt the inner organization of the particles, hence changing their shapes and sizes. This trend was confirmed in figure 5.4 which shows the aspect ratio depending on the quantity of quantum dots used during nanoprecipitation. The more quantum dots were used for nanoprecipitation, the closer the particles were to a sphere (aspect ratio tending toward 1).

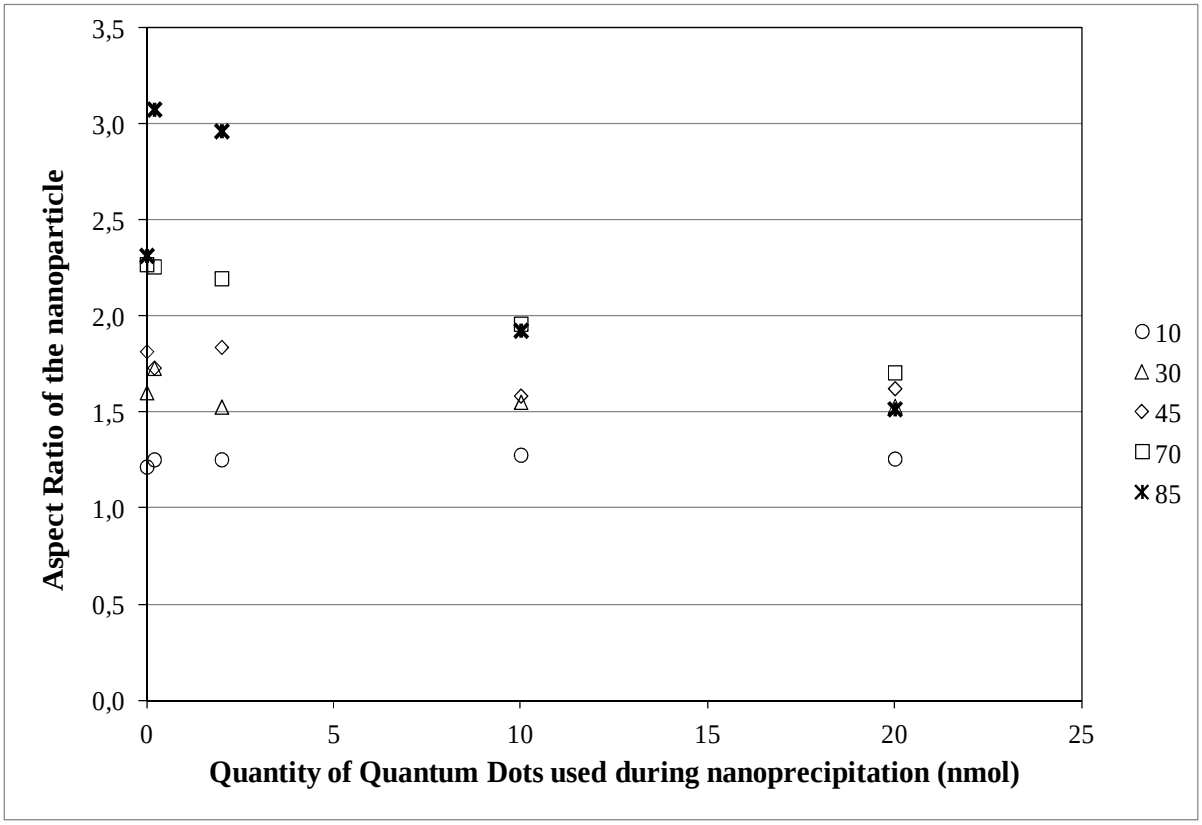

Figure 5.4: Aspect ratio of non spherical nanoparticle depending on the quantity of quantum dots used during the nanoprecipitation. Each series represents a set of nanoparticles made from a polymer of a different molecular weight (see legend for molecular weight in kg.mol^{-1}) leading to different shapes.

As was shown on figures 5.3 and 5.4 the addition of quantum dots in the preparation of nanoparticles changes their shape and size independently of the polymer size. However, small quantities of quantum dots do not impact the shapes and sizes of the nanoparticles too drastically. Up to 10nmol of quantum dots were used in the nanoparticles preparation for fluorescence studies to have a high enough fluorescence while retaining the shape to be studied.

5.2.1.3. Fluorescence study

Nanoparticles prepared with 10nmol quantum dots or 1%, 4%, or 10% PBLG-rhodamine were prepared and analyzed through spectrofluorimetry. Results show that nanoparticles with 10nmol quantum dots and 1% PBLG-rhodamine had similar fluorescence profiles. However nanoparticles with 10% PBLG-rhodamine reveal a much more intense fluorescence, by two orders of magnitude. Thus advantages of using quantum dots (lasting fluorescence,

possibilities of different emissions…), were considerably counterbalanced by this lessening of their fluorescence when encapsulated inside the nanoparticles. The reasons for it are unknown.

The rhodamine labeling was more efficient. These rhodamine-labelled nanoparticles are presented in figure 5.5 and their fluorescence is shown in figure 5.6.

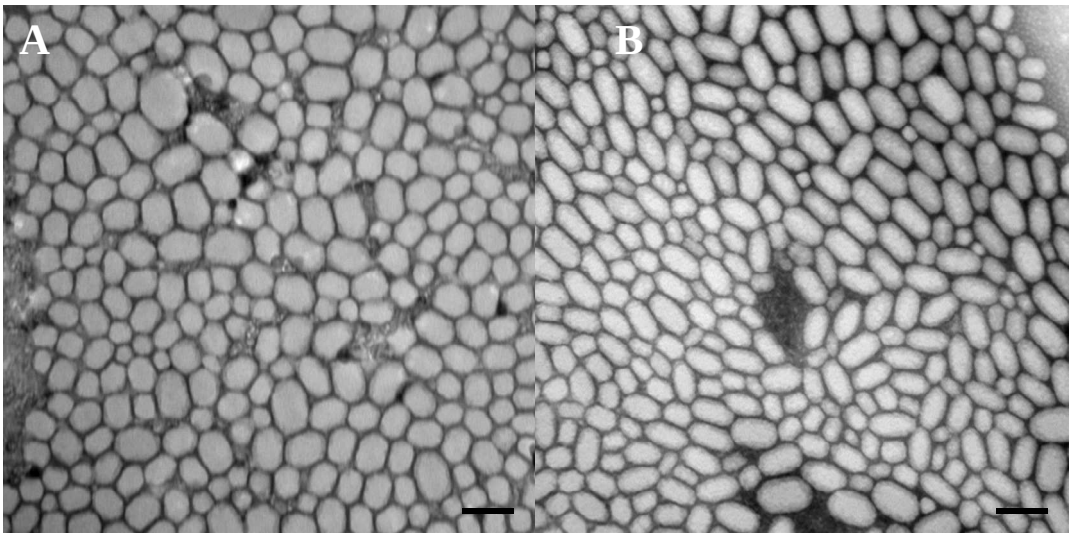

Figure 5.5: TEM pictures of PBLG-PEG-Rhodamine nanoparticles made with polymers of different molecular weights (A) 28kg/mol (B) 55kg/mol. Scale bar = 100nm.

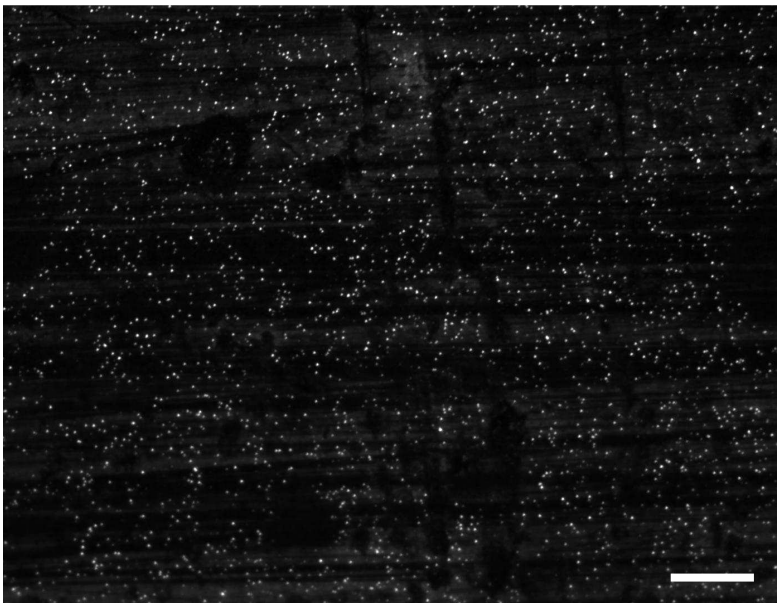

Figure 5.6: Confocal microscopy images of PBLG-PEG-rhodamine nanoparticles (Γ=1.88) Scale bar 10µm.

5.2.2. In vitro assays

When nanoparticles suspensions are injected in the bloodstream, apart from interactions with plasmatic proteins, one type of cells that they will encounter are endothelial cells lining the veins and capillaries. Human Umbilical Vein Endothelial Cells (HUVEC) were thus selected as a model for studying interactions of PBLG nanoparticles with cells.

5.2.2.1. Cytotoxicity assays

Firstly a cytotoxicity assay has been performed. Cytotoxicity assays were made for each particle series using a MTT cell viability test on HUVEC with polymer particles of PBLG-PEG/PBLG (80/20) nanoprecipitated in water with 0.1% poloxamer and adjusted to pH=6.6 and salt concentration 0.9%.

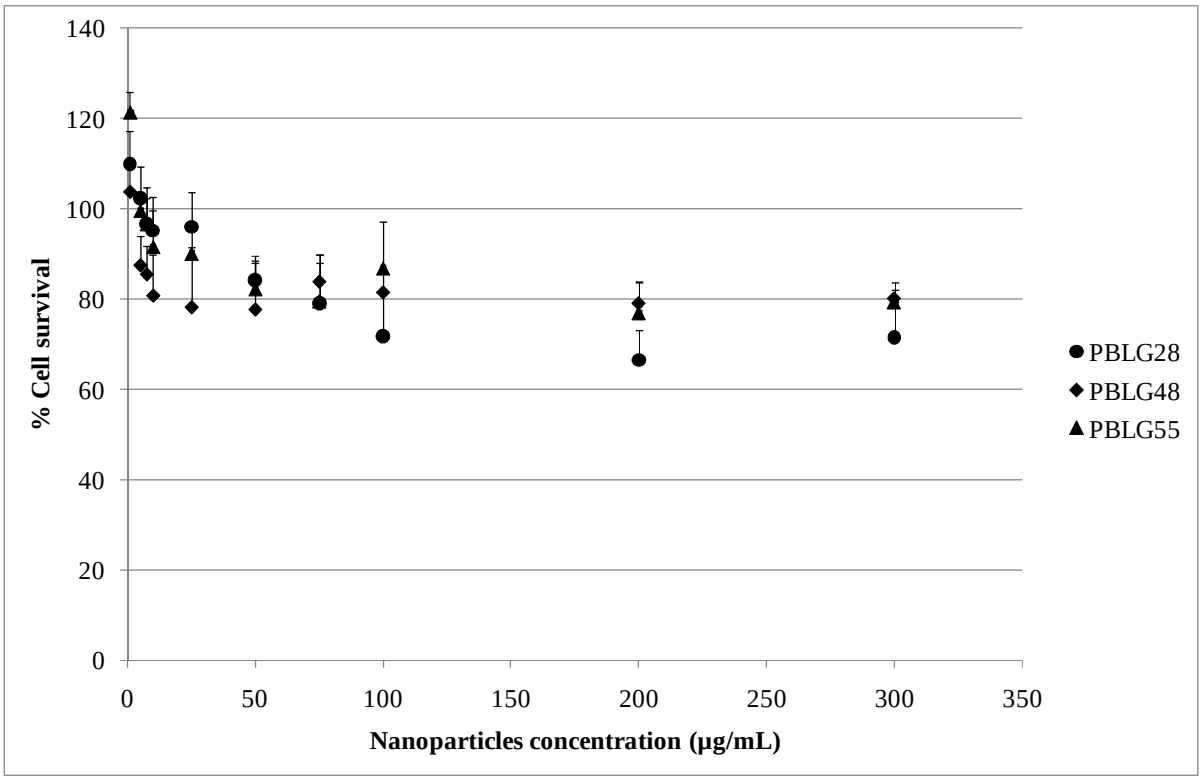

Figure 5.7: MTT Test of the PBLG/PBLG-PEG nanoparticles on HUVEC.

Figure 5.7 shows that the MTT test on PBLG composite nanoparticles revealed no long term toxicity. Even at 300µg.mL^{-1} 70% to 80% of the cells were still viable after 72h.

5.2.2.2. Video and confocal microscopy

Insight into the *in vitro* fate of the nanoparticles was gained by confocal microscopy. Monitoring the nanoparticles internalization by confocal microscopy gave a first look of the particles intracellular localization over time. Confocal pictures revealed that PBLG particles first accumulated on the surface of the cells, and were then internalized and moved to the perinuclear regions of the cells.

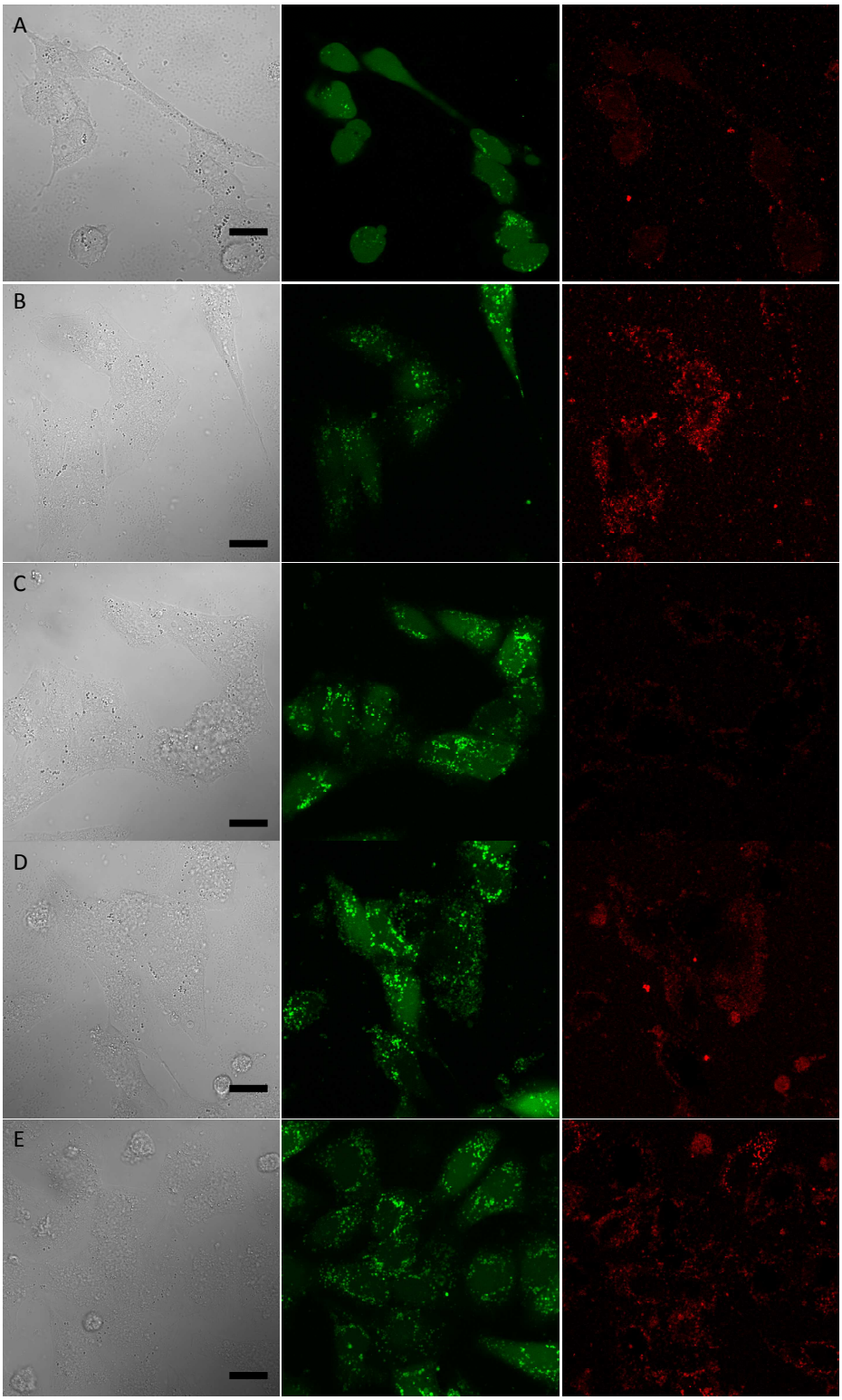

Figure 5.8: Confocal microscopy images of HUVEC after (A)30min, (B)225min, (C)120min, (D)215min and (E)410min of incubation with Γ=1.30(A-B) and Γ=1.88(C-E) nanoparticles. First column is the contrast image, second is calcein marked cells and last is the particles in and out of the cells. Scale bar 20µm

Nanoparticles interactions with cells over time are presented on figure 5.8. We see on these pictures that nanoparticles concentrate over time in the cells. No apparent toxicity of the nanoparticles was noticed, confirming MTT test conclusions.

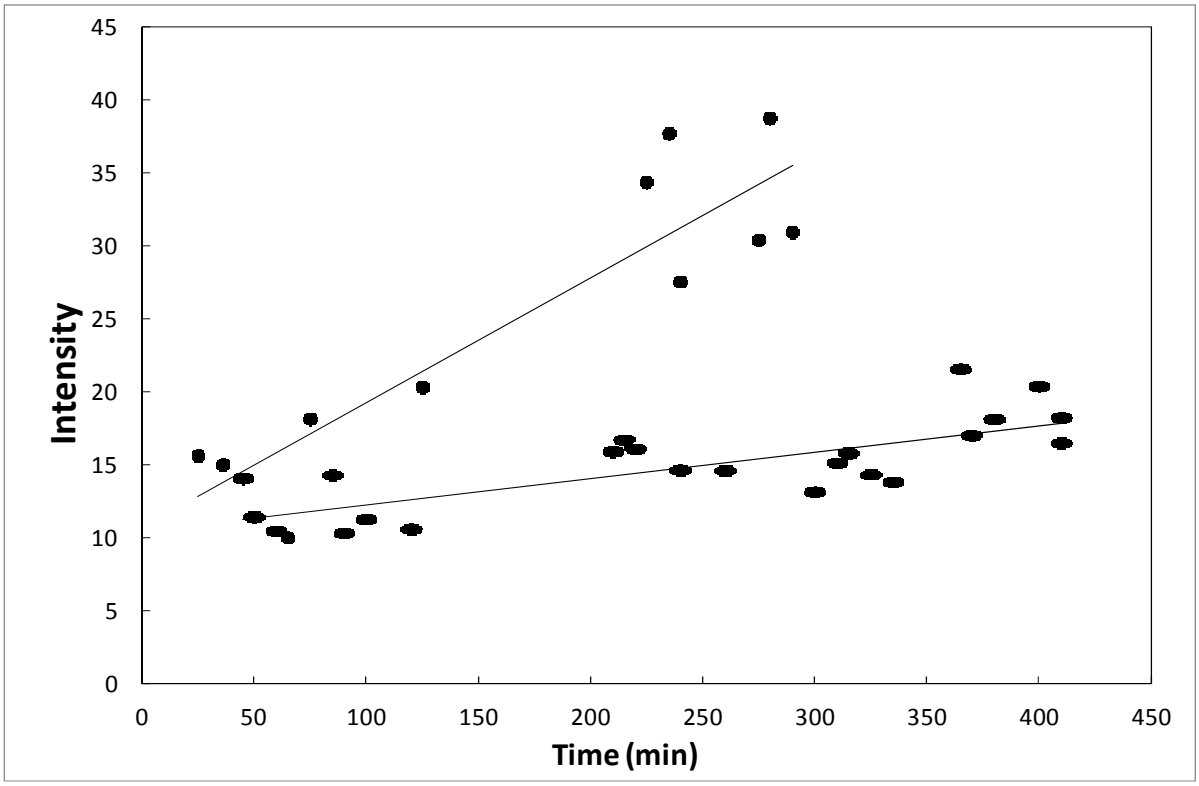

Figure 5.9: Fluorescence intensity in regions of interest over time for nanoparticles of different shapes ● Γ=1.30 and ▲ Γ=1.88

Furthermore attempts were made to determine the kinetics of internalization of the particles. For this purpose, fluorescence in regions of interest was examined over time. As can be seen in figure 5.9, the more elongated nanoparticles were more slowly internalized. Champion et al.[6] found in their study of the interaction of polystyrene microparticles with NR8383 and J774 macrophage cells (see 1.1.3.1) that the more deformation is required from the cell to internalize the particle, the slowly it is phagocyted. So elongated particles should be internalized more quickly if they approach the cell from their pointy end and more slowly or even not at all if they approach the cell from their flat side. Here we have elongated particles that are internalized more slowly, which would suggest a flat side approach.

As a conclusion, particles shape affected the capture by the cells but obviously, more experiments would be necessary for a better understanding of these effects and their mechanisms. The question of using purely spherical nanoparticles as a control has been also

addressed in this work. However, it revealed to be quite problematic to prepare spherical nanoparticles made of the same material and it was decided not to use such a control made of a polymer different from PBLG. Instead further studies could be extended to nanoparticles presenting higher elongation ratios.

Conclusion

After envisioning in chapter 2 and 3 the difficulties of creating regular, well defined, uniform and clean non-spherical particles using polymers of pharmaceutical interest, we have tackled the problem of how to observe these nanoparticles and how to follow them *in vitro.* For this two approaches were developed. First we manufactured quantum dots and studied their association to nanoparticles and we observed that the quantum dots were co-nanoprecipitated with the PBLG. However the addition of quantum dots in the nanoparticles modified their shape and greatly lessened the resulting fluorescence. Second we synthesized PBLG-rhodamine, using a modified rhodamine as initiator for the ring-opening polymerization. After evaluating both these types of nanoparticles we decided to test the possibility to follow our nanoparticles *in vitro* and to make a first series of experiments to assess the effect of shape on nanoparticles-cells interaction. For this we observed human umbilical cord endothelial cells (HUVEC) incubated with nanoparticles of interest up to 7h and noticed that elongation impacted their capture by the particles. Indeed elongated nanoparticles (Γ=1.88) were endocyted more slowly than more spherical particles (Γ=1.30). However these are still preliminary results and should be repeated and completed by a TEM study to see the *in vitro* fate of the particles.

Acknowledgements

We would like to thank Danielle Jaillard (CCME, Paris XI, Orsay) for her help with the TEM measurements, Valerie Nicolas (IFR141-IPSIT-ITFM) for her help with confocal microscopy, and Benjamin Le Droumaguet (UMR 8612) for kindly providing the rhodamine B derivative used for labeling.

References

1. Barbosa, M.E.M., Montembault, V., Cammas-Marion, S., Ponchel, G. & Fontaine, L.
Synthesis and characterization of novel poly(gamma-benzyl-L-glutamate) derivatives tailored for the preparation of nanoparticles of pharmaceutical interest,
Polymer International, 56, 317-324, **2007**.

2. Sicard-Roselli, C., Lemaire, S., Jacquot, J.-P., Favaudon, V., Marchand, C. & Houée-Levin, C.
Thioredoxin Ch1 of Chlamydomonas reinhardtii displays an unusual resistance toward one-electron oxidation,
European Journal of Biochemistry, 271, 3481-3487, **2004**.

3. Mohamed, M.B., Tonti, D., Al-Salman, A., Chemseddine, A. & Chergui, M.
Synthesis of High Quality Zinc Blende CdSe Nanocrystals,
The Journal of Physical Chemistry B, 109, 10533-10537, **2005**.

4. Mahler, B., Spinicelli, P., Buil, S., Quelin, X., Hermier, J.-P. & Dubertret, B.
Towards non-blinking colloidal quantum dots,
Nat Mater, 7, 659-664, **2008**.

5. Smith, A.M., Duan, H., Mohs, A.M. & Nie, S.
Bioconjugated quantum dots for in vivo molecular and cellular imaging,
Advanced Drug Delivery Reviews, 60, 1226-1240, **2008**.

6. Champion, J.A. & Mitragotri, S.
Role of target geometry in phagocytosis,
Proceedings of the National Academy of Sciences of the United States of America, 103, 4930-4934, **2006**.

Chapter VI

Effect of the shape of nanoparticles on pharmacokinetics

Chapter 6. Effect of the shape of nanoparticles on pharmacokinetics

Introduction

Drug targeting is a strategy that consists in modifying the biodistribution properties of a drug by those of a carrier in which it is associated. Consequently understanding the *in vivo* fate of the carriers is a critical step in their development. This strategy aims not only to reduce the amount of administered drugs, but also to improve the benefit/risk ratio for the patient by enhancing the delivery of the carrier in a specific organ, specific cells or subcellular compartments. Ideal carriers should increase specificity while toxic effects caused by non specific delivery should be weakened. Looking to fully efficient various vectors have been proposed, including lipidic or polymeric particulate systems, which are not only able to encapsulate the therapeutic molecules, but are also meant to interact efficiently with target cells. From this point of view, polymer nanoparticles are interesting objects for specifically targeting cells because of a unique combination of a nanometric size and the possibility to considerably modulate their physico-chemical properties and controlling more and more efficiently their surface at a molecular level.

Classical parameters used to tune the properties of these nanoparticles are the size, the surface charge and the nature as well as the conformation of the molecules decorating their surface. Quite surprisingly nanoparticles shape has not been much considered in drug delivery applications so far, although it has been shown in the literature that shape could be important factor to take into account for the *in vivo* fate of the carriers.

At the cellular level Champion et al.[1] studied the effect of shape on the phagocytosis of polystyrene microparticles. Outside of size effects they showed that the particle morphology had a severe impact on the rate of internalization and could even hinder the phagocytosis completely. In fact particle phagocytosis necessitates deformations of the cell membrane, which has been described to form first a cup and then a ring around the point of attachment of the particle. For very flat surfaces this deformation of the membrane requires too much energy, which stops the phagocytosis from happening. Gratton et al.[2] have performed a study on the effects of size, shape, and surface chemistry on cellular internalization where they

showed that changing the shape had a severe impact on the rate of internalization of the particles. Entry into HeLa cells was around four times quicker for particles with an aspect ratio (length over width) equal to 3 (50% in ~12min) compared to cubic particles with an aspect ratio of 1 (50% in ~50min) and gave a similar percentage of internalization (90% vs 85%). Chithrani et al.[3] showed equally that the shape of gold nanoparticles could influence their endocytosis. Entry into HeLa cells was two to five times less (in mass) for particles with an elongation ratio of 5 compared to spherical particles (elongation ratio of 1). In these studies it was always concluded that shape had to be taken into account when designing particles for targeting applications. However the effect of shape was different in these experiments.Gratton et al. and Champion et al. reported modifications of the rate of internalization whereas Chithrani et al. suggested modifications of the amount of particles internalized.

Only very few biodistribution studies focused on the effect of the shape of particles on their *in vivo* fate. Decuzzi et al.[4] have described the effect of the morphology of silica microparticles(0.7-5µm) on biodistribution in a tumor animal model. Female nude (nu/nu) mice (8-10 weeks old) were injected subcutaneously with MDA-MB-231 breast cancer cells. The tumor was allowed to establish for 3 weeks (300-700mm^3). Mice were then injected with 10^7-10^8 silica particles in saline via tail vein (4 mice per group). After two to six hours, mice were sacrificed and the organs (liver, spleen, heart, lungs, kidneys and brain) were excised and weighted. Silica biodistribution was made by elemental analysis of Si and histological evaluations were conducted. These authors reported that spherical, hemispherical and cylindrical particles could be captured by the liver (respectively around 50%, 50% and 65% of the total amount of recovered particles), while discoidal particles tended to accumulate in the lungs (around 40% of the total amount of recovered particles). Therefore, the shape would not only affect the amount of particles reaching the organs, but could be also very selective for specific organs. For example hemispherical particles that might seem uninteresting at first apparently never reach the heart and the lungs in this study.

In this context the aim of this work was to study the influence of shape on the *in vivo* fate of nanoparticles prepared from degradable polymers in view of further targeting applications.

The production of sufficient amounts of polymeric non spherical nanoparticles varying only by the shape is not a trivial task, as most polymers are yielding almost spherical particles. For this purpose, the auto assembling properties of a series of poly(γ-benzyl-L-

glutamate) copolymers was foreseen for preparing ovoid-shaped nanoparticles (see chapter 3). Indeed it has been suggested earlier that the rod-like structure of the chains of these polypeptides in their alpha helices secondary conformation has been shown to yield small and elongated nanoparticles, which aspect ratio can be controlled by the molecular weight of the poly(γ-benzyl-L-glutamate) block. After suitable labeling, it was the aim of this study to investigate their pharmacokinetics and biodistribution in rats.

6.1. Material and methods:

6.1.1. Materials:

HPLC grade chloroform (99%, Aldrich) and tetrahydrofuran (THF, Carlo Erba) were used as received without any further purification. Sodium chloride was purchased from Sigma-Aldrich (Steinheim,Germany). Pluronic F-68, a polyoxyethylene-polyoxypropylene block copolymer (MW = 8.5kg/mol.), was supplied from Sigma-Aldrich (Steinheim,Germany). Heparin (Calciparine, Sanofi Aventis Paris, France) was used as an anticoagulant. Lactated Ringer's solution and 0.9% sodium chloride were purchased from C.M.D. Lavoisier (Paris, France). Water was purified by reverse osmosis (MiliQ, Milipore). All other solvents and chemicals used were commercially available highest grades.

6.1.2. Polymer synthesis

Poly(γ-benzyl-L-glutamate) (PBLG) polymers with varying molecular weights were synthesized in anhydrous DMF by ring-opening polymerization of γ-benzyl-L-glutamate N-carboxyanhydrides (BLG-NCA, ISOCHEM-SNPE, stored at -18°C) using benzylamine (Janssen Chimica, distilled under reduced pressure over KOH and stored under argon atmosphere at room temperature) as initiator according to a slightly modified method described elsewhere[5].

Briefly, BLG-NCA was weighed under argon atmosphere in a degassed three-necked roundbottomed flask equipped with a thermometer, mechanical stirring, a refrigerant with a silica gel guard and a bubble detector. BLG-NCA was dissolved in DMF (volume was adjusted to obtain a BLG-NCA final concentration of 0.5M) at room temperature under mechanical stirring and argon flux. After about 10min, the argon flux was stopped, the solution was heated at 30°C and the initiator solution was added. Immediately after the addition, CO_2 emission was observed. Absence of BLG-NCA auto-polymerization was checked by FTIR spectroscopy of the BLG-NCA solution before addition of the initiator. The reaction mixture was stirred at 30°C until the characteristic BLG-NCA bands disappeared from the FTIR spectrum. The mixture was precipitated in an excess of cold diethyl ether to give a white solid. The precipitate was filtered and washed with diethyl ether. The polymers were washed again with diethyl ether and dried under vacuum at 35°C for at least 12h. A second precipitation, purification and drying procedure was performed for all polymers. FTIR

spectra were recorded to analyze BLG-NCA auto-polymerization and to follow the reaction using a Perkin-Elmer 1750 FTIR spectrometer.

6.1.3. PBLG-rhodamine

A PBLG labelled polymer as been prepared as described above for PBLG using a specific piperidine rhodamine derivate[6-7] as an initiator.

6.1.4. Post-synthesis pegylation

The different molecular weights polymers were then pegylated post-synthesis. For this purpose, methoxy-PEG(6000)-N-hydroxysuccinimide (IRIS Biotech) was coupled to PBLG, which was done overnight in a mix of solvent. Briefly 500mg of PBLG was dissolved in 4mL of 25% THF, 25% DMF and 50% DMSO during 18h. 4mL of methoxy-PEG(6000)-N-hydroxysuccinimide was added to the mix for a final concentration of 1.5 equivalent per mole of PBLG. The mixture was heated at 30°C under magnetic stiring and under argon atmosphere during 24h.

6.1.5. Molecular weight analysis

Matrix-assisted Laser Desorption/Ionization-Time of Flight-Mass Spectrometry (MALDI-TOF-MS) analysis was carried out in positive-ion mode on a Voyager DE-STR MALDI-TOF mass spectrometer (Perseptive Applied Biosystems, Framingham, MA,USA) equipped with a 337nm nitrogen laser. 2-[(2E)-3-(4-tert-Butylphenyl)-2-methylprop-2-enylidene]malononitrile or DCTB (40mg/mL in THF) and potassium trifluoroacetate (50mg/mL in THF) were used respectively as matrix and cationic ionization agent. The polymer/matrix molar concentration ratio was adjusted between 40:1 (for the lowest molecular weight) and 1:3600 (for the highest molecular weight). 20µL of this matrix, 1µL of polymer solutions in THF (at the adjusted concentrations) and 1µL of ionization agent were mixed and deposited onto the sample plate and allowed to dry at room temperature. Spectra of PBLG were acquired with the default calibration (accuracy ca. 0.1 %) under the same condition as those described by Sicard-Roselli et al.[8].

6.1.6. Nanoparticles preparation

Two types of nanoparticles with varying elongation ratios were prepared by nanoprecipitation of mixtures of PBLG (80% w/w), PBLG-PEG (10% w/w) and PBLG-

rhodamine (10% w/w) copolymers. In each cases the derivates comprised an invariant PBLG block with a molecular weight of 28kg/mol or 55kg/mol.

Briefly, 15mg of polymer (1.5mg of PBLG-rhodamine, 1.5mg of PBLG-PEG and 12mg of PBLG) were dissolved in 5mL of THF at 30°C during 18h, without stirring. This solution was added dropwise to 10mL of Poloxamer F68 (0.1% w/v) under magnetic stirring (700rpm). The mixture was left under magnetic stirring for 10min and then transferred in a glass flask. The solvent was gently evaporated in a rotavapor (V850, R124, Buchi) at 40°C, first at 200mbar for 5min and then at 40mbar to yield 5mL of suspension. The pH of each preparation was measured, and the osmolarity of each preparation was adjusted to 0.9% by adding 200µl of NaCl solution with a concentration 225g.L^{-1}. The suspensions were kept at 4°C until use.

6.1.7. Transmission Electron Microscopy

Nanoparticles were further analyzed through TEM (Transmission electron microscope, Philips EM208) at 60kV. 3µl of nanoparticles suspension, after suitable dilution of bulk suspensions in milli-Q water, were placed on a formvar-carbon film previously coated on a copper grid (400 meshes). After 5min deposition, a drop of phosphotungstic acid solution (1%) was placed on the copper grid and on top of the sample. After 30s, the liquid was drained and the sample was placed inside the EM208 and pictures were taken.

6.1.8. Morphology analysis

For each type of nanoparticles, dimensions were measured on different TEM pictures thanks to The Gimp© software. The smallest and the longest dimensions of individual nanoparticles taken from a series of microphotographs were measured and were named width and length, respectively. An average of 200 nanoparticles was measured. The nanoparticles were assimilated to oblates and their elongation ratios, as well as their sphere equivalent diameters in volume, were calculated as follows:

Eq.1

$$Aspect\ Ratio = \Gamma = \frac{Length}{Width}$$

Eq.2

$$Equivalent\ Diameter = \sqrt[3]{Length * width^2}$$

6.1.9. Zeta potential measurements

Nanoparticles zeta potential was determined after suitable dilution of nanoparticles suspensions in a 15mM NaCl solution with a Zetasizer nano ZS (Malvern instruments, Worcestershire, United Kingdom).

6.1.10. Pharmacokinetic studies

Males Wistar rats with catheterized jugular vein, aged 14 weeks and weighing 300-325g were obtained from Charles Rivers (Lyon, France). The rats were allowed free access to water and food and were housed under controlled environmental conditions (constant temperature, humidity, and a 12h dark-light cycle). In a preliminary experiment, two groups (n=3) of rats were used for assessing experimental conditions. Each group received one of the nanoparticles formulations. Each rat was injected with 0.5mL of nanoparticles suspensions at ($3mg.mL^{-1}$), previously adjusted to physiological pH and 0.9% with sodium chloride. All the blood was drawn from the heart at 3 different times (one rat for each time): 30min, 4h and 24h.

For final study, two groups of rats were used. Each group (n=7) received one of the nanoparticles formulation. Each rat was injected with 0.5mL of nanoparticles suspension at $3mg.mL^{-1}$ as a bolus intravenously via a catheter in the jugular vein. Suspensions were previously adjusted in pH and salt concentration to physiologic values. 0.25mL of blood were sampled at 7 different times (pre-injection, 30min, 1h, 2h, 4h, 8h and 24h post-injection) in a syringe with 0.05mL of heparin. Each volume collected was then substituted by an equivalent volume of lactated Ringer's solution. To prevent clogging of the catheter, 0.1mL of heparin solution was injected after each blood collection. The animal experiments were conducted accordingly to the principle of animal care and European legislation recommendation 2007/526/EC (authorization of the farming house n°B92-019-01).

Fluorescently labeled nanoparticles were extracted from blood by mixing 250µL of blood with 1mL of chloroform. After vortexing and resting, 900µL of the supernatant (chloroform and dissolved polymer) was separated to be analyzed. The nanoparticles concentration of each sample was then determined by spectrofluorimetry. For this purpose, a calibration curve of

nanoparticles concentration in Wistar rats blood was previously established. For each nanoparticles formulation, six solutions with increasing polymer concentrations ranging from 0 to 0.15mg/mL in blood were prepared. Each sample underwent a chloroformic extraction as described above. Finally chloroformic solutions were assayed with a spectrofluorimeter (PerkinElmer, California USA) at $\lambda = 560nm$ corresponding to the rhodamine specific fluorescence peak.

6.1.11. Organ distribution

A biodistribution study was performed on the rats following the pharmacokinetics study. After a 72h washing period, 1mL of nanoparticles suspension ($3mg.mL^{-1}$, previously adjusted in pH and salt concentration to physiologic values) was injected every 24h three times. Brains, livers, spleens, kidneys, and heart were collected 24h after the last injection. The organs were congealed and kept at -80°C until use. Further they were grinded with a Potter and the fluorescence was extracted in presence of 1mL of chloroform.

6.2. Results & discussion

Following their administration in the body, considerable variations in the biodistribution and pharmacokinetics of polymeric nanoparticles have been reported in the literature. As for every foreign substance, the overall persistency of nanoparticles in the body depends on a combination of excretion and/or degradation, which rates can be highly variable depending on the material. However there is considerable experimental evidence that their biodistribution in the different organs depends on parameters such as particle size, molecular surface properties, and electric charge. Although available experimental data remains rather limited, the influence of these parameters has been characterized on some nanoparticles systems, including liposomes, polymeric micelles, metallic and polymeric nanoparticles. For instance following IV delivery in blood, it has been shown that nanoparticles could be cleared very rapidly or exhibit prolonged circulations in the blood stream, with half-lives ranging from minutes to many days. Basically surface modification with polyethylene glycol chains reduces and/or modifies the opsonization of the surface of the particles by numerous seric proteins, which decreases their uptake by macrophages and cells belonging to the macrophage-phagocyte system (MPS). Possibly, this effect can be obtained by decoration of the particles surface with other hydrophilic chains. The length of PEG chains, their density, the conformation of other hydophilic macromolecules interplay in a complex way with seric proteins adsorption. Secondly, in the case of spherical particles, the decrease of the diameter of the particles generally results in a decrease in phagocytosis and thus in prolonged circulation in blood, which has been attributed to the fact that a pronounced curvature would decrease proteins adsorption. Finally, electric neutrality leads also to prolonged presence of the particles in blood.

So far, the effect of the morphology of nanoparticles has been much less investigated, due to the difficulty of preparing and characterizing non spherical nanoparticles from degradable polymers. The goal of this chapter is to study the influence of the shape of nanoparticles on their pharmacokinetics and biodistribution. For this purpose, non spherical degradable nanoparticles were prepared from the association of different poly(γ-benzyl-L-glutamate) copolymers.

6.2.1. Nanoparticles characterization

Elongated nanoparticles could be easily prepared by nanoprecipitation of mixtures of different poly(γ-benzyl-L-glutamate) copolymers (figure 6.1) in defined proportions (80% PBLG-Bz, 10% PBLG-PEG, and 10% PBLG-rhodamine, respectively) in a 0.1% w/v poloxamer F68 solution in water, in order to fluorescently label these particles as well as hydrophilizing their surface by using PEG derivatives. Two sets of copolymers were used differing only by the molecular weight of the constant PBLG block.

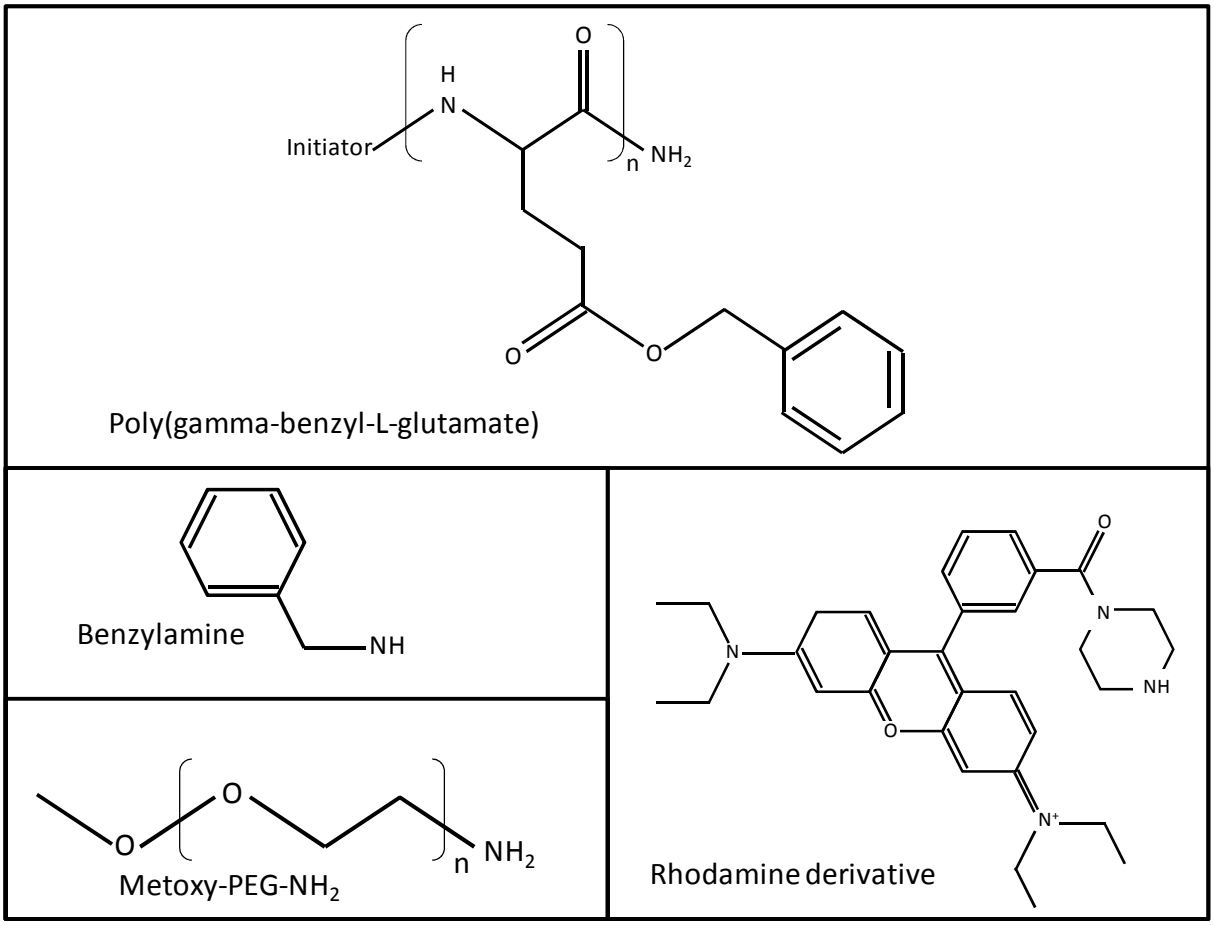

Figure 6.1: Structure of poly(gamma benzyl-glutamate) block and the different moieties introduced during the synthesis of the different PBLG copolymers: benzylamine, methoxy-PEG$_{6000}$ and rhodamine derivative.

As can be seen from transmission scanning microscopy photographs, nanoparticles composed of PBLG derivatives comprising a 28kg.mol^{-1} PBLG block as well as the ones prepared from the derivates with a 55kg.mol^{-1} PBLG block were elongated and ovoid-shaped. Their aspect ratios and mean sphere equivalent diameters in volume were evaluated from

TEM pictures. The geometry of the particles was assimilated to an oblate and aspect ratios of the particles were 1.3 and 1.9 for 28kg.mol^{-1} and 55kg.mol^{-1} PBLG blocks, respectively, which were statistically different. The particles were comparable in term of sphere equivalent diameter in volume, which corresponded to 50-60 nm,

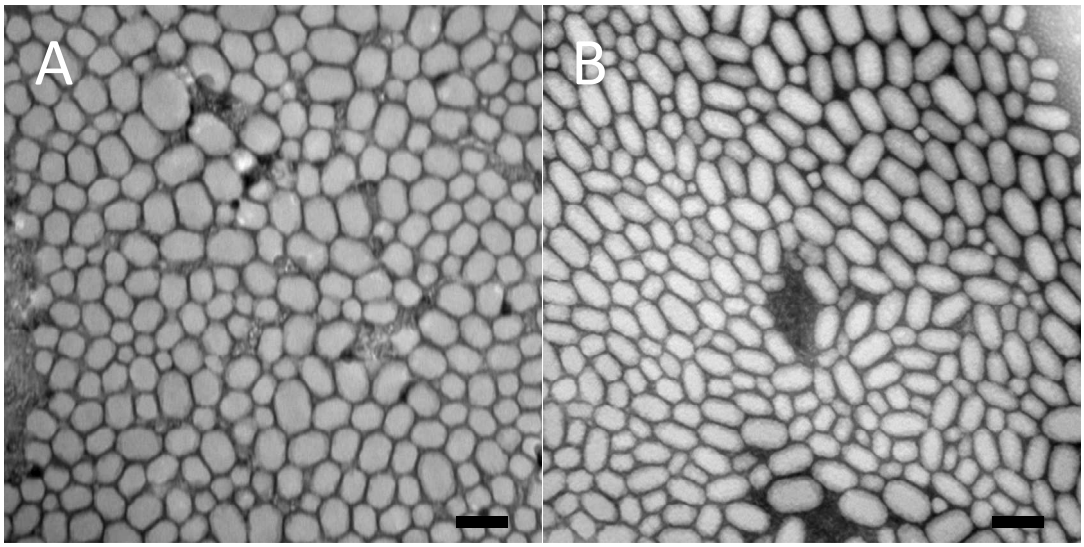

Figure 6.2: Transmission electronic microscopy images of nanoparticles composed of PBLG derivatives (respective ratio: 80% PBLG-Bz, 10% PBLG-PEG, and 10% PBLG-rhodamine). (A) MW = 28kg.mol^{-1} (B) MW = 55kg.mol^{-1} (scale bar 100nm)

The nanoparticles were negatively charged as shown by their zeta potential, which were -29.5 ±4.2mV and -33.4± 3.1mV for mw = 28kg.mol^{-1} and mw = 55kg.mol^{-1}, respectively. Despite pegylation and likely adsorption of poloxamer chains in surface, there was no or only moderate shielding of the negative surface electric charges commonly beared by such particles. However, these values were consistent with literature[9]. Importantly, two types of nanoparticles were obtained with similar surfaces (same polymer and pegylation), similar volume, but with differences in elongation. Suspensions of these particles were administered by the IV route in rats for investigating the effect of this parameter.

Table 6.1: Morphology of nanoparticles determined from TEM images (n= 200)

Molecular Weight (kg/mol)	Width (nm)	Length (nm)	Aspect Ratio	Volume equivalent diameter (nm)
28	56 ± 10	74±18	1.3 ± 0.1	62 ± 12
55	41± 8	78 ± 17	1.9 ± 0.3	51 ± 10

6.2.2. Nanoparticles labeling and recovery in blood

Labeling was required to be able to determine the amount of nanoparticles *in vivo*. As shown in chapter 5 we have envisioned two markers, but the rhodamine based labeling showed a better efficiency than the quantum dots labeling. Direct measurement of fluorescence in the blood or in the grinded organs was not feasible, leading to extract the fluorescence in biological media.

Firstly a simple separation technique using centrifugation has been envisioned. Fresh rat blood was mixed with a known quantity of nanoparticles and attempts were made to separate red blood cells from the plasma by centrifugation at 10,000tr/min during 15min. Nanoparticles concentration in the plasma was measured and only a very low fraction (<0,1%) of the nanoparticles were recuperated. This could be due to an attachment of the particles to the blood cells or sedimentation following aggregation in the plasma.

Thus an alternative method based on a lysis of the blood cells and extraction of the fluorescent polymer to a good solvent of rhodamine-labelled PBLG has been developed. Chloroform has been selected because it is simultaneously a good solvent for PBLG and for rhodamine, and because it is not miscible with water. The recovery of the fluorescence by this technique was more efficient, and it was decided to assess by this technique the total amount of nanoparticles (bound or unbound) in blood.

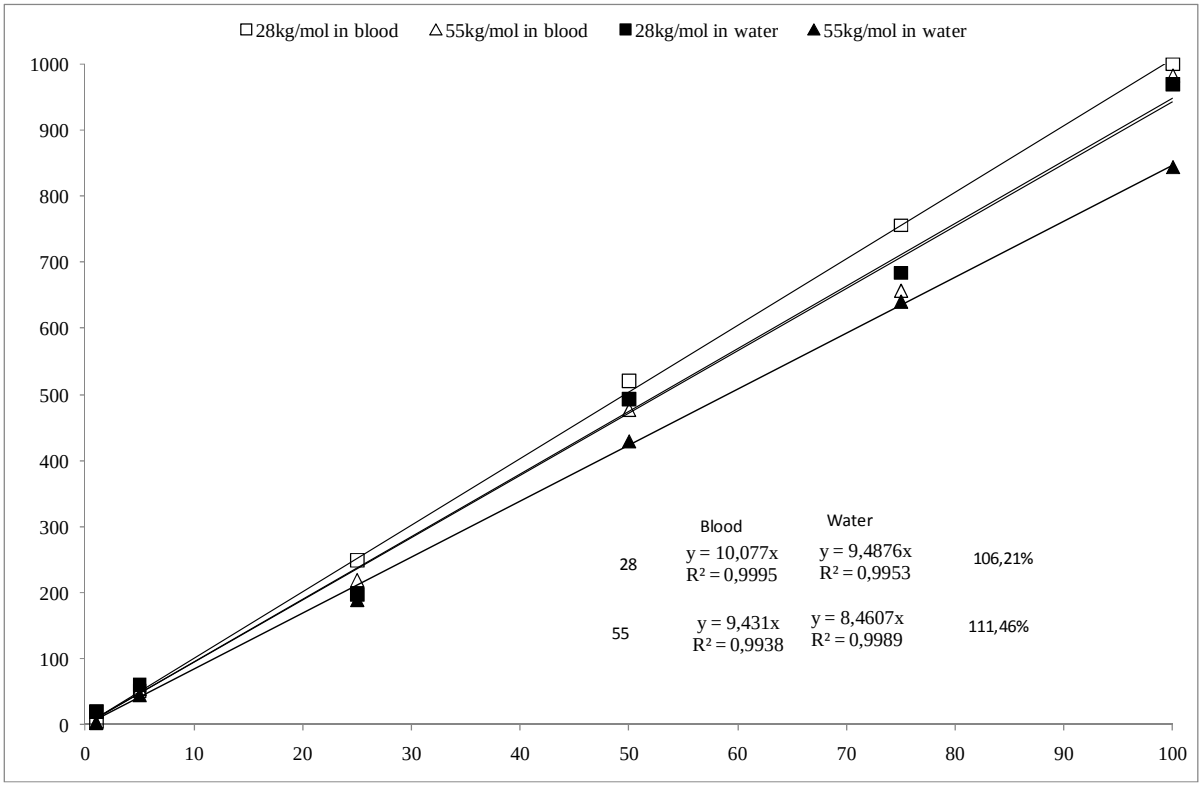

Figure 6.3: Calibration curve of the nanoparticles fluorescence in water and in blood.

As a control, fluorescent nanoparticles suspended in water were treated similarly and their extraction has been compared to the extraction in blood in a concentration range which was expected to be relevant for animal experimentation. Since it was intended to inject 0.5mL of nanoparticles suspensions at $3mg.mL^{-1}$, in rats weighting approximately 300-325g (13mL of blood), it was decided to assay the fluorescence for concentrations ranging from 0 to $0.15mg.mL^{-1}$, corresponding to the dilution of the bolus injection in a final volume of 10mL. As can be seen on figure 6.2, fluorescence extraction from nanoparticles in blood and in water were equivalent, making possible to use these calibration curves for assaying nanoparticles in blood. Some differences could be observed depending on the molecular weight of the poly(γ-benzyl-L-glutamate) copolymers used for preparing the nanoparticles, which was attributed to possible variations in the amount of PBLG-rhodamine copolymer incorporated into the nanoparticles.

6.2.3. Pharmacokinetics analysis

6.2.3.1. Preliminary study

A preliminary pharmacokinetics study has been conducted to establish the timeline of collection by injecting 0.5mL of a 3mg.mL^{-1} nanoparticles suspension in a group of six rats, which were sacrificed, after 30min, 4h, and 24h the rats were sacrificed and blood and organs were collected. As shown in figure 6.4, fluorescent nanoparticles could be easily detected in blood up to 24 hours. However, no fluorescence could be detected in the investigated organs (brain, liver, spleen, kidneys, and heart), whatever the time, suggesting that only very small amounts of particles were distributed in these organs, which was probably not related to the sensitivity of the detection method. To test the hypothesis of a too low sensitivity, the calculated concentration after a hypothetical and uniform distribution of the administered dose in the whole body of rats would be in the range of 5µg.g^{-1} of organ, which were easily detected. Thus, distribution in other organs, including urines and feces should be investigated for clarification.

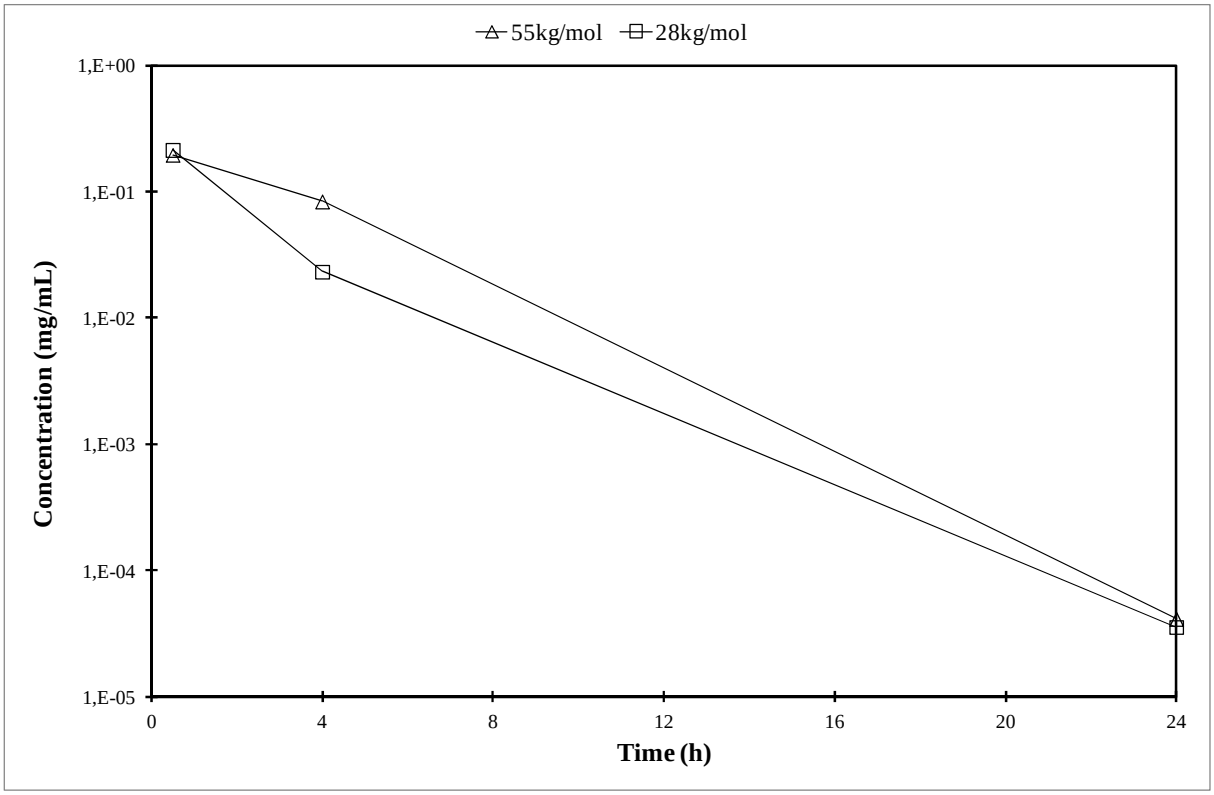

Figure 6.4: Pharmacokinetics preliminary study: Six rats were injected with 0.5mL of nanoparticles solution at 3mg/mL, after 30min, 4h, and 24h the rats were sacrificed and blood and organs were collected.

Figure 6.4 shows the results of the preliminary study. We were able to detect the nanoparticles after injection. After 24h, no nanoparticles were detected. Based on these data pharmacokinetics profiles were obtained for the two types of nanoparticles with blood sampling at 30min, 1h, 2h, 4h, 8h and 24h after injection (figure 5).

6.2.3.2. Pharmacokinetics study

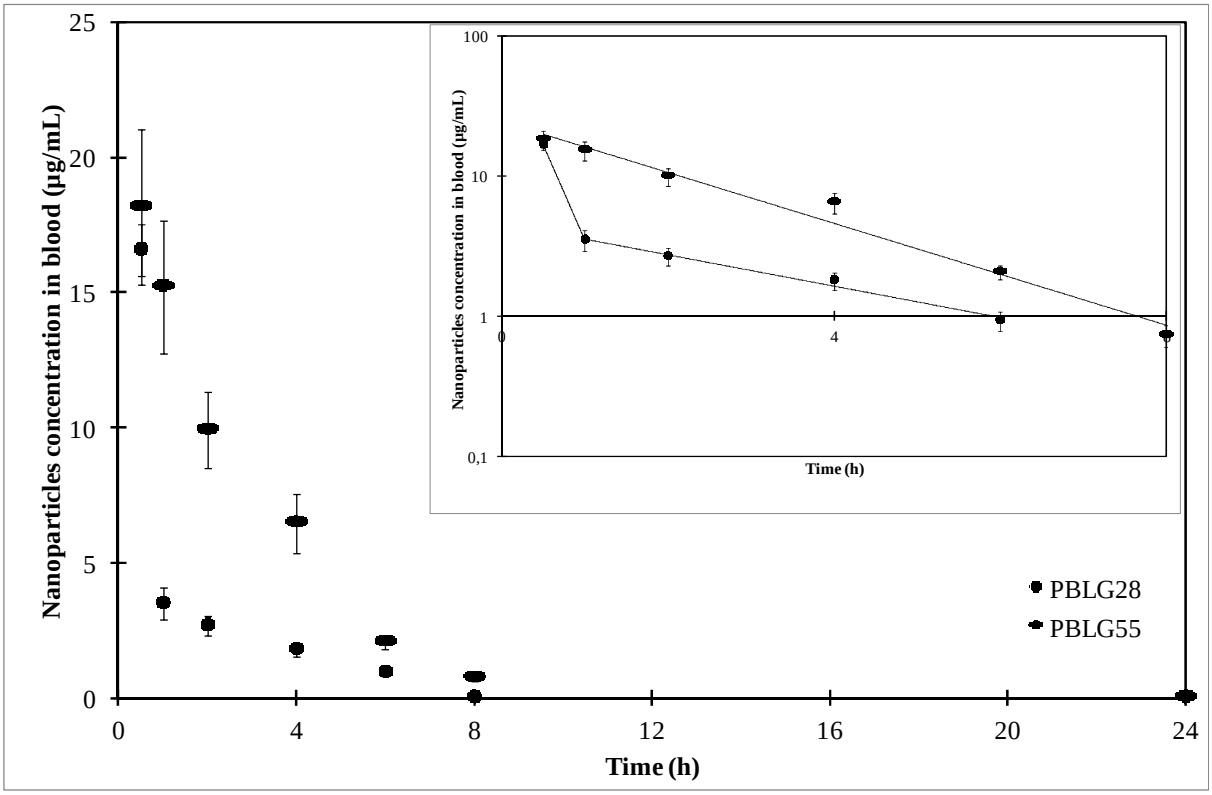

Figure 6.5: Blood profiles of poly(gamma benzyl-L-glutamate) nanoparticles following IV delivery in rats (n=7).

As depicted in figure 6.5, very significant differences in profiles could be noticed depending on the aspect ratio of the particles. The less elongated particles (aspect ratio: 1.3) exhibited a biphasic kinetics characterized by a rapid decrease in the initial part (apparent half-life of 13min), followed by a slower decline (apparent terminal half-life of 2.7h). This phase corresponded only to about 10% of the injected amount, while the rapid initial phase corresponded to the disapearance of more than 90% of the dose. More elongated nanoparticles (aspect ratio: 1.9), were cleared much slowly from blood accordingly to a monophasic kinetics (at least on the 30min-24 hours period.) and the apparent half-life was 1.6 h.

Table 6.2 Pharmacokinetics parameters following IV administration of PBLG nanoparticles with varying elongation ratios. (n=7 rats for each formulation)

	PBLG28 (1rst)		PBLG28 (2nd)		PBLG 55	
$C(t)=C_0*\exp(-Kt)$	Mean	Std Dev	Mean	Std Dev	Mean	Std Dev
C_0(µg/mL)	67.5	13.7	3.81	0.26	20.28	0.42
$K(h^{-1})$	3.14	0.35	0.257	0.014	0.418	0.029
$t_{1/2}=\ln(2)/K$ (min)	13.3	1.4	162.1	9.1	99.9	7.0
Distribution volume (mL) = $Dose/C_0$	22.9	4.2	402.7	65.7	75.1	9.8

The calculated distribution volumes (table 6.2) were quite different for the two types of nanoparticles. The distribution volume of less elongated particles (aspect ratio: 1.3) was 23mL, which compared not so differently to the whole blood volume in rats (approx. 13mL of blood and 7mL of plasma in rat), suggesting their presence mainly in the intravascular space before elimination. This would consistent with the fact that no fluorescence could be detected in investigated organs. On the contrary, more elongated nanoparticles (aspect ratio: 1.9) had an apparent distribution volume of 75mL suggesting a rapid distribution in other organs and/or elimination.

On the whole, these data suggest that the effect of shape on the persistence of nanoparticles in blood can be considered as a relevant parameter as a simple increase of 1.5 fold of the aspect ratio resulted in a half life was multiplied by 7.5. Indeed the other determinants of their pharmacokinetics were identical for the two types of particles including the nature of the polymer, the volume of the particles and the surface properties. These differences seemed related to nanoparticles shape, which is in accordance with various works showing the importance of shape on biodistribution, as shown by Champion et al.[1], Decuzzi et al.[10], and Gratton et al.[2] at the cellular level.

Many factors can be involved to explain the observed trends, including differences in: (i) opsonization and capture by macrophages of the MPS, (ii) extravasation in organs including liver elimination modified by the shape of particles[11], (iii) or even direct interaction of the particles with the surfaces of endothelia. For example, the size of liver sinusoidal endothelial cell fenestrae, which separate the blood in liver capillaries from parenchymal cells, could play a critical role in the extravasation of these nanoparticles to liver cells[12]. The size of these fenestrae has been reported to be 98 ± 13nm[13], which could play a critical role in the sieving of the nanoparticles for which the diameter of the equivalent sphere was 50-60nm. Although no fluorescence could be retrieved in liver whatever the type of nanoparticles, similar behaviors in other organs cannot be excluded.

Conclusion

The present study suggests that the pharmacokinetics of nanoparticles following their administration in the body depends not only from the molecular characteristics in surface of the particles, but also of their morphology. Shape has not been often considered as a critical parameter so far, probably because up to now most nanoparticles investigated in pharmaceutical applications are almost spherical.

The design of ovoid-shaped polymeric nanoparticles made by auto-assembling of poly(γ-benzyl-L-glutamate) copolymers, with similar compositions, surface properties and volume, but only differing by their aspect ratio, allowed to test the effect of the shape parameter on their *in vivo* fate. Considerable differences in blood profiles kinetics were observed. If confirmed by further studies, the elongation of nanoparticles should be considered as an important parameter that can influence their *in vivo* fate and that need to be taken into account when designing a strategy for a specific application in drug targeting.

Acknowledgements

We would like to thank Danielle Jaillard (CCME, Paris XI, Orsay) for her help with the TEM measurements; Valérie Domergue and the team from the “Animalerie et exploration fonctionelle” platform (IFR141, IPSIT) for her help with animal experiments; Vincent Guérineau (IMAGIF) for his help with the Maldi-Tof experiments, and Abdel Atia for his help with animal experiments and analysis.

References

1. Champion, J.A. & Mitragotri, S.
Role of target geometry in phagocytosis,
Proceedings of the National Academy of Sciences of the United States of America, 103, 4930-4934, **2006**.

2. Gratton, S.E.A., Ropp, P.A., Pohlhaus, P.D., Luft, J.C., Madden, V.J., Napier, M.E. & DeSimone, J.M.
The effect of particle design on cellular internalization pathways,
Proceedings of the National Academy of Sciences, 105, 11613-11618, **2008**.

3. Chithrani, B.D., Ghazani, A.A. & Chan, W.C.W.
Determining the Size and Shape Dependence of Gold Nanoparticle Uptake into Mammalian Cells,
Nano Letters, 6, 662-668, **2006**.

4. Decuzzi, P., Godin, B., Tanaka, T., Lee, S.Y., Chiappini, C., Liu, X. & Ferrari, M.
Size and shape effects in the biodistribution of intravascularly injected particles,
Journal of Controlled Release, 141, 320-327, **2010**.

5. Barbosa, M.E.M., Montembault, V., Cammas-Marion, S., Ponchel, G. & Fontaine, L.
Synthesis and characterization of novel poly(gamma-benzyl-L-glutamate) derivatives tailored for the preparation of nanoparticles of pharmaceutical interest,
Polymer International, 56, 317-324, **2007**.

6. Brambilla, D., Nicolas, J., Le Droumaguet, B., Andrieux, K., Marsaud, V., Couraud, P.-O. & Couvreur, P.
Design of fluorescently tagged poly(alkyl cyanoacrylate) nanoparticles for human brain endothelial cell imaging,
Chemical Communications, 46, 2602-2604, **2010**.

7. Nguyen, T. & Francis, M.B.
Practical Synthetic Route to Functionalized Rhodamine Dyes,
Organic Letters, 5, 3245-3248, **2003**.

8. Sicard-Roselli, C., Lemaire, S., Jacquot, J.-P., Favaudon, V., Marchand, C. & Houée-Levin, C.
Thioredoxin Ch1 of Chlamydomonas reinhardtii displays an unusual resistance toward one-electron oxidation,
European Journal of Biochemistry, 271, 3481-3487, **2004**.

9. Upadhyay, K.K., Bhatt, A.N., Mishra, A.K., Dwarakanath, B.S., Jain, S., Schatz, C., Le Meins, J.-F., Farooque, A., Chandraiah, G., Jain, A.K., Misra, A. & Lecommandoux, S.
The intracellular drug delivery and anti tumor activity of doxorubicin loaded poly([gamma]-benzyl l-glutamate)-b-hyaluronan polymersomes,
Biomaterials, 31, 2882-2892, **2010**.

10. Decuzzi, P., Lee, S., Bhushan, B. & Ferrari, M.
A Theoretical Model for the Margination of Particles within Blood Vessels,
Annals of Biomedical Engineering, 33, 179-190, **2005**.

11. Bertholon, I., Vauthier, C. & Labarre, D.
Complement Activation by Core–Shell Poly(isobutylcyanoacrylate)–Polysaccharide Nanoparticles: Influences of Surface Morphology, Length, and Type of Polysaccharide,
Pharmaceutical Research, 23, 1313-1323, **2006**.

12. Braet, F. & Wisse, E.
Structural and functional aspects of liver sinusoidal endothelial cell fenestrae: a review,
Comparative Hepatology, 1, 1-17, **2002**.

13. Fraser, R., Clark, S.A., Day, W.A. & Murray, F.E.
Nicotine decreases the porosity of the rat liver sieve: a possible mechanism for hypercholesterolaemia,
Br J Exp Pathol, 69, 345-350, **1988**.

Chapter VII

General Discussion & Perspectives

Chapter 7. General Discussion

Introduction

The *in vivo* fate of an active ingredient in the body is the result of many phenomena, from the absorption to the elimination phase. At a given dosage, the therapeutic efficiency of these molecules, their eventual side effects and toxicity, all depend on their distribution in the organism, organs, cells and even sub-cellular compartments. This distribution can be very heterogeneous because, for the active ingredient to reach its target, the crossing of many physico-chemical and biochemical barriers is required. In order to better control this distribution, one of the current strategies is to associate the active ingredient to a carrier that will replace the biodistribution properties of this active molecule by its own. These carriers are manufactured to possess the characteristics required to cross these barriers efficiently. Furthermore once the target is reached these carriers must be able to release the active ingredient in the targeted organ or tissue but not during the distribution process itself. Ideally the carrier must be non-toxic and easy to eliminate.

Within this framework, the development of efficient carriers represents a tremendous challenge because these vectors must present successively or at the same time extremely various functionalities. Still this strategy is giving high hopes for the improvement of active ingredient efficiency by increasing their therapeutic index and is currently at the center of a significant research effort.

In this context, particulate carriers present major advantages for this strategy. Currently the parameters that are mostly studied are the size of the carrier (nano, micro or millimeter sized), its surface properties (charge, presented ligands…) and its constitutive materials (polymer, metal, crystal…). The objective of this thesis was to lay the foundation of the study of a “forgotten” parameter: the shape.

However with the recent advances in nanotechnologies, more and more methods to produce non-spherical nanoparticles are available and can be tuned for pharmaceutical applications. This work follows many studies that have presented methods to produce non-spherical particles and focused on two main axis: first the production of non-spherical nanoparticles and their tuning for pharmaceutical purposes, second the study of their *in vitro*

and *in vivo* fate to confirm the relevance of the shape as a major parameter for tuning carriers in the drug delivery strategy.

7.1. Conception of multifunctional non-spherical particles of pharmaceutical interest

7.1.1. Production of non-spherical nanoparticles

As was explained in the first section of this thesis describing previous works in this area (see chapter 1), polymeric hydrophobic nano and microparticles tend to be spherical to minimize the energy of the interaction with water. They naturally tend to minimize their surface tension by reducing their surface thus leading to spheres. Therefore to create non spherical particle one has to find a way to prevent the random coils formed by polymer chains to auto assemble in the geometry of spheres. In the literature, different approaches to solve this problem have been described. Three methods caught our interest, including (i) film stretching, (ii) auto assembly and (iii) particle replication in non wetting templates (PRINT). These methods are the most suitable for pharmaceutical applications because they offer a variety of shapes for different sizes while requiring relatively simple conditions to manufacture the nano or microparticles. That is why we decided to investigate the potential of two of these three methods, because the PRINT method required more complex operations to be carried out.

7.1.1.1. Film stretching strategy

This method consists in trapping micro or nanoparticles in a film or a gel, deforming these particles by stretching the film/gel before or after their liquefaction by the action of heat or of a solvent. The recovery of the particles can then be achieved by dissolution and purification of the film/gel. After purification a suspension of the particles in water is obtained.

Champion et al.[1] have been working on developing this promising method and have achieved in obtaining many shapes, characterized by their aspect ratio (Γ=length/width) from disks ($\Gamma<<1$) to needles ($\Gamma>>1$). They also have been working on modifying the texture of their particles. However they almost only used so far polystyrene particles (non degradable), mostly at the micrometer level. In their most recent study[2] they expanded their research to PLGA nanoparticles.

In chapter 2, we presented the work we did to recreate this method and adapt it to pharmaceutical application by first creating an elongation prototype, then using poly(vinyl alcohol) with glycerol as a filmogen preparation and industrial polystyrene particles and finally by using Eudragit FS30D with triethylcitrate as a filmogen preparation and poly(lactic acid) as nanoparticles material. Eudragit FS30D is an anionic copolymer based on methyl acrylate, methyl methacrylate and methacrylic acid and is insoluble in acidic media, but dissolves by salt formation above pH 7.0 and is commonly used in pharmaceutical technology as a coating agent for tablets. Yet the deformed particles prepared by this technique all presented the same drawbacks for further *in vitro* or *in vivo* testing: (i) the samples were very heterogeneous in terms of size distribution (due to fusion between adjacent melted nanoparticles) as well as shapes (due to heterogeneities in the film stretching); (ii) the filmogen preparation was very difficult to completely eliminate especially on decorated surfaces (PEG, ligand…). However the versatility in aspect ratio was remarkable as we confirmed the possibility to produce disks, barrels, needles… at micrometer level. The deformation of nanoparticles proved to be more difficult.

This method has the potential to be a major contributor to research on the effect of shape on the nanoparticles-cell interaction and on the biodistribution, because it allows the production of micro- or nanoparticles with the same volume but with various shapes. It is our belief that if and when the heterogeneity and fusion problems are resolved, this method will constitute a solid process for the production of particles of all shapes. Despite these positive aspects, some additional drawbacks should be mentioned: (i) the high variability of shapes in a sample obtained from one film; (ii) fusion takes place between particles and (iii) nanoparticles seemed to be less prone to be deformed by elongation. Furthermore we are unsure of the possibility to adapt this technique for pharmaceutical applications because of the use of high temperatures to deform the particles, incompatible with the use of an active ingredient and because of the low yield of this method.

7.1.1.2. Auto assembly method

The second method consists in auto assembling previously prepared macromolecules, including polymers with specific properties (here a specific molecular architecture) to form nanoparticles. We focused our work on poly(γ-benzyl-L-glutamate). PBLG is a degradable polypetidic polymer well known for its ability to form α-helices[3] which has been thoroughly characterized. This work follows those of M.E.Martinez Barbosa[4] and of F. Segura Sanchez[5]

that already dealt with PBLG and PBLG derivative synthesis. These authors created a mini family of copolymer and proved that their auto association could result into multifunctional nanoparticles. Surprisingly these particles, obtained by the well known nanoprecipitation technique, were not spherical but rather ellipsoidal. We studied the reasons behind this and found that because of the presence of α-helices regions in the main chain of the polymer, these nanoparticles were not able to form spheres. The elongation ratio of these nanoparticles proved to be directly proportional to the molecular weight of the polymer. From this we tried to create nanoparticles of controlled shape by increasing the chain length of the polymers. However PBLG synthesis is a ring-opening synthesis and is limited by the presence of impurities. We succeeded to synthesize polymers up to 85kg.mol^{-1} and this polymer was used to create nanoparticles with an aspect ratio of 3.0.

This method is very promising in terms of mass production of nanoparticles. Once the polymer is obtained these particles are easily nanoprecipitated. However it is limited in terms of the obtainable shapes. We also noticed that for the longest polymer, there were different populations appearing in the samples, probably due to the formation of a hairpin like structure. The polymer still formed an α-helix, however the defaults in this structure caused it to fold in two, which led to particles with an aspect ratio corresponding to particles prepared from a PBLG polymer with half the molecular weight. This could be a serious limitation for the range of particles obtainable with this method. It seems that over a certain length the tertiary structure of the polypeptide is not stable enough to produce only very elongated particles. The range of aspect ratios from 1 to 3 (each aspect ratio corresponding to a polymer of a specific molecular weight) was wide enough to undertake *in vitro* and *in vivo* studies of the influence of shape. Furthermore because of their polymeric nature, PBLG nanoparticles could be functionalized in surface by introducing different terminal groups or molecules that allow the formation of multifunctional particles, as already shown previously by Barbosa et al[4].

7.1.1.3. PRINTTM method

The last method that raised our interest was the particle replication in non wetting templates (PRINT) method. In the PRINT method, a master mold is obtained through photolithography. Then a perfluoropolyether (PFPE) mold is imprinted on the master mold with nanometric features. A polymer of interest is then casted in the PFPE mold with pressure. The nanoparticles are removed from the mold by sticking them on an adhesive layer.

Finally the dissolution of the adhesive layer allows the retrieval of the nanoparticles in the form of a suspension.

Any soluble or fusible polymer is eligible for the PRINT process. For example PEG[6], PLA[7] and PLGA[7] particles have already been fabricated. This method offers the advantage of a wide variety of shape despite the fact that all shapes must present a flat surface (air contact) and be removable from the mold. Furthermore filling of the molds in steps allows creating particles with multiple layers[8] or anisotropic particles[9].

This process allows the mass production of particles with dimensions as small as 20nm. Only the fabrication of the master mold imposes limitation to the obtainable shapes. This process requires only mild conditions that should be compatible with the stability of certain drugs to be loaded in (drug, protein, fluorophore…), because it requires moderate heating (depending only on the melting point of the polymer and on the rheological characteristics of the melt polymer) and no solvent out of the dissolution of the adhesive layer are required.

This method is very promising in terms of obtainable shapes and sizes. However it requires complex material for preparing the molds available in nanotechnologies facilities so it is not easy to implement. Still developing this technique would allow the mass production of nanoparticles with a very high homogeneity.

The other drawback of this method is the lack of control of the surfaces. Two main strategies exist to functionalize particles. The first tactic consists in modifying the surfaces after fabrication of the particles and loading with their cargo. This method presents however numerous downsides: especially the possibility of altering the polymer that constitutes the nanoparticle, the possibility of depleting its cargo during the operations and finally the poor reproducibility of the surface modification. This could raise serious issues for pharmaceutical applications as it is now well known how much surfaces dictates the *in vitro* and *in vivo* fates of the nanoparticles. The second approach would be to functionalize the polymers before melting them to form the nanoparticles in the molds. However it is very unlikely that the functionalized groups would be presented on the surface of the particle and would be accessible after production with the PRINT technique.

What can be seen from the surveys on these three methods is that there is yet no perfect method to create surface functionalized nanoparticulate carriers of non spherical shape.

However the merit of these three methods is that they broaden the technological polymers when foreseeing shape studies, depending on the nature of the carrier to be produced.

The film stretching strategy is an excellent manner to modify carriers and to adapt the form to the envisioned application. Unfortunately, we question if this method can be used for preparing carriers with complex surface functionalization, because of the presence of a polymer film that may hide, disorientate, disrupt or worse block the activity of the surface ligands, thus impairing major characteristics such as stealth and/or active targeting.

The PRINT^{TM} strategy allows the creation of a wide variety of shapes, only limited by the creation of the master mold and the extraction of the particles from the mold. Similar problems would arise with the film stretching strategy for the preparation of surface functionalized carriers because molding implies a direct contact of the polymeric chains bearing ligands with polymeric chains of the mold, thus possibly leading to misorientation of these groups, hindrances, which is likely to directly impact their stealth and targeting properties.

For both these techniques it could be theoretically foreseen to add stealth and targeting groups to the surface of non spherical particles after their manufacture and drug loading. However, in the past, this strategy has been proved to be often detrimental for spherical nanoparticles not only to surface control but also to drug load and release kinetics, which can be modified in a way that makes them inoperative. This is a real challenge for both these techniques.

On the other hand, the auto assembly strategy is very tributary of the molecular characteristics of the macromolecules and does not allow the production of many different forms with the same material. For example we were able to make PBLG ovoid nanoparticles with an aspect ratio from 1.0 to 3.0 depending on the molecular weight of the polymer, but it was not possible (at least yet) to form more exotic shapes with this structure. However the literature is full of different shapes obtainable by different materials with this methodology. Furthermore this method is perfect for efficient multifunctionalization. The desired stealth and targeting groups can be covalently linked to the polymer during its synthesis, and nanoparticles with controlled surface can be obtained by a simple co-nanoprecipitation of these different polymers. The co-nanoprecipitation has been shown to lead to a uniform population of nanoparticles as M.E.Martinez Barbosa[4] and F. Segura Sanchez[5] proved during

their PhD work. The influence of the loading of a cargo (e.g. active pharmaceutical ingredient) on the shape of the vector remains to be studied.

7.1.2. Functionalization of non spherical particles

After producing non spherical particles that could be used for *in vitro* and *in vivo* studies, we tried to design multifunctionalized non spherical nanoparticles. These nanoparticles were based on the auto assembly of PBLG chains. We wanted to create an innovative all-purpose system offering the possibility to implement on their surface different ligands for drug targeting purposes by simply mixing ligands extemporaneously to an already manufactured carrier.

This carrier was based on nitriloacetic acid (NTA), which is a polyamino carboxylic acid that can be used as a chelating agent for metal ions such as Ca^{2+}, Cu^{2+}, Fe^{3+}… NTA is well known for its similarity to ethylene diamine tetra acetic acid (EDTA), however NTA is easily degraded and is known to form interesting complexes with Ni^{2+}, which in turn can immobilize an “His-tag”, which is an oligopeptide composed of at least six histidine molecules.

The NTA/Ni^{2+}/His-Tag system has been well studied. The affinities between Ni^{2+} and His-Tag[10] , Ni^{2+} and NTA[11-12] and for the NTA/Ni^{2+}/His-Tag complex[13] have all been characterized in the literature. This could be a strong base for designing a versatile ligand system. Indeed many molecules of interest, such as antibody, or proteins are commercially sold with a terminal His-Tag group. By presenting NTA on the surface of the particles, they could be easily multifunctionalized after their manufacture under mild conditions likely to preserve the activity of sensitive ligands.

NTA is also well known for fixing some radioactive markers such as ^{99}Tc, ^{111}In, and ^{44}Ca with high affinity constants[14]. Thus NTA as a ligand on the surface of carriers could be used alternatively for radioactive labeling, hence allowing the imaging of the biodistribution and of the *in vivo* fate of the carriers in real time.

In chapter 3 the functionalization of the polymer and its characterization were detailed. The formation of multi functionalized non spherical nanoparticles and the characterization of the NTA groups on the nanoparticles were presented. These experiments showed that binding

of Ni^{2+} in solution was equivalent for different shapes of particles with the same number of ligands, whereas interactions on a flat surface revealed that almost spherical nanoparticles (Γ=1.30) had a much higher binding capability than elongated nanoparticles (Γ=1.88). However, isothermal titration calorimetry (ITC) and surface plasmon resonance (SPR) techniques employed for these physico-chemical characterization need to be repeated and completed.

To further study this potentially remarkable ligand attachment system, the next step, after completion of the physico-chemical characterization of these particles would be to test the attachment/detachment of an actual ligand on these particles. Then the attachment of a mix of ligands could be envisioned and the utility of multiple ligand-receptor interactions for the drug targeting strategy could be evaluated.

7.2. Influence of shape on the in vivo fate of the non spherical nanoparticles

After developing different methods to produce non spherical nanoparticles and adapting them for pharmaceutical applications, we wanted to investigate the influence of shape on the *in vivo* fate of the non spherical nanoparticles. However, prior to such a study, one must label these nanoparticles. For this we developed two labeling techniques firstly with quantum dots and secondly with rhodamine. After studying their respective fluorescence in the nanoparticles (see chapter 4), we chose rhodamine, which was more efficient than quantum dots for labeling purposes.

In the literature, only very few articles tackle the influence of shape during *in vitro* experiments with cell cultures or on *in vivo* studies. No real study dedicated to the influence of shape has been done up until now at the nanometric level and very few exist at the micrometric level. We will discuss here different effects that involve shape *in vitro* or *in vivo*.

7.2.1. Influence of shape on the nanoparticles-cells interactions

Major factors can be influenced by the shape of the nanoparticles: the internalization rates, kinetics and pathways and the toxicity.

7.2.1.1. Internalization rates, kinetics and pathways

In chapter 5 we have presented a preliminary piece of work focused on the internalization of non-spherical particles in human umbilical vein endothelial cells. We chose those cells as a model of endothelial cells, because they are the first type of cells that nanoparticles are likely to encounter after intravenous injection. We have found that particles with a small aspect ratio (Γ=1.30) entered the cells faster than the more elongated particles (Γ=1.88).

In the literature different works around this thematic can be found. As discussed in the first section of the thesis, they generally aim either to elucidate the pathway used for particles internalization, or to compare the rates or speeds of internalization for particles of different shapes.

For the pathway elucidation, biochemical inhibitors of energy dependant processes, clathrin-mediated endocytosis, caveole-mediated endocytosis and macropinocytosys were used to treat cells. In their study Gratton et al.[15] demonstrate that (i) PRINT particles of all sizes (150nm up to 3µm) and shapes (see chapter1.1.3.1, figure1.14) were internalized by HELA cells, contrary to current scientific thought that particles >150nm are not internalized in non phagocytic cells[16-18], and that (ii) PRINT particles follow multiple pathways into the cells, independently of the shape. Furthermore they also tackled the question of internalization rates, and found that PRINT particles with a higher aspect ratio were internalized faster at equal volumes. It also appears that after 4h these elongated particles were more internalized than their spherical counterpart. This disagreed with our results, but no definitive conclusion can be drawn and such discrepancies should only prompt more intensive work on this topic.

There is a clear effect of shape on the internalization of the particles. However this phenomenon does not seem to be linked to the pathway of the internalization.

Champion et al.[19] shed light on this problem. According to their study the contact angle Ω between the cell and the surface of the particle at the point of attachment is a critical parameter. They have found that an actin cup ring was forming around the microparticles being internalized and that there is a critical angle (45°) over which there is no internalization:

the cell cannot deform its membrane enough to begin the internalization of the particle. They even go further by showing that the smaller the angle Ω the faster and the higher amount of particles is internalized. It is noteworthy that this study was only performed on microparticles and that this phenomenon might not be reproduced at the nanometric level. Deforming the cell membrane to internalize a nanoparticle requires notably less energy than for a microparticle. Decuzzi and Ferrari[20] have theorized this in the case of nanoparticles of fixed volume (volume of a sphere with R=50nm). Their simulation characterizes the wrapping length and the half wrapping time of non spherical particles (ellipsoids) lying flat on the cell membrane depending on the aspect ratio of the particles at constant volume (This does not describe all the possible approaches of the cell by nanoparticles.). They have shown that there is a critical aspect ratio under which no engulfment happens. Furthermore with the deformation of particles (aspect ratios smaller or bigger than 1) the internalization speed will decrease. From an aspect ratio of 1 to 4 the kinetics of internalization was decreased seven times[20].

This is in complete agreement with what was depicted in chapter 5, which would indicate that it is more probable to have cell nanoparticles interactions with particles lying flat on the membrane. The limiting factor appears to be the deformation of the membrane required to engulf the particle, which explains why at the micrometer level the angle at the first contact point is an essential parameter, whereas at the nanometer level it is the elongation ratio. Still this does not explain why for Gratton et al.[15] elongated particles were faster internalized than spherical particles.

As a conclusion, it appears that particle shape has a major impact on particle cell interactions, but also that the shape effect will be essentially different at the micro and nanoscale levels.

To complete our study, it would be interesting to undergo an in-depth internalization study, by blocking all the internalization pathways but one, to evaluate the percentage of internalization for each pathway and see how shape changes the mechanism of internalization for these objects. If it does, this would maybe give a further possibility for tuning the properties of the carrier for its application by favoring a shape that uses an internalization pathway that corresponds to the desired application or that escapes an unwanted pathway.

7.2.1.2. Toxicity caused by shape

Is there an intrinsic toxicity caused by the shape? This question is very relevant for pharmaceutical applications. Kolhar et al[2] have recently demonstrated the ability of needle-shaped particles to permeabilize cell membrane for intracellular drug delivery. One of the plausible explanations they advanced was that the nanoparticles cause a membrane poration and then entered the cell. Indeed the nanoneedles with their pointy edge only require a strength superior to 1nN to perforate the lipid bilayer[21]. Studies have shown that the cells can repair the hole created in the membrane[22-23]. This fact, although interesting, raises the question of the toxicity. If too many holes are created at the same time in the cell, can its ability to regenerate keep up, or will cells die? The MTT assays seem to indicate cell death. PLGA that lose their sharpness over time lead to 20% more cell viability than PLGA nanoneedles that keep this property[2]. Our own toxicity assays did not reveal an influence of shape on the toxicity. However our elongation ratios only rose up to 3.0, their nanoneedles aspect ratio is clearly higher, but was not characterized.

7.2.2. Influence of shape on the biodistribution of micro and nanoparticles

The overall influence of shape on the biodistribution of micro and nanoparticles is obviously of major interest for targeting applications. There are many phenomena that play a major role in the biodistribution of a particle. Although some of these factors are now better understood, there is not yet any systematic relationship between our knowledge of surface structure and biodistribution. Thus our aim was solely to test the impact of shape on the fate of the particles in the body and to see if the shape must be considered as a parameter to tune to change the biodistribution profile of a particle. As we have seen in the literature [24-25] and in our biodistribution study in chapter 6, shape does play a major role, at least in the blood persistence and probably in the organ distribution. So where do these differences stem from? We believe that the displacement of the nanoparticles in biological fluids, their margination, their capacity to interact and adhere to vessel walls and endothelial cells are strongly impacted by the change in shape.

The displacement of non spherical particles in motionless or moving fluids has been thoroughly studied. We detailed it in the first chapter of this thesis and we found that the more the aspect ratio derived from 1 (sphere) the more complex the particle movement was and the more it explored space within the fluid, thus increasing the probability for a contact with cells.

In the blood stream the spherical particles tend to stabilize at a definite distance from the wall and to follow a definite stream line, whereas a disc tend to rotate and drift from one side of the capillary to the other. Hence one can easily see that non spherical particles will tend to explore more space in the capillary tube and thus have more chance to explore the walls[26-27].

In a practical study[28] R. Toy et al. have compared the circulation of two series of gold nanoparticles coated with PEG of different shapes using 60nm nanospheres and nanorods 56nm in length and 25nm in diameter (Γ=2.2), which were allowed to circulate in PDMS microchannels (175µm in width x 100µm in height) under the physiologic flow rates expected in tumor microcirculation. They have found that the rods showed a propensity to deposition eight folds higher than the sphere.

Nanoparticles with an aspect ratio that diverges from 1 will marginate faster than spherical particles. Hence they have a higher probability to deposit themselves on the vessel wall. Furthermore, as we have shown in chapter 4, nanoparticles with an aspect ratio that diverges from 1 will also have a smaller surface presented to the fluid motion and will have a smaller probability to be detached from the wall.

When we compare all these data with our own biodistribution data, we can hypothesis some of the differences between the two particle types. For the pharmacokinetics, an increase of the aspect ratio by a factor 1.5 (1.30 compared to 1.88) resulted in an increase in the half life of the nanoparticles in blood of a factor of 7.5. It could be hypothesized that the more elongated nanoparticles (Γ=1.88) had covered the vessel walls to a higher extent. By adhering to the wall they have less chance to be cleared from blood. However detachment may be also feasible due to blood flow, thus leading to free particles, able to adhere again. This could explain why the more elongated nanoparticles persisted longer in the blood flow. Our further investigations of the distribution of the particles in organs failed to detect any particles in main organs (brain, heart, kidney, spleen, and liver), which could support the idea of an attachment to the walls of blood vessels but could also be due to yet unidentified phenomena, including premature degradation, fast elimination before organ retrieval, among other hypothesis. Obviously an interesting study would be to investigate the presence of nanoparticles on the vessel wall, as well as clarifying these observations relative to distribution.

Conclusion

This entire work aimed to identify and answer as well as possible the question of the importance of the shape as a parameter to tune when designing nanoparticles and microparticles carriers for drug targeting applications. Not only did we create non-spherical particles in a controlled manner, but the comparison of different manufacturing techniques for the preparation of elongated nanoparticles helped to identify key elements for the use of these nanoparticles: if microparticles and nanoparticles manufactured by PRINT or made with the film stretching strategy offered a tremendous variety of shape which can be helpful for studying the effects of changing the shape on the *in vitro* and *in vivo* fate of the particles, the self-assembled particles seemed to be a much more efficient way of preparing surface functionalized carriers, because their surfaces are better controlled and more precisely engineered. Apart from these technological considerations, the strong influence of nanoparticle shape on their behavior in the body was strongly suggested by our own data and was consistent with the few studies available in the literature.

All these results lead us to the conclusion that shape is a major parameter that has to be considered to better control and even to increase the efficiency of any drug targeting strategy.

References

1. Champion, J.A., Katare, Y.K. & Mitragotri, S.
Making polymeric micro- and nanoparticles of complex shapes,
Proceedings of the National Academy of Sciences, 104, 11901-11904, **2007**.

2. Kolhar, P., Doshi, N. & Mitragotri, S.
Polymer Nanoneedle-Mediated Intracellular Drug Delivery,
Small, 7, 2094-2100, **2011**.

3. Klok, H.-A., Langenwalter, J.F. & Lecommandoux, S.
Self-Assembly of Peptide-Based Diblock Oligomers,
Macromolecules, 33, 7819-7826, **2000**.

4. Barbosa, M.E.M., Montembault, V., Cammas-Marion, S., Ponchel, G. & Fontaine, L.
Synthesis and characterization of novel poly(gamma-benzyl-L-glutamate) derivatives tailored for the preparation of nanoparticles of pharmaceutical interest,
Polymer International, 56, 317-324, **2007**.

5. Segura-Sánchez, F., Montembault, V., Fontaine, L., Martínez-Barbosa, M.E., Bouchemal, K. & Ponchel, G.
Synthesis and characterization of functionalized poly([gamma]-benzyl-l-glutamate) derivates and corresponding nanoparticles preparation and characterization,
International Journal of Pharmaceutics, 387, 244-252, **2010**.

6. Rolland, J.P., Maynor, B.W., Euliss, L.E., Exner, A.E., Denison, G.M. & DeSimone, J.M.
Direct Fabrication and Harvesting of Monodisperse, Shape-Specific Nanobiomaterials,
Journal of the American Chemical Society, 127, 10096-10100, **2005**.

7. Euliss, L.E., DuPont, J.A., Gratton, S. & DeSimone, J.
Imparting Size, Shape, and Composition Control of Materials for Nanomedicine,
ChemInform, 38, **2007**.

8. Hernandez, C.J. & Mason, T.G.
Colloidal Alphabet Soup: Monodisperse Dispersions of Shape-Designed LithoParticles,
The Journal of Physical Chemistry C, 111, 4477-4480, **2007**.

9. Zhang, H., Nunes, J.K., Gratton, S.E.A., Herlihy, K.P., Pohlhaus, P.D. & DeSimone, J.M.
Fabrication of multiphasic and regio-specifically functionalized PRINT particles of controlled size and shape,
New Journal of Physics, 075018, **2009**.

10. Zhang, Y., Akilesh, S. & Wilcox, D.E.
Isothermal Titration Calorimetry Measurements of Ni(II) and Cu(II) Binding to His, GlyGlyHis, HisGlyHis, and Bovine Serum Albumin: A Critical Evaluation,
Inorganic Chemistry, 39, 3057-3064, **2000**.

11. Stora, T., Hovius, R., Dienes, Z., Pachoud, M. & Vogel, H.
Metal Ion Trace Detection by a Chelator-Modified Gold Electrode: A Comparison of Surface to Bulk Affinity,
Langmuir, 13, 5211-5214, **1997**.

12. Hull, J.A., Davies, R.H. & Staveley, L.A.K.
1033. Thermodynamics of the formation of complexes of nitrilotriacetic acid and bivalent cations,
Journal of the Chemical Society (Resumed), 5422-5425, **1964**.

13. Hart, B.R. & Shea, K.J.
Molecular Imprinting for the Recognition of N-Terminal Histidine Peptides in Aqueous Solution,
Macromolecules, 35, 6192-6201, **2002**.

14. Anderegg, G.
Critical survey of stability constants of NTA complexes,
Pure and Appl. Chem., 54, 2693-2758, **1982**.

15. Gratton, S.E.A., Ropp, P.A., Pohlhaus, P.D., Luft, J.C., Madden, V.J., Napier, M.E. & DeSimone, J.M.
The effect of particle design on cellular internalization pathways,
Proceedings of the National Academy of Sciences, 105, 11613-11618, **2008**.

16. Conner, S.D. & Schmid, S.L.
Regulated portals of entry into the cell,
Nature, 422, 37-44, **2003**.

17. Gary, D.J., Puri, N. & Won, Y.-Y.
Polymer-based siRNA delivery: Perspectives on the fundamental and phenomenological distinctions from polymer-based DNA delivery,
Journal of Controlled Release, 121, 64-73, **2007**.

18. Oupický, D., Koňák, Č., Ulbrich, K., Wolfert, M.A. & Seymour, L.W.
DNA delivery systems based on complexes of DNA with synthetic polycations and their copolymers,
Journal of Controlled Release, 65, 149-171, **2000**.

19. Champion, J.A. & Mitragotri, S.
Role of target geometry in phagocytosis,
Proceedings of the National Academy of Sciences of the United States of America, 103, 4930-4934, **2006**.

20. Decuzzi, P. & Ferrari, M.
The Receptor-Mediated Endocytosis of Nonspherical Particles,
Biophysical journal, 94, 3790-3797, **2008**.

21. Obataya, I., Nakamura, C., Han, Nakamura, N. & Miyake, J.
Nanoscale Operation of a Living Cell Using an Atomic Force Microscope with a Nanoneedle,
Nano Letters, 5, 27-30, **2004**.

22. Denoual, M., Chiral, M. & LePioufle, B.
Cell cultures over nanoneedle fields,
NanoBioTechnology, 1, 389-394, **2005**.

23. Hoshino, T., Konno, T., Ishihara, K. & Morishima, K.
Live-Cell-Driven Insertion of a Nanoneedle,
Jpn. J. Appl. Phys., 48, **2009**

24. Geng, Y., Dalhaimer, P., Cai, S., Tsai, R., Tewari, M., Minko, T. & Discher, D.E.
Shape effects of filaments versus spherical particles in flow and drug delivery,
Nat Nano, 2, 249-255, **2007**.

25. Decuzzi, P., Godin, B., Tanaka, T., Lee, S.Y., Chiappini, C., Liu, X. & Ferrari, M.
Size and shape effects in the biodistribution of intravascularly injected particles,
Journal of Controlled Release, 141, 320-327, **2010**.

26. Decuzzi, P., Pasqualini, R., Arap, W. & Ferrari, M.
Intravascular Delivery of Particulate Systems: Does Geometry Really Matter?,
Pharmaceutical Research, 26, 235-243, **2009**.

27. Broday, D., Fichman, M., Shapiro, M. & Gutfinger, C.
Motion of spheroidal particles in vertical shear flows,
American Institute of Physics, **1998**.

28. Toy, R. & et al.
The effects of particle size, density and shape on margination of nanoparticles in microcirculation,
Nanotechnology, 22, 115101, **2011**.

General Conclusion

General Conclusion & Perspectives

This entire work aimed to identify and answer as well as possible the question of the importance of the shape as a parameter to tune when designing nanoparticles and microparticles for drug targeting or other delivery applications.

Most techniques available so far for the preparation of polymeric nano or microparticles yield spheres. Thus, in a first step, we have investigated two different strategies for the preparation of non spherical particles making possible a precise control of their morphology, as well as their other characteristics. On the one hand, we confirmed that the film stretching technique could help to create nanoparticles and microparticles with a wide variety of shapes, although it may be more difficult in the case of small particles. Moreover, this strategy presents important drawbacks when drug targeting applications are envisioned because: (i) the samples obtained critically lacked uniformity in shape, due to inhomogeneities in the film stretching, (ii) it should be difficult to modulate the surface properties, for example, the introduction of recognition ligands, due to the difficulty to completely eliminate film residues after shape of modification, and (iii) poor yields of fabrication. On the other hand spheroïdal nanoparticles of controlled shape and with elongation ratios ranging from 1 to 4 were prepared from poly(γ-benzyl-L-glutamate), by taking advantage of the auto assembly properties of these polypeptide chains in the conformation of α-helices during a very simple nanoprecipitation process. A direct correlation was found between the elongation ratio of the particles and the molecular weight of the polymer that they are made of. Clearly this latter technique offers a wide flexibility when functionalizing the surface of the particles by various molecular entities is requested. A first approach for an “on demand” surface functionalization of these particles by His-tagged proteins is presented.

The second part of the work aimed to investigate some aspects of the fate of these non spherical nanoparticles after their intravenous delivery. These studies showed clearly that particle shape could influence the interactions of the particles with cells, as well as their internalization, which was investigated *in vitro* in HUVEC cells cultures. Furthermore *in vivo* experiments in rats revealed a clear impact of the shape on the pharmacokinetics of the particles in blood, consistent with the scares reports found in the literature about the question of shape.

As a general conclusion we believe that shape is a major parameter that has to be considered in view of increasing the specificity of distribution in any drug targeting strategy. A better understanding of the effect of shape on distribution is also believed to be important from the point of view of toxicology of particulate systems. However, it should be recognized that there is yet no a sufficient amount of available experimental data in this area of pharmaceutical technology and biopharmacy. Indeed assessing, comparing and understanding the effect of shape on the various mechanisms which govern the distribution in living organisms represents an emerging field of research. However it still in its infancy and much more data should be accumulated for establishing stronger conclusions. A few key points can be suggested, including: (i) the recognition and comparison of the effects of various shapes on the biodistribution using surface controlled non spherical nanoparticles, (ii) the investigation of the relationships between nanoparticles shape, their surface functionalization and their interactions with cells and biological molecules. These are some of the fascinating scientific challenges opened to pharmaceutical scientists in the field of drug targeting.

Synthèse

Synthèse de la thèse en français

Introduction

Quelque soit la voie d'administration dans l'organisme, un principe actif est soumis à de nombreux phénomènes depuis son absorption jusqu'à son élimination. A une dose donnée, l'efficacité thérapeutique de ces molécules, leurs éventuels effets secondaires et leur toxicité dépendent de leur biodistribution dans l'organisme (organes, cellules et compartiments subcellulaires). Cette distribution repose uniquement sur les propriétés physico-chimiques de ces molécules, combinées aux propriétés spécifiques des barrières physiologiques et biologiques du patient. L'efficacité thérapeutique d'un principe actif dépend donc de sa capacité à atteindre les cellules ciblées, ce qui résulte principalement de la capacité du principe actif à passer au travers des barrières physico-chimiques et biochimiques entre le site d'administration et la cible thérapeutique. Afin de mieux contrôler cette biodistribution, une des stratégies actuelles consiste à associer le principe actif à un transporteur qui substitue les propriétés de biodistribution du principe actif par les siennes, jusqu'à atteindre la cible. Idéalement, ce transporteur possède une série de caractéristiques qui lui permet de traverser chacune des barrières de manière efficace. Une fois la cible atteinte le transporteur doit alors être capable de libérer le principe actif dans les organes ou tissus visés. Enfin, le transporteur doit être facile à éliminer. Cette stratégie devrait permettre d'augmenter la concentration locale en principe actif au niveau de la cible thérapeutique et/ou de diminuer les effets indésirables dans le reste du corps.

Si cette stratégie est porteuse de grands espoirs pour le développement de nouvelles thérapies, par exemple pour le traitement de cancers ou d'autres pathologies, elle requiert d'être capable de créer des vecteurs possédant simultanément des fonctionnalités très différentes. Malgré la difficulté de réaliser de tels vecteurs, cette stratégie est prometteuse

pour l'amélioration de l'efficacité thérapeutique par l'augmentation de l'index thérapeutique et est à l'heure actuelle au centre d'un effort considérable de recherche aussi bien au niveau académique qu'industriel.

Ces efforts de recherche sont principalement focalisés sur la création de vecteurs efficaces, basés sur des structures variées, allant de la macromolécule aux vecteurs particulaires. Dans le cas des vecteurs particulaires, plusieurs paramètres sont classiquement ajustés, incluant la taille du vecteur, la charge de surface du vecteur, les groupes chimiques ou les molécules plus complexes présentés à la surface des vecteurs. Si l'impact de chacun de ces paramètres est maintenant bien maîtrisé, on peut se demander comment améliorer encore l'efficacité de ces vecteurs.

Une revue des vecteurs particulaires actuels destinés à des applications pharmaceutiques montre que la forme est un paramètre qui a été cruellement négligé jusqu'à présent. En effet, de nombreux vecteurs avec différentes structures internes ont été imaginés et fabriqués, mais ces vecteurs, tant au niveau des microparticules que des nanoparticules, sont dans leur immense majorité des sphères.

Dans ce contexte, le but de cette thèse était d'étudier l'influence de la forme de nanoparticules polymères non sphériques sur leurs interactions avec les cellules et sur leur distribution après injection par voie intraveineuse. Pour cela différentes stratégies ont été développées pour produire suffisamment de nanoparticules possédant des formes autres que sphériques. Ces particules ont été caractérisées, et finalement testées *in vitro* et *in vivo.*

Le présent mémoire se divise en sept chapitres. Le premier chapitre passe en revue différentes études publiées sur l'effet de la forme des particules sur différents phénomènes biologiques et physiques impliqués dans leur biodistribution. Ce chapitre comprend aussi une présentation des différentes techniques de fabrication de particules non sphériques, en prenant

en compte le fait que ces particules doivent être utilisées à des fins pharmaceutiques. Le second chapitre est dédié à la préparation de micro et nanoparticules non sphériques par la méthode d'étirement dans des films, une méthode qui consiste à encapsuler des particules polymères sphériques dans un film polymère, à les liquéfier puis à étirer le film pour déformer ces particules avant de les solidifier. Le troisième chapitre décrit comment l'auto-assemblage de polymères particuliers permet la création de particules non sphériques. Dans notre cas, le poly(γ-benzyle-L-glutamate), un polypeptide qui forme des hélices α, a été utilisé pour empêcher les nanoparticules de devenir sphériques et former des ellipsoïdes. Les travaux expérimentaux ont permis de montrer que le rapport d'élongation des particules (longueur sur largeur) dépendait de la masse molaire des polymères qui les composent. Le quatrième chapitre présente l'effet de la forme des nanoparticules ellipsoïdales, décorés en surface par des ligands de reconnaissance, sur leurs interactions avec des surfaces portant des récepteurs. Pour cela, un modèle théorique et un modèle expérimental ont été développés. Ce dernier est constitué de nanoparticules facilement fonctionnalisables après leur production, par la mise en œuvre d'une stratégie originale, qui consiste à profiter de la possibilité d'accrocher des protéines His-taggées à des groupes nitriloacétiques en présence de Ni^{2+}. En effet, de nombreux ligands His-taggés potentiellement intéressants sont disponibles commercialement. En utilisant les particules ellipsoïdales formées par auto-assemblage, le chapitre cinq rapporte une étude *in vitro* décrivant l'impact de la forme sur les interactions entre cellules et nanoparticules. Le sixième chapitre présente une étude *in vivo* de l'effet de la forme sur leur biodistribution chez le rat, qui démontre l'impact de la morphologie sur le devenir des particules dans l'organisme. Enfin la discussion générale permet de synthétiser les différents résultats expérimentaux obtenus, montre leur intérêt pharmaceutique et ouvre sur les possibles futures études sur cette thématique.

Chapitre 1 : Forme et vectorisation

Ce premier chapitre passe en revue les études existantes concernant deux questions d'intérêt : quelle est l'influence de la forme des particules sur leur devenir *in vivo* ? Comment fabriquer des nanoparticules non sphériques ?

Lorsqu'un vecteur nanoparticulaire est administré dans l'organisme, il est tout d'abord soumis aux fluides dans lesquels il se déplace, qu'ils soient immobiles (par exemple, le liquide interstitiel) ou en mouvement (par exemple, le sang). Dans les liquides statiques, les nanoparticules sont soumises au mouvement brownien, les particules sphériques se déplacent de façon anisotrope, alors que les ellipsoïdes se souviennent de leur position initiale lorsqu'ils rencontrent un objet et explorent alors l'espace dans la direction de leur axe le plus long. Dans les liquides en mouvement, et en particulier dans le sang, les particules se déplacent au cœur du fluide, et vont selon leurs caractéristiques physiques et physico-chimiques rejoindre les parois des vaisseaux plus ou moins rapidement. Une fois les parois atteintes, les particules vont soit revenir au cœur du fluide et continuer leur trajet, soit adhérer aux parois et/ou les traverser. Dans ce type de flux les particules non sphériques ont des mouvements plus chaotiques que les particules sphériques et explorent donc plus l'espace. On peut donc s'attendre à ce que les cinétiques d'interaction avec les endothelia ou d'autres surfaces biologiques soient modifiées. L'adhésion et le détachement aux parois sont traités dans le chapitre 4.

La biodistribution des nanoparticules et leurs interactions avec les cellules mettent en jeu des mécanismes extrêmement complexes qui ont été largement étudiés. Ces phénomènes ont été décrits comme influencés par la nature du matériau qui les compose, leur taille et particulièrement par leurs propriétés de surface. Cependant, il n'existe que peu d'études au niveau nanométrique et les effets décrits semblent différents.

Chapitre 2 : Fabrication de micro et nanoparticules polymères non sphériques par la méthode d'étirement dans les films : conditions et limitations

Après avoir mis en valeur certaines des possibilités des particules non sphériques, il est intéressant de se préoccuper de leur fabrication. Avant tout il est essentiel de comprendre pourquoi les particules polymères ont tendance à être sphériques. Pour minimiser leur énergie de surface lors de la fabrication des nanoparticules en milieu liquide (donc peu contraint),, les chaînes polymères qui existent très généralement dans une conformation de type pelote statistique (random coil) ont tendance à s'associer et former une particule dont la géométrie présente la surface minimale à l'interface, c'est-à-dire la sphère. Pour fabriquer des nanoparticules non sphériques, il faut donc trouver un moyen d'empêcher les polymères formant les particules d'adopter cette géométrie sphérique. Pour cela différentes techniques peuvent être imaginées consistant soit en la formation directe de particules non sphériques, soit en la déformation de particules initialement sphériques.

Les techniques de préparation directe de nanoparticules de formes originales peuvent être classées en deux grandes catégories mettant en œuvre soit l'auto-assemblage soit la préparation sous contrainte. L'auto-assemblage est une méthode qui permet la formation de nanoparticules non sphériques dans le cas où les « briques » constitutives des particules ont une structure définie qui permet leur assemblage en une super structure qui permettra la formation de particules de formes originales. Parmi ces briques, on trouve certains peptides, certains polymères, les molécules amphiphiles, et des structures cristallines. La préparation sous contrainte consiste à appliquer des contraintes spatiales sur une quantité donnée de matériau. Trois méthodes sont à regrouper dans cette catégorie: la réplication de particules dans des moules hydrophobes (PRINT), l'électrospinning, et la micro/nanofluidique. En

résumé, dans ces méthodes, le matériau utilisé pour produire les nanoparticules, généralement un polymère, est fondu puis soumis à des contraintes physiques. Cela nécessite un appareillage externe capable d'imposer leur forme aux particules. Le matériau composant les particules subit alors un stimulus qui cause la solidification des particules.

A côté de ces diverses stratégies, deux méthodes de préparation indirectes de particules non sphériques sont décrites dans la littérature. La première méthode consiste à encapsuler des particules initialement sphériques dans un film ou dans un gel, puis à liquéfier les particules par l'action de la chaleur ou d'un solvant. Les particules sont alors déformées par étirement du film/gel puis solidifiées dans leur nouvelle forme. L'autre méthode, consiste à agréger de manière anisotrope des particules sphériques par liaison covalente ou par émulsion/évaporation.

Toutes ces méthodes permettent la formation de particules non sphériques, cependant elles ne sont pas toutes équivalentes d'un point de vue pharmaceutique. On notera en particulier que toutes les méthodes comprenant l'encapsulation des particules auront des conséquences drastiques sur la surface des particules considérée à l'échelle moléculaire. Les méthodes mettant en œuvre un chauffage ou l'utilisation d'un solvant peuvent abîmer un principe actif encapsulé dans les particules… De plus, elles ne permettent pas toutes d'avoir accès à la même variété de formes géométriques. Les méthodes d'étirement dans les films/gels et la méthode PRINT donnent accès aux géométries les plus variées, mais c'est l'auto-assemblage qui semble le plus propice à être utilisé à des fins pharmaceutiques.

Dans ce contexte, le deuxième chapitre de cette thèse s'intéresse à la mise en place d'une technique expérimentale pour la fabrication de micro et nanoparticules polymères non

sphériques par la méthode d'étirement dans les films pour des applications pharmaceutiques, en insistant sur les conditions et limitations d'application de cette méthode.

Cette méthode consiste à encapsuler des nanoparticules dans un film polymère. Une fois le film coulé et séché, les particules sont liquéfiées par l'action de la chaleur ou d'un solvant. Le film est alors étiré. Enfin les particules sont solidifiées dans leur nouvelle forme par refroidissement ou évaporation du solvant. Les particules sont alors récupérées par dissolution du film dans lequel elles sont encapsulées.

Pour mettre en place cette technique, nous avons créé un prototype d'étirement de film. Ce prototype, constitué d'une étuve, d'un moteur et d'un ensemble de poulies et de rotors, nous a permis de reproduire cette méthode initialement décrite par Champion et al. (*PNAS*, 2007) pour la préparation de microsphères polymère non sphériques. Pour cela, nous avons coulé des suspensions de nano ou microparticules de polystyrène (PS) dans une solution d'alcool polyvinylique (PVA) utilisé comme filmogène et du glycérol comme plastifiant, sur des lames de verre. Après séchage, ces films ont subi le processus d'étirement et de récupération des particules décrit précédemment, ce qui a permis la formation de nanoparticules non sphériques. La morphologie de ces nanoparticules a été observée par microscopie électronique à transmission. Cependant, deux inconvénients ont été mis en évidence : des problèmes de répétabilité inter échantillons et des problèmes d'uniformité de taille et de forme au sein d'un échantillon. Après une étude approfondie, nous nous sommes aperçus que ces problèmes d'uniformité provenaient de la déformation non uniforme des films au sein desquels les particules sont déformées et également de la fusion de plusieurs particules pendant l'étirement.

Malgré ces problèmes nous avons décidé d'adapter cette méthode au domaine pharmaceutique. Pour cela nous avons remplacé le PVA, difficile à éliminer, par un film déjà

utilisé en pharmacie. Après essais de différentes formulations, un copolymère méthacrylique (Eudragit FS30D) communément utilisé pour le pelliculage des formes solides et plastifié par le triéthylcitrate (TEC) a présenté les meilleures propriétés d'étirement et d'élimination. Pour le matériau constituant les nanoparticules, différents polymères ont aussi été testés : le poly(γ-benzyle-L-glutamate), dont la conformation des chaînes en hélices alpha (étudiée au chapitre 3) semble avoir empêché la déformation, et le poly(acide lactique) dont les chaînes adoptent un conformation en pelote statistique qui a permis la déformation de particules comme dans le cas du PS. Cependant les inconvénients repérés dans le début de cette étude restent présents (non uniformité et fusion).

Cette technique permet la production de micro et nanoparticules de formes variées, cependant elle ne semble pas facilement utilisable telle quelle dans le cadre d'études *in vitro* et *in vivo*. Beaucoup de travail est nécessaire pour perfectionner cette technique, résoudre les problèmes d'uniformité et préparer des lots de particules importants.

Chapitre 3 : Contrôle de l'élongation de nanoparticules dégradables de poly(γ-benzyle-L-glutamate)

Le troisième chapitre traite de la fabrication de nanoparticules polymères non sphériques par auto-assemblage. Le poly(γ-benzyle-L-glutamate) (PBLG), un polymère dégradable connu pour former des hélices α dans certains solvants, a été sélectionné puis utilisé pour fabriquer des nanoparticules.

Différents PBLG de masses molaires comprises entre 28kg.mol^{-1} et 85kg.mol^{-1}ont été synthétisés par polymérisation par ouverture de cycle de l'anhydride de Leuchs correspondant, puis caractérisés par spectrométrie de masse (MALDI-TOF) pour déterminer leur masse molaire, et par dichroïsme circulaire pour déterminer la conformation (hélices α ou

non) de leur chaîne principale. Enfin ces polymères ont été utilisés pour la fabrication de nanoparticules par nanoprécipitation. Ces nanoparticules ont été caractérisées à leur tour par dichroïsme circulaire pour confirmer l'existence des chaînes de PBLG dans la conformation en hélice alpha puis par microscopie à transmission électronique (MET) pour observer leur morphologie.

L'analyse en MET a révélé que les nanoparticules étaient ovoïdes et que leur élongation dépendait de la masse molaire du polymère utilisé pour les fabriquer. Une hypothèse raisonnable serait que la conformation des chaînes polymère serait à l'origine de l'élongation des nanoparticules, en raison de phénomènes d'empilement régulier des hélices alpha. Grâce à ces observations, nous avons pu déterminer que le ratio d'élongation des particules (longueur/largeur) était proportionnel linéairement à la masse molaire du polymère qui les compose. Un autre élément important à noter est que les particules, quelle que soit leur forme, présente toujours le même volume.

La méthode présentée dans ce chapitre est donc une méthode directe, de type « bottom up » qui permet la fabrication de nanoparticules (de même volume) dont la forme est contrôlée par la masse molaire du polymère qui les compose, ce qui est attribuable à la conformation en hélice α du polymère. De plus, cette méthode parait aisément transposable pour la production de grandes quantités

Chapitre 4 : Interactions des particules non sphériques avec les surfaces: Approche théorique et développement de particules ovoïdes décorables à la demande grâce au système acide nitriloacétique-Nickel-molécule His-taggée

Dans le quatrième chapitre de ce mémoire, deux approches du problème des interactions des particules ovoïdes avec les membranes biologiques sont traitées. Tout d'abord, d'un point de vue théorique, en simulant les interactions spécifiques entre une particule et une paroi, puis d'un point de vue pratique, en développant des nanoparticules susceptibles d'être décorées à la demande par des ligands de reconnaissance spécifique.

Les interactions entre une particule et une paroi sont proportionnelles à la quantité de ligands présentés par la particule et disponibles pour interagir avec les récepteurs portés par la paroi. Nous avons donc modélisé ces interactions en supposant que les ligands sont répartis de manière uniforme à la surface de la particule et que les récepteurs sont en excès à la surface de la paroi. Nous avons donc évalué la surface de la particule concernée par l'établissement de liaisons avec la paroi en fonction de la forme et de la façon dont la particule approche la paroi. Il est apparu qu'un facteur 10 dans le rapport d'élongation de la particule avait un impact sur la surface disponible pour les interactions de 4 ordres de grandeur. Pour obtenir la force (probabilité) du lien entre la particule et la paroi, il faut comparer cette force à la force de détachement appliqué à la particule. Dans notre cas, il a été considéré que la force appliqué provenait par exemple du déplacement des liquides (extracellulaire, sang…) exerçant ainsi une force sur la particule. Cette force est proportionnelle à la section de la particule présentée aux fluides. De même que pour la surface disponible pour les interactions, les modélisations suggèrent que cette probabilité d'attachement est très fortement dépendante de la forme des particules.

Une fois encore l'impact de la forme des particules sur les modalités d'interactions avec les surfaces est évident. L'angle d'approche de la particule semble être aussi un élément majeur dans ses interactions.

La deuxième partie de ce chapitre s'attache à développer des nanoparticules modèles décorables à la demande afin de disposer de particules modèles utilisables dans des expérimentations visant à conforter les comportements prévus par modélisation. Pour cela, nous avons synthétisé différents dérivés du PBLG possédant un bloc PBLG de masse molaire variable et portant des ligands différents : polyéthylèneglycol (PEG, 5000g.mol^{-1}) et PEG-acide nitriloacétique (PEG-NTA). Des nanoparticules composites de PBLG, PBLG-PEG et PBLG-PEG-NTA ont ensuite été synthétisées par co-nanoprécipitation. Enfin, la fonctionnalité des dérivés NTA a été vérifiée par calorimétrie de titration isotherme (ITC), et par résonance plasmonique de surface (RPS) en mesurant les interactions entre les particules et les ions nickel et également les ions nickel complexés à un dérivé his-taggé. L'ITC a confirmé qu'en suspension les interactions sont les mêmes quelle que soit la forme des particules. Par contre la RPS semble indiquer que les particules de formes différentes auront des interactions différentes avec la même surface. Ces résultats restent cependant à confirmer.

Chapitre 5 : Etude préliminaire *in vitro* de l'influence de la forme des nanoparticules sur leur internalisation par les HUVEC.

Le cinquième chapitre de cette thèse décrit la mise en place d'essais *in vitro* visant à étudier l'influence de la forme des nanoparticules sur leur internalisation par les cellules. Lorsque des nanoparticules sont administrées à un patient, elles sont directement injectées dans la circulation sanguine. Les premières cellules rencontrées sont des cellules endothéliales. Nous avons donc décidé d'observer les interactions entre les nanoparticules de PBLG présentées au chapitre 3 et des cellules endothéliales humaines HUVEC, provenant du cordon ombilical.

Dans un premier temps, les nanoparticules ont été marquées pour pouvoir mesurer leurs interactions avec les cellules et leur internalisation. Deux voies ont été suivies. Un premier marquage a été réalisé par co-nanoprécipitation de quantum dots préalablement synthétisés et caractérisés. Un deuxième marquage a consisté à utiliser un polymère fluorescent préparé à partir d'un dérivé de la rhodamine B utilisé comme initiateur de la synthèse de PBLG.

L'absence d'impact du marquage sur la forme des particules a ensuite été vérifiée. Il est apparu que la présence de quantum dots dans les nanoparticules les déformait en les rendant plus sphériques et plus grosses. En revanche, comme la fluorescence des nanoparticules marquées à la rhodamine était plus importante que pour les quantum dots et que la modification du polymère n'aboutissait pas à la déformation des nanoparticules, ce marquage a été exclusivement utilisé pour le reste des études.

La toxicité des nanoparticules de PBLG sur les cellules HUVEC a été étudiée en premier lieu au moyen d'un test MTT. Jusque 300µg/mL, aucune toxicité franche des particules n'est apparue, puisque 70-80% des cellules survivaient après 72h.

Enfin, les interactions entre les HUVEC et les nanoparticules de PBLG de formes variées marqués par la rhodamine ont été examinées par microscopie confocale. Nous avons constaté dans un premier temps un accrochage des nanoparticules aux membranes cellulaires, puis l'entrée des nanoparticules dans les cellules. De plus, il semblerait que les nanoparticules allongées entrent plus lentement que des particules plus sphériques dans les HUVEC.

Chapitre 6 : Effet de la forme des nanoparticules sur leur pharmacocinétique

Le sixième chapitre de cette thèse présente une étude de biodistribution de deux types de nanoparticules de PBLG de formes différentes chez le rat en se servant du marquage

développé au chapitre 5. Dans ce but, une méthode de mesure de la quantité de nanoparticules dans le sang a été préalablement mise au point, mettant en œuvre une extraction chloroformique du polymère flurorescent inclus dans les particules présentes dans le sang et avec un taux de récupération de 100%.

Une étude pharmacocinétique portant sur deux séries de particules a ensuite été menée chez le rat (n=7). Les nanoparticules presque rondes (rapport d'élongation=1.30) et les autres plus allongées (rapport d'élongation=1.88) présentent des profils pharmacocinétiques fort différents, puisque les particules allongées ont été éliminées plus lentement que les particules sphéroïdes. Ce résultat parait attribuable uniquement à l'élongation plus ou moins grande des particules, puisque les particules étaient constituées du même polymère, seule variant la masse molaire.

Chapitre 7 : Discussion générale

Ce travail avait pour but de répondre autant que possible à la question de l'incidence du facteur forme sur divers mécanismes mis en jeu lorsque des vecteurs micro et surtout nanoparticulaires sont utilisés afin de vectoriser des principes actifs. Pour réaliser cet objectif, il a été nécessaire de créer des nanoparticules non sphériques de manière contrôlée. La comparaison de différentes techniques de production pour la fabrication de particules non sphérique a ainsi permis de sélectionner les techniques les plus adaptées, capables de préserver un certain nombre de caractéristiques physico-chimiques importantes pour leur utilisation. Les méthodes PRINT et d'étirement des particules dans des films de polymères permettent d'accéder à une variété importante de géométries, ce qui permettrait d'étudier l'incidence de la morphologie sur le devenir *in vitro* et *in vivo* des particules. En revanche, la méthode d'auto assemblage semble plus appropriée pour la production de particules fonctionnalisées, parce que cette méthode qui opère en milieu aqueux permet un bien meilleur

contrôle de leurs surfaces à l'échelle moléculaire. En dehors de ces considérations technologiques, une forte influence de la morphologie particulaire sur le devenir *in vivo* des nanoparticules a été fortement suggérée par nos expériences, cohérents en cela avec les quelques études disponibles dans la littérature.

Conclusion et perspectives

En conclusion, nos travaux suggèrent que la morphologie des nanoparticules polymères pourrait influencer considérablement leur devenir dans l'organisme puisque leur biodistribution notamment parait dépendre fortement de ce paramètre. Ainsi, la morphologie particulaire représente certainement une caractéristique importante qui doit être pris en considération, tant dans le cadre d'applications pharmaceutiques dans le domaine de la vectorisation que du point de vue de la toxicité de ces systèmes. A ce jour, les travaux dans ce domaine sont émergents. Il est vraisemblable que le manque actuel de données dans ce domaine sera progressivement comblé car s'il était confirmé que le paramètre morphologique était capable de gouverner efficacement la distribution dans les organismes vivants, il représenterait alors un paramètre nouveau à prendre en compte lors de la conception de nouveaux vecteurs, permettant peut être un meilleur contrôle de la distribution. Ainsi, nous suggérons de s'intéresser en particulier : (i) .aux développement de méthodes permettant de produire dans des conditions parfaitement contrôlée de telles particules, (ii) à l'effet de la forme et de la surface des nanoparticules lors de leurs interactions avec les cellules et les molécules biologiques et (iii) bien entendu à l'accumulation d'études de biodistribution de séries variées de nanoparticules tant au niveau des organes que cellulaires, seules études capables de rendre compte de l'impact de la morphologie particulaire dans le domaine de la vectorisation.

ABSTRACT

The drug targeting strategy aims not only to reduce the amount of administered drugs, but also to improve the benefit/risk ratio for the patient. Specific cellular delivery is raised while toxic effects caused by non specific delivery are weakened. To be fully efficient various vectors have been proposed, which are not only able to encapsulate the therapeutic molecules, but are also meant to interact efficiently with target cells. From this point of view, polymer nanoparticles are interesting objects for specifically targeting cells because of a unique combination of a nanometric size and the possibility to considerably modulate their physico-chemical properties.

To this day the influence of the morphology of micro- and nanoparticles on their biodistribution is mostly unknown. However only a few studies suggest that the shape of objects introduced in the body has a major influence on their fate in fluids[1], *in vitro* [2], and *in vivo*. Thus the observation of micro-organisms shows that shape not only influences their displacement, but also their capacity to interact with cells and the capture by macrophages.

Understanding, at the micro- and nanometric levels the influence of shape on the interaction between particles and cells presents an undeniable scientific and pharmaceutical interest. Within this framework, the objective of our project is to identify the different mechanisms or phenomena that the shape might impact, and to try to quantify their significance. More and more studies on the fabrication of micro- and nanoparticles are emerging, but almost no data referred to the influence of shape on the behavior of these objects.

To realize this study, we focused on producing non spherical particles of controlled shape and surface, either by auto-assembly of copolymers of poly(gamma-benzyl-L-glutamate) or by deformation of spherical nanoparticles. Then we studied the influence of shape on the *in vitro* interactions with characterized surfaces through surface plasmon resonance, on the interactions with cells (Human umbilical vein endothelial cells, HUVEC), and on the *in vivo* fate of the particles. All these elements demonstrated that the morphology of micro- and nanoparticles must be considered as a major factor to modulate their *in vivo fate.*

[1] Decuzzi P.; Ferrari M., Design maps for nanoparticles targeting the diseased microvasculature. *Biomaterials*, **2008**, *29*(3):377-384
[2] Champion J.A.; Mitragotri S., Role of target geometry in phagocytosis. *Proc Natl Acad Sci*, **2006**, *103*(13):4930-4934.

KEY WORDS: Nanoparticles, shape, morphology, PBLG, self assembly, biodistribution

LABORATOIRE DE RATTACHEMENT :
UMR CNRS 8612 – Laboratoire de Physico-chimie, Pharmacotechnie et Biopharmacie.
5, Rue Jean Baptiste Clément
92296 Châtenay-Malabry, France
POLE : PHARMACOTCHENIE ET PHYSICO-CHIMIE

UNIVERSITE PARIS-SUD 11
UFR « FACULTE DE PHARMACIE DE CHATENAY-MALABRY »
5, Rue Jean Baptiste Clément
92296 Châtenay-Malabry, France